



IMPROVEMENT OF THE ONE-WAY AND TWO-WAY SHAPE MEMORY EFFECTS IN TI-NI SHAPE MEMORY ALLOYS BY THERMOMECHANICAL TREATMENTS

Cristina Urbina Pons

Dipòsit Legal: T. 1349-2011

ADVERTIMENT. La consulta d'aquesta tesi queda condicionada a l'acceptació de les següents condicions d'ús: La difusió d'aquesta tesi per mitjà del servei TDX (www.tesisenxarxa.net) ha estat autoritzada pels titulars dels drets de propietat intel·lectual únicament per a usos privats emmarcats en activitats d'investigació i docència. No s'autoritza la seva reproducció amb finalitats de lucre ni la seva difusió i posada a disposició des d'un lloc aliè al servei TDX. No s'autoritza la presentació del seu contingut en una finestra o marc aliè a TDX (framing). Aquesta reserva de drets afecta tant al resum de presentació de la tesi com als seus continguts. En la utilització o cita de parts de la tesi és obligat indicar el nom de la persona autora.

ADVERTENCIA. La consulta de esta tesis queda condicionada a la aceptación de las siguientes condiciones de uso: La difusión de esta tesis por medio del servicio TDR (www.tesisenred.net) ha sido autorizada por los titulares de los derechos de propiedad intelectual únicamente para usos privados enmarcados en actividades de investigación y docencia. No se autoriza su reproducción con finalidades de lucro ni su difusión y puesta a disposición desde un sitio ajeno al servicio TDR. No se autoriza la presentación de su contenido en una ventana o marco ajeno a TDR (framing). Esta reserva de derechos afecta tanto al resumen de presentación de la tesis como a sus contenidos. En la utilización o cita de partes de la tesis es obligado indicar el nombre de la persona autora.

WARNING. On having consulted this thesis you're accepting the following use conditions: Spreading this thesis by the TDX (www.tesisenxarxa.net) service has been authorized by the titular of the intellectual property rights only for private uses placed in investigation and teaching activities. Reproduction with lucrative aims is not authorized neither its spreading and availability from a site foreign to the TDX service. Introducing its content in a window or frame foreign to the TDX service is not authorized (framing). This rights affect to the presentation summary of the thesis as well as to its contents. In the using or citation of parts of the thesis it's obliged to indicate the name of the author.

Cristina Victoria Urbina Pons

IMPROVEMENT OF THE ONE-WAY AND TWO-WAY SHAPE
MEMORY EFFECTS IN TI-NI SHAPE MEMORY ALLOYS BY
THERMOMECHANICAL TREATMENTS

THESIS



UNIVERSITAT ROVIRA I VIRGILI

Department of Mechanical Engineering

IMPROVEMENT OF THE ONE-WAY AND TWO-WAY SHAPE MEMORY EFFECTS IN TI-NI SHAPE MEMORY ALLOYS BY
THERMOMECHANICAL TREATMENTS
Cristina Victoria Urbina Pons
DL: T.1349-2011

IMPROVEMENT OF THE ONE-WAY AND TWO-WAY SHAPE MEMORY EFFECTS IN TI-NI SHAPE MEMORY ALLOYS BY
THERMOMECHANICAL TREATMENTS
Cristina Victoria Urbina Pons
DL: T.1349-2011

IMPROVEMENT OF THE ONE-WAY AND TWO-WAY SHAPE MEMORY EFFECTS IN TI-NI SHAPE MEMORY ALLOYS BY
THERMOMECHANICAL TREATMENTS
Cristina Victoria Urbina Pons
DL: T.1349-2011

Cristina Victoria Urbina Pons

IMPROVEMENT OF THE ONE-WAY AND TWO-WAY SHAPE
MEMORY EFFECTS IN TI-NI SHAPE MEMORY ALLOYS BY
THERMOMECHANICAL TREATMENTS

THESIS

Supervised by Dr. Francesc Ferrando Piera and Dra. Silvia De la Flor Lopez

Department of Mechanical Engineering



UNIVERSITAT ROVIRA I VIRGILI

Tarragona

2011

IMPROVEMENT OF THE ONE-WAY AND TWO-WAY SHAPE MEMORY EFFECTS IN TI-NI SHAPE MEMORY ALLOYS BY
THERMOMECHANICAL TREATMENTS
Cristina Victoria Urbina Pons
DL: T.1349-2011

Dr. Francesc Ferrando i Dra. Silvia De la Flor, professors titulars del Departament d'Enginyeria Mecànica de la Universitat Rovira i Virgili

FEM CONSTAR

que el present treball que porta el títol

IMPROVEMENT OF THE ONE-WAY AND TWO-WAY SHAPE
MEMORY EFFECTS IN TI-NI SHAPE MEMORY ALLOYS BY
THERMOMECHANICAL TREATMENTS

que presenta en/na Cristina Urbina per optar al grau de Doctor per la Universitat Rovira i Virgili, ha estat realitzat sota la seva direcció en els laboratoris del Departament d'Enginyeria Mecànica de la Universitat Rovira i Virgili, i que tots els resultats presentats i la seva anàlisi són fruit de la investigació realitzada per l'esmentat/da doctorant.

I per a que se'n prengui coneixement i tingui els efectes que correspongui, signo aquesta certificació.

Tarragona, 23 de Maig de 2011

Dr. Francesc Ferrando
Professor Titular d'Universitat

Dra. Silvia De la Flor
Professor Titular d'Universitat

IMPROVEMENT OF THE ONE-WAY AND TWO-WAY SHAPE MEMORY EFFECTS IN TI-NI SHAPE MEMORY ALLOYS BY
THERMOMECHANICAL TREATMENTS
Cristina Victoria Urbina Pons
DL: T.1349-2011

A Sergio,

*Por los caminos recorridos,
por las cumbres alcanzadas,
por todo lo que nos queda por descubrir.*

IMPROVEMENT OF THE ONE-WAY AND TWO-WAY SHAPE MEMORY EFFECTS IN TI-NI SHAPE MEMORY ALLOYS BY
THERMOMECHANICAL TREATMENTS
Cristina Victoria Urbina Pons
DL: T.1349-2011

Agradecimientos

A través de estas líneas me gustaría dar las gracias a todas aquellas entidades y personas que han colaborado, pero que también me han ayudado y apoyado durante la realización de esta tesis doctoral.

A mis directores de tesis, la Doctora Silvia De la Flor y el Doctor Francesc Ferrando, por haber depositado su confianza en mí y creer que sería capaz de llevar a cabo este trabajo. Todos estos años me han dirigido de una forma experta y profesional, no sólo dándome el necesario soporte técnico o buscando las fuentes de financiación que tan necesarias han sido, sino también su apoyo personal y amistad.

Al Servei de Recursos Científics i Tècnics de la URV, por su inestimable contribución a esta tesis.

A todos y cada uno de mis compañeros del Departamento de Ingeniería Mecánica. A Vicenç Puig, Josep Maixé y José Rodríguez, por su fundamental colaboración en la construcción de la parte experimental. A todo el personal de administración y servicios del DEM, por su eficiencia, gentileza y paciencia. Siempre dispuestos a ayudarte. Y en especial, a mis compañeros de Área que, de una forma u otra, siempre me han mostrado su apoyo durante todo este tiempo.

A mi familia y amigos, de aquí y de allí, por soportar mis abandonos y ausencias. Al fin se terminó.

A mi madre, quien me ha enseñado que pase lo que pase y pese a todo, siempre hay motivos para seguir adelante. Gracias por tu dedicación, optimismo y apoyo incondicional.

Y, por encima de todo, a Sergio. Por hacer de nuestra vida en común una maravillosa aventura compartida. Gracias por tu amor e incondicional apoyo en cualquier situación y en cualquier momento. Siempre a mi lado. Sin ti, y tú lo sabes mejor que nadie, yo no habría llegado hasta aquí.

IMPROVEMENT OF THE ONE-WAY AND TWO-WAY SHAPE MEMORY EFFECTS IN TI-NI SHAPE MEMORY ALLOYS BY
THERMOMECHANICAL TREATMENTS
Cristina Victoria Urbina Pons
DL: T.1349-2011

Resumen

El objetivo principal de esta tesis es establecer los **vínculos existentes** entre los **cambios** producidos **en las transformaciones de fase** por procesos termomecánicos y **las propiedades funcionales** en aleaciones con memoria de forma de Ti-Ni, tal que nos permita hallar los procesos termomecánicos más adecuados que proporcionen una **mejora substancial** en las propiedades funcionales de estas aleaciones. La determinación de estas relaciones, prestando especial atención a la fase-R, nos debe proporcionar las claves para incrementar las propiedades de memoria de forma y doble memoria de forma.

Las Aleaciones con Memoria de Forma (SMA) son una clase de materiales inteligentes que pueden sufrir transformaciones de fase micromecánicas reversibles cambiando su estructura cristalográfica. Estas transformaciones de fase pueden ser inducidas por cambios en la temperatura (T) y/o en la tensión, permitiendo mostrar sus especiales propiedades funcionales a nivel macroscópico. Las propiedades resultantes de este comportamiento son principalmente tres: la superelasticidad, la memoria de forma y la doble memoria de forma. El mecanismo subyacente es una **transformación martensítica** termoelástica reversible **entre dos fases** en estado sólido, la fase de alta temperatura (**austenita, A**) y la fase a baja temperatura (**martensita, M**). Bajo determinadas condiciones como la aplicación de un ciclado térmico, un tratamiento térmico (TT) previo, composición química, nivel de deformación, etc., durante la transformación de A a M, puede aparecer una fase denominada **fase-R**, produciendo un proceso de transformación en dos pasos. Por tanto, las propiedades funcionales de las SMA son gobernadas por las transformaciones de fase y se caracterizan por el rango de T's en las cuales se muestran estas propiedades.

Sin embargo, **las transformaciones de fase son altamente dependientes de la composición de la aleación, así como de la historia térmica y mecánica** previa al uso de la SMA. Pero no sólo los tratamientos previos al uso de la SMA condicionan sus propiedades funcionales, sino que el uso cíclico bajo determinadas condiciones termomecánicas de las SMA puede causar la degradación de sus propiedades (fatiga funcional): cada ciclo termomecánico suele comprender una transformación de fase completa, provocando la formación y acumulación de defectos en la microestructura inducidos por transformación, produciendo cambios en las subsiguientes transformaciones de fase. Los efectos en las transformaciones de fase debido a los

diferentes tratamientos termomecánicos es todavía un tema abierto de discusión en la literatura especializada.

Por tanto, el principal objetivo de esta tesis es el estudio exhaustivo de los efectos de los tratamientos termomecánicos en las transformaciones de fase y, en especial en la fase R, y la influencia de estos cambios en las propiedades funcionales de memoria de forma y de doble memoria de forma.

Para la consecución de este objetivo se han usado **diferentes técnicas de caracterización** experimental: **variación de la resistividad eléctrica con la temperatura (ER)**, **difractometría de rayos X (DRX)**, **ensayos de tracción isotérmicos**, **ciclos térmicos a tensión constante** y **ciclos térmicos a tensión nula**. La ER es una técnica muy adecuada para conocer la evolución de las transformaciones de fase puesto que la resistividad eléctrica de las diferentes fases varía notablemente con la T. Los resultados obtenidos con esta técnica en el caso de aleaciones donde la presencia de la fase-R sea escasa o inexistente pueden ser, sin embargo, inconcluyentes o contradictorios, con lo que es necesario complementarla con la DRX. La DRX se ha empleado tradicionalmente para la caracterización de la estructura cristalina, o bien para la caracterización cualitativa de las fases presentes en las SMA. En esta tesis se presentan por primera vez resultados de DRX de caracterización cuantitativa: se ha cuantificado la fracción en peso de las diferentes fases, pudiéndose detectar con mayor precisión los cambios de las transformaciones de fase debido a tratamientos termomecánicos. Esta caracterización se ha realizado mediante el procesamiento de los resultados de DRX por métodos matemáticos y software adecuado (TOPAS). Para la consecución del objetivo principal, se utilizaron alambres Ti-Ni de diámetro 1mm con composición 49.33 Ni (at%) Se realizaron cuatro tratamientos térmicos a 450°C, 475°C, 500°C y 525°C para asegurar diferentes presencias de fase-R, por tanto diferentes transformaciones de fase, en las muestras.

El **primer paso** fue estudiar experimentalmente cómo un repetitivo **ciclado térmico a tensión nula** en todo el rango de temperaturas de transformación **cambia las transformaciones de fase, y en especial, desarrolla y/o estabiliza la fase R, dependiendo de la T del TT previo aplicado a la aleación**. Complementando los resultados obtenidos mediante ER con los obtenidos mediante DRX, **se ha propuesto una nueva interpretación de las curvas de resistividad** dependiendo de la forma de estas curvas, que mejora substancialmente la anterior interpretación. Posteriormente, y **mediante el cálculo de los parámetros mecánicos** que definen las propiedades de

memoria de forma, se determinó la influencia de la evolución de las transformaciones de fase con la T del TT y con el posterior ciclado térmico a tensión nula en las propiedades de memoria de forma. Este exhaustivo análisis experimental nos permitió **establecer los procedimientos térmicos más adecuados previos al uso de la aleación que mejoran las propiedades de memoria de forma simple**. Las propiedades mecánicas tales como la tensión crítica de transformación, módulos de elasticidad y capacidad de recuperación de deformación mejoran si la aleación es ciclada térmicamente a tensión nula previo a su uso. Esta mejora es sustancial siempre y cuando esta aleación haya sido previamente tratada térmicamente a temperaturas iguales o superiores a 500°C. La ventaja de aplicar este proceso, **una adecuada temperatura de TT seguido de un número mínimo de ciclos a tensión cero**, es que este proceso proporciona una mejora de las propiedades de memoria de forma, **evitando deformaciones permanentes** en la aleación que podrían influir negativamente en una futura aplicación de la aleación.

La doble memoria de forma (TWSME) es una propiedad funcional de las SMA que permite que la SMA sea capaz de recuperar la forma original a alta T y la forma impuesta por deformación a baja T, aplicando únicamente cambios de temperatura e incluso actuando contra una fuerza. La TWSME no es una propiedad intrínseca de las SMA, sino que se desarrolla mediante la aplicación de adecuados procesos termomecánicos, llamados adiestramientos. **La TWSME es extremadamente sensible al proceso de transformación de fase, sin embargo, no existe una opinión contrastada sobre la influencia de la fase-R en la TWSME**. Manteniendo el mismo objetivo de optimización de la memoria explicado previamente, se pretendió investigar **si las dislocaciones introducidas** en la microestructura de la aleación **por el ciclado térmico a tensión nula** podrían tener una influencia positiva en el desarrollo de la TWSME. Así, **la segunda fase** de esta tesis fue la **optimización de las propiedades de TWSME** mediante la aplicación de un adecuado TT previo al adiestramiento. Para ello, se determinó inicialmente la **influencia del tipo de transformación de fase y de la presencia inicial de la fase-R** que muestra la aleación antes del adiestramiento en el desarrollo efectivo de la TWSME. Posteriormente, la influencia de la evolución de las transformaciones de fase y de la fase-R con el adiestramiento en los **parámetros de adiestramiento y en las temperaturas de activación** fue exhaustivamente analizada. Los resultados obtenidos sugieren que para obtener un **aumento en las propiedades de TWSME**, es decir, un incremento de la deformación de memoria doble recuperable,

junto con una minimización de la deformación permanente desarrollada durante el proceso de adiestramiento y unas temperaturas de activación del efecto doble memoria apropiadas, **el alambre de Ti-Ni debe ser tratado térmicamente a T superior a 500°C**. Con ello se obtiene una transformación de fase adecuada, caracterizada por la evolución simultánea de la fase-R y de la martensita. Posteriormente, **ciclar el alambre a tensión nula para desarrollar la fase-R** en el material y consiguiendo que ésta incida mínimamente en la formación de la forma a recordar durante el adiestramiento. Finalmente, **el alambre debe ser adiestrado mediante ciclos térmicos a tensión constante**. Por tanto, un ciclado térmico a tensión nula previo al adiestramiento produce un incremento en la eficiencia del entrenamiento, en la doble memoria de forma conseguida y un decrecimiento en la deformación permanente acumulada si se compara con un alambre que recibe el mismo TT pero no ciclado térmicamente a tensión nula previo al adiestramiento.

Como resultado del exhaustivo análisis de la evolución de las transformaciones de fase con el TT, con el ciclado térmico y con los procesos de adiestramiento se ha conseguido que esta aleación comercial **muestre una gran variedad de comportamientos de memoria de forma**. Un TT a $T < 500^{\circ}\text{C}$ proporciona una transformación de fase caracterizada por una fase-R completamente desarrollada y que hace que la aleación sea apropiada para aplicaciones cíclicas de one-way memory effect (memoria de forma simple). Mientras que un tratamiento a $T > 500^{\circ}\text{C}$ proporciona una transformación de fase adecuada para aplicaciones cíclicas de la TWSME.

Finalmente, el **último paso** de esta tesis ha sido el estudio de la **eficiencia de la optimización de la TWSME** conseguida. Se midió el trabajo generado por los alambres previamente adiestrados según el proceso explicado anteriormente y frente a diversos niveles de fuerzas opositoras. **Los resultados muestran que estos alambres ciclados térmicamente antes del adiestramiento generan hasta un 15% más de trabajo que los alambres que NO han sido ciclados térmicamente previos al adiestramiento, debido a su mayor capacidad de deformación recuperable.**

A través del estudio exhaustivo de las transformaciones de fase, se ha aportado una nueva interpretación de las curvas de resistividad para el cálculo de las temperaturas de transformación, se ha determinado la influencia de la fase-R en las propiedades funcionales de las SMA y se han mejorado substancialmente las propiedades de memoria simple y doble memoria de forma mediante procesos térmicos que evitan deformaciones permanentes antes del uso de la aleación.

ABSTRACT

The main objective of this thesis is to establish the relationships between the changes in **Ti-Ni phase transformation behaviour** caused by thermomechanical processes, especially in the R-phase range, and the **functional properties** of the Ti-Ni shape memory alloys (SMAs). Establishing these relationships should allow us to find **appropriate thermomechanical processes** to substantially **improve the Ti-Ni one-way and two-way shape memory effects**.

The functional properties of SMAs, such as shape memory effect (or one-way memory effect), superelasticity and the two-way shape memory effect (TWSME), are derived from **thermoelastic reversible crystallographic phase transformation which occurs when an SMA is subject to a process in which it passes from a high temperature phase called austenite to a lower temperature phase called martensite**. Under certain circumstances, such as the application of thermal cycling, heat treatment, chemical composition, deformation, etc., an intermediate phase known as **R-phase** is present in the alloy during the austenite to martensite transformation, which results in a two-stage transformation. Therefore, the SMA's functional properties are characterized by the transformation behaviour between the alloys' phases and their temperatures, which are known as transformation temperatures.

However, the **Ti-Ni phase transformation behaviour is very sensitive to the thermal and mechanical history of the alloy**. Thermomechanical cycling through the full transformation range may degrade the Ti-Ni functional properties (functional fatigue). These repeated transformation cycles cause changes in the SMA phase transformation behaviour due to the formation and accumulation of defects in the alloy microstructure. Therefore, **the changes that thermomechanical processes cause in the phase transformation behaviour of Ti-Ni SMA are still an open discussion** in the SMA scientific community.

Consequently, the main objective of this thesis is the exhaustive study of the effects of the most common Ti-Ni SMA thermomechanical processes on the Ti-Ni phase transformation behaviour and their influence on the one-way and two-way shape memory effects. This experimental study should help to determine the most appropriate thermomechanical processes for substantially improving Ti-Ni functional properties. **The study will pay special attention to the development and stabilization of the R-phase** that results from these thermomechanical processes and to the influence of the R-phase on the Ti-Ni functional properties.

To achieve this objective, **several experimental techniques are used including measuring variations of the electrical resistivity with temperature (ER), X-ray diffraction (XRD), isothermal tension testing, thermal cycling under constant stress, and thermal cycling under zero stress.** ER is one of the best and frequently used experimental techniques to characterize phase transformation behaviour because SMA phase transitions are accompanied by significant variations in electrical resistivity. The main reason for these variations seems to be the appearance of the R-phase in the ER curves of the Ti-Ni wires; that is, the R-phase has significantly higher electrical resistivity compared to the austenite or martensite phases. However, if there is no R-phase in the alloy, or if this alloy has received thermomechanical treatments, it is very difficult to interpret the alloy phase transformation behaviour from the ER curves. This has been a source of controversy among several authors. For this reason, the ER results were compared and complemented by XRD measurements; that is, the phase transformation behaviour in Ti-Ni SMA wires was quantified by XRD as a function of temperature after various thermomechanical processes. Normally, XRD is used to characterize the crystalline structure of the SMA alloy or to characterize the phases present in the SMA alloy in a qualitative way. In this thesis, the quantitative characterizations of the SMA phases, which are derived from XRD profiles, are introduced as a weight fraction (%wt) of the SMA phases as a function of temperature. The weight fraction evolution is derived from XRD profiles using the Rietveld method and specific software (TOPAS).

A commercial Ti-Ni wire with a nominal composition of 49.33 Ni (at%) and a diameter of 1 mm was used throughout this study. A heat treatment was applied to the Ti-Ni material that consisted of annealing four sets of the material at temperatures of 450°C, 475°C, 500°C, and 525°C. The aim was to obtain four different initial phase transformation behaviours with different levels of R-phase.

The **first step** of this thesis was to study experimentally how repetitive thermal cycling at zero stress through the full transformation range changes the phase transformation behaviour and develops or stabilizes the R-phase, depending on the temperature applied in the previous heat treatment. Combining the ER results with the XRD data, **a new interpretation of the ER curves is proposed to measure the transformation temperatures as a function of the shape of the ER curve.** We think that this new interpretation of the ER substantially clarifies the ER measurements.

Following this, by calculating the mechanical parameters that define the shape memory properties of these alloys, we analyzed and determined how **the evolution of the phase transformation behaviour with heat treatment and subsequent thermal cycling at zero stress influences the SMA functional properties**. This wide ranging analysis allowed us to **establish which are the most appropriate thermal processes for improving the mechanical properties of the Ti-Ni wires**. The critical transformation stresses, the apparent modulus of elasticity and the recovery strain are improved for this alloy. **This improvement occurs whenever the alloy is thermally cycled at zero stress prior to use and after a heat treatment at a temperatures equal to or higher than 500°C**. The **great advantage** of this process of adequate heat treatment temperature followed by a minimum number of thermal cycles at zero stress, is that **the process prevents permanent strains** in the martensitic phase that can negatively influence future applications of the SMA.

In the shape memory effect, only the shape of the parent phase is memorized; however, the martensitic shape can be remembered when the alloy is under certain thermomechanical conditions. The SMA alloy can learn to remember both shapes after a training process. This is known as the Two-Way Shape Memory Effect (TWSME). **The TWSME is extremely dependent on the transformation sequence; however, there is no general agreement regarding the resulting phase transformation after alloy training, or the role of the R-phase in the development and stability of the TWSME**. Keeping in mind our objective of improving the functional properties of the SMA by means of thermal processes, we thought that the **dislocations introduced in the alloy by thermal cycling at zero stress could play an important role during the development of the TWSME**. Therefore, the **second step** of this thesis was to use **an adequate thermal process prior to training to improve the TWSME**. To achieve this objective, we determined the influence of the initial phase transformation and the initial presence of the R-phase on the development of the TWSME. The training parameters and the activation temperatures were analyzed for each of the training procedures; these being, thermal cycling under constant stress and isothermal tensile deformation under martensite state. The results suggest that **to improve the TWSME**, that is, to obtain a substantial two-way memory strain together with minimum irreversible strain and TWSME activation at room temperatures, the **Ti-Ni wire should be heat treated at temperatures equal to or higher than 500°C**. This heat treatment temperature creates a convenient phase transformation that allows the TWSME to be developed. This phase

transformation is characterized by a simultaneous evolution of the R-phase and the martensite phase during all the transformation process. Afterwards, **the wire should be thermally cycled at zero stress to develop the R-phase**. If this is done, the R-phase seems to interfere a little with the TWSME development. **The last part of the process involves training the wire by thermal cycling under constant stress**. This thermal cycling prior to training improves the training efficiency, increases the two-way memory strain and decreases the permanent strain accumulated during training. Consequently, samples thermally cycled prior to training generate a higher two-way memory strain than samples non-thermally cycled prior to training (0.5% higher).

Depending on the heat treatment temperature, thermal cycling at zero stress, and the training method applied, **an important variety of behaviours** for this commercial SMA is obtained. The optimal combination for obtaining TWSME behaviour is the one described above. To obtain **one-way behaviour**, the samples have to be **heat treated at $T < 500^{\circ}\text{C}$** . These heat treatment temperatures **generate a two-step phase transformation behaviour and a well-developed R-phase on cooling, thus producing a very stable one-way behaviour under isothermal cycling conditions**.

Finally, the **last step** of this thesis was to study the **efficiency of the TWSME improvement**. We measured the work production of the wires during repeated thermomechanical cycling under various levels of constant stresses. The wires had received a heat treatment at a temperature equal to or greater than 500°C , followed by repetitive thermal cycling at zero stress. They had then been trained by constant stress training. The results show that **samples thermally cycled prior to the TWSME training produced more work (15% more) than samples non-thermally cycled prior to TWSME training**. This is due to the recovery strains developed during thermomechanical work, which were always larger for thermally cycled samples than for non-thermally cycled samples.

The present exhaustive study of the phase transformation changes caused by thermomechanical processes has led to a new way of interpreting resistivity curves for calculating the transformation temperatures. Moreover, we have determined how the R-phase influences the functional properties of SMA and, finally, we have substantially improved the properties of one-way and two-way shape memory effects by using thermal processes that avoid permanent deformation of the alloy.

Publicaciones

Parte del contenido más relevante de esta tesis ha sido publicado en revistas y congresos de prestigio internacional, los cuales se listan a continuación (por orden de publicación).

Revistas Internacionales Indexadas

- Urbina, C., De la Flor, S., Gispert-Guirado, F., Ferrando, F.

Quantitative XRD analysis of the evolution of the TiNi phase transformation behaviour in relation to thermal treatments,

Intermetallics 18 (8), 2010, pp.1632-1641. Índice de Impacto 2009: 2.231. Revista situada en el año 2009 en la posición 4/70 (primer tercio) de la clasificación: Metallurgy & Metallurgical Engineering.

- Urbina, C., De la Flor, S., Ferrando, F.

R-phase influence on different two-way shape memory training methods in NiTi shape memory alloys,
Journal of Alloys and Compounds 490, 2010, pp.499-507. Índice de Impacto 2009: 2.135. Revista situada en el año 2010 en la posición 5/70 (primer tercio) de la clasificación: Metallurgy & Metallurgical Engineering. El artículo ha sido citado 1 vez según Scopus.

- Urbina, C., De la Flor, S., Ferrando, F.

Effect of thermal cycling on the thermomechanical behaviour of NiTi Shape Memory Alloy,

Materials Science and Engineering A501 (1-2), 2009, pp.197-206. Índice de Impacto 2009: 1.901. Revista situada en el año 2009 en la posición 53/214 (primer tercio) de la clasificación: Materials Science-Multidisciplinary. El artículo ha sido citado 4 veces según Scopus.

- De la Flor, S., Urbina, C., Ferrando, F.

Effect of mechanical cycling on stabilizing the transformation behaviour of NiTi Shape Memory Alloys,

Journal of Alloys and Compounds, 469(1-2), 2009, pp.343-349. Índice de Impacto de la Revista (según Journal Citation Reports) en el año 2009: 2.135. Revista situada en el año 2009 en la posición 5/70 (primer tercio) de la clasificación: Metallurgy & Metallurgical Engineering. El artículo ha sido citado 3 veces según Scopus.

- De la Flor, S., Urbina, C., Ferrando, F.

Constitutive model of shape memory alloys: Theoretical formulation and experimental validation,

Materials Science and Engineering A, 427(1-2), 2006, pp.112-122. Índice de Impacto de la Revista (según Journal Citation Reports) en el año 2006: 1.490. Revista situada en el año 2006, en la posición 52/176 (primer tercio) de la clasificación: Materials Science-Multidisciplinary. El artículo ha sido citado 3 veces según Scopus.

Congresos Internacionales

- Urbina, C., De la Flor, S., Gispert-Guirado, F., Fabregat, A., Ferrando, F.

Characterization of phase transformation and shape memory behaviour of Ti-Ni 54.4 wt% by heat and thermal treatments,

10th Biennial Conference on Engineering Systems Design and Analysis ESDA. Estambul, Turquía. Proceedings of the ESDA, 25071, 2010.

- **Urbina, C., De la Flor, S., Ferrando, F.**

TWSME improvement by thermal cycling at zero stress in NiTi shape memory alloys,
2nd International Conference on Smart Materials and Nanotechnology in Engineering, Weihai
(China), Proceedings of SPIE. Vol. 7493-74930L. 2009.

- **De la Flor, S., Urbina, C., Ferrando, F.**

*Caracterización de la evolución de las transformaciones de fase con el TT previo en aleaciones NiTi
con memoria de forma,*

9º Congreso Iberoamericano de Ingeniería Mecánica. CIBIM 9, Las Palmas de Gran Canaria (España),
2009.

- **Urbina, C., De la Flor, S., Ferrando, F.**

*Thermal Cycling Effect on different two way shape memory training methods in NiTi Shape Memory
Alloys,*

36th Solid Mechanics Conference, SOLMECH 2008, Gdansk (Polonia), 2008.

- **De la Flor, S., Urbina, C., Ferrando, F.**

Comportamiento termomecánico de actuadores NiTi: Modelo numérico y contrastación experimental,
8º Congreso Iberoamericano de Ingeniería Mecánica. CIBIM, Cuzco (Perú), 2007.

- **De la Flor, S., Urbina, C., Ferrando, F.**

Modelization and experimental analysis of a NITI shape memory alloy actuator,
6th European Solid Mechanics Conference, ESMC, Budapest (Hungria), 2006.

Proyectos financiados

Optimización de la doble memoria de forma en actuadores termomecánicos helicoidales de NiTi,
MCIN - Ministerio de Ciencia e Innovación. 2010.

Investigadora Principal: Silvia De la Flor López. DPI2009-13216

Revistas Nacionales

- **De la Flor, S., Urbina, C., Ferrando, F.**

*Adaptación de modelos macromecánicos para la simulación del comportamiento a flexión de
alambres NiTi: implementación numérica y verificación experimental,*

Anales de Ingeniería Mecánica, 16, 2006, pp. 945-951.

Congresos Nacionales

- **De la Flor, S., Urbina, C., Ferrando, F.**

*Adaptación de modelos macromecánicos para la simulación del comportamiento a flexión de
alambres NiTi: implementación numérica y verificación experimental,*

XVII Congreso Nacional de Ingeniería Mecánica, Gijón, (España), 2006.

GENERAL INDEX



IMPROVEMENT OF THE ONE-WAY AND TWO-WAY SHAPE MEMORY EFFECTS IN TI-NI SHAPE MEMORY ALLOYS BY
THERMOMECHANICAL TREATMENTS
Cristina Victoria Urbina Pons
DL: T.1349-2011

GENERAL INDEX

CHAPTER ONE: MOTIVATIONS OF THIS STUDY	27
1. Motivations of this study	
CHAPTER TWO: INTRODUCTION	43
1. Introduction: Shape Memory Alloys and their Functional Properties	
2. The R-phase transformation and its influence on the Functional Properties of Ni-Ti SMA	
3. The Two-Way Shape Memory Effect	
CHAPTER THREE: MATERIALS AND METHODS	93
1. Test in Ni-Ti SMA alloys: initial considerations	
2. Selected Material	
3. Experimental procedures and equipment	
CHAPTER FOUR: EFFECT OF HEAT TREATMENT AND THERMAL CYCLING ON THE MECHANICAL BEHAVIOUR OF THE TI-NI SMA WIRES	123
1. ER measurements of the effect of heat treatment and thermal cycling at zero stress on the SMA phase transformation behaviour	
2. XRD quantification of the effect of the heat treatment and thermal cycling at zero stress on the SMA phase transformation behaviour	
3. Effect of thermal cycling at zero stress on the Ni-Ti Functional Properties	
4. Summary and conclusions	

CHAPTER FIVE:
IMPROVEMENT OF THE TWO-WAY SHAPE MEMORY
EFFECT BY THERMAL CYCLING AT ZERO STRESS PRIOR
TO TRAINING **191**

1. Influence of heat treatment and thermal cycling at zero stress on the constant stress training method
2. Influence of the heat treatment and thermal cycling on isothermal tensile deformation below M_f training method
3. Summary and conclusions

CHAPTER SIX:
WORK PRODUCTION OF THE IMPROVED Ti-Ni WIRES **271**

1. Operating mode
2. Work production of samples 500TCs
3. Work production of samples 525TCs
4. Comparison between samples
5. Quantification of the changes in phase transformation behaviour due to thermomechanical cycling
6. Summary and conclusions

CHAPTER SEVEN: CONCLUSIONS **305**

REFERENCES **317**

ANNEX 1: SM495 QUALITY CERTIFICATE **343**

ANNEX 2: XRD ANALYSIS **347**

CHAPTER 1

MOTIVATIONS OF THIS STUDY



CHAPTER ONE: MOTIVATIONS OF THIS STUDY

Introduction

1 Motivations of this study

<i>1.1 What is wrong with the Functional Properties of Ni-Ti SMA?</i>	31
<i>1.2 Improvement of the Functional Properties of Ni-Ti SMA</i>	35
<i>1.3 Objectives of this thesis</i>	37
<i>1.4 Organization of this thesis</i>	42

Introduction

Shape memory is a generic term used to describe a group of alloys that shows exceptional mechanical and thermal responses. Shape Memory Alloys (SMAs) have the ability to recover previously defined large strains when subjected to an appropriate mechanical or thermal process. As such the alloys are able to recover their original geometry and it is in this shape change that their technological interest lies.

The functional properties of the SMAs, such as shape memory effect (SME), superelasticity and the two-way shape memory effect (TWSME) [VHU, 2001], are the result of a martensitic phase transformation that occurs between the high temperature phase (known as the austenite phase) and the different variants of the low temperature phase (known as the martensite phase). Evidence of the martensitic transformation was first obtained by Otsuka et al. [OTS, 1970], who unambiguously demonstrated a correspondence between the shape memory effect and the thermoelastic martensitic transformation in Cu-Al-Ni alloy.

By applying mechanical loading to the SMA in the martensitic state, its martensitic variants are forced to reorient (through detwinning) into a single variant, thus resulting in large macroscopic strains. After heating to the above austenitic temperatures, the martensitic phase returns to the austenitic phase, and the strains and the original shape of the alloy are recovered. The shape change is observable macroscopically. This behaviour is one of the Functional Properties of the SMA and is known as *Shape Memory Effect* (SME). Since only *one shape is memorized*, this property is also called *one-way memory effect*.

An alloy with Two-Way Shape Memory Effect (TWSME) has the ability to remember a geometrical shape at a high temperature above the austenite finish temperature and another shape at a low temperature below the martensite finish temperature. During repetitive heating and cooling the material changes its shape, through a hysteresis loop, moving from a hot shape linked to the austenite phase and a cold shape linked to the martensite phase. However, in contrast with the SME (or pseudoelasticity which will be described in the next paragraph) this functional property only occurs in Ni-Ti alloys after particular training procedures that usually involve thermomechanical treatments [ZHA, 2006].

The shape memory effect and the TWSME described above require temperature changes; that is, they are based on temperature-induced transformation. In contrast, the functional property known as *pseudoelasticity* is based on the formation of martensite by stress, is isothermal in nature, and involves the storage of potential energy. *Pseudoelasticity* is observed when the martensitic phase transformation is induced by applying thermomechanical loading to an SMA sample in austenite condition, which results in detwinning martensite being directly produced from austenite [DUE, 1990]. The process is associated with large strains, which are recovered upon unloading due to a reverse phase transformation that returns the SMA to the austenitic phase [WAY, 1990].

As has been seen, the SMA's Functional Properties are characterized by the transformation behaviour which occurs between phases of the alloy at four specific temperatures known as transformation temperatures (A_S and A_F , for the initial and final austenite transformation; and M_S and M_F , for the initial and final martensite

transformation). Under certain circumstances, such as the application of thermal cycling, heat treatment, chemical composition, deformation, etc., an intermediate phase known as R-phase is present in the alloy during the austenite to martensite transformation that results in a two-stage transformation. The transformation behaviour of the R-phase is defined by two characteristic temperatures, R_S and R_f . These transformation temperatures and the differences M_S-M_f , R_S-R_f and A_S-A_f , are important factors in the characterization of shape memory behaviour.

Therefore, the Functional Properties of the SMAs are highly dependent on the temperature at which the stress is applied to them. An increase in temperature results in shape recovery even under high-applied loads and therefore results in high actuation energy densities. In addition, under specific conditions, Ni-Ti SMA can absorb and dissipate mechanical energy by undergoing a reversible hysteretic shape change when subject to mechanical cyclic loading. These unique Functional Properties have made SMAs popular for sensing and actuation, impact absorption and vibration damping applications.

1 Motivations of this study

1.1 What is wrong with the Functional Properties of Ni-Ti SMA?

Cyclic loading is one of the generic features of many current applications of Ni-Ti shape memory alloys. These applications exploit both mechanical (pseudo-elasticity) and thermal shape memory (one-way/two-way memory effect). In many applications, a thermomechanical loading path using the pseudoelastic or shape memory effect can be repeated and can often involve a large number of transformation cycles.

Depending on the material history (fabrication process, heat treatments) or types of loading such as stress, strain, and temperature variations, cyclic martensitic transformations induce microstructural modifications such as defects on grain boundaries that result from strain incompatibilities. Therefore, one of the most critical aspects when developing SMA devices is to ensure the stability of their thermomechanical response in repeated sequences of one-way, two-way or

pseudoelastic effects; that is, the maximum memory effect, strain and/or stress, are restricted according to the number of cycles required.

SMA cycling loading is known to decrease the SMAs' Functional Properties as the number of cycles increases, which in turn affects their overall lifespan. This is known as functional fatigue [EGG, 2004] and indicates that the shape memory effect decreases with increasing the number of cycles.

Although the term functional fatigue was proposed by [EGG, 2004], Morgan et al. [MOR, 2001] distinguished between, on the one hand, the failure by fracture of the SMAs due to thermal cycling under stress/strain (conventional fatigue) and, on the other hand, the changes in physical, mechanical and memory properties due to pure thermal cycling at zero stress or under stress/strain through the transformation region (functional fatigue). This separation is useful, as [MOR, 2001] showed, because it separates classic fatigue effects from transformation cycling effects. Failure by fracture encompasses conventional fatigue mechanisms and crack growth whilst changes in physical, mechanical and memory properties describe a process whereby these properties change due to repeated phase transformations.

Consequently, the cyclic degradation of the Ni-Ti SMA memory properties represents a critical roadblock regarding the use of these active materials in applications that require more than one transformation loading cycle. These repeated transformation cycles change aspects of the transformation behaviour such as the critical transformation stresses, the transformation temperatures, the recoverable strain and the mechanical hysteresis, depending on whether the technique involved is mechanical cycling in martensitic range [LIU, 2002] or in pseudoelastic range [MIY, 1986], [STR, 1995], thermal cycling [MIY, 1986]b, [LIU, 1994], [LIU, 2006], or thermomechanical cycling to develop the two-way shape memory effect [LIU, 1990]. Miyazaki et al. [MIY, 1986] showed that during thermomechanical cycling the phase boundaries propagate forward and backward, which induced defects such as dislocations that hindered the interface movement in subsequent cycles. These accumulations of local residual defects influence the macroscopic shape memory behaviour of Ni-Ti. As Liu et al. discuss [LIU, 2006], all these effects have been attributed to the modification of the microstructure by the transformation cycling; that is, repeated thermal cycling under no

stress generates dislocation arrays that interfere with the transformation accommodation mechanism, thus reducing the martensite start temperature ([MIY, 1986]b, [LIU, 1994], [LIU, 2002], [LIU, 2006]b, and [PATT, 2007]). Thermal cycling also changes the phase transformation behaviour of the alloy, which in turn causes the R-phase because of the decrease in the martensitic start temperature, as will be explained in chapter 2, section 2.2.

An extensive study on the cyclic pseudoelastic response of Ni-Ti demonstrated that it depends on the heat treatment, material composition and testing temperature [MIY, 1986]. The Ni-Ti SMA pseudoelasticity hysteresis loops drift down with the number of cycles ([MIY, 1986], [STR, 1995]) and the Ni-Ti strain hardening behaviour changes [TOB, 1991], [TOB, 1992], [TOB, 1992]b and [LIM, 1994].

Cycling Ni-Ti by pure isothermal mechanical cycling decreases the critical transformation level and increases residual strain with cycling [LIU, 1994], [SAI, 2006]. De la Flor et al. [DFO, 2009] experimentally demonstrated that the mechanical properties obtained in near equiatomic Ni-Ti wires that had been stabilized by cycling depend significantly on the cycling temperature. Irrespective of the cycling temperature, De la Flor et al. [DFO, 2009] demonstrated that isothermal mechanical cycling tends to lower the transformation stress, thus moving the transformation lines on the stress-temperature plane in the direction of low stress and high temperature as the cyclic deformation progresses. This effect was much more pronounced in those samples cycled at higher temperatures, which indicates that if the SMA wire has to be used throughout the transformation range, the sample should be cycled at the lowest temperature at which it would be used, to obtain the best mechanical properties (i.e. critical stress). Moreover, the martensitic transformation temperatures tended to increase slightly as the cycling proceeded and this effect was more pronounced in the samples cycled at higher temperatures. If the mechanical cycling is well above or below the R_S and R_f , the R-phase tends to vanish or diminish as the mechanical cycling progresses. All these parameters vary significantly in the early cycles and they are more pronounced for the samples cycled at lower temperatures; however, the amount of variation decreases as the number of cycles increases. [DFO, 2009] found that the samples cycled at lower temperatures had the best mechanical properties and stable behaviour for at least 100 mechanical cycles.

Poor cyclic stability during thermal cycling under stress has often been reported ([STAC, 1988], [TAN, 1992], [LIU, 1999]b, [MIL, 2001] and [WAD, 2005]). In these studies, martensite start temperature increases and thermal hysteresis decreases with an increasing number of cycles, while the transformation strain decreases and the permanent strain (irrecoverable strain) increases with the number of thermal cycles under stress. Moreover, repeated thermal cycling under stress changes the phase transformation behaviour by increasing the martensitic start temperature and seems to cause the martensitic and R-phase transformation to overlap.

As has been seen, the Functional Properties of Ni-Ti alloys change in a substantial way depending on the type of thermomechanical cycling. Moreover, we should not forget that martensitic and austenitic transformation temperatures determine almost all the functional properties of shape memory alloys, including the One-Way and Two-Way Shape Memory Effects, because they determine at which temperature range such effects can be observed. This is crucial for practical applications. However, the SMAs' transformation temperatures are very sensitive to exact composition, grain size, processing and loading conditions, and this significantly alters their functional properties [OTS, 2002]. Moreover, the transformation temperatures are greatly influenced by the application of an annealing treatment. In near equiatomic Ni-Ti SMAs, low temperatures of annealing (350-450°C) produce martensitic temperatures under room temperature and austenitic temperatures near 60°C. As the annealing temperature increases the martensitic and austenitic temperatures also increase. The values obtained for the transformation temperatures can vary depending on the method of measurement [LUO, 2004].

The selection of annealing temperature has a strong influence on the properties of the alloy. Annealing the alloy prior to the SMA use is a common treatment for restoring a shape memory effect that has been reduced by cold rolling. The annealing temperature also affects the shape memory behaviour [LIU, 1989] by decreasing the critical stress and increasing the shape memory strain as the annealing temperature increases. For binary Ni-Ti alloys (Ni<50.4at%), pseudoelasticity is observed in specimens which have been cold worked and then annealed at temperatures below their recrystallization temperature. For Ni-rich alloys (Ni>50.6at%), pseudoelasticity may be developed

during ageing after a solution treatment. Full-annealed near-equiatomic Ni-Ti alloys exhibit no pseudoelasticity.

It can be seen that the main parameters to consider when studying the functional properties of the SMA are temperature, stress, and macroscopic shape strain [VHU, 1999]. However, all these macroscopic parameters are controlled by the microstructural phase transformation within the alloy. Continuous thermomechanical cycling through the complete transformation range introduces and accumulates defects in the alloy microstructure, thus producing changes in the phase transformation behaviour, transformation temperatures, thermal hysteresis, and the accumulation of permanent strains.

To conclude, it is clear that the SMA phase transformation behaviour is very sensitive to the thermal and mechanical history of the alloy, the composition of the alloy, the testing methods and the conditions (the type of loading and the strength of the austenite and martensite phases) [MOR, 2001], [HOR, 2004]. Therefore, understanding which phase transformation changes are associated with which thermomechanical cycling effects is crucial to defining how temperature, stress, and strain relate to the optimal application of SMAs.

1.2 Improvement of the Functional Properties of Ni-Ti SMA

Many methods have been proposed to improve the functional properties of near equiatomic Ni-Ti alloy. Among these are grain refinement, specific texture formation and strain hardening, which consist of cold working, cold working followed by low-temperature annealing, and severe plastic deformation, respectively [MIL, 2001], [WADA, 2005]. Conventional cold working techniques such as rolling, drawing, and extrusion can impose large strains and refine the microstructure, which improves cyclic stability. However, one or more dimensions of the processed samples are significantly reduced during these processing techniques. It is known that cold working causes an overall decrease in the austenite and martensite transformation temperatures. This decrease is due to a suppression of the martensite phase which is caused when an increase in the dislocation density inhibits interface mobility [LIU, 1989], [FIL, 1995], [PRA, 1997]. Similar to cold working, hot rolling increases dislocation density, impedes

the martensitic transformation and thus decreases the transformation temperatures [MIY, 1986]b. This makes it difficult, if not impossible, to use the SMA in several applications.

Several studies have proposed different methods to optimize the functional properties of SMAs. [HEC, 2002] stated that aging at 500°C for 6 min. in order to obtain dislocation in addition to particles in a Ni-Ti alloy (50.7%atNi) will inhibit the formation of new undesired defects during cycling. These defects increase the yield stress of the parent phase without decreasing the martensite transformability, thus improving the fatigue of the alloy. Morgan et al. [MOR, 2001] found that the most stable superelastic and thermal actuator alloys are those that have the highest resistance to slip: increasing the critical shear stress for dislocation slip minimizes plastic accommodation and martensite stabilization.

[HOR, 2004] found that the Ni-Ti alloys hardened by thermomechanical treatments are the most promising SMAs for safe use under cycle loading conditions. They found that the cyclic stability prevents the formation and accumulation of defects during thermomechanical cycles. Therefore, to achieve high cyclic stability they proposed that plastic deformation of martensite has to be avoided and that the yield strength of the austenite should be high. They achieved this by introducing favourable textures to maximize the strain from austenite to martensite and vice versa, or by introducing dislocations networks into the austenite phase (without spoiling the transformability). These extrinsic dislocations were transferred into martensite and back into austenite during transformation cycles [HOR, 2004]. They proposed ausforming (hot rolling in austenite state) or marforming (cold rolling in martensite state) plus tempering to provide an effective means of additional strengthening for all types of SMA.

However, the defects induced during these thermomechanical treatments prior to using the SMA also induce a permanent strain that will not participate either in further transformation during stress or in thermally induced transformation. Therefore, these defects can adversely influence the functional fatigue behaviour of the SMA by degrading their functional properties. More research is required to find processes to optimize the functional properties of SMAs without introducing irreversible strains in the Ni-Ti alloy.

Although it has not been implemented yet, another method that modifies the functional properties of SMAs is **repeated thermal cycling at zero stress throughout a complete temperature transformation range**. Thermal cycling at zero stress has significant and irreversible effects on the transformation behaviour of an SMA because it modifies the alloy's microstructure by delaying the beginning of the martensitic and the austenitic transformations. Because of these effects, [MOR, 2001] and [EGG, 2004] consider that thermal cycling at zero stress is a type of functional fatigue, but [HOR, 2003]-[HOR, 2004] also considers that performing thermal cycling at zero stress prior to using the SMA could improve the fatigue resistance of the alloy; that is, the process not only prevents plastic deformation in the martensite phase, but can also give high yield strength in the austenite phase. **One of the objectives of this thesis is to determine whether thermal cycling at zero stress can improve the functional fatigue of the SMAs.**

1.3 Objectives of this thesis

The main objective of this thesis is to **establish the relationships** between the changes in **Ti-Ni phase transformation behaviour** caused by thermomechanical processes (especially in the R-phase range) and the **functional properties** of the Ti-Ni shape memory alloys. By determining these relationships, we aim to **find adequate thermomechanical processes** that substantially **improve the Ti-Ni one-way and two-way shape memory effects**.

To achieve this, the following **experimental techniques** will be used: **measuring variations in the electrical resistivity with temperature (ER), X-ray diffraction (XRD), isothermal tension test, thermal cycling under constant stress, and thermal cycling under zero stress**. Published studies have used various experimental techniques to investigate how heat treatment, repeated thermal cycling at zero stress, and mechanical and thermomechanical cycling affect phase transformation behaviour and, in particular, the R-phase of the Ni-Ti SMA. These techniques included differential scanning calorimetry (DSC), electrical resistivity measurements (ER), thermomechanical analysis (TMA), internal friction probes (IF), X-ray diffraction (XRD) and neutron diffraction [UCH, 1998], [PEL, 1998], [LUK, 2002], [LIU, 2002],

[MAT, 2003], [MAT, 2004], [SIT, 2006]b, [PATT, 2007], [UCH, 2007] and [URB, 2009]. Measuring the variations in electrical resistivity is one of the most widely used of all these techniques for studying the phase transformation behaviour in SMA wire specimens and for evaluating their transformation temperatures. **The phase transitions are accompanied by significant variations in the ER which often make the results difficult to interpret** [LIN, 1980], [AIR, 1994], [WUK, 2006]. The main reason for these variations seems to be the appearance of the R-phase in the ER curves of the Ni-Ti wires. The R-phase has significantly higher electrical resistance compared to austenite or martensite phases; however, if there is no R-phase in the alloy, as occurs in fully annealed Ni-Ti wires, or when the alloy has received thermomechanical treatments, it is very difficult to interpret the phase transformation behaviour or to find the transformation temperatures of the SMA alloy. This has been a source of controversy in the research community. For this reason, our ER results will be compared and complemented by XRD measurements; that is, the phase transformation behaviour of Ni-Ti SMA wires after various thermomechanical processes will be quantified by XRD as a function of temperature. In this thesis, the quantitative characterizations of the SMA phases, which are derived from XRD profiles, are introduced as a weight fraction (%wt) of the SMA phases as a function of temperature. The weight fraction diagrams are obtained from XRD profiles using the Rietveld method [RIE, 1969], [CHE, 1992] and TOPAS software [BRU, 2003].

Moreover, **this thesis pays special attention to the R-phase transformation zone** and its mechanical parameters because, although R-phase transformation appears as an intermediate phase in most commercial Ni-Ti SMAs, there is still a lack of experimental results regarding the macromechanical properties of the R-phase. The main reason for this, according to [DUE, 2006], is that R-phase deformation/transformation processes are very difficult to detect from macroscopic stress-strain temperature curves. Furthermore, different opinions have been published on how the R-phase affects the functional response of a Ni-Ti SMA ([LIU, 1988]b, [LI, 1991], [POZ, 1999] and [CHAN, 2001]). In fact, the mechanical properties of the R-phase are the least studied of all and the transformation zone for the R-phase in the critical-stress temperature diagram has only recently been characterized ([NG, 2006], [SIT, 2006], [HE, 2006] and [TOM, 2006]). Finally, the most widely accepted macromechanical models do not

include the transformation zone for the R-phase in their critical stress-temperature diagrams ([TAN, 1986], [LIA, 1990], [BRI, 1993], [AUR, 1997]a). Associated with the previously described R-phase problems is the role of the R-phase in the development of the TWSME. Although this is not still clear, different opinions have been published concerning the influence of the R-phase on the TWSME, such as whether or not the TWSME trainings develops the R-phase, or whether the R-phase decreases the two-way memory strain. Despite this, **the influence of the R-phase on the SMA functional properties is not clear.**

To achieve the main objective of this thesis, it is necessary to break it down into a series of smaller objectives. **The first of these** is to study experimentally **how a repeated thermal cycling at zero stress** throughout the full transformation range may **change the Ti-Ni phase transformation behaviour** and the R-phase depending on the temperature of the heat treatment previously applied. **The second objective** is to calculate the mechanical parameters that define the shape memory properties of these alloys in order to determine how the evolution of the phase transformation behaviour with heat treatment and subsequent **thermal cycling at zero stress influences the SMA mechanical parameters. This wide-ranging analysis will determine which is the most appropriate thermal process** to apply before the SMA use in order to **improve the SMA mechanical properties. The thermal process should prevent the formation of permanent strains** in the martensitic phase that can negatively influence future applications of the SMA.

The third objective of this thesis is to determine **how the phase transformation behaviour of the Ti-Ni wires is affected by the TWSME training procedures.** In the shape memory effect, only the shape of the parent phase is memorized; however, under certain thermomechanical conditions, the alloy can remember the martensitic shape. The SMA alloy can learn to remember both shapes after a training process. This is the Two-Way Shape Memory Effect (TWSME). Nevertheless, the TWSME is extremely dependent on the transformation sequence; moreover, there is no general agreement regarding the resulting phase transformation after alloy training, or the role of the R-phase in the development and stability of the TWSME. Hence the importance of determining how the training procedures affect the phase transformation behaviour of the Ti-Ni wires.

To date, various training procedures have been investigated in effort to develop a TWSME of both high magnitude and stability ([SAB, 1974], [PER, 1984] and [LIU, 1990]). One of the best improvements in the TWSME was made by Wada et al. [WADA, 2005]b, who found that an adequate pre-strain of the SMA wire in the martensite phase improves the TWSME and decreases the plastic strain accumulated during posterior training cycling under constant stress. This method of training allows the introduction of an optimum amount of dislocations, thus creating preferentially oriented martensite which is rearranged by subsequent training at constant stress. This combination of methods increases the TWSME. However, it introduces large permanent strains to the alloy in martensitic state.

To avoid this important problem, keeping in mind our objective of improving the functional properties of the SMA by means of thermal processes, we think that **the dislocations introduced in the alloy by thermal cycling at zero stress can play an important role during the development of the TWSME**. The most important advantage is that thermal cycling at zero stress does not produce any permanent deformation on the alloy. Therefore, **the fourth objective of this thesis is to improve the two-way shape memory effect** by applying adequate thermal processes prior to training. The training methods that we will apply to our SMA alloys are thermal cycling under constant stress and isothermal tensile deformation under M_f .

When applied in actuators, the SMA is subjected to thermal cycling under a given load across the transformation range, this process generally being referred to as thermomechanical cycling. The actuator is thermally cycled under a constant load and, in contrast to TWSME thermal cycling, the cooling and the heating are performed under constant stress. The actuators are expected to perform the desired operation repeatedly without any deterioration in their strain response. However, it is known that thermal cycling under external constant stress changes the transformation temperatures and the phase transformation behaviour. Moreover, it accumulates an irreversible strain that changes the hot and cold shape of the sample. Nevertheless, studies have shown that these changes are quite significant during the initial few cycles and that the material tends to stabilize with further thermal cycling [PER, 1984], [WAY, 1990], [TUR, 2000], [MIL, 2001] and [BRA, 2001]. Evidence for this can be found in the microscopic reproducibility

and stability of the martensite transformation path after these few initial cycles [STA, 1992]c.

It is known that the formation of oriented martensite creates significant macroscopic strain and that the formation of self-accommodated martensite creates little macroscopic strain. At different stress levels, the microstructure of martensite is different, oriented martensite forms at high stress level, self-accommodated martensite forms at low stress level, and partially oriented martensite forms at intermediate level. Therefore, the formation of different structures of martensite at different stress levels causes variation in the transformation strain [WUX, 2003]. All this reveals a very important trend. **When Ni-Ti wire has to work against low levels of stress**, it is important to **orient its martensite variants prior to work** in order to maximize the work production of the Ni-Ti wire. In this way, the Ti-Ni wire will produce the highest possible macroscopic strain under low levels of stress because the oriented martensite path is already generated in the alloy. This oriented martensite path can be achieved if the sample is trained using TWSME methods prior to work [STA, 1992]c. Moreover, Stalmans et al. found that after a sufficient number of training cycles, the martensite formation path is stabilized in such way that it hardly changes when resisting stresses are applied in subsequent transformation cycles. Hence, it seems that TWSME trained samples are highly resistance to the formation and growth of variants that are different from those developed by training, meaning that the trained SMA can withstand considerable forces during cooling. Likewise, Liu et al. [LIY, 2004] proposed several recommendations for obtaining the best performance in a Ti-Ni wire: **“prior to work, train the SMA to have a TWSME, and preferentially, use the wire under tension”**. He suggests that this method will fully use the capacity of the SMA wire by uniformly distributing the deformation and recovery strain.

Consequently, the **fifth and last objective of this thesis** is to measure the work production generated by the trained wires under various opposing forces. The changes caused by thermomechanical cycling in recovery strain, transformation temperatures, and phase transformation behaviour will be analyzed and measured for all the samples.

1.4 Organization of this thesis

This chapter has described the objectives of this thesis. Chapter 2 contains a short introduction to the most important features of the SMAs. Chapter 3 gives a broad description of the material, test equipment, and experimental procedures used. Chapter 4 analyzes the effect of heat treatment and thermal cycling at zero stress on the phase transformation and mechanical behaviour of the Ti-Ni SMA wires. Chapter 5 describes the improvements made to the TWSME by thermal cycling at zero stress prior to training. Chapter 6 measures the work production achieved by these trained Ni-Ti wires, and the last chapter summarizes the work that has been carried out and the conclusions that can be drawn.

CHAPTER 2

INTRODUCTION



CHAPTER TWO: INTRODUCTION

Introduction

1 The Shape Memory Alloys and their Functional Properties

<i>1.1 The Memory Effect and the Shape Memory Alloys</i>	46
<i>1.2 The Functional Properties of the Shape Memory Alloys</i>	47
1.2.1 Phenomenology of the martensitic transformation	48
1.2.2 Shape memory effect	53
1.2.3 Two-way shape memory effect	54
1.2.4 Pseudoelasticity	56
<i>1.3 Commonly used Shape Memory Alloys</i>	59
1.3.1 Ni-Ti	59
1.3.2 Cu-based alloys	63
1.3.3 Other SMA alloys	63
<i>1.4 Applications of the Ni-Ti SMA alloys</i>	64

2 The R-phase transformation and its influence on the Functional Properties of the Ni-Ti SMAs

<i>2.1 Origin of the R-phase</i>	67
<i>2.2 How to obtain R-phase transformation in near equiatomic Ni-Ti SMA</i>	70
<i>2.3 Influence of the R-phase on the Ni-Ti Functional Properties</i>	76
2.3.1 Influence on shape memory effect and pseudoelasticity	76
2.3.2 Influence on the Two-Way Shape Memory Effect	77

3 The Two-Way Shape Memory Effect

<i>3.1 Particular Characteristics of the TWSME</i>	79
3.1.1 Training procedures for Ni-Ti alloys	81
3.1.2 Optimum thermomechanical training conditions for near equiatomic Ni-Ti alloys	88
<i>3.2 Mechanisms of the TWSME</i>	90

Introduction

The objective of this chapter is to perform a little revision of the most common macroscopic behaviour of the Shape Memory Alloys. It does not want to be an exhaustive study about the metallurgy, crystallography, or material mechanics. Moreover, as wire is the most common shape that a shape memory alloy can be found in market, all the descriptions will be referred to this common shape.

1 The Shape Memory Alloys and their Functional Properties

1.1 The Memory Effect and the Shape Memory Alloys

The remarkable properties of the SMA have been known since the 1930's when A. Ölander made the first related observations in the Au-Cd system in his study of a "rubber like effect" [OLA, 1932]. Lately, in 1938, Greninger y Mooradian [GRE, 1938] observed that in Cu-Zn alloys the martensitic phase appeared and disappeared with changes in the alloy temperature. However, it was many years later that Chang and Read [CHA, 1951] first reported the relationship between the martensite transformation and the shape recovery. The research became much more active after the shape memory effect was found in Ni-Ti alloys by Buehler and co-workers of the U.S. Naval Ordnance Laboratory [BUE, 1968], who introduced the phrase "shape memory effect" as a

material property and called the Ni-Ti alloy as Nitinol, as a reference to the initials of the laboratory. Essentially, Nitinol is an alloy containing approximately 50at% Ni and 50at% Ti. The Nitinol became quite popular soon after the discovery, partly by the worldwide publicity by the people in Naval Ordnance Laboratory, and partly by the good mechanical properties of the alloy, which were suitable for applications.

In spite of this welcome to shape memory alloys in the 1960's, the understanding of the phenomena of the martensitic transformation, from which phenomena originate, did not develop rapidly. In fact, as it was reported first by J.V. Humbeeck and later by Otsuka [VHU, 1999], [OTS, 2005], it took about 25 years before SMA became a well-known and well established functional material due to their complex behaviour. They depend crucially on their chemical composition, cold work, heat treatment, and thermomechanical cycling.

To date, about 30 alloys are reported to show a shape memory effect [JAN, 2005]. However, the alloys that have only been commercially exploited are Cu-Zn-Al, Cu-Al-Ni and Ni-Ti system alloys. The initial competition between Cu-based and Ni-Ti based alloys contributed to a more detailed and fundamental research, which finally led to the superiority of Ni-Ti based alloys. By far, and, although Ni-Ti based alloys have common characters with other SMAs, they are the most important commercial shape memory alloys. At present, more than 90% of all SMA applications are based on Ni-Ti or ternary Ni-Ti-Cu and Ni-Ti-Nb alloys, which are commercially available in the shape of thin wires, tubes, and thin films.

1.2 The Functional Properties of Shape Memory Alloys

The behaviour of the SMAs is more complex than that of common materials, but this complexity is the basis of their use in many applications. Different effects are observed according to the thermomechanical loading path and the loading history of the material. The two key effects in SMAs associated with the martensitic transformations are the shape memory effect and pseudoelasticity. In this section, they are briefly described together with the Two-Way Shape Memory Effect (TWSME).

1.2.1 Phenomenology of the martensitic transformation

The martensitic transformation is a shear dominant diffusionless solid-state phase transformation occurring by nucleation and growth of the martensitic phase from the parent phase [OLS, 1982]. Martensitic transformations are usually divided into two groups (thermoelastic and non-thermoelastic). The non-thermoelastic transformations occur mainly in ferrous alloys and are associated with non-mobile martensite-parent phase interfaces. These transformations are crystallographic non-reversible in the sense that the martensite cannot revert to the parent phase in the original orientation. The thermoelastic martensitic transformations are associated with mobile interfaces between the parent and martensitic phases. These interfaces are capable of backward movement during the reverse transformation (martensite to austenite transformation, $M \rightarrow A$) by shrinkage of the martensitic plates rather than nucleation of the parent phase, which leads to a crystallographically reversible transformation [OTS, 1999]. Therefore, unique properties of SMAs (i.e., shape memory effect, pseudoelasticity) are the result of thermoelastic martensitic transformation. The main characteristics of martensitic phase transformations that distinguish them among other solid-state transformations can be consulted in a wide range of excellent studies, as the ones of [DEL, 1991], [WAY, 1992], [GIL, 1998] and [PAT, 2006].

In SMA materials, the martensitic phase transformation is a rate independent, reversible, crystallographic reorientation process between the two stable phases. In absence of stress, the martensitic transformation (austenite-to-martensite) occurs when the free energy of martensite becomes less than the free energy of austenite at a temperature below a critical temperature (T_0) at which the free energies of the two phases are equal [DEL, 1991]. In absence of stress applied to the SMA, this temperature is M_S . The transformation finishes when the temperature reaches the M_f temperature. When the SMA is heated from the full martensitic phase in the absence of stress, the reverse transformation (martensite-to-austenite) begins at the temperature A_S , higher than T_0 . The transformation concluded when the temperature A_f is reached and the material is entirely in austenitic phase. The equilibrium temperature T_0 is approximately [OTS, 1999]:

$$T_o = \frac{(M_s + A_f)}{2} \quad (\text{eq.2.1})$$

Figure 2.1 represents the direct and reverse transformation processes, above described. As seen in this figure, the direct transformation and the reverse transformation follow different paths as a consequence of the transformation hysteresis. From a microscopic point of view, this hysteresis can be associated to the friction produced by the mobility of the martensite variants during the transformation process [WAY, 1990]. The hysteresis wide is defined as the difference between the austenite pick and the martensite pick. The austenite pick and the martensite pick (A_p , M_p), are defined as the temperature at which the 50% of the material is already transformed. The wide of the hysteresis loop depends of the alloy system, but hysteresis loops ranges are usually between 20°C-40°C for Ni-Ti SMA alloys [FUN, 1987].

As martensitic transformation takes place, numerous physical properties are modified between martensite and austenite. During the transformations, a latent heat associated with the transformation is absorbed or released based on the transformation direction.

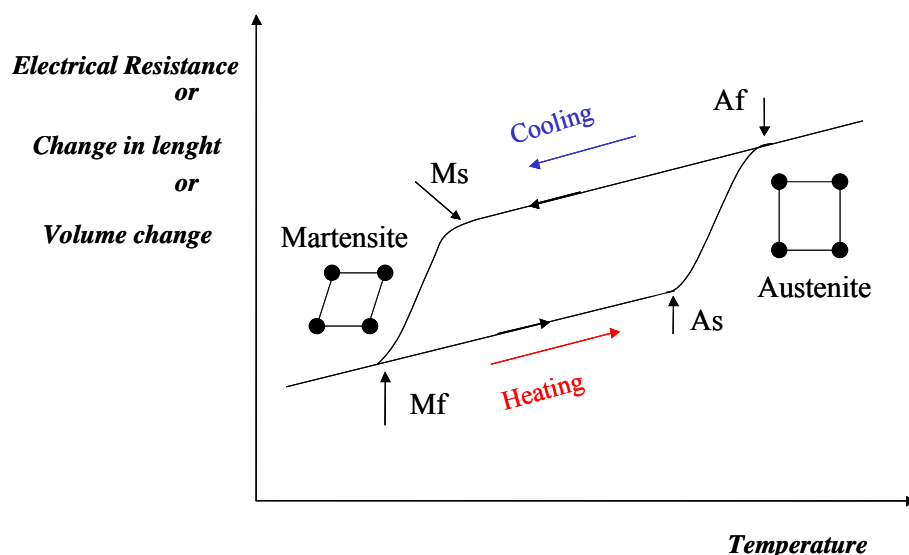


Figure 2.1 SMA Martensitic transformations: representation of the change in SMA properties. The austenite is represented by squares and the martensite by rhombohedra. In the figure, there are the transformation temperatures.

The forward transformation, austenite-to-martensite ($A \rightarrow M$), is accompanied by the release of heat corresponding to a change in the transformation enthalpy (exothermic phase transformation). The reverse transformation, martensite-to-austenite ($M \rightarrow A$), is an endothermic phase transformation accompanied by absorption of thermal energy. For a given temperature, the amount of heat is proportional to the volume fraction of the transformed material. The two phases also have different electrical resistivity due to their different crystallographic structures [HAR, 1990], thus, their phase transformations are associated with a change in the electrical resistivity of the alloy. These changes allow the measurement of the transformation temperatures.

Moreover, the martensite not only can be formed by a change in the temperature of the alloy, but also due to an application of stress, whenever this stress is applied at temperature higher than M_s . This martensite formed by stress is called stress-induced martensite (SIM) [DUE, 1990]. Figure 2.2 shows the necessary stress to produce SIM. The stress to induce martensite increases when the temperature is increased.

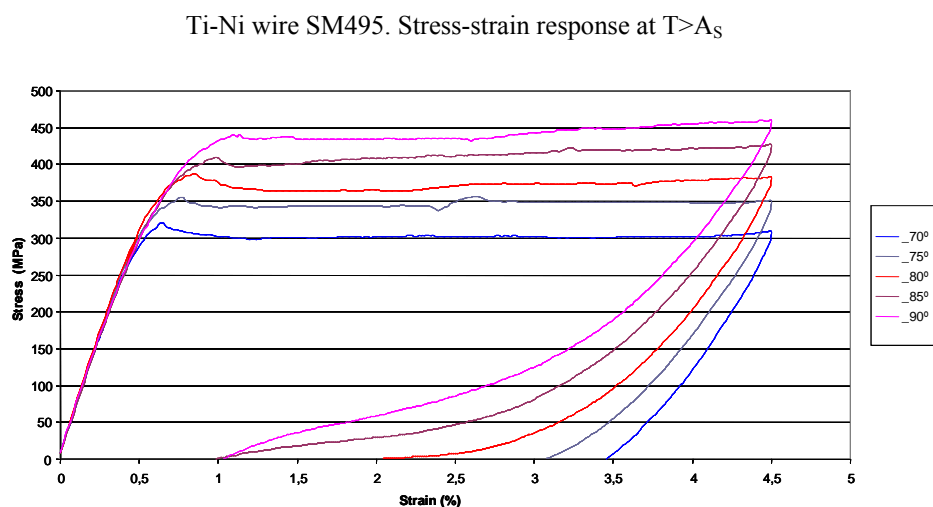


Figure 2.2 Stress-strain response for a near equiatomic Ni-Ti SMA. The necessary stress to produce SIM increases with the increase in temperature.

The lineal variation of the stress with temperature is in agreement with the Clausius-Clapeyron equation. This equation 2.2 is usually expressed as:

$$\frac{dP}{dT} = \frac{\Delta H}{\Delta V} \quad (\text{eq.2.2})$$

Where P is the pressure, T is the temperature, ΔH is the latent heat, and the ΔV is the volume change during the transformation. In terms of SMAs, this equation 2.2 is usually expressed as:

$$\frac{d\sigma}{dM_s} = - \frac{\Delta H}{\varepsilon_o} \quad (\text{eq.2.3})$$

Where σ and ε_o are respectively the applied stress and the transformation strain during the tension test. The complexity to produce SIM increases with the increase in temperature up to a certain value of temperature is reached. This temperature is called M_d . Above this temperature, plastic deformation of the SMA occurs prior to martensite transformation: plasticity by movement of dislocations becomes the dominant strain mechanism, thus the martensite transformation does not occur. Consequently, M_d is the highest possible temperature to induce martensite by stress [DUE, 1996]. In Ni-Ti SMAs M_d is usually higher than A_f .

As seen, the SMA complex behaviour is a function of stress, strain, and temperature and the corresponding rate of change of these parameters. To predict the thermomechanical response of the SMAs, macroscopic constitutive models are commonly used. These models have most often been used in technological applications because they are easier to interpret, their parameters can be obtained experimentally, and they can be more easily implemented in numerical methods. They are based on experimentally determined critical-phase transformation diagrams in the stress-temperature space. These are the models of Tanaka [TAN, 1986], Liang-Rogers [LIA, 1990], Brinson [BRI, 1993], Auricchio [AUR, 1997]a,b, Zhang [Zhang, 1997] and De la Flor [DFO, 2005].

Representing these parameters in a stress-temperature diagram (figure 2.3), it is possible to observe how the SMA transformation temperatures change with the level of stress applied, displacing them towards higher values with the increase in stress. In the figure 2.3, the critical stress-temperature diagram from De la Flor is shown [DFO,

2006]. An important SMA parameter is obtained from this diagram; that is, the stress influence coefficient (C_A or C_M for austenite and martensite respectively).

Moreover, figure 2.3 shows the critical stress required to start the martensitic transformation versus temperature. For given temperature T , the critical stress to start the martensite transformation and to finish it is denoted by σ_S^{CR} and σ_F^{CR} , respectively. For more information about experimentally determined critical-phase transformation diagrams in the stress-temperature space, please consult the studies of Brinson [BRI, 1993], Auricchio [AUR, 1997]a,b and De la Flor [DFO, 2006].

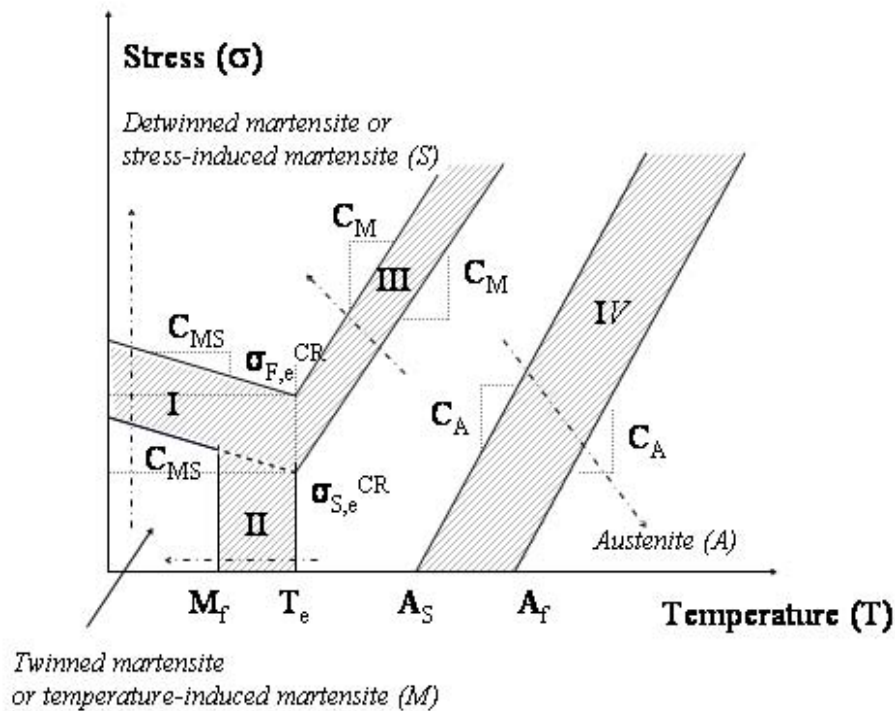


Figure 2.3 Critical stress-temperature diagram showing the special relationship that SMA develop between the stress and temperature [DFO, 2006].

1.2.2 Shape memory effect

When a shape memory alloy undergoes a martensitic phase transformation, as cooling the alloy at zero stress, the variants of the martensitic phase usually arrange themselves in a self-accommodating manner through twinning, resulting in a non-observable macroscopic shape change. By applying mechanical loading to the alloy in the martensitic state ($T < M_f$), the martensitic variants of the shape memory alloy are forced to reorient (detwinning) into a single variant leading to large macroscopic inelastic strains. After heating above $T > A_f$, the martensitic phase returns to the austenitic phase, and the inelastic strains and the original shape of the alloy are recovered. The shape change is observable macroscopically. This behaviour is one of the functional properties of the SMA and is known as *Shape Memory Effect* (SME).

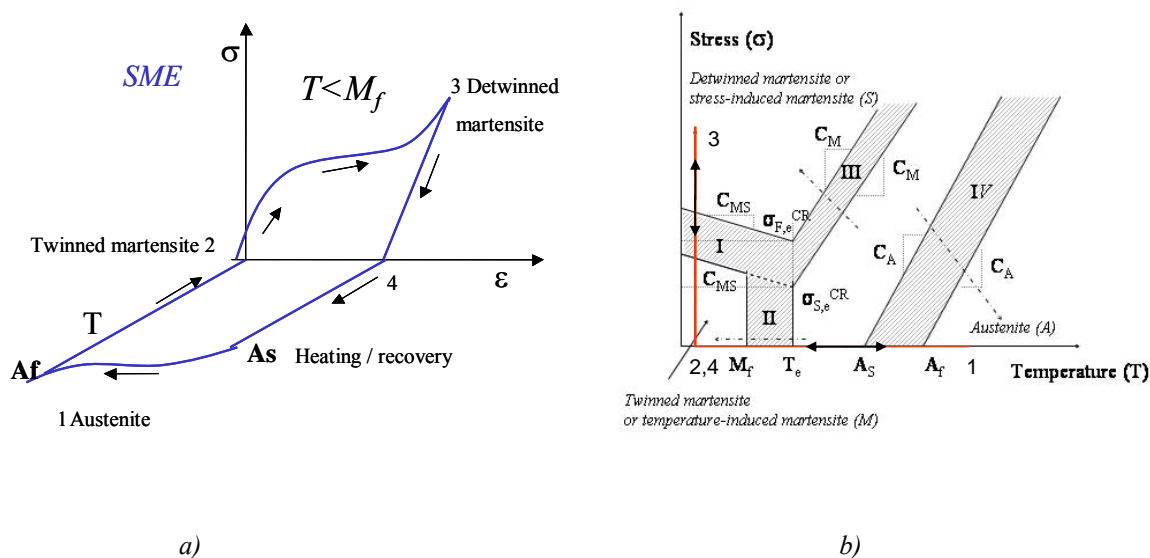


Figure 2.4 a) Schematic critical stress-strain-temperature diagram of the crystallographic changes in the shape memory effect and b) Critical stress-temperature diagram by [DFO, 2006], showing the relationship that occurs between the stress and temperature during the shape memory effect (red lines).

A typical loading path, 1→2→3→4→1, in which the SME is observed is shown in figure 2.4a. The same path is shown in figure 2.4b, schematically plotted in the stress-strain-temperature space proposed by De la Flor [DFO, 2006]. The parent phase (1→2) transforms to twinned martensite during cooling process. The material is then loaded

(2→3) causing stress induced detwinning and development of inelastic strains. Upon unloading (3→4) the material remains in detwinned state and the inelastic strains are not recovered. Finally, when the material is heated above A_f (4→1), the SMA returns to its parent phase and the inelastic strains are recovered.

The crystallographic features of the SMA alloy changes during the SME. The stress-free cooling of austenite produces self-accommodating growth of the martensitic variants (1→2) such that there is no macroscopic transformation strain. The self-accommodated morphology is a characteristic of the crystallography of the alloy used. The growth of such groups produces no macroscopic transformation strain, but the multiple interfaces present in these structures (boundaries between the martensite variants and twinning interfaces) are very mobile. This great mobility is at the heart of the shape memory effect. Movement of these interfaces accompanied by detwinning is obtained at stress levels far lower than the plastic yield limit of martensite. This mode of deformation, called reorientation of variants, dominates at temperatures lower than M_f . During the second stage (2→3), the mechanical loading in the martensitic phase leads to reorientation of the variants and results in development of large inelastic strains. This inelastic strain is not recovered upon unloading (3→4). During the last step (4→1), heating the sample above A_f induces the reverse transformation and recovers the inelastic strain. When the temperature approaches A_f , the martensitic phase becomes unstable in the absence of stress. This results in a complete transformation to the parent phase. Since martensite variants have been reoriented by stress, the reversion to austenite produces a large transformation strain having the same amplitude but opposite direction to the inelastic strain. As a result, the SMA returns to the original shape that it had in the austenitic phase.

1.2.3 Two-way shape memory effect

There is no transformation strain induced during the cooling of the material in the SME. If transformation strains are generated during both heating and cooling of the material, then this property is known as the Two-Way Shape Memory Effect and was observed for the first time by Perkins [PER, 1974]. Therefore, an alloy with TWSME allows remembering a geometrical shape at high temperature, above austenite finish

temperature (A_f) and another shape at low temperature, below martensite finish temperature (M_f). However, in contrast with the SME (or pseudoelasticity which will be described in the next section) this functional property only occurs in Ni-Ti alloys after particular training procedures that usually involve thermomechanical treatments [ZHA, 2006].

By inducing a non-homogeneous plastic strain (torsion, flexion) at a martensitic or austenitic phase or, by aging under applied stress in the austenitic phase, or in the martensitic phase or by thermomechanical cycling, either isothermal mechanical loading or thermal cycling are possible to develop the TWSME. All these training procedures involve repeated deformation and transformation between the austenite and martensite, producing a dislocated structure in the matrix. There is not yet general agreement about the exact nature of this mechanism and the precise way in which it facilitates the two-way memory effect.

The most accepted theory is that this structure creates an anisotropic stress fields that favours the formation of the preferentially oriented martensite variants, resulting in a macroscopic shape change between the phase transformation temperatures [WAD, 2008]. In any case, the generation of permanent defects eventually creates a permanent internal stress state, which allows for further formation of the preferred martensitic variant when cooled in the absence of the external load.

The training leads to secondary effects, like changes in the transformation temperatures, change in the hysteresis size and a decrease in the macroscopic transformation strain. These effects are similar to those observed during thermomechanical fatigue tests performed on the SMA alloy [LAG, 1999]. It is important to define optimal conditions of training, because an insufficient number of training cycles produces a non-stabilized two-way memory effect and over-training generates unwanted effects that reduce the efficiency of training [LIU, 1990], [STA, 1992].

In any case, from the several modes of using the shape memory alloys, the two-way shape memory effect is the most suitable to apply in actuators since no resetting force has to be considered in design [PRE, 2008]. Ni-Ti actuators using the one-way shape memory effect require a residual strain to be created before actuating, while no

preparing operation is required when using a TWSME actuator. Consequently, the main part of this thesis is dedicated to improve the Two-Way Shape Memory Effect. The TWSME will be widely described in section 3 of this chapter.

1.2.4 Pseudoelasticity

The aforementioned shape memory effect and TWSME require temperature changes; that is, they are based in temperature-induced transformation. In contrast, the functional property known as *Pseudoelasticity* is based on the formation of martensite by stress, is isothermal in nature, and involves the storage of potential energy. The *Pseudoelasticity* is observed when the martensitic phase transformation is induced by applying a stress to a SMA sample in austenite condition ($A_f < T < M_d$). Detwinning martensite is directly produced from austenite during the pseudoelastic effect [DUE, 1990]. The process is associated with large inelastic strains that are recovered upon unloading due to reverse phase transformation that returns to the austenitic phase [WAY, 1990]. Under most general conditions, pseudoelastic thermomechanical loading paths start at zero stress in the austenitic region, then move to the detwinned martensite region and then unload again to the starting point. Figure 2.5 shows the pseudoelastic path $A \rightarrow B \rightarrow C \rightarrow D \rightarrow E \rightarrow F \rightarrow G \rightarrow H$.

As the material is loaded at a temperature above A_f , the austenite undergoes up to a critical stress level called transformation stress (initial path $A \rightarrow B$, $\sigma_T^{A \rightarrow M}$). At this stress level, the material undergoes a stress induced phase transformation ($\sigma^{A \rightarrow M}$, $B \rightarrow C$) from austenite to martensite, at which large inelastic strains are developed. Any subsequent loading in the detwinned martensitic region ($C \rightarrow D$) does not produce further phase transformation, although reorientation of the martensitic twins may occur in multiaxial loading conditions. When the point (D) is reached, the reverse transformation begins (martensite-to-austenite), leading to recovery of the inelastic strains. From D to F an elastic restoration of the martensite occurs. When ($\sigma_T^{M \rightarrow A}$) the reverse transformation is initiated. The material is fully transformed to austenite at G. The final segment of the loading path ($G \rightarrow H$) is characterized by recovery of the thermoelastic strains, leading to zero macroscopic strains upon completion of the path.

The transformation process results in a hysteresis, which reflects the energy dissipated by the cycle. A similar path schematically plotted using the stress–strain–temperature space of De la Flor et al. is shown in figure 2.6 [DFO, 2006]. The a-b-c-d-g-h path showed in figure 2.6 explains the same features than the A→B→C→D→E→F→G→H path showed in figure 2.6 and it reveals the relationship between the pseudoelastic effect and the martensitic and austenitic domains.

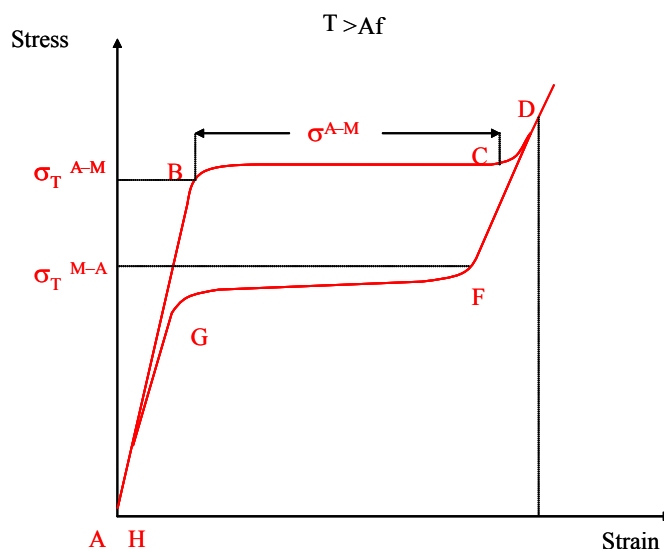


Figure 2.5 Stress-Strain diagram for an ideal SMA that shows the pseudoelastic behaviour.

To conclude, the Functional Properties of the SMAs are highly dependent on the temperature at which the stress is applied to them. Figure 2.7 shows a resume of the possible SMA behaviours versus temperature.

In the next section, the properties of common SMAs with different chemical compositions are summarized.

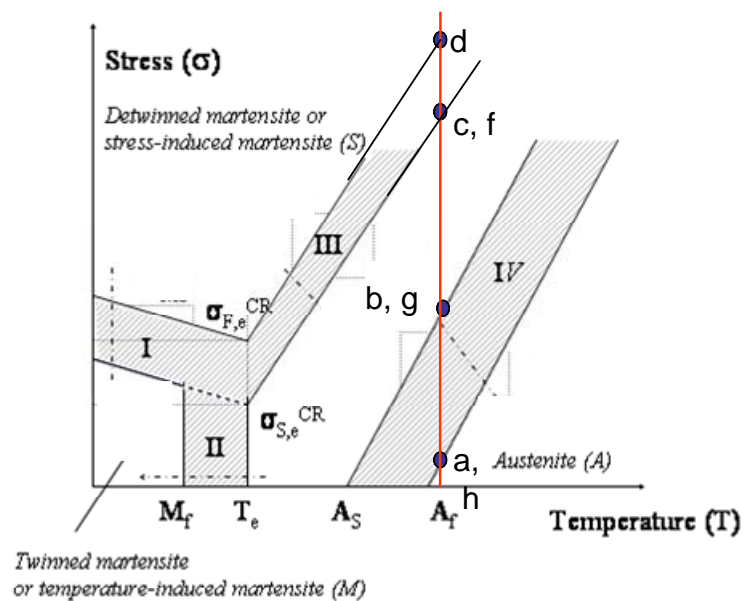


Figure 2.6 Critical Stress-Temperature diagram showing the relationship between the pseudoelastic effect and the austenitic and martensite domains [DFO, 2066].

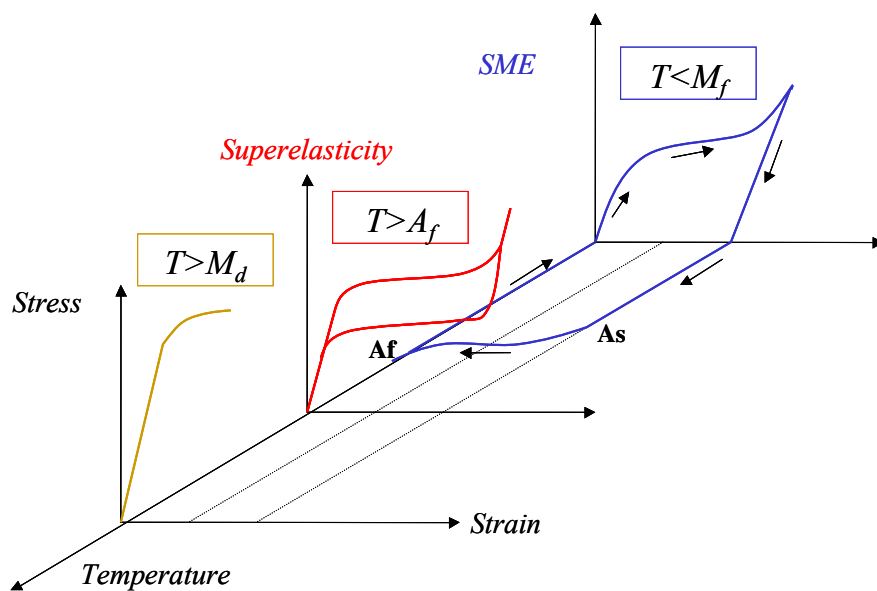


Figure 2.7 Representation of the stress-strain response in function of temperature. In the case of $T > M_d$, the behaviour of the alloy is the same that the behaviour that a conventional metallic alloy can show: an elastic zone is followed by a plastic zone. In the case of $T > A_f$, pseudoelasticity occurs. In the case of $T < M_f$ the alloy develops the shape memory effect.

1.3 Commonly used shape memory alloys

1.3.1 Ni-Ti

Nickel-titanium shape memory alloy, Nitinol (Ni-Ti), is a functional material whose shape and stiffness can be controlled with temperature. It has very large recoverable strains, high working stresses, high ductility, excellent corrosion and abrasion resistance and medical biocompatibility that have really set this alloy apart in terms of commercial application. To illustrate this fact, table 2.1 shows the property values of selected shape memory alloys [OTS, 1999].

As mentioned in section 1.1, in the early 1960s, Buehler and co-workers first explored the shape memory effect in an equiatomic Ni-Ti alloy. In fact, their initial research was focused in the corrosion resistance of the Nitinol. On the Nitinol surface a thin film of titanium oxide is formed, which is very stable and resistant to many forms of potentially corrosive attack. This corrosion resistance has led to studies on the compatibility of Ni-Ti and a number of applications. Although its cost is still high for special forms as tubes, it is popular due to its strong shape memory effect with transformation strains around 8% [MEL, 1990]. Ni-Ti TWSME has transformation strains near of 3% [LIU, 1990]. Typical pseudoelastic strain for this material is 8% [STÖ, 2001].

For Ni-Ti alloys, a wide range of transformation temperatures has been reported in the literature [WAY, 1990]. In the Ni-Ti system alloys, the transformation temperatures can be modified by only a little variation of the chemical composition [OTS, 2002]. Ti-rich Ni-Ti differs from equiatomic Ni-Ti in that the additional Ti increases the transformation temperatures. Transformation finish temperatures for a representative alloy have been observed at $M_f=40^\circ\text{C}$ and $A_f=85^\circ\text{C}$ [TOD, 1986]. Ni-rich Ni-Ti differs from equiatomic Ni-Ti in that increasing Ni content decreases the transformation temperatures: M_s drops significantly when the composition of Ni increases from 50 to 51at%.

The commonly used Ni-Ti SMAs have close to equiatomic composition, but adding a third element may result in an improvement of some properties. Ni-Ti-Cu is formed by substituting Ni for Cu in binary Ni-Ti. This decreases and stabilizes the hysteresis and reduces aging effects by suppressing precipitate formation. It also reduces the

sensitivity of the material to small composition differences in Ni or Ti. Addition of Cu suppresses the drop in M_s temperature caused by excess in Ni, making the material more suitable for commercial use, for example as actuator.

Representative transformation finish temperatures are $M_f = 30^\circ\text{C}$ and $A_f = 67^\circ\text{C}$ for Ti50-Ni40-Cu10 [STR, 1995]. Temperature ranges of $M_f \pm 20^\circ\text{C}$ and $A_f \pm 10^\circ\text{C}$ are observed throughout the literature and are due to varying the ratio of Ni to Ti while holding the at% of Cu constant as well as varying levels of cold work and thermomechanical treatment. However, these ranges are much smaller than those observed in a Ni-Ti SMA. The addition of Cu beyond $\geq 10\text{at}\%$ causes the material to become brittle [OTS, 1999]. SME transformation strains of 3% have been observed for Ti50-Ni40-Cu10 [MOB, 1990].

Ti-Ni-Zr is formed when Ti is substituted for zirconium in binary Ni-Ti. This high temperature alloy was explored by Eckelmeyer [ECK, 1976] who exposed that a small amount of Ti replaced by Zr increases the M_s temperature of Ni-Ti SMA. With the Zr content above 10at% and Ni ≥ 49.5 at%, the M_s temperature can be raised above 120°C . Representative transformation temperatures for Ti-Ni-Zr are $M_f = 100^\circ\text{C}$, and $A_f = 230^\circ\text{C}$. It is also observed that for Ni47-Ti53-Zrx, where x is the at% of Zr, transformation temperatures increase by 13°C for every at% of Ti substituted [HSI, 1998].

Among ternary alloys developed for high temperature applications, Ti-Ni-Hf shows some of the most promise. Compared to other ternary alloys like Ti-Ni-Zr or Ti-Ni-Pd, the percentage of Hf required to obtain similar transformation temperatures is much smaller. A typical transformation temperature set is $M_f = 148^\circ\text{C}$ and $A_f = 231^\circ\text{C}$ for Ti36-Ni49-Hf15 [WAN, 1999]. On average, if the percentage of Ni is held near 49 at%, A_f increases 12°C for every atomic percentage Ti of substituted for Hf assuming that the at% of Hf is greater than 3%. The material transformation temperatures are also affected by the percentage of Ni. While the transformation temperatures remain relatively constant for Ni compositions varying from 40 to 50 at%, Ni exceeding 50at% results in a steep fall in the transformation temperatures [THO, 1999]. The mechanical properties of the material are also dependent on the material composition. Low Ni ($< 40\text{at}\%$) causes brittleness [BES, 1999]. The material exhibits SME at various test temperatures and a transformation strain of 3% has been observed. However, the material exhibits

poor pseudoelastic properties due to plastic deformation coupled with transformation leading to partial recovery on unloading above A_f [WAN, 1999]. Addition of Cu to Ti-Ni-Hf results in small decrease in the transformation temperatures [MEN, 2002].

Property	Unit	Ni-Ti	CuZnAl	CuAlNi
Young's modulus	GPa			
Austenite		70-98	70-100	80-100
Martensite		27	70	80
Yield strength	MPa			
Austenite		100-800	150-300	150-300
Martensite		50-300	80-300	150-300
Ult. Tensile strength	MPa			
Austenite		800-1500	400-900	500-1200
Martensite		700-2000	700-800	1000-1200
Elongation at failure	%			
Austenite		15-20		
Martensite		20-60	10-15	8-10
Recovery Strain	%	8	3.5	3
Max recovery stress	MPa	600-900	400-700	300-600
Specific Damping capacity	%	15-20	30-85	10-20
Fatigue strength $N=10^6$	MPa	350	270	350
Resistivity	$\Omega m \cdot 10^{-6}$			
Austenite		0.5	0-0.7	0.1
Martensite		0.8	0.13	0.14

Table 2.1 SMA mechanical properties of the main commercial alloy.

Ti-Ni-Pd alloys are formed when Pd in binary Ni-Ti substitutes Ni. Early investigations of Ti-Pd materials generated interests in their high transformation temperatures and thermal hysteresis. Addition of Pd leads to an initial decrease of transformation temperature with increasing Pd content; but at higher Pd concentrations, transformation temperature increases with increasing Pd [LIQ, 1990]. These transformation temperatures can be further varied by altering the composition of Ti. As the composition of Ti increases from 50 to 51at% (where Pd is kept constant and Ni reduced), the transformation temperatures gradually decrease with increasing Ti [TIA, 2002]. A transformation strain of up to 2.8 to 3% has been observed assuming a total applied strain of 7–7.2% [WUJ, 2003]. Pseudoelasticity has also been observed in this material with a recoverable strain of up to 7% at high temperature [WUJ, 2003].

NiTiPt is formed when Ni is substituted by platinum in binary Ni-Ti. During the 1990's Liddquist and Wayman investigated the NiTiPt alloys, including the variation of transformation temperature with composition and SME properties [LIQ, 1990]. The alloys with more than 30 at% Pt become brittle. Recoverable strain of NiTiPt is approximately 2% for an applied strain of 3.5%.

Other elements, which can be alloyed with Ni-Ti, include niobium and iron. Niobium ($\approx 9\text{at}\%$) in the form of precipitates, stabilizes the martensite by shifting the transformation temperatures. Fe (1–3 at%) promotes the R-phase transformation with very low hysteresis and good fatigue performance. Others elements as carbon or oxygen can change the temperatures or can inhibit the SMA mechanical properties. Their penetration occurs during production and/or processing of the alloy. Therefore, in commercial alloys, a certificate indicating the exact chemical composition of the Ni-Ti SMA is fundamental to work safely.

1.3.2 Cu-based alloys

The main copper-based alloys are the Cu–Zn and Cu–Al systems. The presence of a third element allows the adjustment of the transformation temperatures. Their transformation temperatures are highly dependent on the composition. Copper-based alloys generally exhibit less hysteresis than Ni-Ti. The Cu–Zn–Al alloy is easy to create and rather cheap. However, it exhibits a high tendency of decomposing into its equilibrium phases when is overheated, thus bringing about a stabilization of the martensite. Addition of boron is also used to improve the ductility of the material.

Cu–Al–Ni is less sensitive to stabilization and aging phenomena. This alloy exhibits less hysteresis than Ni-Ti and becomes brittle as Ni increases beyond 4at% [TAD, 1999]. Generally, as higher is the Al content, the stability of martensite increases [WU, 1990]. The substitution of Al for Cu decreases its transformation temperatures. This variation is linear, ranging from $M_f = -70^\circ\text{C}$ and $A_f = -23^\circ\text{C}$ for 14.4at%Al, to $M_f = 35^\circ\text{C}$ and $A_f = 75^\circ\text{C}$ for a content in Al of 13.6at% [TAD, 1999]. Although the temperatures can be manipulated over a wide range, the practical upper limit for transformation is 200°C . Above this temperature, there is a rapid degradation in the transformation due to aging effects. The pseudoelastic strain for a typical Cu based SMA is 4–6%. However, with successive martensite-to-martensite transformation very high pseudoelastic strain levels can be obtained [WU, 1990], [OTS, 1979].

Developed in 1982, the Cu–Al–Be alloy has been studied during the last few years. Its nearly eutectoid composition gives it a good thermal stability. Beryllium, in small amounts (about 0.6 wt%), enables adjustment of the transformation temperatures from near 200°C to 150°C .

1.3.3 Other SMA alloys

Iron based alloys are known to exhibit less SME than many other alloys types. $\text{Fe}_{59}\text{Mn}_{30}\text{Si}_6\text{Cr}_5$ alloy is an example of a Fe based SMA [LINH, 2006]. The martensitic transformation, considered non-thermoelastic, leads to one-way shape memory effect near of 2%. The performance of these alloys is very sensitive to thermomechanical treatments.

Ni-Al alloys have attracted attention due to their very good high temperature strength and resistance to corrosion. Chakravorty and Wayman [CHK, 1976] performed early crystallographic studies on the thermoelastic martensitic behaviour of this material. Ni-Al materials exhibit good SME but are extremely brittle and exhibit a high sensitivity of the transformation temperatures due to varying Al content. Addition of Fe makes the control of M_s by annealing the alloy at appropriate temperatures. The addition of Fe to the alloy greatly increases its ductile properties and lowers the transformation temperatures of the alloy, but these effects can be compensated by adding Mn or by lowering the Al content. The ductility of this material can also be improved by the addition of B or Cr.

We have chosen near equiatomic Ni-Ti SMA alloys as the kind of SMA alloys to study in this thesis because of these alloys show important advantages in front of the others SMA. Moreover, these Ni-Ti are relatively easy to find in the market.

1.4 Applications of the Ni-Ti SMA alloys

SMA's engineering applications appeared within 10 years or so after the discovery of the shape memory effect in Ni-Ti alloys. To date, most SMA applications have been one dimensional in nature, where wires, strips, and rods were employed. Emerging applications of Ni-Ti SMA include micro-electro-mechanical systems (MEMS), [FU, 2004], biomedical devices and implants [MOR, 2004], robotics systems [VEL, 2005], civil engineering [DOL, 2011], [DLO, 2001]b, [JAN, 2005], and deployable aerospace structures [KUM, 2008]. The success of these applications hinges on the ability of Ni-Ti to perform multiple one-way memory, two-way memory, or pseudoelastic transformation sequences.

Many excellent and unique devices have been constructed for the medical industry and the market is still growing at a considerable pace. Because of its shape memory property, it provides a possibility to prepare self-locking, self-expanding, self-compressing, and other functional implants activated at body temperature. Furthermore, because of its superelasticity, it can be used in implants exposed to continuous distortion or kinking. The reported biocompatibility that has Ni-Ti, makes it a safe implant material, which is at least equally good as stainless steel or titanium alloys. This

good biocompatibility allied to the less complicated design procedure for superelastic applications, it has resulted in high number of devices utilizing this effect. Guide wires for non-invasive surgery, orthodontic arch wires, highly flexible surgical tools and stents for the re-canalization of arterial and oesophageal structures, have all been successfully produced out of Ni-Ti superelastic wires. About these medical applications, many excellent published studies can be consulted ([DUE, 1996], [GIL, 1998]_b, [RYH, 1999], [SAB, 2000], [GLE, 2000], [PELT, 2003], [PIE, 2003], [MAC, 2003], [MOR, 2004], [KUM, 2008], [PELT, 2008]).

The area of thermal application has the greatest potential of SMA application based on the hypothesis of using the SMA element as a thermal actuator that will convert electrical or thermal energy into work production [VHU, 1997], [OTS, 2002]_b, [CAI, 2005]. The function of the SMA actuator is essentially changing its shape within a change in temperature. The SMA actuator is capable of generate high forces/stresses (up to 500 MPa over large displacements/strain, 4%-8%). The temperature change can be done by change in the air temperature [YOO, 2008], [ZHUI, 2008], [KIH, 2008] or by electrical heating via Joule effect [WANZ, 2004], [DUT, 2005], [ZHO, 2006]. In the first case, the actuator is used as a sensor and thermal actuator. In the second case, the SMA is electrical actuator. This last mode of SMA use enables inexpensive mechanical actuation with electronic control.

The electrical actuators can be maintained in fixed positions or applying constant forces, controlling the electricity power. They have been used in valves and integrates in composites to control structural noises and vibrations in structures [DOL, 2001]_a, [DOL, 2001]_b, [SAA, 2002]. One of the major problems that the electrical actuator has is its cooling process that cannot be controlled as easy as its heating process. It has to be used natural air convection, or coolant fluids to cool the SMA. This fact places an inherent bound on the operating frequency of SMA electrical actuators. These problems seem overpasses by SMA thin films. They have been used in the field of MEMS, since it can be patterned with standard lithography techniques and fabricated in batch process [FU, 2004]. Thin film SMA has only small mass to heat and cool, thus the response time is reduced substantially, and the speed of operation can be increased. It facilitates the simplification of the mechanism, giving flexibility in the design and non-vibration movement. They have generated interest as micro-valves and micro-fasteners.

About engineering applications that use the recovery stress that can be generated by the Ni-Ti alloy, the first successful application was designed by Raychem Corp. for fasteners and tube couplings (to employ constrained recovery in joining pipes together in the Grumman F-14 aircraft) [MEL, 1999]. A ring of Ni-Ti-Fe alloy was expanded at very low temperatures and fitted over the coupling area of the pipes. As the ring returned to comparatively higher ambient temperatures it tried to contract to its original diameter and thus exerted high forces on the pipes resulting in a very strong and reliable coupling. The fastener type applications, all utilizing the constrained recovery effects, have the advantages that are easy to install, have a great behaviour in front of vibrations and impacts. Since then, SMAs have attracted a great deal of interest in various fields of industrial applications ranging from aerospace to naval applications. SMA technology implementation in the aerospace industry has spanned the areas of fixed-wing aircraft, rotorcraft, and spacecraft [KUM, 2008], [MATO, 2010].

To date, the devices with commercial success are those that have been designed allied to stringent actuator research and development programs (Matsushita Electrical Industrial Company Limited, [TAM, 1984]; Mercedes-Benz Company [SCH, 2000]). In most of these applications, Ni-Ti actuators or sensors are often expected to perform the desired operation repeatedly, without any significant change in their functional properties, as the working displacement in a shape memory effect application or the dissipated energy in a pseudo-elastic damping accumulation. However, because of the complicated design criteria of matching the desired motion, fatigue life and actuation temperatures the number of successful repeatable behaviour is limited. Therefore, as shape memory alloys gain acceptance as actuators in the engineering applications, the necessity for characterization of the Ni-Ti SMA thermomechanical response, (which shows complex mechanical behaviour that is dependent on the stress, strain, and temperature and production process) has become greater and it is essential that these responses could be reliably predicted. Therefore, information on changes in the SMA functional properties when the SMA is operating in cycling applications or the effect of prior to use processing conditions on these functional properties are essential for design engineers and essential for the commercial future of SMA actuator devices.

To conclude, properties and phenomena that are inherent to the SMA, such as transformation temperatures, hysteresis profiles, cyclic stability under load, etc, need to

be evaluated to provide the type of data essential for the design of high technology SMA products and their subsequent commercial acceptance.

2 The R-phase transformation and its influence on the Functional Properties of the Ni-Ti SMAs

In this section, the origin of the R-phase, the thermomechanical conditions to obtain R-phase in a near equiatomic Ni-Ti SMA alloy, and its influence on the functional properties of the Ni-Ti SMA alloys are described.

2.1 Origin of the R-phase

In the case of near equiatomic Ni-Ti SMA, the phase transformations may undergo in two different paths depending on the thermomechanical treatment condition of the alloy [OTS, 1999]. Ni-Ti alloys can exhibit one step phase transformation from cubic B2 austenite directly into monoclinic B19' martensite (B2→B19' transformation path), or via the formation an intermediate R-phase, causing a two-step transformation from the B2 to the R-phase to the B19'; that is, B2→R→B19' transformation path.

Initially, the R-phase was considered to be a premartensitic behaviour (precursor effect) prior to the subsequent martensitic transformation. However, no close structure relation between the R-phase and the B19' was found [GOO, 1985]. Lately, the R-phase transformation was considered to be a rhombohedra distortion of the B2 structure, from which derives its name [GOO, 1985], [WU, 1989], [HARA, 1997] [SHY, 2002]. Nowadays, the R-phase is considered as a martensitic transformation itself, which competes with the subsequent martensitic transformation, and only sometimes B19' martensite forms directly from B2 phase without forming R-phase (e.g. in quenched Ti-Ni alloys). A complete review of the structure of the R-phase can be found in [OTS, 2005].

The R-phase appears prior to B19' transformation under certain conditions. The transformation sequence may vary depending on the relative values of the R-phase transformation temperatures (R_S and R_f) and martensitic transformation temperatures

(M_S and M_f). It is clear that martensite can be formed from R-phase or B2. When M_S temperature is less than R_f , the transformation sequence is $B2 \rightarrow R \rightarrow B19'$. If M_S is greater than R_S , the R-phase transformation is pre-empted by the martensitic transformation. Studies about Ti49.5-Ni50.5 at% showed that a temperature below R_S , the $B2 \rightarrow R$ transformation seems to occur simultaneously with the $B2 \rightarrow B19'$ transformation, with the R-phase transforming to martensite at lower temperature, as published by [GOO, 1985] and [STAC, 1988].

The B2 to R transformation has attracted much attention since the stress-temperature-strain response associated to this transformation shows a small temperature hysteresis (1°C - 5°C) and does not vary much with cycling through the transformation range [TOD, 1986], [STAC, 1988]. The R-phase can be detected by electrical resistivity values due to the sharp increase that is produced during the B2 to R transformation (the R-phase has the highest electrical resistivity of the three phases [LIN, 1980]). Figure 2.8 shows the evolution of the electrical resistivity in front of temperature for two near equiatomic (SM 495) Ni-Ti alloys, with different heat treatment temperature [URB, 2010].

As seen in figure 2.8, on cooling, sample heat treated at 475°C shows a clear two-stage transformation $B2 \rightarrow R \rightarrow B19'$, which is identified as a sharp increase in the electrical resistivity during $B2 \rightarrow R$ transformation (R_S point), followed by a resistivity plateau. A decrease in electrical resistivity characteristic of the $R \rightarrow B19'$ transformation (M_S point) is produced after this resistivity plateau. The range of increase in electrical resistivity that characterizes the R-phase transformation was measured by [WUK, 2006]. To consider that the R-phase transformation occurs in a SMA alloy, the increase in electrical resistivity value during the $B2 \rightarrow R$ transformation should be around of 10–16 $\mu\Omega\cdot\text{cm}$, which is about 12–20% of resistivity change. Figure 2.8 also shows a sample heat-treated at 525°C with no increase in its electrical resistivity curve during the transformation path. This ER curve shows a situation that can be interpreted as the sample has a one-step transformation path during cooling ($B2 \rightarrow B19'$), with no signal of the R-phase transformation.

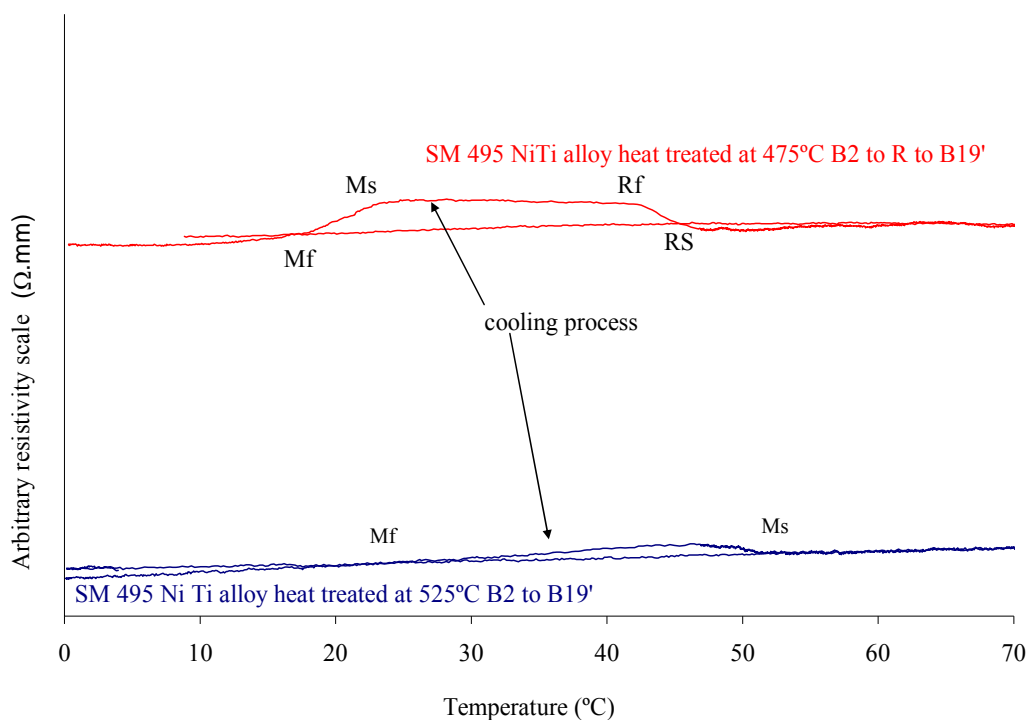


Figure 2.8 Electrical resistivity versus temperature for two annealed Ni-Ti wires. The transformation temperatures are indicated on the figure according to Lin and Kaplow [LIN, 1980].

The small lattice distortion of the R-phase transformation implies less damage to the microstructure and lower sensitive to structure modifications, hence resulting in higher reversibility and stability. The small hysteresis implies high response rate and high reversibility. R-phase transformation has excellent functional fatigue properties associated with the B2 ↔ R transformation, which is commonly ascribed to its small transformation strains (less than 1%). Fast expiration of the R-phase volume fraction upon heating was found to be the reason for the limited achievable recovery strain due to the R→B2 transformation [SIT, 2006].

In contrast, on cooling, the R→B19' and B2→B19' transformations are associated with much larger transformations strains and temperatures hysteresis (20°C-70°C). Moreover, R-phase has strong stress-temperature dependence (17Mpa/°C, [MIY, 1988], [TOB, 1994]). Ultrasonic pulse transmission measurements of elastic properties in Ni-49.5at%Ti suggest that the lowest value of modulus of elasticity corresponds to the modulus of the R-phase near the R_f temperature [SIT, 2006].

Owing to these unique characteristics, the R-phase transformation is of particular interest for many applications as sensors or actuators. Early studies on polycrystalline and single crystalline Ni-Ti alloys reported phenomena such as pseudoelasticity, shape memory, and recovery stress generation associated with the R-phase transformation. In fact, the R-phase has a contribution to the SME and SE [MIY, 1984], [MIY, 1986]c, [MIY, 1988], [TOB, 1994], [TOB, 1996] and it has a significant influence on the Two-Way Shape Memory Effect [LIU, 1990].

2.2 *How to obtain R-phase transformation in near equiatomic Ni-Ti SMA*

The basic approach to study the R-phase transformation is to recognize that we have two competing transformations: the R-phase and the martensitic transformation [OTS, 1990]. Thus, the R-phase can be developed by suppressing the martensitic transformation relative to the R-phase. Initially, [MIY, 1986]b established three ways to obtain the R-phase in near equiatomic Ni-Ti alloys:

a) **Adding a third element** [HON, 1980], [SAL, 1985]. Alloying elements not only change transformation temperatures (as explained in section 1.3), but also often change the product of the transformation or the transformation route. A typical example is that Ti-Ni undergoes a direct B2-B19' transformation; but with the addition of Fe, the Ti-Ni-Fe alloy shows a two-stage transformation B2-R-B19'. As published by [SAL, 1985] the addition of small amounts of iron suppresses the martensitic transition, permitting a detailed study of "premartensitic" effects. Using X-ray and neutron-diffraction data, they showed that two distinct phases appear.

b) **Under certain ageing conditions Ni-rich Ti-Ni alloys (typically Ni>50.6at%) exhibit complex transformation behaviour.** Ageing these alloys at proper temperatures ($T < 500^\circ\text{C}$) cause the precipitation of Ti_3Ni_4 particles in the B2 matrix. These precipitates are lens-shaped, which suppress the martensite transformation and induce the R-phase. These precipitates give a strong resistance to the formation of B19' and are associated with a large lattice deformation: these fine precipitates destabilize martensite with large transformation strain (B19'), but hardly affect the stability of martensite with small transformation strain (the R-phase has a significant smaller lattice deformation and is much less affected by the presence of particles). Therefore, the

formation of Ti_3Ni_4 by aging treatments favours the R-phase transformation prior to B19'.

Zhu et Gotthardt [ZHU, 1988] first reported an internal friction measurements demonstrating two-stage martensitic transformation on cooling in a Ti-51at%Ni alloy after ageing at 500°C. Airoidi et al. presented the first differential scanning calorimetry (DSC) evidence of multistage martensitic transformation in an aged Ti-50.6 at%Ni and suggested that this behaviour be not related to precipitates, despite the previously ageing treatment [AIR, 1989]. Later, Favier et al. presented DSC evidence of the same transformation behaviour directly induced by ageing in a Ti-50.2at%Ni and they ascribed the effect to ageing-induced precipitates, although they discovered no evidence of such precipitates in their 50.2at%Ni alloy [FAV, 1993]. Since then, a number of investigations have been reported [NIS, 1984], [MIY, 1986]b, [GYO, 1996], [SOM, 1999], [REN, 2001], [KHA, 2002] to explain this phenomena. [BAT, 1998] reported by transmission electron microscopy (TEM) in situ investigations of the transformation behaviour of a Ti-51at%Ni alloy. They observed at TEM scale two discrete steps of martensite formation from the R-phase in regions near Ti_3Ni_4 precipitates and ascribed them to “stressed” and “unstressed” regions. Based on this observation, they proposed that the influence on the martensitic transformation is believed to originate from the strain field that might occur in the surrounding matrix. During the martensitic transformation B2 lattice is distorted into martensite lattice. However, Ti_3Ni_4 precipitates do not transform; thus, they do not follow such a shape change. Lately, by TEM techniques was possible to measure these strain fields surrounding the small precipitates [TIR, 2005]. Early, theoretical calculations concerning these strain fields were performed by [GALL, 1999]. However, the scientific community has not an accepted mechanism for this phenomena, otherwise, appears a common acceptance that ageing induce two-stage transformation process and is related to the formation of Ni-rich precipitates, in particular Ti_3Ni_4 , which are formable in Ni-rich alloys.

c) Annealing at intermediate temperatures (400°C-500°C, below recrystallization temperatures) after cold work to create rearranged dislocation structures in equiatomic Ni-Ti alloys (50at%Ni). As stated first by [MIY, 1986]b and lately by Liu et al. [LIU, 1990]-[LIU, 1994], the high density of dislocations remaining from the cold work in the specimens annealed at temperatures under recrystallization

temperature ($T < 500^\circ\text{C}$ in Ni-Ti) is regarded as being responsible for the possible formation of the R-phase. These dislocations depress the martensitic transformation but promote the R-phase transformation. High density of dislocations acts as a resistance to lattice distortion (martensite transformation) similar to precipitates. The resistance is much larger for transformation involving large lattice distortion like B19', while the effect becomes very small for transformation involving small lattice distortion like R-phase.

With the increase in cold working rate, there is an increase in R-phase and in the temperature interval range between M_s and R_f [MIY, 1986]b, [JIN, 1992], [FIL, 1995]. As annealing temperature increases, the interval becomes narrow and the R-phase tends to disappear. R-phase does not occur in samples annealed at higher temperatures ($T \geq 500^\circ\text{C}$) because as higher is the temperature, higher is the decrease in the number of dislocations in the matrix. In this case, only the $B2 \rightarrow B19'$ occurs (figure 2.8, sample heat treated at 525°C). In other words, the defects introduced by cold working depress the martensitic transformation but promote the R-phase. During annealing these defects continuously die out, and the residual stress decreases simultaneously. Therefore, the effects of cold work on transformation temperatures decrease with increasing annealing time and temperature. This leads to the feature that R-phase decreases while M temperature increases with the increasing annealing time and temperature. Studies performed by X-ray diffraction detected the R-phase in annealed 49at%Ni-51at%Ti alloys (400°C - 500°C , [PAU, 2004]). In the same way Uchil et al. found that the XRD analysis is more sensitive in detecting smaller volume fractions of the R-phase in specimens heat treated from 400 to 560°C [UCH, 2007].

In addition to these three forms proposed by Miyazaki et al. the R-phase can be developed in a Ni-Ti alloy by thermal cycling at zero stress [MIY, 1986]b.

1. R-phase can be developed in near equiatomic alloys by thermal cycling at zero stress in the cooling part of the transformation cycle, but not in the heating part (transformation to B2) of the transformation cycle (figure 2.8). [MIY, 1986]b found that the martensitic transformation is hidden and delayed, favouring the development of the R-phase during the thermal cycling process. At the same time, they found that thermal cycling at zero stress does not influence samples that already contain

a high density of dislocations, as Ni-Ti alloys annealed at temperatures under recrystallization ($T \leq 500^\circ\text{C}$) or in Ni-rich specimens. This fact is due to that once the dislocations are stabilized by annealing, the effect of the thermal cycling is also suppressed. It can be said that the presence of high-density dislocations in samples annealing at temperatures under recrystallization stopped the introduction of new dislocations by thermal cycling.

In posterior studies, Matsumoto et al. investigated the transformation behaviour of an equiatomic Ni-Ti alloy by electrical resistivity and by differential scanning calorimeter [MAT, 1993]. They found that the temperature region of transformation depends on the number of thermal cycles at zero stress and the intermediate phase appears progressively during cooling with increasing thermal cycles, resulting in a two-stage transformation, while the reverse transformation during heating remains a one-stage transformation.

[LIU, 1994]b interpreted, in terms of changes in the elastic energy, the formation of the R-phase as an intermediate phase during cooling, but not during heating: this is a direct consequence of the irreversible energy dissipated during martensitic transformation.

Furthermore, Uchil et al. [UCH, 2002] studied the required number of thermal cycles at zero stress to stabilize the R-phase in the alloy and its relationship with the stability of the M_s temperature using electrical resistivity measurements. The near equiatomic 40% cold worked Ni-Ti wire was heat treated in the temperature regions of $340\text{--}620^\circ\text{C}$. Their results showed that, in the samples having only $M \rightarrow A$ transformations after heat treatment, successive thermal cycles promote and result in the stabilization of intermediate R-phase. During the initial thermal cycles, M_s was found to decrease facilitating the development of intermediate R-phase as indicated by the emergence of resistivity peak in the cooling part of the transformation profile. Once the R-phase was completely developed, the transformation parameters such as M_s , M_f and peak resistivity of the transformation profile remained unaffected during thermal cycling. Uchil et al. proposed a critical number of thermal cycles for the complete development of the R-phase and that this critical number is in function of the heat treatment temperature.

Lately, Matsumoto et al. found that for equiatomic Ni-Ti the anomalous behaviour such as enhancement of a resistivity-peak, the increase in the electrical resistivity of the low-temperature phase and the nonlinear relation between the resistivity and the temperature in the high-temperature phase were attributable to the appearance of an intermediate phase (R-phase) [MAT, 2004].

All the above studies were done for equiatomic Ni-Ti alloys or Ni-rich Ni-Ti alloys. However, Pelosin et al. [PEL, 1998] published that Ti-rich Ni-Ti alloys showed the same behaviour than equiatomic Ni-Ti alloys: the martensitic transformation is delayed after repeated thermal cycling at zero stress, leading to show the evidence of the R-phase. In posterior studies, Matsumoto et al. found in Ti-rich (52% at) that the transformation has a tendency to change from one stage to two stages with increasing the number of thermal cycles [MAT, 2003]. The defects generated by the deformation contribute to the formation of the intermediate phase.

Consequently, the chemical composition of the Ni-Ti alloy and the initial dislocation structure obtained after heat treatment determine whether the alloy is affected by the thermal cycling at zero stress. The process of R-phase developing is appreciably dependent on the composition of the alloy, but the number of defects introduced by thermal cycling also contributes to increase the stability of the R-phase. As a final point, thermal cycling is effective in introducing the R-phase transformation prior to the martensitic transformation, and this is ascribed to the introduction of random dislocations in the matrix.

Furthermore, the R-phase is found in:

2. **Ti-rich Ti-Ni alloy thin films fabricated by sputtering formed Ti_2Ni precipitates** [GYO, 1996], [KAJ, 1996], [ISH, 2001], [NAM, 2002], [NAM, 2007]. Similar to Ti_3Ni_4 , the Ti_2Ni particles suppress the B19' martensite and induce the R-phase transformation (strengthening the parent phase), and thus the $B2 \rightarrow R \rightarrow B19'$ transformation occurs in Ti-rich thin alloys films.

3. There are different opinions about if **thermal cycling under constant induces the R-phase in Ni-Ti**. Stachowiak et al. have shown in near equiatomic Ni-Ti alloy (50.2

%at. Ni) that R-phase vanishes on thermal cycling under constant load using strain recovery measurements [STAC, 1988]. The R-phase seems to disappear because the overlapping of the $B2 \rightarrow R$ and $B2 \rightarrow B19'$ transformations, increasing the M_s temperature through cycling. The dislocation structure developed during cycling assists the nucleation of the preferred stressed variants of martensite during cooling, thus increasing the M_s temperature and decreasing the hysteresis. In opposition, Li et al. found by electrical resistivity and X-ray measurements (51.3%atNi) that the R-phase is induced through successive thermal cycling under stress, proposing that the internal stresses formed by the dislocations introduced by thermal cycling induce the R-phase [LI, 1991]. Pozzi et al. found in equiatomic Ni-Ti wires that the R-phase is suppressed whenever a value of stress high enough is applied to the alloy [POZ, 1999]. Wu et al. studied by ER that the R-phase seems to disappear due to the high stress applied to annealed Ni-rich Ni-Ti alloys, but their results are really confuse [WUX, 2000]. Uchil et al. states by ER experiments that thermal cycling under a constant stress promotes R-phase transformation in the direct and reverse transformations in heat-treated samples, independent of the initial transformation path of the alloy [UCH, 2002]b. The reason for this is ascribed to the dislocations that may pin down the motion of the martensite plates depending on their density and interaction. Pinning down the motion of the martensite plates paves the way for the formation of the R-phase. Recently, Novak et al. measured the evolution of the electrical resistivity during thermal cycles under stress and by micromechanical model simulations, they considering that two-stage transformation was formed in the alloy after thermal cycling under stress [NOV, 2008]. However, they found that under high values of stresses, the Ni-Ti alloy did not show any signal of the R-phase transformation.

Consequently, the discussion if thermal cycling under stress promotes or not the R-phase is still open. One of the objectives of this thesis is to clarify this fact.

2.3 Influence of the R-phase on the Ni-Ti Functional Properties

As seen, the R-phase transformation can commonly appear as an intermediate phase in most of the commercially available cold worked/annealed Ni-Ti wires [MIL, 2001]. Although the R-phase related to deformation processes seems to affect the overall thermomechanical behaviour of the SMAs, the R-phase often seems to be neglected in Ni-Ti mechanical studies [HUAN, 2001]. In fact, the R-phase processes are the least explored among all deformation/transformation processes in Ni-Ti because their activity is very difficult to detect just from macroscopic stress-strain temperature curves due to the small crystallographic strain associated with the R-phase [SIT, 2006]. Therefore, the influence of the R-phase in the functional properties of near equiatomic alloys, that is, in the shape memory effect, the pseudoelasticity, and the Two-Way Shape Memory Effect are still unclear.

2.3.1 Influence on shape memory effect and pseudoelasticity

Miyazaki et al. developed an extensive experimental study in aged Ti-Ni alloys [MIY, 1981]. They found that Ni-rich Ti-Ni alloy might reach 100% pseudoelasticity after ageing in the temperature range of 300°C-500°C, but no pseudoelasticity occurred after ageing above 600°C. They suggested that the appearance of perfect pseudoelasticity was due to fine Ti_3Ni_4 precipitates that exist after ageing the alloy between 300°C and 500°C. Lately, in 1986, Miyazaki et al. found that aged Ni-Ti samples after cold work present an increase in the critical stress for moving the interface between the martensite variants in temperatures below and over R_s [MIY, 1986]c. The reason was attributable to the presence of dislocations. The critical stress in the cold work specimens was more than three times higher than that for a specimen with the precipitate structure (Ni-rich alloy). They concluded that dislocations could prevent more strongly the interface movements in the martensite and R-phase than precipitates do.

In 1991, Li et al. published that the effects of ageing and thermal cycling on the shape memory effect and on the pseudoelasticity are attributable to the increase in R-phase [LI, 1991]. Li et al. proposed that the increase in R-phase is caused by the internal tensile stress introduced by coherent Ti_3Ni_4 precipitates in the case of ageing and the

dislocations in the case of thermal cycling at zero stress. Therefore, according to the results of the previous studies by the authors mentioned above, the shape memory effect and the pseudoelasticity may be improved if the R-phase is present in the alloy.

In 1996, Tobushi et al. studied in detail the thermomechanical properties of the SME and the pseudoelasticity due to the martensitic and R-phase transformations by various loading-unloading and heating-cooling tests in Ti-55.33wt%Ni SMA wire [TOB, 1996]. They found that the thermomechanical properties due to the R-phase transformation vary little with cyclic deformation, and thus, in applications that demand a sample with excellent cyclic properties and fast response, the R-phase transformation should be used. The temperature interval needed to cause the transformation strain associated with the R-phase is small and stable; therefore, the response of the sample to heating/cooling cycles is fast.

2.3.2 Influence on the Two-Way Shape Memory Effect

Usually, studies concerning the TWSME of Ni-Ti SMA have focused on the efficiency of the training method applied ([LIU, 1990], [LIU, 1999], [KAF, 1998], [HUA, 2000] and [LAH, 2002]), on the influence on the type of training and the training parameters in the transition temperatures ([LIU, 1990], [PRA, 1997], [LAH, 2002] and [WANZ, 2003]), on the stability of the TWSME achieved ([HEB, 1995], [SCHE, 1999] and [SCHE, 2002]), and, on the micromechanical origin of the TWSME [MAN, 1993]. Moreover, the training routes reported in these studies are mainly associated with B2→B19' transformation path. However, little work has been done on training methods that consider R-phase transformation to be an essential part of the training process. In fact, different opinions have been published concerning the influence of the R-phase on the TWSME, [LIN, 1980], [TOD, 1986], [LIU, 1990], [POZ, 1999] and [UCH, 2002]b.

The TWSME is extremely dependent on the transformation sequence. The dislocations introduced during the training procedure are given as the main reason why an intermediate transformation between austenite and martensite is a negative factor in obtaining a substantial two-way memory strain (ϵ_{tw}) ([TOD, 1986], [LIU, 1988], [STAC, 1988], [LIU, 1999], [LAH, 2004]). The ϵ_{tw} is developed in relation to the

establishment of dislocated structures and associated local stress fields in the SMA's microstructure during training. These both favour the formation of the preferred orientation of martensite during cooling, which is transformed into a net shape change of the SMA. Because the stress fields are in function of the transformation strain, the transformation strain is reduced when there are two separate transformations, and this could reduce the development of the ϵ_{tw} . Authors as [TOD, 1986], [LIU, 1998] and [STAC, 1988] stated that the formation of R-phase diminishes the extent of obtained reversible strain as well as the stability of the TWSME. Wang et al. investigated the effect of the heat treatment conditions on training procedures and found that, after training by the same means, a sample heat treated at 550°C showed a Two-Way Shape Memory Effect that was three times as strong as for sample heat treated at 400°C, which showed two stage transformation on cooling [WANZ, 2003]b. The results of their study give support to the conclusion made by [LIU, 1990] that a single stage transformation between martensite and austenite is essential for producing a significant TWSME.

However, other authors have found that the formation of the R-phase before B19' transformation helps to increase the stability of the TWSME ([CHI, 1999], [SAT, 1998], [FIL, 2001], [CHG, 2001], [GYO, 2001], [WANZ, 2002] and [WAD, 2005]). Moreover, although the recoverable strain associated with the B2→R transformation is small (less than 1%) in comparison with the B2→B19' transformation ([MIY, 1984], [STAC, 1988]), other studies used the two-way memory strain associated with the R-phase transformation to develop micro actuators because the transformation temperature hysteresis of the Ni-Ti R-phase is extremely small and stable ([SAT, 1998], [FIL, 2001], [UCH, 2002]c and [TOM, 2006]).

As seen, further studies are needed to clarify how the R-phase contributes to the TWSME. One of the objectives of this thesis is to investigate the role of the R-phase developed by thermal cycling at zero stress on the two-way shape memory effect.

3 The Two-Way Shape Memory Effect

3.1 Particular Characteristics of the TWSME

In the shape memory effect, only the shape of the parent phase is memorized; however, the martensitic shape can be remembered when the alloy is under certain thermomechanical conditions. The SMA alloy can learn to remember both shapes after a training process. This is known as the Two-Way Shape Memory Effect (TWSME). Training is a cyclic thermomechanical treatment creating a microstructure and stress fields, which enforce austenite to transform to exactly those martensite variants (and through this to the same outer shape) that were introduced by previous deformation in martensite state. This effect was first called “the reversible shape memory effect” [NAG, 1974], [SAB, 1974], but Tas et al. proposed first the term “two way memory effect” (TWME) to designate the spontaneous reversible shape change during cooling and heating, which was observed after thermomechanical procedures, and afterwards, this is the term used [TAS, 1972].

Different magnitudes of TWSME could be seen according to the training method used. The result of the TWSME can be seen as a linear shape change in each SMA specimen during thermal cycling at zero stress after training. Then, after training, the two-way memory strain (ϵ_{tw}) is measured and is obtained from the difference between the strain of the sample in the martensite state (ϵ_m) and the strain of the sample in the austenite state (ϵ_a) (see Figure 2.9).

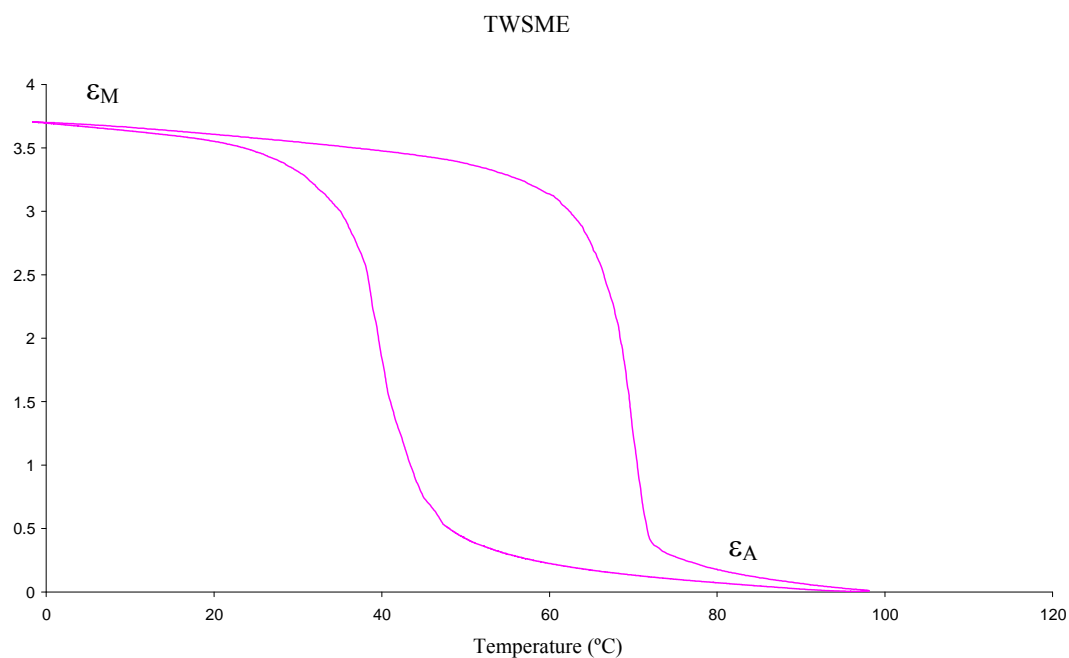


Figure 2.9 Two-way memory strain response in annealed Ni-Ti wire (500 °C) after constant stress training [URB, 2010]b .

The first report of TWSME was due to Wang and Buelher [WANF, 1972] for a Ti-Ni alloy, but the condition to realize the effect was too complex and it was hard to know what was essential, as criticized by Nagasawa et al. [NAG, 1974]. This author reported that two-way shape memory effect is obtained when specimens are severely deformed below M_S temperature, and they observed the effect for Ti-Ni, Cu-Zn, and Ni-Al alloys. [SAB, 1974] also found the same effect by high deformation in Cu-Zn-Ga alloy in a persistent manner. Since that time, many papers on the TWME have been published.

Ni-Ti SMA wires have two important advantages in front of Cu-Zn-Al and Cu-Al-Ni wires when all are trained under the same thermomechanical conditions. These advantages are that, firstly, the TWSME is higher in Ni-Ti systems: 4.5% in superelastic Ni-Ti alloys [LAH, 2004] in front of near 2.5% for Cu-Zn-Al alloys [REY, 1986] and near of 2.5% for Cu-Al-Ni alloys [KNE, 2008]. This fact is because of the easier occurrence of the martensite reorientation process in Ni-Ti alloys than in the Cu based alloys. The martensite reorientation requires considerable higher stresses for Cu-based alloys when is compared with Ni-Ti alloys [SHCE, 2002]. Secondly, the capacity of the

Ni-Ti alloys to work against a constant stress is also higher for Ni-Ti alloys than Cu-Zn-Al wires [BIG, 1996]. However, the stability is weaker in Ni-Ti than Cu based alloys [SHCE, 2002], [KNE, 2008]. Their degradation due to cyclic application is related to instabilities in the high and low temperature transformation.

In the following, the TWSME in near equiatomic Ti-Ni alloys wires is discussed in more detail.

3.1.1 Training procedures for Ni-Ti alloys

It is well known that the memory of both, a hot shape and a cold shape, is not a natural feature of the alloy, but rather it is a learned or trained behaviour. [PER, 1984] investigated in Cu-Zn-Al the relation between the cyclic training routine and the ability of the sample to exhibit the TWSME, giving the first classification and clear explanation of the training routes reported since that time. A recognized classification was made by Guilemany et al. who differentiated the so-called “Passive training”, where the martensite is formed via SIM from the “Active training”, where the martensite is thermally formed, without the application of stress [GUIL, 1987]. A valuable and modern reviews of all methods of training are those performed by [ZHA, 2006] and [LUO, 2007]. By now, there are reported more than 20 different training procedures, which have as a common feature that an external applied stress should be used, such as tension, compression, torsion or bending. However, there are some training methods without applied load, but inducing internal stress, such as quenching, laser or iron irradiation, sputter-deposited thin film or external magnetic field. Please, consult [ZHA, 2006] for more information and references for these training methods.

Therefore, several training methods involving stress have been proposed. They received different classifications and names depending on the author. In general, the main training methods can be classified in three types: one-time martensite deformation, thermomechanical cycling treatment and introduction of precipitations. These training procedures are summarized in the following table 2.2.

The **one time martensite deformation method** or **martensite reorientation training** developed by martensite reorientation [LIU, 1999], is accomplished simply, by deforming the heat-treated alloy sample in the martensite phase. Liu et al., who found

that the magnitude of the two-way memory strain induced by simple tensile deformation of the martensite is comparable to the two-way memory effect developed through conventional training procedures, developed this method. Equiatomic Ni-Ti deformation to the end of the stress plateau (6.2%) causes a two-way memory strain of 1.44% with a permanent strain of 0.7% (measured by TMA, thermomechanical analyzer). However, this two-way memory strain is small compared with others training methods. If the level of the alloy tensile deformation is amplified beyond of the value of the maximum recoverable strain of the alloy (for the alloy studied by Liu et al. this level was 13.3%), a two-way memory effect of 4.1% can be reached, which was comparable to the best two-way memory effects achieved by other training methods until that dates by the same author [LIU, 1990]. Far than a pre-strain of 15%, the two way memory strain decreases. However, the large amount of plastic strain introduced by such high level of deformation will seriously deteriorate the memory of the hot shape. These findings suggest that the choice of deformation strain in martensite dictates a trade-off between the two-way recovery strain and the loss of the hot shape, when developing TWSME by the single-step deformation of martensite. As a result, optimal training conditions cannot be expected with this training method.

The first one TWSME effect obtained by **introduction of precipitates** in Ni-Ti was the one reported by Nishida and Honma [NIS, 1984] as “all-round shape memory effect” (ARME), and then followed by [NIS, 1984]b, [FUK, 1997], [HUA, 2000], [HUA, 2001], [CHG, 2001], [ZEL, 2003] and [SHA, 2009]. The ARME or TWSME is associated with the internal stress fields between coherent Ti_3Ni_4 particles and Ti-Ni matrix. The particular stress orientation accounts for the promotion of the variants of R-phase (and B19' later) with only certain, preferential orientation during cooling of the specimen, which result in TWSME. Therefore, the Two-Way Shape Memory Effect using Ti_3Ni_4 precipitates was very interesting, especially from the scientific point of view, because the mechanism of the TWSME was rather clear. However, the available two-way memory strain was not so large (1%), and the increase in Ni to obtain the precipitates resulted in the lowering on M_s temperature. These results are not advantageous for industrial applications. Thus researchers, especially in the field of applications, are interested in create two-way by deformation and/or cycling technique

of Ni-Ti equiatomic in order to obtain optimum conditions for industrial application, as convenient temperatures for activation the TWSME.

Type	Training procedure	
One time martensite deformation or martensite reorientation	i. ii. iii.	Cool the specimen below M_f Deform it in martensite state Unload it completely
Introduction of precipitates	i.	Heat treatment procedure with the specimen fixed in another shape in Ni-rich alloys
Thermomechanical cycling treatment		
a) Shape memory cycling or isothermal tensile deformation under M_f training	i. ii. iii. iv. v.	Cool the specimen below M_f Load it in martensite state to a desired cold shape Unload it completely Heat it to a temperature above A_f Repeat the above steps a number of times
b) Pseudoelastic cycling	i. ii. iii. iv.	Heat the specimen above A_f and below M_d where superelastic behaviour is expected Load it in austenitic state to a desired shape Unload it completely Repeat steps ii and iii a number of times
c) Combined cycling: pre-strain and thermal cycling under stress	i. ii. iii. iv. v. vi. vii viii	Cool the specimen below M_f Deform it in martensite state Unload it completely Heat it to a temperature above A_f Cool the specimen below M_f Load it in martensite state to a desired cold shape Heat and cool it in the constrained condition through M_f and A_f Repeat step vii a number of times
d) Thermal cycling under constant stress or constrained cycling	i. ii. iii. iv.	Cool the specimen below M_f Load it in martensite state to a desired cold shape Heat and cool it in the constrained condition through M_f and A_f Repeat step iii a number of times

Table 2.2 Main TWSME training methods for Ni-Ti SMA.

Thermomechanical cycling treatment is based on the repetition of a cycle that must include the transformation from austenite to preferentially oriented martensite or from deformed martensite to austenite. The **shape memory cycling or isothermal**

tensile deformation under M_f training (SME training) involves repeated cycles of deformation of the alloy by a tensile deformation in martensite state and recovery of the deformation by a reverse transformation by heating under no stress at $T > A_f$ ([SCO, 1977], [PER, 1984], [TOB, 1990] and [FAL, 2007]). The effects of this type of training on the stress-strain response can be summarized in figure 2.10 [URB, 2010]b. Annealed 49.3%at Ni-Ti wire was used to perform this SME training. The figure shows the profiles for the first training cycle, several intermediate training cycles, and the last training cycle. The following observation can be made. When the number of training cycles increases, a hardening of the material is observed, resulting in a large stress level, together with a decrease in the stress for the onset of the detwinning. The effect of the training is a high slope of the reorientation plateau after several training cycles. This hardening process is due to the formation of a dislocation structure that benefits the two-way shape memory behaviour of the material [LIU, 1999]. Recently published values of the two-way memory strain obtained by this method are near of 3% [FAL, 2008] for Ni-51at%Ti sheets of 1.15 mm of thick.

Pseudoelastic cycling is simply a mechanical cycling process in pseudoelasticity through the stress-induced martensitic transformation and the reverse transformation that proceeds against the external stress ([PER, 1984] and [CON, 1990]). This method obtains values of two-way memory strain of 1.36% in Cu-Zn-Al alloys and 0.8% in Ni-Ti alloys. [LUO, 2007] published that the reason for this poor results can be that loading and unloading occur in full austenite. The introduction of dislocations is probably difficult due to the high stability of the austenite phase, thus the amount of dislocation arrangements produced (those that give rise to the formation of the cold shape) is too small to remind the cold shape of the sample. The training also causes a decrease in the critical stress for the forward transformation and it has a little influence on the critical stress for the reverse transformation, decreasing the stress hysteresis [MIY, 1986]. The reversible pseudoelastic strain is also decreased whilst a residual deformation is being accumulated during training.

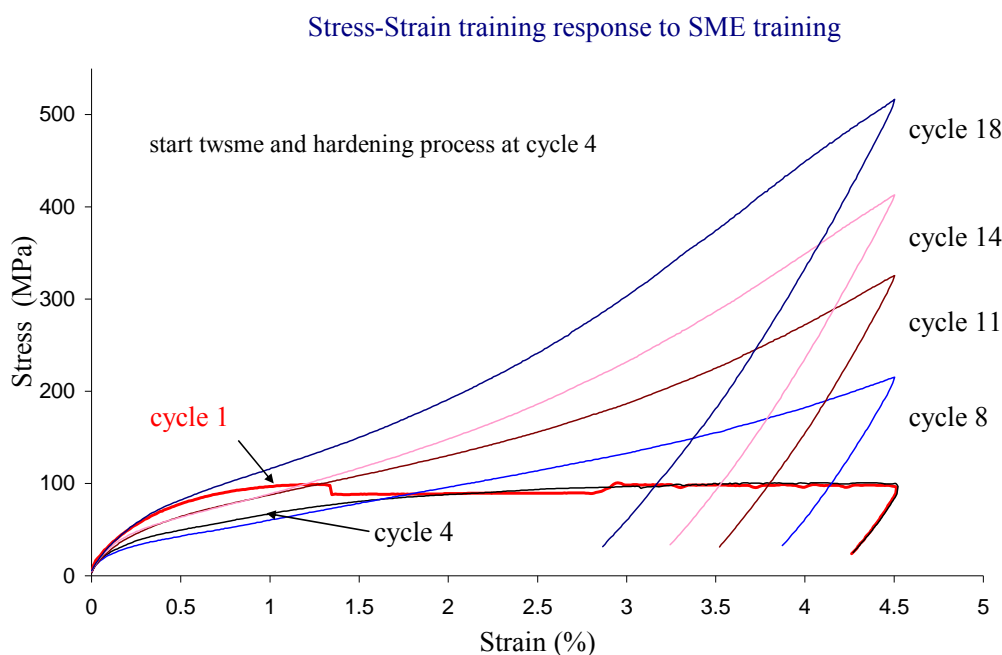


Figure 2.10 Stress-strain response during SME training in annealed Ni-Ti wire [URB, 2010]b.

Similar to the training method of martensite reorientation, the **Combined cycling: pre-strain and thermal cycling under constant stress** was studied by Wada et al. [WAD, 2005], [WAD, 2005]b, who first applied this training on an annealed Ni-Ti alloy. Two kinds of deformation procedures were performed: test (1), fixed pre-strain with variable constrained stress; and test (2), fixed constrained stress with variable pre-strain. They obtained that the maximum two-way memory effect (4.3%) is generated at about 13% pre-strain, owing to the optimum amount of dislocations and preferentially oriented martensite produced. They found that the development of maximum TWSME was independent of the order of deformation procedures and it was predominantly determined by the magnitude of martensitic strain generated during either pre-deformation or thermal cycling. However, this training procedure introduces large permanent strains in the alloy in martensitic state. In fact, the growth of preferentially martensite variants favouring the TWSME is disrupted by the plastic accommodation between the stress assisted martensite variants generated by thermal cycling under stress and the retained martensite variants generated by the tensile pre-strain [WADA, 2008].

This plastic accommodation process becomes the principal factor for lowering the magnitude of the two-way memory strain.

Thermal cycling under constant stress or constrained cycling involves subjecting the alloy to repeat thermal transformation cycles under the influence of an external bias stress ([TOD, 1986], [LIU, 1988], [LIU, 1990], [STA, 1992], [BIG, 1996], [SCHE, 1998], [TUR, 2000] and [MIL, 2001]). During thermal cycling against applied load training, stress fields are generated that assist the martensite transformation. Associated with the development of the two-way memory effect an increase in transformation temperatures and changes in the transformation sequences are observed. This method has been proved to be as the most effective in introducing two-way memory effect ([LIU, 1990], [DER, 1995], [TUR, 2000] [SCHE, 2002] and [LAH, 2004]). Several different strains may be distinguished during a thermomechanical training cycles, as illustrate in Figure 2.11, and defined first by Stalmans et al. [STA, 1992], and lately, by [SHE, 2002] in a clear way. During cooling from the high temperature, martensite is stress-induced upon reaching the M_S temperature. As the forward transformation occurs under an external load, the present stress field causes a preferred nucleation and growth of those variants that have the highest compatibility with the stress field. Consequently, a number of martensite variants are oriented and the growth of this oriented martensite results in a macroscopic strain in the direction of applied stress, called SAMS (stress assisted martensitic strain). Most part of this SAMS is recovered when the alloy transforms back to the austenite, forced to restore the associate original shape change. This is the purpose of the training, to teach the microstructure to keep building these variants preferentially during cooling, even without external load. However, the original shape in the austenite state is not restored perfectly. In other words, there is an imperfect one-way shape memory recovery. As suggested by [STA, 1992] this imperfect recovery can be due as a result from a true plastic deformation and/or from some local martensite stabilization. While the true plastic deformation is irrecoverable, the second contribution can be recoverable by an overheating. In any case, both effects are undesirable effects because of the training.

Finally, the stress-assisted transformation effect SATE is the shape change from the austenite shape to the martensitic shape under the effect of the training constant stress. Lately, SATE was defined as SATWME (stress-assisted two-way memory effect) in

which martensitic transformation would be assisted by an external stress [BIG, 1996]. The evolution of these strains during training can be observed in figure 2.12, where an annealed 49.3%at Ni-Ti wire was subjected to this type of training during 8 full transformation cycles [URB, 2010]b.

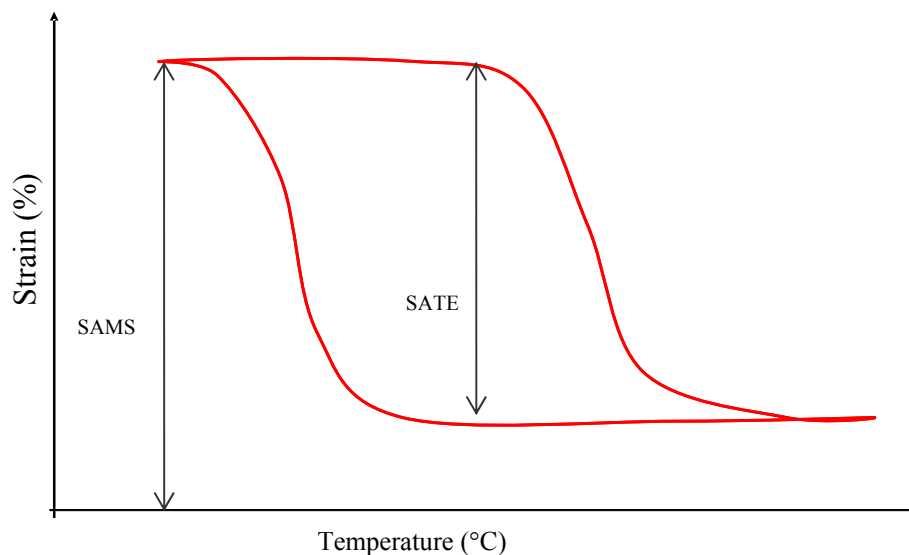


Figure 2.11 Different strains involved in a training cycle under constant stress.

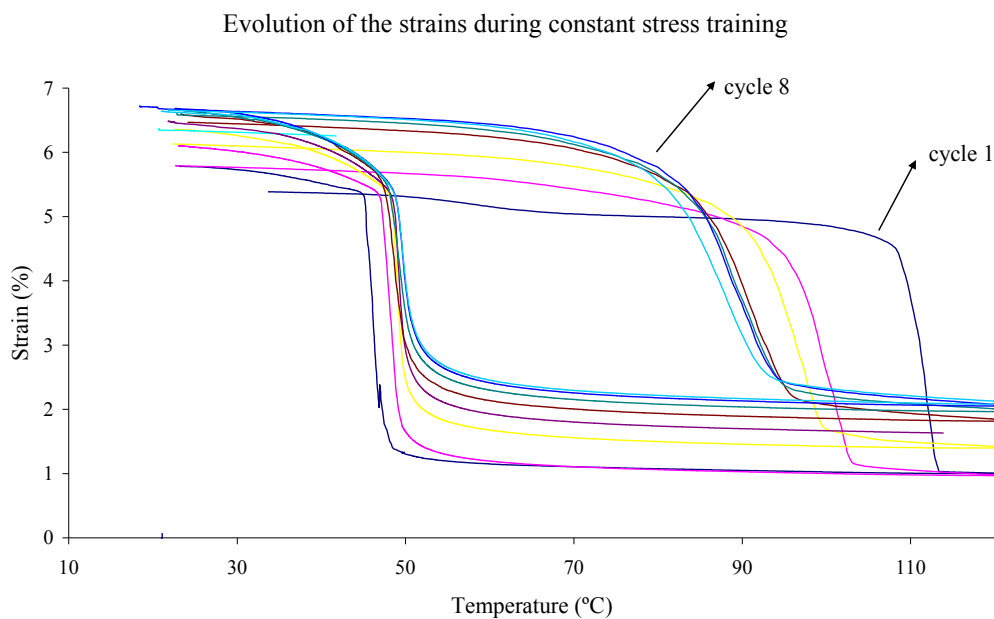


Figure 2.12 Evolution of the different strains involved in a training cycle under constant stress as a function of number of training cycles.

According to the above described, this thesis is focused on **isothermal tensile deformation under M_f training** and **thermal cycling under constant stress training** methods to obtain substantial two-way shape memory effect.

3.1.2 Optimum thermomechanical training conditions for near equiatomic Ni-Ti alloys

The two-way training parameters were widely studied by Perkins et al. and Stalmans et al. in [PER, 1984] and [STA, 1992]. The training parameters help to control the training procedure in order to obtain an optimum two-way memory strain. Although these parameters were defined for Cu-Zn-Al, the scientific community extended them to any type of SMA alloys. These parameters are:

- Heat treatment condition of the wire prior to training.
- Training stress (σ_{tr}) or training strain (ε_{tr}) to apply in case of thermal cycling under constant stress training or isothermal tensile deformation training, respectively.
- SATWME or recovery strain, ε_r , the shape change from the austenite shape to the martensitic shape under the effect of the training stress.
- ε_a , residual deformation in austenitic state.
- Number of training cycles (n).

Thermomechanical factors influencing the development of two-way shape memory under different tensile stresses on a thermal cycling were widely studied by Liu et al. [LIU, 1990]. They used near equiatomic Ni-Ti wire (50.2at%Ni), annealed at various temperatures between 190°C and 930°C and air cooled to room temperature. The scientific community accepts these results since then. The factors affecting the development of the TWSME are listed next.

- Liu et al. measured the effect of annealing temperature on the two-way memory strain, reporting that a single-stage martensitic transformation was a prerequisite for obtaining a significant two-way memory strain in Ni-Ti. One reason for

this is that parent phase is hardened when R-phase is introduced, and thus, the introduction of dislocations becomes more difficult [OTS, 2005].

- The near proportionality that exists between the two-way memory strain obtained and the SATWME developed during training suggest that the dislocation structure responsible for the growth of the SATWME with cycling is also responsible for the development of the two-way memory strain. Lately, [WADA, 2008] suggested that both strains are directly correlated with the strain in martensitic state: an increase in martensitic strain through constrained cooling increases SATWME and TWMS. However, experimental results show that a martensitic strain over 20% reduces the SATWME and the TWSME.

- A decrease in two-way memory strain with increasing training stress values and with increasing number of training cycles has been observed. Consequently, there is an optimum number of training cycles for a value of constant stress.

- Maximum two-way memory strain is associated with values of training stress and number of training cycles, which are high enough to induce a full one-way transformation strain. The values of two-way strain decrease with increasing training stress for stresses greater than the stress required to induce full one-way strain in the first training cycle.

- The optimum training procedure is that yields the highest values of two-way memory strain in the minimum cumulative of residual deformation in austenite state. This may produce partial or complete loss of transformability and therefore memory.

An important goal to achieve by this thesis is the improvement of the training parameters and the consequent improvement of the TWSME through a thermal process that does not imply a severe residual deformation of the sample prior to training.

3.2 *Mechanism of the TWSME*

The mechanism that develops TWSME was initially perceived as follows: the plastic deformation in the martensitic state introduces dislocations; upon heating, detwinned

martensite variants disappear to form austenite in the matrix, but the presence of dislocations makes the shape recovery incomplete [PER, 1974]. The remaining dislocations create a specific internal stress field, which directs the nucleation and growth of martensite variants into a preferential orientation [RIO, 1987], [MAN, 1993]. The formation of these preferred variants on cooling bring about the spontaneous shape change of the alloy, causing the TWSME ([SCHR, 1977], [MAN, 1993]). It was proposed by Contardo et al. that those internal stress fields favour the nucleation and the beginning of growth of some preferential variants, since the residual stresses are relaxed by the accompanying large shape change [CON, 1990]. Assuming that these dislocations have created internal stress fields, then, during cooling, this stress field should prevent the self-accommodation of martensite variants, producing a macroscopic deformation. That is, during further cooling those preferential variants grow without any assistance, thus causing the TWSME. Based on the assumption that those dislocations are linked with plasticity, a plastic deformation was still considered as being essential for the TWSME ([PER, 1984], [RIO, 1987]).

On the other hand, the presence of locally stabilized martensite retained above the austenite finish temperature A_f , was proposed to be another development mechanism of the TWSME. The increased volume fraction of retained martensite due to the repeated number of cycles was claimed to be favourable to the TWSME ([PER, 1984], [DUE, 1990]).

Later on, Stalmans et al. in [STA, 1991], [STA, 1992] and [STA, 1992]b established that the reproducibility of the TWSME is the macroscopic consequence of the microscopic reproducibility of the transformation path: in subsequent cycles, the same martensite variants are formed in the same sequence during cooling. In the same way, they proposed that the stability of the TWSME was the consequence of a stable transformation path, which is generated by training. The martensite variants corresponding with this training path even grow when opposing stresses are applied. Since the transformation is thermoelastic, the growth of those stable variants must be energetically favoured to other variants. These variants are growing in the dislocation structures having the lowest energy. This conclusion was in contrast with the two before explained, which were both based on spontaneous growth [DUE, 1990]. Therefore, [STA, 1992]b proposed a new mechanism for the TWSME: dislocations are generated

by transformation cycling (training) and consequently, the martensite transformation path is stabilized. At the same time, they invalidate the two before explained mechanisms with the following experimental observations:

- Stalmans et al. [STA, 1992]b found that an increasing amount of stabilized martensite is accumulating during training cycle. However, those martensite remnants that are retained above the original A_f could be removed by overheating without a significant magnitude of the TWSME is erased. This observation made the second mechanism improbable. In addition, Miller and Lagoudas demonstrated that increasing the fraction of retained martensite results in higher plastic strains with a lower two-way memory strain [MIL, 2000].
- The residual deformation was an undesirable side effect of overtraining and not a pre-requisite to obtain TWSME.

The results of Stalmans et al. [STA, 1992]b, showed that the TWSME is directly determined by the transformation strain, which is repeatedly induced in the training procedure and by the number of training cycles. This transformation stress is caused by the stress applied during the transformation from austenite to martensite (SATE, figure 2.11) in which martensitic transformation would be assisted by the external stress.

Posterior studies by Manach et al. confirmed the presence of internal stress fields after training, analyzing the experimental results obtained during Ni-Ti superelastic training cycles [MAN, 1993]. Therefore, Manach et al. suggested that the dislocation arrays are not only a source of internal stresses, but also they create an important friction for the variants that have been not activated during the training. It becomes thus thermodynamically more difficult to obtain the self-accommodation of the martensite variants. To conclude given by Manach et al., the thermodynamic anisotropy suggested by Stalmans et al. lies in the development during training of friction barriers which are not the same for all martensite variants. In order to form them during cooling, the disadvantaged variants have to overcome this friction energy. This effect contributes significantly to the TWSME.

[MOR, 2003] studied a number of Ni-Ti alloy wires which were thermally cycled against constant applied stress, analyzing the changes in transformation temperatures and heats of transformation. They concluded that first, during thermal cycling against

applied load anisotropic stress fields are generated that assist the martensite transformation. Concurrent with the internal stress assistance, there is a rise in the M_S temperature. Second, the stress field created within the alloy follows the Clausius-Clayperon relationship resulting in a $d\sigma/dM_S$ stress rate gradient that is the same that had the alloy before cycling. Third, concurrent with the stress fields that favour the martensite transformation, a back stress generated during cycling results in an increase in the elastic energy stored during the martensite transformation. This back stress opposes the martensite transformation but favours the austenite transformation. Finally, depending upon the number of training cycles and the level of applied stress either the changing level of internal stress assisting the martensite transformation or the changing level of internal elastic energy opposing the martensite transformation will dominate.

Recently, [WAD, 2008]b found the same experimental results than [MOR, 2003]: the increase and decrease in M_S can be associated with the formation of internal forward and back stresses, respectively. Their results indicate that the high magnitude of the TWSME results from a dominant internal forward stress. The dominance of internal back stress reduces the martensite strain and results in a TWSME decrease. In addition, [WAD, 2008]b studied the influence of the retention of martensite in the generation and development of SATWME and two-way memory strain. Based on their experimental observations they concluded that the generation of the maximum TWSME and SATWME does not result from the retention of the martensite, but it is rather predominantly determined by the favourable dislocations and internal stress fields created during training.

To conclude, it is possible to accept that the mechanism that develops TWSME by thermomechanical cycling lies in developing reminders of the desired cold shape in the austenite phase (know as dislocation arrangement) by repeating the transformation cycle between martensite and austenite phases with the application of an external training stress. These dislocation arrangements create an anisotropic stress field in the matrix of austenite, which guides the nucleation growth of the martensite variants towards the preferred orientations in relation to the deformation adopted in the training procedure. Therefore, the maximum TWSME is generated because of the optimum density of dislocations and magnitude of internal stress.

CHAPTER 3

MATERIALS AND METHODS



CHAPTER THREE: MATERIALS AND METHODS

Introduction

1 Test in Ni-Ti SMA alloys: initial considerations	
1.1 <i>Influence of the test conditions on the properties of the samples</i>	96
1.2 <i>Influence of the cold work and the heat treatment performed on the properties of the samples</i>	98
1.3 <i>How to obtain the transformation temperatures</i>	100
2 Selected Material	103
3 Experimental procedures and equipment	104
3.1 <i>Heat treatment</i>	107
3.2 <i>Electrical resistivity measurements</i>	107
3.3 <i>Thermal cycling under zero stress test</i>	109
3.4 <i>Tension test</i>	110
3.5 <i>How to measure the constitutive parameters</i>	113
3.6 <i>Training to develop two-way shape memory effect</i>	116
3.6.1 <i>Thermal cycling under constant stress training</i>	116
3.6.2 <i>Isothermal tensile deformation below M_f</i>	120
3.6.3 <i>Test to measure the TWSM strain</i>	121
3.7 <i>X-ray diffractogram: a quantitative analysis of the SMA phase transformation behaviour</i>	121

Introduction

This chapter describes the complete methodology used to determine the mechanical parameters and the critical stress-temperature diagrams of our SMAs. Following these, the material selected, test machinery used and auxiliary equipments are described. Finally, the experimental procedures used to develop the TWSME and to measure the work production of our SMAs are described.

1 Test in Ni-Ti SMA alloys: initial considerations

1.1 Influence of the test conditions on the properties of the samples

De la Flor et al. [DFO, 2005] published an exhaustive study in relation to the initial considerations that are necessary to take into account before testing a Ni-Ti SMA wire. Their study detected the main differences between authors' procedures and the main handicaps that can present tension and constant stress tests. The revision of De la Flor et al. allow implementing the most rigorous and convenient experimental methodology to test SMA depending on the material and equipments. Therefore, the study of De la Flor et al. is taken as a reference for our test procedures.

As explained in the previous chapter, the functional properties of the SMA material are highly dependent on the environmental test conditions and prior thermomechanical history of the alloy. Therefore, both the environmental test conditions and the thermomechanical history, have to be well defined prior to performing any experimental test. The most important test conditions are:

- The ratio of heating/cooling of the sample during any kind of test will be slow enough to detect its phase transformations. The heating and cooling rate that we use is 1°C/min [NUR, 2008].
- To perform accurately tension test under isothermal conditions, the selected test strain rate is very important ([GAD, 2002], [PIEC, 2006]). Elevated strain rates ($4 \cdot 10^{-1} \text{s}^{-1}$ and $4 \cdot 10^{-2} \text{s}^{-1}$) may produce on the material local temperature changes that can alter its transformation stresses ([SHA, 1995], [TOB, 1998], [VIT, 2005]). The

strain rate used in this thesis is 1.5 mm/min for samples with 100 mm of length between machine jaws. That means a strain rate of $0.25 \cdot 10^{-3} \text{ s}^{-1}$.

- The type of control for our isothermal tension test will be *strain control by maximum strain* (hard mode).
- Although heating the sample by electrical current is faster and cheaper, the resistivity of the wires change with the change in temperature producing variations in the temperatures measured and increasing the difficult to control the alloy temperature. Consequently, all thermal cycling through the temperature transformation range will be performed by *air which is forced by convection*.

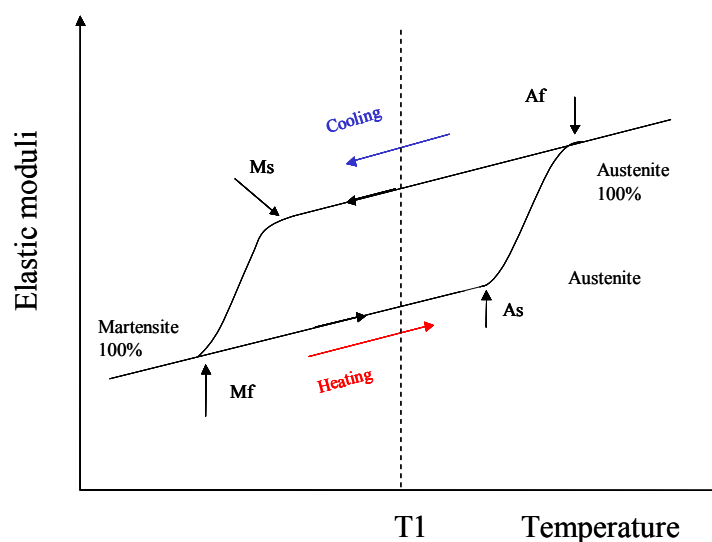


Figure 3.1 Schematic representation of the evolution of the elastic module versus temperature variation. The elastic module changes depending on the thermal origin of the sample.

- The fraction of the martensite changes depending on the thermal origin of the sample, that is, if the sample arrives to the test temperature from austenite state or it arrives from martensite state. The value of the SMA elastic module depends on the martensite fraction, as seen in figure 3.1. At temperature $T1$ (between M_S and A_S) the alloy will have different elastic module depending on the sample arrives to $T1$ from austenitic state or from martensitic state. On stress-strain curve, this implies a higher

stress values because the elastic module is higher for the austenite than for the martensite state.

1.2 Influence of the cold work and the heat treatment performed on the properties of the samples

The processing history and the microstructure of the Ni-Ti alloys have an evident effect on their mechanical properties ([MIY, 1981], [FIL, 1995], [PRAD, 1997], [HUA, 2000]). The level of the critical stress and the value of the shape memory strain would be different depending on the temperature of the alloy heat treatment. As seen in figure 3.2, where these alloys have received a heat treatment at different temperatures (475°C and 525 °C) for 1h. and subsequent quenching in water, as higher is the heat treatment temperature applied on the sample, a decrease in critical stress and an increase in recovery strain are produced.

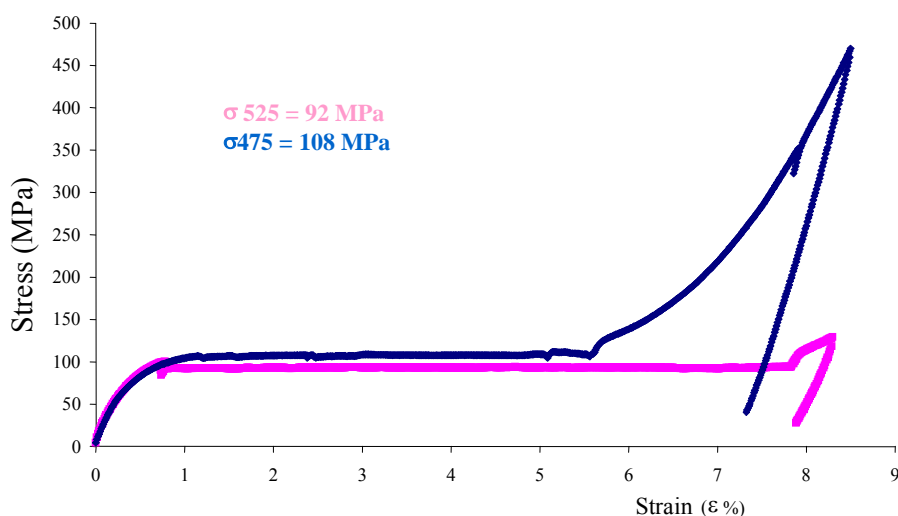


Figure 3.2 Stress-strain curves for different heat treatment temperatures (475°C and 525°C) applied on a 49.3at%Ni alloy, As seen, a decrease in heat treatment temperature means an increase in critical stress and a decrease in recovery strain [URB, 2010]c .

The combination of heat treatment temperature and prior cold work is fundamental in establishing good mechanical properties and stable memory effect in SMA Ni-Ti alloys. The Ni-Ti alloy in the as-received condition will usually have an amount of residual

cold work resulting from the wire drawing process. If no annealing process is carried out, the mechanical yield strength of the SMA alloy will be high but its memory properties will be poor and low values of recoverable strains will be possible for this non-annealed alloy. If an annealing step is carried out, the dislocation structure introduced in the alloy by the cold work becomes rearranged which results in improved memory characteristics but low values of internal stress for this annealed alloy. Low values of internal stress result in low values of critical stress and low values of yield strength for the annealed alloys. A minimum stress to produce reorientation of the martensite variants or stress induced martensite occurs when the alloy is heat treated at temperatures near of its recrystallization temperature (approximately 500-600°C for a near equiatomic Ni-Ti alloy [LIU, 1989]).

Concurrent with the decrease in internal stress is an increase in martensitic and austenitic transformation temperatures, that is, a change in the transformation behaviour is produced. The high density of dislocations remaining from the cold work in the Ni-Ti specimens annealed at temperatures between 350-500°C is regarded as being responsible for the possible formation of the R-phase in the alloy ([MIY, 1986], [LIU, 1994]b, [PEL, 1998], [UCH, 2002], [URB, 2010]). These dislocations depress the martensitic transformation but promote the R-phase transformation. The R-phase has a higher dislocation density than the martensitic and austenitic phases [MAT, 1992]. The R-phase does not occur in samples heat-treated at higher temperatures ($T \geq 500$ °C) because this range of temperatures decreases the number of dislocations in the matrix. Therefore, with the convenient heat treatment in time and temperature is possible to adjust the phase transformation behaviour of the alloy.

In the case of commercial alloys, the company may indicate the adequate heat treatment temperature range for its SMA alloy. However, this information is usually too unspecific or inexistent. Finding commercial material with the exact conditions of the straight annealed treatment performed is difficult. Another inconvenient to sum is the fact that the material is rolled for easy selling. This process of rolling produces a strain of the material, which can be erased by a new heat treatment of the material. Nevertheless, to perform a heat treatment, time and temperature have to be determined experimentally for each composition, shape and set alloy for giving the best memory properties.

1.3 *How to obtain the transformation temperatures*

Several methods have been reported for determining SMA transformation temperatures, of which differential scanning calorimetry (DSC), electrical resistance method (ER), A_f active test, applied loading method and lately, XRD patterns are the most commonly used. We describe the last four methods, with the intention that they will be used in this thesis.

The **electrical resistance method** (ER) is based on Ni-Ti alloy showing changes in resistance as it is heated and cooled throughout the transformation temperature range [LIN, 1980]. A drop in resistance occurs during the transformation from austenite to martensite upon cooling, and an increase in resistance accompanies the reverse transformation upon heating. The specimen forms part of an electrical circuit. As the resistivity is function of the crystalline structure, by monitoring the resistance change with temperature, the transformation temperatures can be obtained. The advantages of this method are firstly, that is very simple to apply and secondly, the resistivity of the alloy can be measured during the industrial application of the SMA. However, the interpretation of these increments and decrements in resistivity, especially those under load, is a cause of controversy between authors ([LIN, 1980], [AIR, 1994], [HOD, 1999], [WU, 2006], [ANT, 2007]). The main reason for these different opinions seems to be the appearance of the R-phase in the electrical resistivity curves of the Ni-Ti wires: the R-phase has significantly higher electrical resistance compared to austenite or martensite phases; however, if there is no R-phase in the alloy, as occurs in fully annealed Ni-Ti wires, it is very difficult to interpret the phase transformation behaviour or to find the transformation temperatures of the SMA alloy. Please, see figure 2.8 for an example of ER measurements.

The **second method is called the A_f active test**, which consists of bending the specimen at martensitic temperature until the strain of the wire is about 4% [HOD, 1999]. The temperatures corresponding to the recovery of the straight shape are recorded during slow heating of the alloy in a furnace (1-2°C/min). This experiment gives the austenite transformation temperatures, A_s and A_f , and this method is useful when it is necessary to obtain the austenitic temperatures in an easy and fast way [GOR, 2006], [RYK, 2008]. A representation of the process is represented in figure 3.3. When

the wire begins its austenitic transformation, the recovery movement starts. The recovery strain process finishes recovering the initial horizontal shape of the alloy (180°). The recovery angle and the temperature can be represented and then, the value of the austenitic transformation temperatures calculated. As a recommendation to avoid a permanent strain in the alloy during the process, the initial bending strain of the sample would be limited to 45° [DFO, 2005].

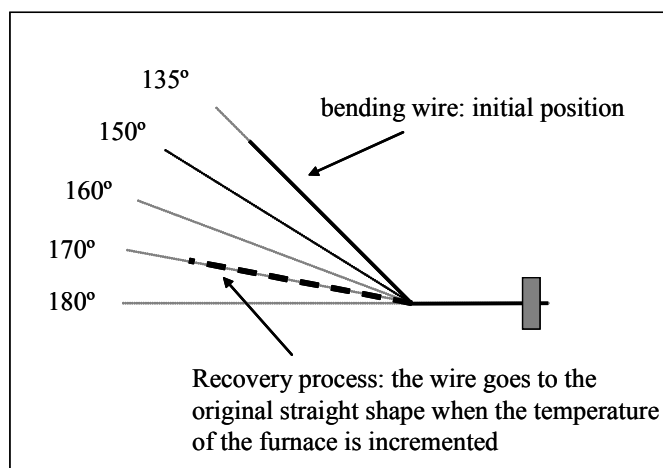


Figure 3.3 Figure representing the A_f active test.

The third method, applied loading method, has as a principle that, the transformation to martensite and the reverse transformation are accompanied by a large deformation when an external force is applied to the sample during cooling and a shape recovery during heating. Therefore, the temperature at which occurs a large change in geometry can be used to determine the transformation temperatures. This method obtains the SMA stress-strain behaviour at different temperatures and, through the lineal relationship between stress and temperature (Clausius-Clapeyron), the transformation temperatures at zero stress are calculated. To use this method implies to accept that the relation between stress and temperature of the SMA is lineal, as it was previously explained by equation 2.3. Next figure 3.4 shows how the transformation temperatures are obtained by the applied loading method.

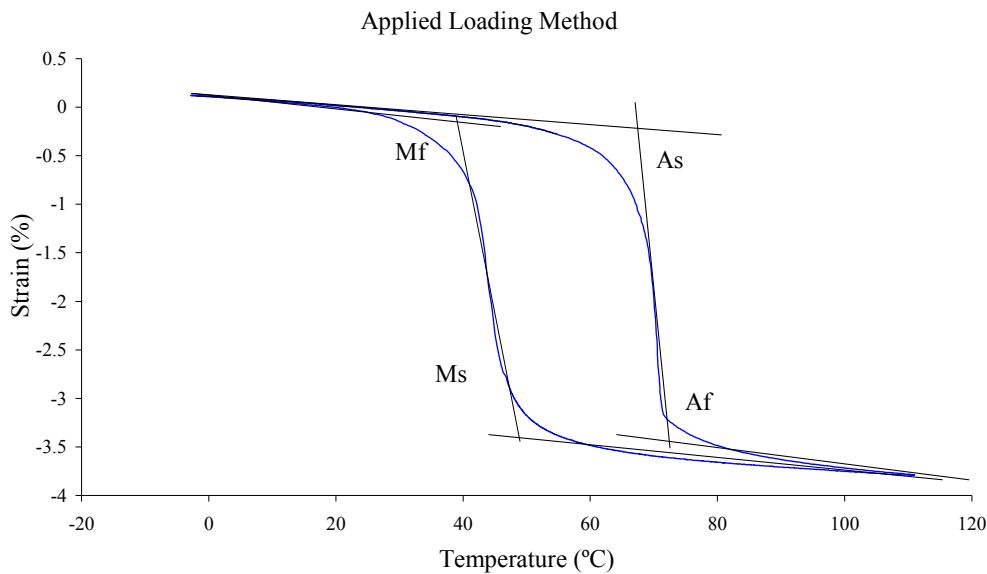


Figure 3.4 Figure representing the applied loading method. The transformation temperatures are calculated by tangent lines.

Finally, **the X-ray diffraction technique** is usually used to characterize the crystalline structure of the SMA alloy [MCN, 2003], [GRY, 2004], [KIM, 2005] or to characterize the phases present in the SMA in a qualitative way [LIN, 1980], [TUR, 2000], [PAU, 2004], [IIJ, 2004], [PAU, 2006], [IIJ, 2008]. Uchil et al. measured for the first time the SMA austenitic transformation temperatures, which were obtained from the analysis of the XRD peak profiles [UCH, 2007].

All these methods are widely reported in the literature, but their accuracy and coherence are seldom discussed. An example is [ABE, 2004] who published that the transition temperatures obtained by DSC did not correspond to those measured by the resistance and applied loading methods. Moreover, Abel et al. recommended as did [ANT, 2007], the resistance method to measure the M_S and M_F temperatures in cases where the R-phase is present during the cooling process of the alloy due to the distinct characteristic points in the cooling curve (the method to calculate these temperatures were proposed by [LIN, 1980]). Moreover, [PAT, 2007] and [PAU, 2008] published that the ER technique is in a better position to found R-phase temperatures than DSC technique. For A_S and A_F temperatures they recommended the applied loading method: real load values are applied to simulate conditions in practice.

In this thesis the experimental techniques of ER, applied loading methods, Af active test and for the first time, the weight fraction diagrams (XRD) are used to measure, to compare and to discuss the transformation temperatures obtained by each of these methods.

2 Selected Material

A binary near-equiatomic Ni-Ti with a nominal composition of Ti-rich 49.33at%Ni-50.67at%Ti in a form of a wire with a diameter of 1 mm manufactured by Euroflex (SM 495) is used throughout this study. The selection of Ti-rich is not a careless selection. The transformation temperatures and mechanical properties can be altered easier for Ti-rich Ni-Ti SMA than for Ni-rich SMA through adequate thermal and/or mechanical processes. Up to now, there are more studies published about equiatomic or Ni-rich alloys than about Ti-rich Ni-Ti alloys.

The material used has a certificate performed by the company, where it certifies its composition and properties (annex one). This material is straight annealed and is in martensitic state at room temperature. The material is served rolled; therefore, this deformation must be erased prior to use it. The commercial sheet data has not information about heat treatment (time and temperature) or the transformation temperatures of the material. The given more relevant data is in table 3.1. However, we have been characterized the as-received material in our laboratory in previous studies [DFO, 2005].

Physical properties	
Electrical Resistivity	76 $\mu\Omega$ -cm
Elastic module	28-41*10 ³ MPa
Expansion thermal coefficient	6.6*10 ⁻⁶ /°C
Mechanical properties	
Yield strength (min)	1100 MPa
Maximum strain (min)	10%
Shape memory properties	
Stress plateau (3%)	100 MPa
Recoverable stress (min)	8%
Final austenite temperature (A_f)	60-80°C
Chemical composition	
Ni	54,4 wt%
Ti	Balance
Oxygen	0.0033 wt (%)
Carbon	0.0046
Hydrogen	0.001 wt (%)

Table 3.1 Sheet data for Ti-Ni SM495.

3 Experimental procedures and equipment

Next tables 3.2 and 3.3 present a summary of the procedures that we have applied to each set of samples used in this thesis. We think that these tables help to clarify the experimental study done in this thesis. The information is separated into two tables because the samples used in this thesis are divided into two big sets: samples with heat treatment and samples with heat treatment a subsequent thermal cycling at zero stress. Each of the procedures and equipment used is explained in the next sections (3.1 to 3.7). However, we have indicated the number of the section where it is possible to find the explanation of the process to clarify the information of the tables 3.2 and 3.3.

Samples with heat treatment, 1h, water quenched (3.1)							
450		475		500		525	
Measurement of the transformation temperatures and determination of the phase transformation behaviour by ER and XRD (3.2, 3.7)		Measurement of the transformation temperatures and determination of the phase transformation behaviour by ER and XRD		Measurement of the transformation temperatures and determination of the phase transformation behaviour by ER and XRD		Measurement of the transformation temperatures and determination of the phase transformation behaviour by ER and XRD (3.2, 3.7)	
Calculus of the constitutive parameters and determination of the critical stress-temperature diagram (3.4, 3.5)		Calculus of the constitutive parameters and determination of the critical stress-temperature diagram (3.4, 3.5)		Calculus of the constitutive parameters and determination of the critical stress-temperature diagram (3.4, 3.5)		Calculus of the constitutive parameters and determination of the critical stress-temperature diagram (3.4, 3.5)	
TWSME trainings (3.6)		TWSME trainings (3.6)		TWSME trainings (3.6)		TWSME trainings (3.6)	
Determination of the training parameters for thermal cycling under constant stress training	Determination of the training parameters for isothermal tensile deformation under M_f	Determination of the training parameters for thermal cycling under constant stress training	Determination of the training parameters for isothermal tensile deformation under M_f	Determination of the training parameters for thermal cycling under constant stress training	Determination of the training parameters for isothermal tensile deformation under M_f	Determination of the training parameters for thermal cycling under constant stress training	Determination of the training parameters for isothermal tensile deformation under M_f
450cs	450it	475cs	475it	500cs	500it	525cs	525it
Thermal cycling under constant stress	Isothermal tensile deformation under M_f	Thermal cycling under constant stress	Isothermal tensile deformation under M_f	Thermal cycling under constant stress	Isothermal tensile deformation under M_f	Thermal cycling under constant stress	Isothermal tensile deformation under M_f
Measurement of the two-way memory strain	Measurement of the two-way memory strain	Measurement of the two-way memory strain	Measurement of the two-way memory strain	Measurement of the two-way memory strain	Measurement of the two-way memory strain	Measurement of the two-way memory strain	Measurement of the two-way memory strain
Transformation temperatures by ER, XRD and applied loading method	Transformation temperatures by ER, XRD and applied loading method	Transformation temperatures by ER, XRD and applied loading method	Transformation temperatures by ER, XRD and applied loading method	Transformation temperatures by ER, XRD and applied loading method	Transformation temperatures by ER, XRD and applied loading method	Transformation temperatures by ER, XRD and applied loading method	Transformation temperatures by ER, XRD and applied loading method
Determination of the phase transformation behaviour by ER and XRD	Determination of the phase transformation behaviour by ER and XRD	Determination of the phase transformation behaviour by ER and XRD	Determination of the phase transformation behaviour by ER and XRD	Determination of the phase transformation behaviour by ER and XRD	Determination of the phase transformation behaviour by ER and XRD	Determination of the phase transformation behaviour by ER and XRD	Determination of the phase transformation behaviour by ER and XRD
Training selection		Training selection		Training selection		Training selection	
One-way applications 450it		One-way applications 475it		Thermal cycling under constant stress 500cs		Thermal cycling under constant stress 525cs	
50 Thermomechanical cycles under various levels of stress (29 to 104 MPa)							
Measurement of the work production				Measurement of the work production			
Phase transformation behaviour by XRD				Phase transformation behaviour by XRD			

Table 3.2 Summary of the processes applied to each set of samples heat-treated.

Samples with heat treatment, 1h, water quenched plus 50 thermal cycles at zero stress (3.3)							
450TC50		475TC50		500TC50		525TC50	
Measurement of the transformation temperatures and determination of the phase transformation behaviour by ER and XRD		Measurement of the transformation temperatures and determination of the phase transformation behaviour by ER and XRD		Measurement of the transformation temperatures and determination of the phase transformation behaviour by ER and XRD (3.2, 3.7)		Measurement of the transformation temperatures and determination of the phase transformation behaviour by ER and XRD (3.2, 3.7)	
Determination of the minimum number of thermal cycles to stabilize the R-phase		Determination of the minimum number of thermal cycles to stabilize the R-phase		Determination of the minimum number of thermal cycles to stabilize the R-phase		Determination of the minimum number of thermal cycles to stabilize the R-phase	
450TC (8 cycles)		475TC (8 cycles)		500TC (12 cycles)		525TC (25 cycles)	
Calculus of the constitutive parameters and determination of the critical stress-temperature diagram (3.4, 3.5)		Calculus of the constitutive parameters and determination of the critical stress-temperature diagram (3.4, 3.5)		Calculus of the constitutive parameters and determination of the critical stress-temperature diagram (3.4, 3.5)		Calculus of the constitutive parameters and determination of the critical stress-temperature diagram (3.4, 3.5)	
TWSME trainings (3.6)		TWSME trainings (3.6)		TWSME trainings (3.6)		TWSME trainings (3.6)	
Determination of the training parameters for thermal cycling under constant stress	Determination of the training parameters for isothermal tensile deformation under M_f	Determination of the training parameters for thermal cycling under constant stress	Determination of the training parameters for isothermal tensile deformation under M_f	Determination of the training parameters for thermal cycling under constant stress	Determination of the training parameters for isothermal tensile deformation under M_f	Determination of the training parameters for thermal cycling under constant stress	Determination of the training parameters for isothermal tensile deformation under M_f
450TCcs	450TCit	475TCcs	475TCit	500TCcs	500TCit	525TCcs	525TCit
Thermal cycling under constant stress	Isothermal tensile deformation under M_f (3.6.2)	Thermal cycling under constant stress	Isothermal tensile deformation under M_f	Thermal cycling under constant stress	Isothermal tensile deformation under M_f	Thermal cycling under constant stress	Isothermal tensile deformation under M_f
Measurement of the two-way memory strain	Measurement of the two-way memory strain	Measurement of the two-way memory strain	Measurement of the two-way memory strain	Measurement of the two-way memory strain	Measurement of the two-way memory strain	Measurement of the two-way memory strain	Measurement of the two-way memory strain
Transformation temperatures by ER, XRD and applied loading method	Transformation temperatures by ER, XRD and applied loading method	Transformation temperatures by ER, XRD and applied loading method	Transformation temperatures by ER, XRD and applied loading method	Transformation temperatures by ER, XRD and applied loading method	Transformation temperatures by ER, XRD and applied loading method	Transformation temperatures by ER, XRD and applied loading method	Transformation temperatures by ER, XRD and applied loading method
Phase transformation behaviour by ER and XRD	Phase transformation behaviour by ER and XRD	Phase transformation behaviour by ER and XRD	Phase transformation behaviour by ER and XRD	Phase transformation behaviour by strain-T, ER and XRD	Phase transformation behaviour by strain-T, ER and XRD	Phase transformation behaviour by strain-T, ER and XRD	Phase transformation behaviour by strain-T, ER and XRD
Training selection		Training selection		Training selection		Training selection	
One-way applications 450TCit		One-way applications 475TCit		Thermal cycling under constant stress 500TCcs		Thermal cycling under constant stress 525TCcs	
50 Thermomechanical cycles under various levels of stress (29 to 104 MPa)							
Measurement of the work production				Measurement of the work production			
Phase transformation behaviour by XRD				Phase transformation behaviour by XRD			

Table 3.3 Summary of the processes applied to each set of samples heat-treated and thermally cycled at zero stress.

3.1 Heat treatment

The heat treatment applied to the as received Ni-Ti material consisted of annealing four sets of the material at the following temperatures: 450°C, 475°C, 500°C, 525°C [DFO, 2005], [URB, 2010]. This is done for one hour before quenching the sets in water in order to ensure different initial phase transformation behaviours, with different transformation temperatures and levels of R-phase in each of the heat-treated alloys. The samples heat-treated at 450°C were called 450 samples; those heat-treated at 475°C were called 475 samples; those heat-treated at 500°C, 500 samples; and those heat-treated at 525°C, 525 samples.

The equipment to perform the heat treatments is composed by:

- **Programmable Furnace Labotherm**, model N 20/H ($T \leq 1400^\circ\text{C}$). This furnace is also used to heat the samples to $T > A_f$ after tension test or after isothermal training in order to recover the residual strain.
- **Straight shape memory device**: it has the mission to teach the desirable shape that the wire has to remember in austenitic shape. It is selected the straight form. This device can treat 15 samples at the same time. Thus, a great number of samples with a maximum of homogeneity in heat treatment characteristics is obtained.

3.2 Electrical resistivity measurements

As been explained in section 1.3 of this chapter, the ER measurements have been a well-known technique for understanding the Ni-Ti behaviour. Based on the change of the electrical resistivity versus temperature that has the Ti-Ni alloys, their transformation temperatures and their phase transformation behaviours are characterized. In this study, we used precise heating/cooling controller equipment and an accurate resistivity measurement equipment to minimize the errors. Thus, very precise resistivity values for all samples have been obtained.

The electrical resistivity measurements are taken using a homemade four-probe setup and data is extracted using a precise digital equipment (HBM MGC plus). The control of the MGC plus equipment is via PC using the software CATMAN professional. The

temperature is varied in a controlled way using a thermal chamber (FRIOCELL 707). Then, a total automatic process is assured. The temperature is acquired via thermocouples, type J, which can be introduced into the thermal chamber, as seen in figure 3.5, where it is represented the equipment used to measure the transformation temperatures by ER. The accuracy of the electrical resistivity measurements is $\pm 0.03\Omega$ and for temperature measurements it is $\pm 0.03^\circ\text{C}$. The ER stress-free transformation temperatures are measured through the application of Ling and Kaplow's tangent lines method [LIN, 1980].

The auxiliary ER equipment is:

- **Thermal chamber Friocell 707 by forced air.** The work temperature range of this thermal chamber is $-9^\circ\text{C} < T < 115^\circ\text{C}$. The heating/cooling rate and the number of thermal cycles to perform are fully programmable. The maximum heating rate is $3.2^\circ\text{C}/\text{min}$ and the maximum cooling rate is $1^\circ\text{C}/\text{min}$.
- **HBM MGC plus** [HBM, 2010], is a modular measurement system that can measure force, displacement, pressure, temperature, torque, acceleration, strain, stress, voltage, current, frequency or resistance at low or high speeds. As MGCplus is a modular system, it is possible to select exactly the components that you need for current measurement tasks. This equipment can be fully computer-controlled. The accuracy for half and quarter-bridge strain gages, transducers, voltages and currents and thermocouples are 0.03. The module used for the resistance measurement is the ML35B with amplifier AP01 and for the thermocouple is ML801B with the amplifier AP 801.
- **Catman Software 5.0 Professional** [CAT, 2005] comprises software modules for setup and measured-value data acquisition. Data is recorded using a multichannel data server during measurement while the system's client-server architecture enables real-time data visualization.

Finally, Af active test uses the same furnace Friocell 707.



Figure 3.5 Equipment to measure the SMA transformation temperatures.

3.3 Thermal cycling under zero stress test

Thermal cycling at zero stress test consists of applying repeated thermal cycles under zero stress to samples 450, 475, 500 and 525 to study the evolution of the R-phase and transformation temperatures and the possibility to improve the mechanical behaviour of the Ni-Ti SMA used. Each of the thermal cycles at zero stress performed started by cooling the sample from $T > A_f$ to $T < M_f$. The sample was then heated again to a temperature of $T > A_f$. The temperature was varied using the thermal chamber Friocell 707 with cooling/heating rate of $1^\circ\text{C}/\text{min}$ by forced air.

Different number of thermal cycles at zero stress will be performed:

- 50 thermal cycles at zero stress are performed in order to study the evolution of the Ni-Ti phase transformation behaviour with thermal cycling at zero stress. These samples are called 450TC_{50} , 475TC_{50} , 500TC_{50} , and 525TC_{50} .

- We experimentally determine the minimum number of thermal cycles at zero stress that is necessary to apply to our Ti-Ni alloy to fully develop its R-phase ([MIY, 1986], [LI, 1991], [MAT, 1992], [UCH, 1998], [PEL, 1998], [MAT, 2003], [MAT, 2004] and [URB, 2009]). The value of the R-phase resistivity peak during thermal cycling is measured to determine whether the R-phase in samples 450, 475, 500 and 525 had been completely developed. Uchil et al. [UCH, 2002] took a constant value of the R-phase peak resistivity as a sign of the complete development of the R-phase in the alloy. The average value and the standard deviation of the resistivity peak over ten successive cycles are then calculated. When the standard deviation value is under 1% and this condition is repeated for at least five consecutive values, the R-phase was considered developed in all the samples. Afterwards, thermal cycling at zero stress is considered completed and the samples are ready to be tested. These samples are called 450TC, 475TC, 500TC, 525TC.

3.4 *Tension test*

A complete set of isothermal tension tests within the transformation temperature range is performed to compare the mechanical behaviour of the thermally cycled wires after a minimum number of thermal cycles at zero stress (450TC, 475TC, 500TC and 525TC samples) and the mechanical behaviour of the non-thermally cycled ones (450, 475, 500 and 525 samples). Isothermal tension tests are conducted under displacement-controlled loading conditions using a Zwick 1445 Tensile Test Machine with specially designed grips and a specially designed controlled thermal chamber [URB, 2002]a, [URB, 2002]b, [URB, 2002]c. Before each tension test, the specimens are cooled from a higher temperature to achieve the desired phase for the test (i.e. R-phase). All isothermal tests are performed by imposing a certain value of strain that ensured that a complete martensitic transformation took place (and that all the constitutive parameters could be obtained [DFO, 2006]).

The Zwick 1445 Tensile Test Machine has a test capacity of 10 kN with a working course of 1460 mm (figure 3.6):

- **Load cell, EA18-350:** 10 kN.
- **Extensometer:** Postflach 4350, with 50mm of distance between extensometer grips and a capacity of a 60 mm of deformation. It has no problem with high temperature tests.
- **Software:** specific Zwick software to control and record the test results.
- **Grips:** they were specially designed by the author of this thesis [URB, 2002], [URB, 2002]b, [URB, 2002]c. They are capable to test different wire diameters and to support high and low temperatures. The grips work by friction, without the introduction of bending or torsion stresses in the wire. The grips are also completely adapted to the specially designed thermal chamber (figure 3.7).



Figure 3.6 Tension test equipment.



Figure 3.7 Grips and extensometer.

- **Thermal chamber** (figure 3.8): the thermal chamber was designed by the author of this thesis to be able to perform tension tests through the full range of transformation temperatures that require the macrostructural characterization of the Ni-Ti material ($-30^{\circ}\text{C} < T < 250^{\circ}\text{C}$) [URB, 2002], [URB, 2002]b, [URB, 2002]c. The thermal chamber was fully constructed at the laboratory of the URV in 2004. The thermal chamber is made of AISI 316L, with isolation of basaltic roc (Banroc 511). The contact materials between the inner and exterior walls are made of Teflon to avoid thermal bridges. The circulation of the forced air is by centrifuge ventilator (2DTR45 225x40 R, ECOFIT). Four electrical resistances (1000 W, M shape) heat the air. The situation of the resistances is beside of the ventilator. The measurement of the temperature is made by a thermocouple J (Epcoc, diameter 3mm). Eurotherm 880 PID system device that connects and disconnects the resistances depending on the desired temperature, regulates the temperature of the thermal chamber. The dimensions of the chamber are 800x450x410 mm.

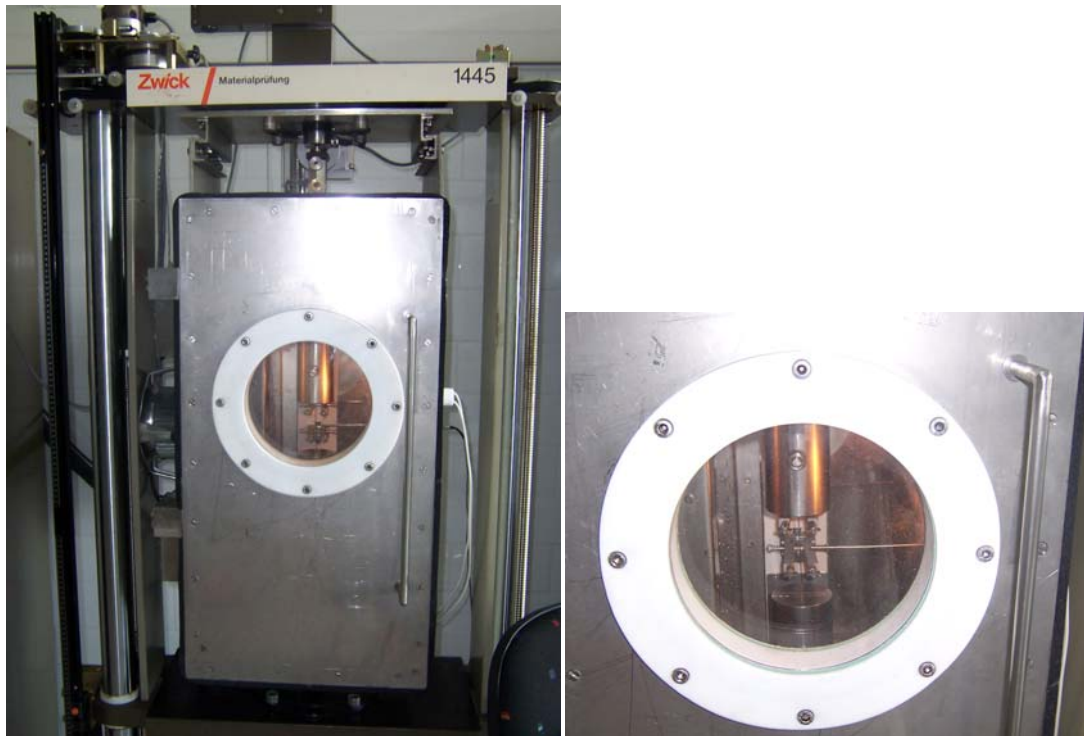


Figure 3.8 Thermal chamber installed on the Zwick test machine. On the right is possible to see the grips, the extensometer, the thermocouple, and the Ni-Ti wire during a tension test.

3.5 How to measure the constitutive parameters

Because SMAs are used in engineering applications due to their unique functional responses, it is essential that these responses are understood and can be reliably predicted. To predict the thermomechanical response of SMAs, macroscopic constitutive models are commonly used. These models have most often been used in technological applications because they are easier to interpret, their parameters can be obtained experimentally, and they can be more easily implemented in numerical methods. They assume that the behaviour of the material is a function of stress, strain and temperature and the corresponding rate of change of these called constitutive parameters. They are based on experimentally determined critical-phase transformation diagrams in the stress-temperature space. These are the models of Tanaka [TAN, 1986], Liang-Rogers [LIA, 1990], Brinson [BRI, 1993], Auricchio [AUR, 1997], [AUR,

1997]b and De la Flor [DFO, 2006]. In terms of cyclic applications, it is desirable to study the change of the constitutive parameters before these diagrams are obtained. Previous studies conducted by the authors proved that the constitutive parameters of a Ni-Ti SMA change considerably under mechanical cycling [DFO, 2009]. Now, in the present thesis, the influence of heat treatment temperature and thermal cycling at zero stress on the thermomechanical behaviour of a Ni-Ti SMA are investigated. To achieve this objective, **the constitutive parameters of the samples heat treated and thermally cycled at zero stress (450TC, 475TC, 500TC and 525TC samples) and the samples heat treated with no thermal or mechanic cycling (450, 475, 500 and 525 samples) will be analyzed and compared.**

The constitutive parameters are extracted from the stress-strain profiles for 450, 475, 500 and 525 samples and for 450TC, 475TC, 500TC, and 525TC samples. These constitutive parameters are: the transformation temperatures at zero stress; the stress influence coefficients that represent the relationship between stress and temperature ($C=d\sigma/dT$); the start and the final critical stresses to transform martensite (M) into detwinned martensite (S), σ_S^{CR} and σ_F^{CR} respectively, the critical stress to transform R-phase into martensite, $\sigma_{R \text{ to } M}^{CR}$, the maximum recoverable strain ϵ_L and the apparent modulus E_A , E_R and E_M of the initial linear elastic region and the apparent modulus for detwinned martensite E_S .

In more detail, the constitutive parameters are:

- **C_M , $C_{M \text{ to } R}$, C_R , $C_{A \text{ to } R}$ and C_A stress influence coefficients**

The stress influence coefficients represent the relationship between stress and temperature ($C=d\sigma/dT$) and give the variation rate of the stress with temperature for each phase. The process to obtain these coefficients consists on performing several isothermal tension tests through the SMA transformation temperature range. Later on, for any stress-strain curve is obtained the start and final critical stresses to transform. For temperatures within shape memory effect, the start and the final critical stresses to transform martensite (M) into detwinned martensite (S), σ_S^{CR} and σ_F^{CR} respectively, and the critical stress to transform R-phase into martensite, $\sigma_{R \text{ to } M}^{CR}$ are calculated (figure 3.9a). In the case of superelastic temperatures, we calculate four stresses: σ_S^{CR} y σ_F^{CR}

and σ_{Ai}^{CR} and σ_{Af}^{CR} . The last ones are the initial and final critical stresses to transform the stress induced martensite into austenite (figure 3.9b).

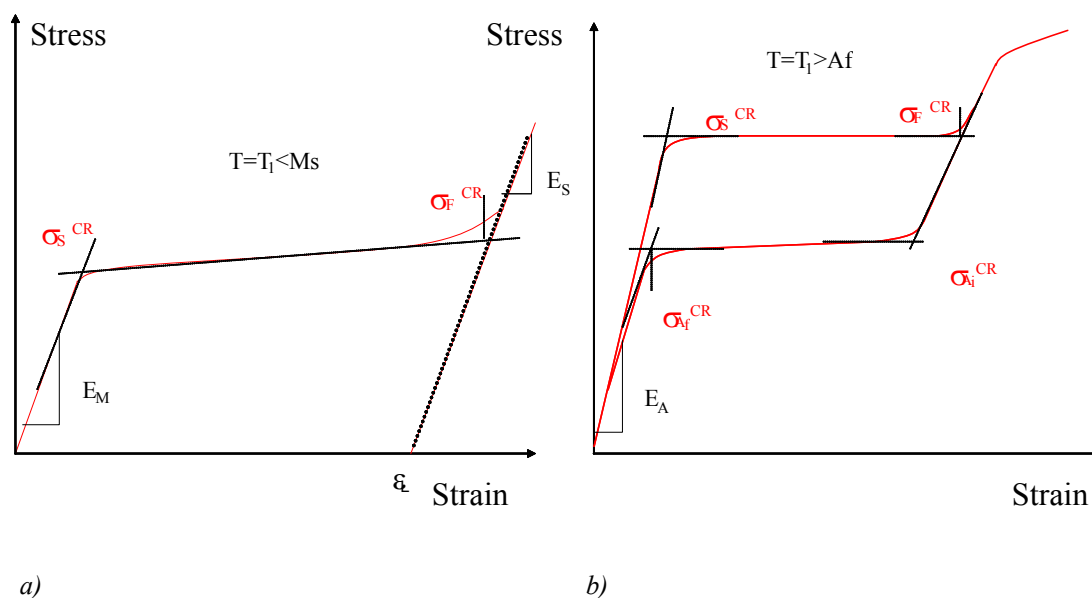


Figure 3.9 Schematic representations of the constitutive parameters obtained from a) stress-strain in martensitic range and b) stress-strain in austenitic range.

- **Maximum recoverable strain ϵ_L**

The maximum recoverable strain ϵ_L , will be determined from the stress-strain curves for each temperature after unloading the sample, and results from the remaining deformation that can be totally recovered after heating the sample above A_f . The condition to validate this data is that the unloading process has to be inside of the elastic range of the detwinning martensite ([BRI, 1993], figure 3.9a).

- **Apparent modulus, E_A , E_R and E_M**

The apparent modulus is calculated for pure martensite and pure austenite, i.e. the slope of the initial linear elastic region of the stress-strain curve at a temperature of $T < M_s$ for the martensitic apparent modulus (E_M) and a temperature of $T > A_s$ for the austenitic apparent modulus (E_A). The value of the R-phase apparent modulus (E_R) is also obtained from the slopes at R-phase temperatures ($M_s < T < A_s$), following the same

process; E_S is calculated from the slope corresponding to the deformation of the detwinned martensite for each test temperature (figures 3.9a and b).

The strain and temperature applied to each set of samples will be specified in the respective chapter of results and discussion.

3.6 *Training to develop two-way shape memory effect*

The objective of training is to study how heat treatment temperature, thermal cycling at zero stress and R-phase developed by heat treatment or by thermal cycling at zero stress influence the TWSM training procedures and the training parameters. The training procedures to develop TWSME are applied to 450, 475, 500 and 525 samples and 450TC, 475TC, 500TC and 525TC samples. The training procedures are thermal cycling under constant stress training and isothermal tensile deformation below M_f training, because these are effective methods for developing TWSME in Ni-Ti SMA.

3.6.1 Thermal cycling under constant stress training

Each couple of thermal and non-thermally cycled samples, 450-450TC, 475-475TC, 500-500TC and 525-525TC are subjected to the same training procedures and the same training parameters when both were trained by thermal cycling under constant load to compare the results. These parameters are a constant training stress (σ_{tr}) and a number of training cycles (n). According to Liu et al. the optimum training stress (σ_{tr}) corresponds closely to that required to form fully oriented martensite in one-step of the deformation process [LIU, 1990]. Simultaneously, the optimum number of training cycles (n) is associated with training conditions that should minimize the permanent strain (ϵ_p) that can be developed on the alloy during training. According to the stresses shown in figure 3.10 for samples non-thermally cycled, training involves applying a stress of a $\sigma_{tr}=104$ MPa for samples 450, 475, 500, and 450TC, 475TC, 500TC, on the alloys at fully martensite state. For samples 525 and 525TC the applied stress is $\sigma_{tr}=72$ MPa. The value of the training stress for samples 450, 475, 500, and 450TC, 475TC, 500TC is the same to facilitate the testing process. For 525 and 525TC samples, the value of the training stress applied is almost 22 MPa less than the training stress

recommended by Liu et al. [LIU, 1990]. This fact is due to the limitation in test temperature that our extensometer has (figure 3.11). Samples 525 have a value of the final austenite transformation temperature near of 135°C when they are under a stress near of 90 MPa. This temperature is not sustained by our extensometer.

The constant stress was applied using specially designed equipment installed in the thermal chamber FRIOCELL 707. Figures 3.11 and 3.12 show the equipment. The load is constantly applied to the alloy while this alloy is thermally cycled throughout the full transformation range. The number of training cycles applied to each type of samples to develop TWSME is specified in chapter 4.

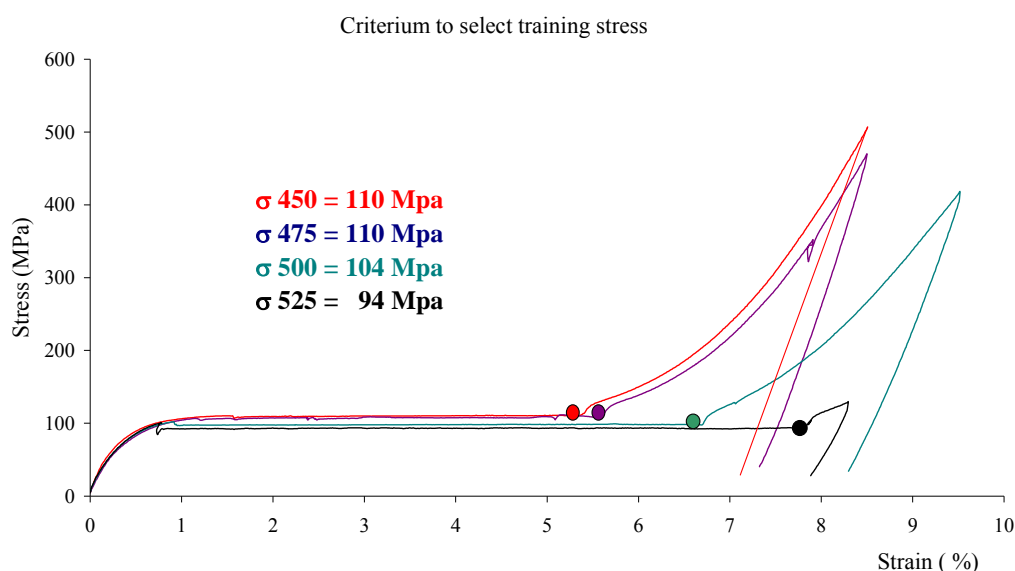


Figure 3.10 Stress-strain responses for 450, 475, 500 and 525 samples in order to select their optimum training stresses.

The equipment to perform thermal cycling under constant stress training is composed by (figures 3.11 and 3.12):

- **Wire load device:** the load device is designed to obtain the desired stress state of the wire. The device consist of a gravity mass ($0.5 < P < 10\text{kg}$) that hangs from the free end of a stainless steel bar. This bar is rigid enough to avoid undesirable deformations. The length of the bar has to be long enough to guarantee that the load applied keeps the

linearity with the wire (660 mm). On the other end of this bar a stainless steel hold-drill is mounted, which allows subjecting the wire avoiding slip and crushing wire situations. Another hold-drill is fixed to the furnace tray to complete the device load system. The device stiffness is high enough to assure the linearity of the system.

- **Strain gauge extensometer:** the extensometer has been self-designed and constructed. The reference length of the extensometer is 50mm, with a deformation capacity of $\pm 2.5\text{mm}$ ($\pm 5\%$). This deformation capacity is high enough to measure the Ni-Ti strains. The operation mode of the extensometer is based on a cantilever beam. The extensometer is instrumented with a full bridge strain gauge located near of the embeded join. As seen in figure 3.11, the upper part of the extensometer is fixed to the wire and acts as a support of the extensometer when the extensometer is mounted on the wire. The mobile end of the extensometer is the exterior end of the cantilever beam that is displaced by the displacement of the wire during the test. The mobile end is subjected to the wire through a punctual contact that is guaranteed by a silicone tensile device (figure 3.11). The design of the extensometer was made paying special attention to the SMA temperature range, but always thinking in the security of the equipment. Thanks to the facts that the strain gauge material is polyester substrate (HBM, it is fixed by an special adhesive), and that the connecting cable from the extensometer to the HBM equipment is made by copper recovered with Teflon, the extensometer is able to work at adequate Ni-Ti alloy temperature range (-20°C to 115°C).

- **Thermal chamber Friocell 707 by forced air** (figure 3.5).
- **HBM MGC plus**, [HBM, 2010]. The module of the MGC plus for the strain measurements is ML801B with the amplifier AP810.
- **Catman Software, 5.0 Professional**, [CAT, 2005] recorded the variation of the strain with temperature.

The samples trained by constant stress training are called 450cs, 475cs, 500cs, 525cs, 450TCcs, 475TCcs, 500TCcs and 525TCcs samples.

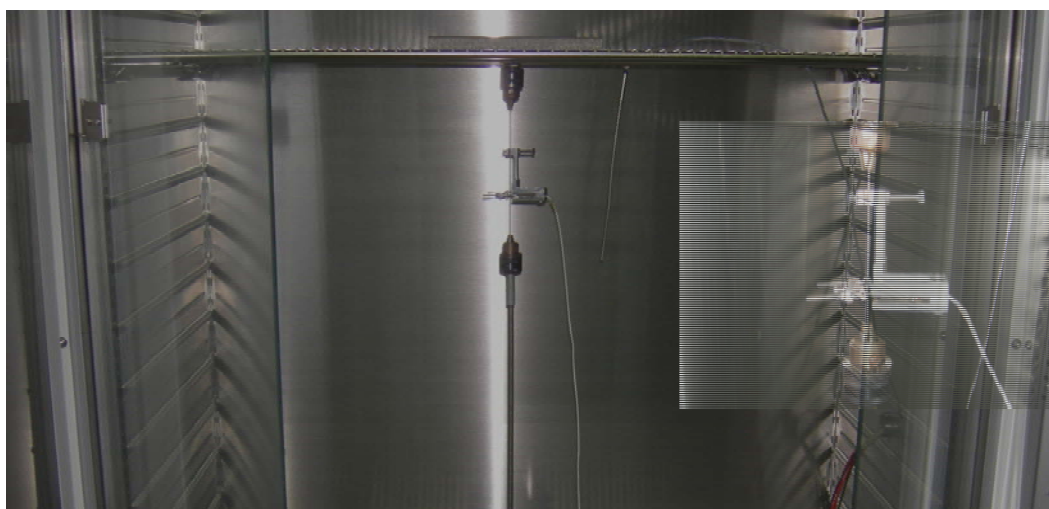


Figure 3.11 Equipment to perform the TWSME constant stress training. The equipment is inside the FRIOCELL thermal chamber, where is possible to see the grip-load system, the extensometer and the thermocouple. On the right, there is a detail of the extensometer and the grip system attached to the wire.

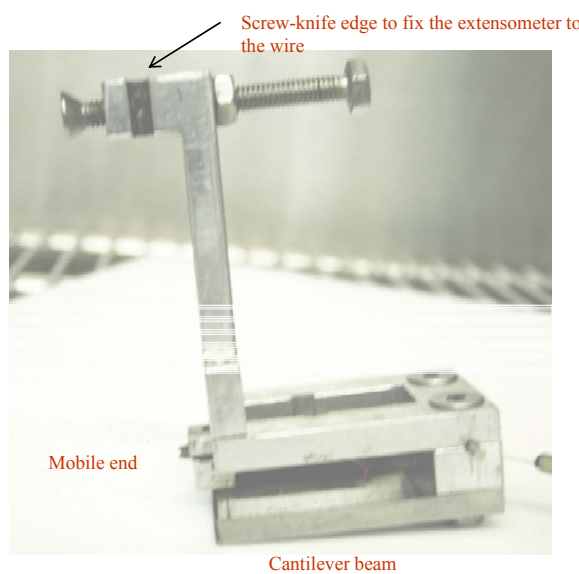


Figure 3.12 Extensometer detail.

The different types of strain measured during TWSME training are the strain in the martensite state (ϵ_m), the strain in the austenite state (ϵ_a) and the recovery strain (ϵ_r), the

latter being the remainder of the strain in martensite and the strain in austenite. According to the definition of the strains, for all samples, the loss of recovery of the alloy in austenite state for each cycle during the training procedure is ε_a .

The change in the transformation temperatures during the constant stress training is studied using the applied loading method.

3.6.2 Isothermal tensile deformation below M_f

The second training method, isothermal tensile deformation below M_f , was carried out using the same test equipment used for tension tests, Zwick 1445 Tensile Test Machine, described before. This training is performed by repeating thermomechanical cycles composed of five subsequent steps:

- a) Cooling the specimen to below 0°C to assure a fully martensitic state;
- b) Applying an isothermal training strain;
- c) Unloading the sample completed and recording the residual strain;
- d) Heating the specimen above A_f to measure the recovery strain (ε_r) and the permanent strain (ε_p);
- e) Cooling the sample to below 0°C and recording the increase in ε_{tw} during training.

This training is applied to the 450, 475, 500, 525, 450TC, 475TC, 500TC and 525TC samples with the following training strains: $\varepsilon_{tr} = 4.5\%$ for 450-450TC, 500-500TC and 525-525TC samples and $\varepsilon_{tr} = 4.75\%$ for 475-475TC samples at $T < M_f$. Each training cycle started after the cooling stage of the previous cycle had finished. This training was considered finished if the ε_{tw} of the sample did not increase during five consecutive training cycles.

The samples trained by isothermal training are called 450it, 475it, 500it, 525it, 450TCit, 475TCit, 500TCit and 525TCit samples.

3.6.3 Test to measure the TWSM strain

Different magnitudes of TWSME could be seen according to the training method used. The result of the TWSME training can be seen as a linear shape change in each wire during thermal cycling at zero stress after training. Then, thermal cycling between the whole transformation temperature ranges was repeated on 450, 475, 500, 525, 450TC, 475TC, 500TC and 525TC samples, to measure the ε_{tw} and its evolution during thermal cycling after training. The ε_{tw} was obtained from the difference between the strain of the sample in the martensite state (ε_m) and the strain of the sample in the austenite state (ε_a). A small force of 5 N was applied to keep the specimens stretched during these tests. The equipment is the same used for the constant stress training.

3.7 X-ray diffractogram: a quantitative analysis of the SMA phase transformation behaviour

To complement and to clarify the interpretation of the phase transformation behaviour made by ER measurements, weight fraction diagrams are also used in this thesis to analyze the changes in the phase transformation behaviour caused by thermomechanical treatments. The weight fraction diagrams are obtained from XRD profiles using the Rietveld method [RIE, 1969] and TOPAS 4.2 [BRU, 2003] software. The quantitative phase analysis was carried out on the XRD powder profiles. The results obtained by XRD are always combined and compared with those results obtained by electrical resistivity.

XRD analysis is done on 450, 475, 500 and 525 samples after heat treatment, on 450TC₅₀, 475TC₅₀, 500TC₅₀, 525TC₅₀ samples after thermal cycling at zero stress; on 450cs, 475cs, 500cs, 525cs, 450TCcs, 475TCcs, 500TCcs and 525TCcs samples after constant stress training method; on 450 it, 475it, 500cs, 525 it, 450TC it, 475TC it, 500TCit and 525TCit samples after isothermal training method; and on 500cs, 500TCcs, 525cs and 525TCcs samples after thermomechanical cycling under various levels of constant stress.


XRD measurements were made using a Siemens D5000 diffractometer equipped with an Anton-Paar TTK low temperature chamber. The angular 2θ diffraction range

was between 37° and 48°, step size 0.016° and 0.4s of step time. Ni-filtered $\text{Cu}_{k\alpha}$ radiation (30 mA, 40 kV) and a Braun position sensitive detector (PSD) were used. The profiles were collected at $\Delta T=1^\circ\text{C}$ after 30s of delay time and at a heating/cooling rate of 0.1°C/s. A static air-atmosphere was used throughout the measurement. All samples were heated at 130°C, cooled at 0.1°C/s down to -20°C, and heated again up to 100°C, and one diffractogram was taken every 1°C during both the cooling and heating processes.

Please consult annex two for extensive information about the quantitative analysis of the XRD profiles by the Rietveld method and TOPAS 4.2 software.

CHAPTER 4

***EFFECT OF HEAT TREATMENT AND
THERMAL CYCLING ON THE MECHANICAL
BEHAVIOUR OF THE TI-NI SMA WIRES***



CHAPTER FOUR: EFFECT OF HEAT TREATMENT AND THERMAL CYCLING ON THE MECHANICAL BEHAVIOUR OF THE TI-NI SMA WIRES.

Introduction

1 ER measurements of the effect of heat treatment and thermal cycling at zero stress on the SMA phase transformation behaviour	128
2 XRD quantification of the effect of heat treatment and thermal cycling at zero stress on the SMA phase transformation behaviour	132
3 Effect of thermal cycling at zero stress on the Ti-Ni functional properties	
3.1 <i>Effect of heat treatment and thermal cycling on transformation temperatures</i>	<i>146</i>
3.1.1 Effect of heat treatment on transformation temperatures	<i>146</i>
3.1.2 Effect of thermal cycling at zero stress on transformation temperatures	<i>152</i>
3.2 <i>Minimum number of thermal cycles at zero stress to develop the R-phase</i>	<i>152</i>
3.3 <i>Effect of thermal cycling on the stress-strain behaviour and on the apparent modulus</i>	<i>155</i>
3.3.1 Martensite state results	<i>157</i>
3.3.2 R-phase state results	<i>159</i>
3.3.3 Stress induced R-phase from austenite plus R-phase state	<i>162</i>
3.3.4 Austenite state results	<i>164</i>
3.3.5 Evolution of the apparent modulus with temperature	<i>165</i>
3.4 <i>Effect of thermal cycling on maximum residual strain</i>	<i>171</i>

<i>3.5 Effect of thermal cycling on the overall thermomechanical behaviour: critical stress-temperature diagrams</i>	<i>176</i>
4 Summary and conclusions	<i>185</i>

Introduction

This chapter analyses the influence of heat treatment and posterior thermal cycling at zero stress on the Ti-Ni thermomechanical response in the martensitic, R-phase and austenitic transformation ranges. This analysis has as a main objective finding the adequate thermal processes that can provide an improvement in the SMA functional properties. The thermal process that is studied in this experimental analysis is heat treatment following by a minimum number of repeated thermal cycling at zero stress.

It is known that the Ni-Ti mechanical behaviour is modified by performing repeated thermal cycling at zero stress throughout a complete temperature transformation range [MIY, 1986], [LIU, 1994], [PEL, 1998], [LIU, 2006], [SAI, 2006], [PAT, 2007]. Thermal cycling at zero stress has significant and irreversible effects on the transformation behaviour of an SMA because it modifies the alloy microstructure (such as delaying the beginning of the martensitic and the austenitic transformations). Because of these effects, [MOR, 2001] and [EGG, 2004] consider that thermal cycling at zero stress is a type of functional fatigue, but [HOR, 2003]-[HOR, 2004] also considers that performing thermal cycling at zero stress prior to using the SMA could improve the fatigue resistance of the alloy; that is, the process not only prevents plastic deformation in the martensite phase, but can also give high yield strength in the austenite phase. The accumulation of defects on the alloy microstructure increases the thermal hysteresis of the transformation behaviour, promotes the hardening of the thermally cycled alloy and improves the shape memory effect.

In the R-phase, thermal cycling at zero stress also has considerable effects on alloy microstructure. Li et al. [LI, 1991] have shown that thermal cycling can improve the shape memory effect of Ti-Ni alloys and this improvement can be attributed to the

increase in R-phase caused by thermal cycling. Matsumoto [MAT, 1993] found that the R-phase appears progressively during cooling with an increase in the number of thermal cycles. Uchil et al. [UCH, 1998] used electrical resistivity measurements to determine that R-phase is quite stable within a range of heat treatment temperatures, that it has a fixed start temperature (R_S) and that it has a high resistivity value. Furthermore, Uchil et al. [UCH, 2002] studied the number of thermal cycles at zero stress needed to stabilize the R-phase in the alloy and its relationship with the stability of the M_S temperature. In later studies, Matsumoto [MAT, 2003], [MAT, 2004] found that the process of R-phase stabilization is appreciably dependent on the composition of the alloy, but the number of defects introduced by thermal cycling also contributes to the stability of the R-phase. Several opinions have been published on how thermal cycling affects not only R-phase mechanical properties, but also the functional response of a Ti-Ni SMA [LIU, 1990], [STA, 1992], [POZ, 1999], [CHA, 2001], [WAD, 2005].

Therefore, the first objective of this chapter is to quantify the effects of heat treatment and repeated thermal cycling at zero stress on the Ti-Ni phase transformation behaviour. To achieve this objective, the study uses different sets of Ti-Ni wire. One set is heat treated at different temperatures to obtain different transformation paths, whereas the other set has the same heat treatment followed by repeated thermal cycling at zero stress. The number of cycles applied is 50. The study then uses the experimental techniques of ER and weight fraction diagrams to analyze how heat treatment and thermal cycling affect the phase transformation behaviour of these samples. Comparing these two experimental techniques will not only help to improve and clarify the interpretation of the ER measurements, regardless of whether there is an R-phase in the alloy or not, but will also give information about the SMA dynamic transformation behaviour between austenite, R-phase and martensite.

Following this, the minimum number of thermal cycles at zero stress that is necessary to apply in order to achieve the full development and stability of the R-phase is found for each sample. Thirdly, an in-depth study compares the mechanical properties of the samples thermally cycled at zero stress and the samples without thermal cycling, introducing their critical stress-temperature diagrams. The comparison study pays special attention to the R-phase transformation zone and its parameters in order to detect

a possible improvement of SMA functional properties brought about by the application of minimum number of thermal cycles at zero stress.

1 ER measurements of the effect of heat treatment and thermal cycling at zero stress on the SMA phase transformation behaviour

The ER measurements were taken for samples 450, 475, 500, and 525 after heat treatment and for samples 450TC₅₀, 475TC₅₀, 500TC₅₀, and 525TC₅₀ during each of the 50 thermal cycles at zero stress. In accordance with [UCH, 2002] the R-phase resistivity peak during thermal cycling was measured in order to determine when the R-phase had completely developed in all samples: a constant value of the peak resistivity is a sign that the R-phase has completely developed. The increase in the resistivity ($\Delta\rho$) resulting from the transformation from austenite to R-phase was also measured as the percentage increase between the value of the resistivity in austenite and the value of resistivity at the end of the R-phase transformation. An $\Delta\rho$ value of more than 12% is considered to indicate that the R-phase is present in the alloy [WUK, 2006] and an $\Delta\rho$ increase during thermal cycling at zero stress is considered to indicate that the R-phase has developed in the alloy [MAT, 2004].

Figure 4.1 shows the resistivity measurements as a function of heat treatment temperature (450, 475, 500 and 525 samples) and their evolution after 50 thermal cycles under zero stress for samples 450TC₅₀, 475TC₅₀, 500TC₅₀ and 525TC₅₀. In order to simplify the results discussion, the points for the martensitic and R-phase transformation temperatures are marked on the ER curves according to the most used interpretation for these temperatures, which was defined by Ling and Kaplow [LIN, 1980]. Figure 4.1 also shows for each sample the increase in resistivity values ($\Delta\rho$ in %) due to the transformation from austenite to R-phase.

Figure 4.1 also shows the changes in phase transformation behaviour resulting from heat treatments and thermal cycling at zero stress. The ER curves for the samples heat treated at temperatures 450, 475 and 500°C follow the two stage B2→R→B19' transformation on cooling in agreement with the values of the $\Delta\rho$. On heating, a single-

stage B19'→B2 transformation is shown by these samples, showing ER curves with no peaks or changes in the electrical resistivity slope. Liu et al. [LIU, 1994] state that the formation of the R-phase as an intermediate phase during cooling, but not during reverse transformation on heating, is a direct consequence of the irreversible energy dissipated during martensitic transformation.

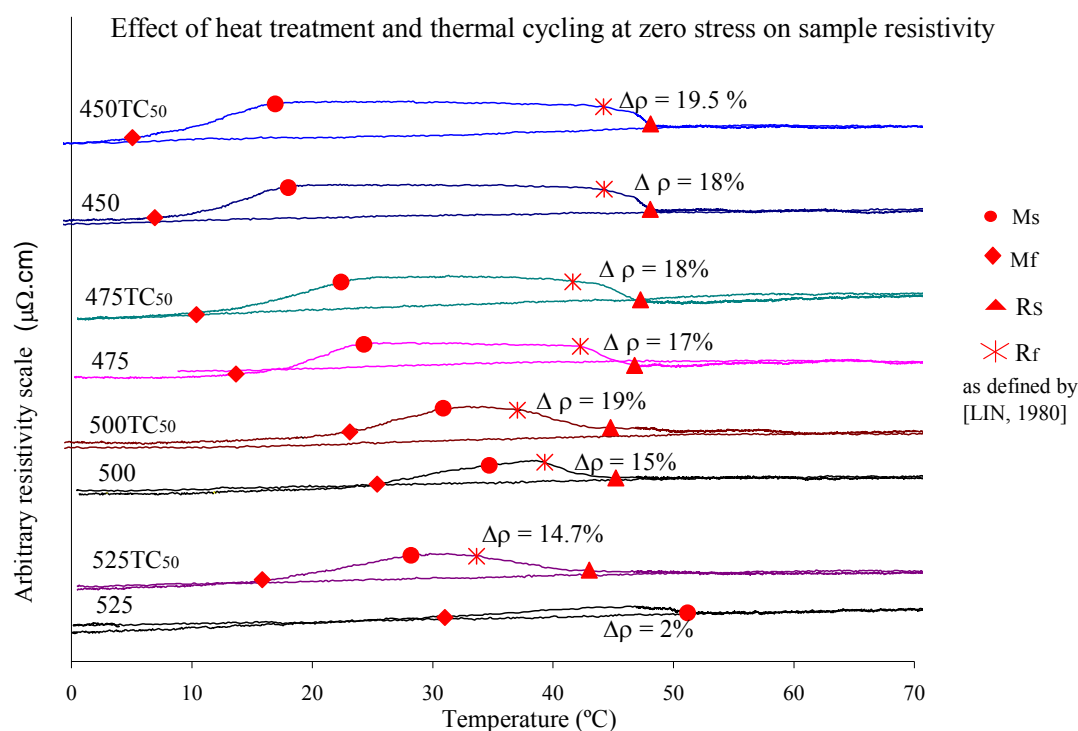


Figure 4.1 Effect of heat treatment and thermal cycling at zero stress on the samples electrical resistivity. To prevent the curves from overlapping due to similar resistivity values, the data have been modified in order to show the increment in resistivity more clearly.

As seen in figure 4.1, samples 450 and 475 show a well-developed hump that marks the presence of the R-phase as well as the highest $\Delta\rho$ values after heat treatment. Moreover, as their martensitic transformation temperatures are clearly lower than the R-phase transformation temperatures, their R-phase can be clearly observed as a pre-martensitic transformation. As the heat treatment temperature increases, the temperature interval between the ends of the R-phase to the beginning of the B19' decreases. When this temperature interval is very narrow, the martensite may form either from the B2 or

the R-phase, or indeed the B2→R transformation may occur simultaneously with the B2→B19' transformation [GOO, 1985]. However, these results are difficult to extract from the ER curves. The ER curves for the sample heat treated at 525°C show a single-stage B2↔B19' transformation path on cooling and heating according to the values of $\Delta\rho$ measured; that is, the R-phase seems to be absent and no peaks in the resistivity were measured, suggesting that the R-phase transformation is hidden by the martensitic transformation. In this case, the martensite seems to be formed only from B2.

After 50 thermal cycles at zero stress, (see figure 4.1) samples 450TC₅₀ and 475TC₅₀ do not show appreciative changes in the ER curves or the $\Delta\rho$ values and maintain the two stage transformation on cooling. This suggests that, for these two samples, the R-phase could have already fully developed after the heat treatment. This fact agrees with studies published by [MIY, 1986], [UCH, 1998] and by [WUK, 1999], whose found that thermal cycling does not influence samples that already contain a high density of dislocations. Once the dislocations are stabilized by annealing, the effect of the thermal cycling is also suppressed: it can be said that the presence of high-density dislocations in samples annealing at temperatures under 500°C stopped the introduction of new dislocations by thermal cycling. Thus, the ER measurements show that repeated thermal cycling at zero stress had no discernible effect for samples 450TC₅₀ and 475TC₅₀. In contrast, there are important changes in the ER results for samples 500TC₅₀ and 525TC₅₀. For sample 500TC₅₀, the ER curve shows an increase in $\Delta\rho$ that may mean that the thermal cycling causes the R-phase to develop. The ER curve for sample 525TC₅₀ now shows a clear hump between austenitic and martensitic states that is typical of the existence of the R-phase. This indicates that the transformation path of sample 525TC₅₀ has changed: the sample now shows a two-step transformation path on cooling. This evolution for samples 500TC₅₀ and 525TC₅₀ is the manifestation of a change in the microstructure, which implies that dislocations are introduced by the successive thermal cycles, which affect mainly the martensitic transformation. The martensitic transformation is hidden and delayed, favouring the development of the R-phase during the thermal cycling process [MIY, 1986], [LIU, 1994], [PEL, 1998], [UCH, 1998], [SOM, 1999], [WUK, 1999] and [UCH, 2002]. On heating, all ER curves again show no peaks or changes in the electrical resistivity slope for all thermally cycled samples, as it is the case for the non-thermally cycled samples (see figure 4.1).

Therefore, the initial dislocation structure obtained after heat treatment determines whether or not the alloy is affected by the thermal cycling at zero stress.

As stated above, the maximum values of the R-phase resistivity peak during each thermal cycle were measured during thermal cycling at zero stress in order to determine the relationship between the increase in resistivity and the development of the R-phase.

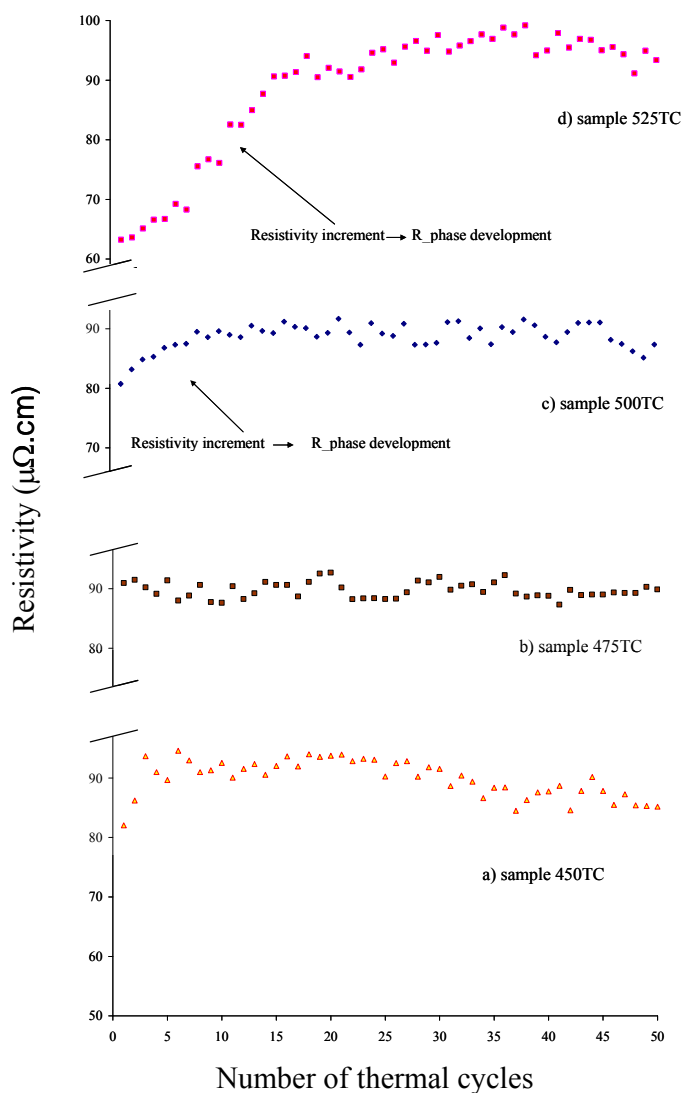


Figure 4.2 Evolution of the resistivity peak during 50 thermal cycles at zero stress for a) 450TC₅₀, b) 475TC₅₀, c) 500TC₅₀, and d) 525TC₅₀ samples.

Figures 4.2 compare these values in terms of the number of thermal cycles and show that the development of peak resistivity depends strongly on the temperature of the heat

treatment. Sample 450TC₅₀ peak resistivity increases during the first three cycles and then tends to decrease slightly until the 50th thermal cycle (figure 4.2a). The average peak resistivity value is 92.5 μΩ.cm, which is nearly equal to the resistivity associated with a well-developed R-phase [UCH, 1998]. Sample 475TC₅₀ peak resistivity remains almost constant throughout the thermal cycling (figure 4.2b), and has an average peak resistivity value of 90.5 μΩ.cm.

In contrast, sample 500TC₅₀ peak resistivity increases until the ninth cycle and then remains almost constant until the end of thermal cycling (figure 4.2c). The value of the peak resistivity once the constant value has been reached is 89 μΩ.cm. Sample 525TC₅₀ (see figure 4.2d) has a high increase in peak resistivity until the 18th thermal cycle; after this, the increase is smaller until the 25th cycle, at which point peak resistivity becomes constant with values of 95 μΩ.cm. Consequently, the evolution of the peak resistivity is not a very useful method for deducing the effects of thermal cycling at zero stress on the phase transformation behaviour for samples heat-treated at 450 and 475°C. In fact, figures 4.2a and 4.2b suggest that thermal cycling did not affect these samples. The evolution of the peak resistivity and its relation to the development of R-phase with thermal cycling at zero stress is actually useful if this value increases, as occurs with samples 500TC₅₀ and 525TC₅₀. That is, the R-phase peak resistivity increases to a maximum value that indicates the development of the R-phase, as is states by [UCH, 2002].

2 XRD quantification of the effect of heat treatment and thermal cycling at zero stress on the SMA phase transformation behaviour

The Rietveld method and TOPAS software were used to make a quantitative analysis of the XRD powder profiles in order to determine how heat treatment and thermal cycling under no stress influences the SMA phase transformation behaviour. Figures 4.3 to 4.6 show for each sample the phase transformation behaviour after heat treatment and its evolution after thermal cycling at zero stress. The results are given for each sample and treatment and they show the percentage of the weight fraction (wt%) of each phase

that is present in the sample as a function of temperature. The shape of the corresponding electrical resistivity curve is added in each diagram to correlate the ER measurements with the wt% results. In each of the diagrams is indicated the points at which each phase begins to transform and finishes its transformation (maximum value of the phase in wt%). These points are marked as M_f , M_s , R_f , R_s , A_s and A_f to correlate these values with the transformation temperatures in section 3.1 of this chapter.

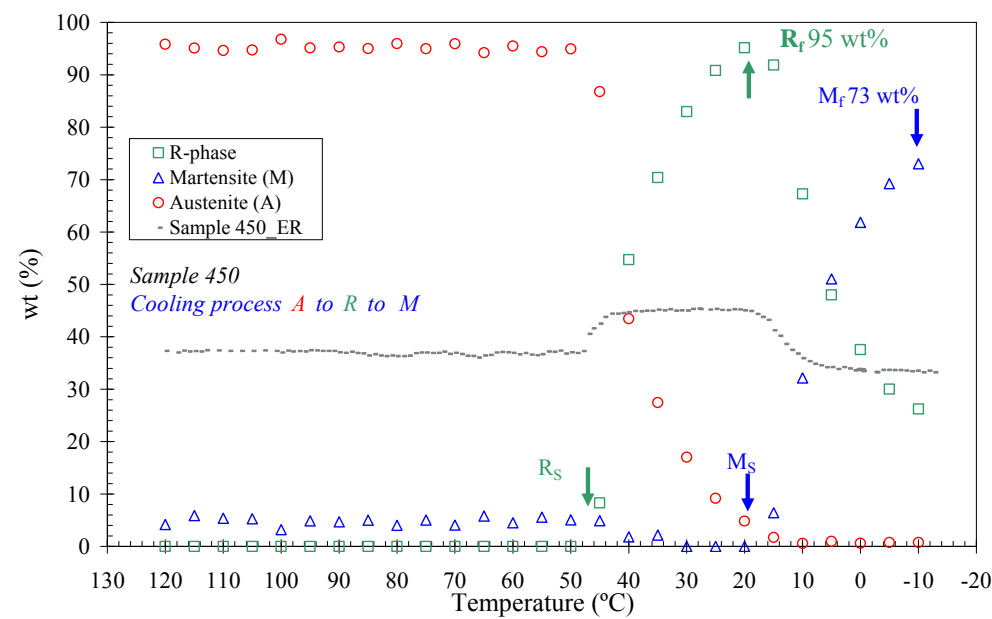
The weight fraction diagrams presented in this section are calculated by the Parametric Rietveld refinement. To consult the same data and results calculated by Conventional Rietveld Refinement, please see [URB, 2010].

Figures 4.3a and 4.3b show the effect of the 450°C heat treatment (sample 450) during the cooling and heating process, respectively. Figures 4.3c and 4.3d show how 50 thermal cycles under no stress (sample 450TC₅₀) affect the phase transformation behaviour. The analysis first focused on how heat treatment affected the phase transformation behaviour of sample 450. On cooling, the transformation path of the weight fraction is as follows: the austenite phase (A) transformed into R-phase, and then the R-phase transformed in martensite (M) (see figure 4a). In detail, this transformation path is as follows. The heat treatment produces a well-developed R-phase that starts from $R_s=45^\circ\text{C}$ (the austenite starts to transform into R-phase) and that reaches the R-phase with a maximum of 95wt% at 18°C ($R_f=18^\circ\text{C}$). At 18°C, the R-phase turns into M with no contribution from the austenite phase, as seen in figure 4a. From this point, the R-phase only transforms into martensite and the wt% of austenite remains constant. This transformation of the R-phase into martensite seems to finish at -5°C. The martensite phase reaches a 73wt% of transformation at the end of the process with some residual R-phase. Figure 4b also shows the three phases involved in the heating process: the residual R-phase (26wt%) transforms simultaneously with M into austenite ($A_s=40^\circ\text{C}$). The austenite transformation finishes at 68°C.

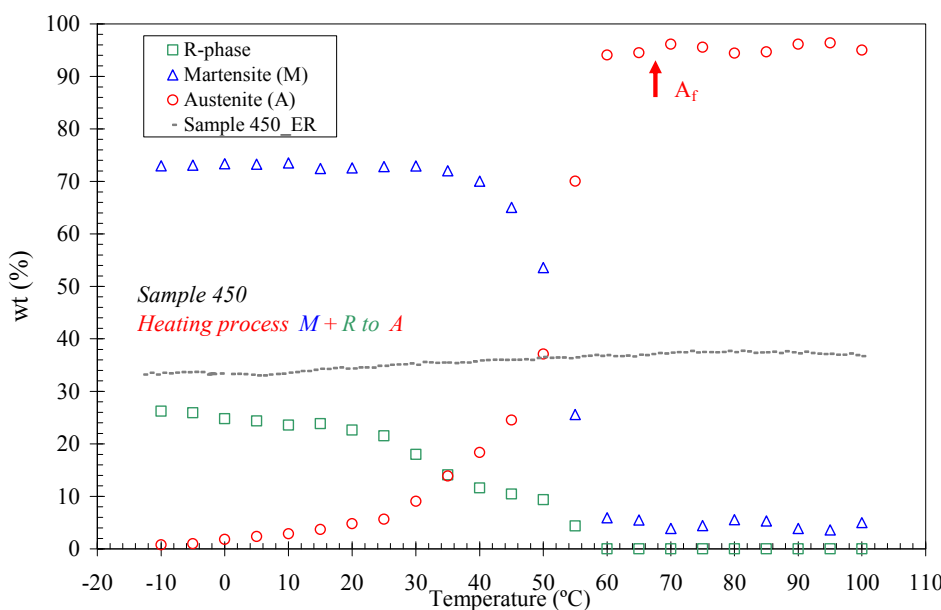
Comparing the wt% results (figure 4.3a) with the ER measurements shows that the R_s point on the wt% diagram coincides with the R_s point in the ER measurements. However, the end of the R-phase transformation (R_f) found in the wt% diagram does not correspond with the R_f point of the ER measurements proposed by [LIN, 1980], (see figures 4.1). According to the wt% results, the R_f does not occur at the end of a large

increase in resistivity, but rather it is found at the end of the plateau of resistivity, which is formed after this increase. [LIN, 1980] considered this point as the beginning of the transformation to martensite phase M_S (see figure 4.1). Thus, the end of the transformation to R-phase and the beginning of the martensite transformation occur at the same point ($R_f=M_S$) and if the wt% diagram and the ER curve are compared, it can be seen that they are situated at the end of plateau resistivity in the ER curve. As seen in figure 4.3a, the resistivity plateau starts when more than 50% of the austenite has transformed into R-phase; consequently, it can be said that the increase in the resistivity values and the subsequent plateau is only due to the R-phase transformation. The resistivity starts to decrease when the R-phase starts to transform into M. The end of the sharp decrease in the resistivity curve coincides with the point at which the R-phase is almost all transformed. Regarding the heating process (figure 4.3b), the fact that the R-phase contributes little to the transformation into austenite phase (only 23wt%) could be the reason why it is not detected in the resistivity curve; that is, the quantity of the R-phase is too low to cause a hump in the resistivity.

Figure 4.3c quantifies the effect of repeated thermal cycling at zero stress on the phase transformation behaviour during cooling for sample 450TC₅₀. As can be seen, the wt% of the R-phase does not increase compared with the wt% of the R-phase for the non-thermally cycled 450 sample; in fact the R-phase decreases by 4 wt% due to thermal cycling. Figure 4.3a shows that at around 100°C the wt% distribution of the non-thermally cycled 450 sample for each phase is 0 wt% for R-phase, 4 wt% for martensite and 96 wt% for austenite. After thermal cycling at zero stress (see figure 4.3c), the wt% distribution for sample 450TC₅₀ at around 100°C is 0wt% for R-phase, 8 wt% for martensite and 92wt% for austenite. The wt% of non-transformed martensite (residual martensite) has thus been increased cycle by cycle, there being less austenite to transform at the beginning of each thermal cycling.

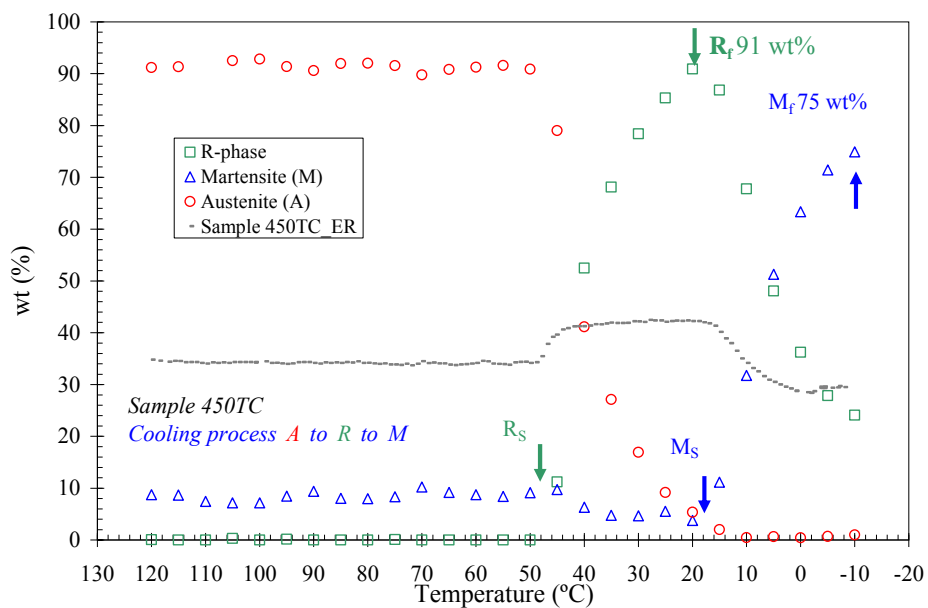


a)

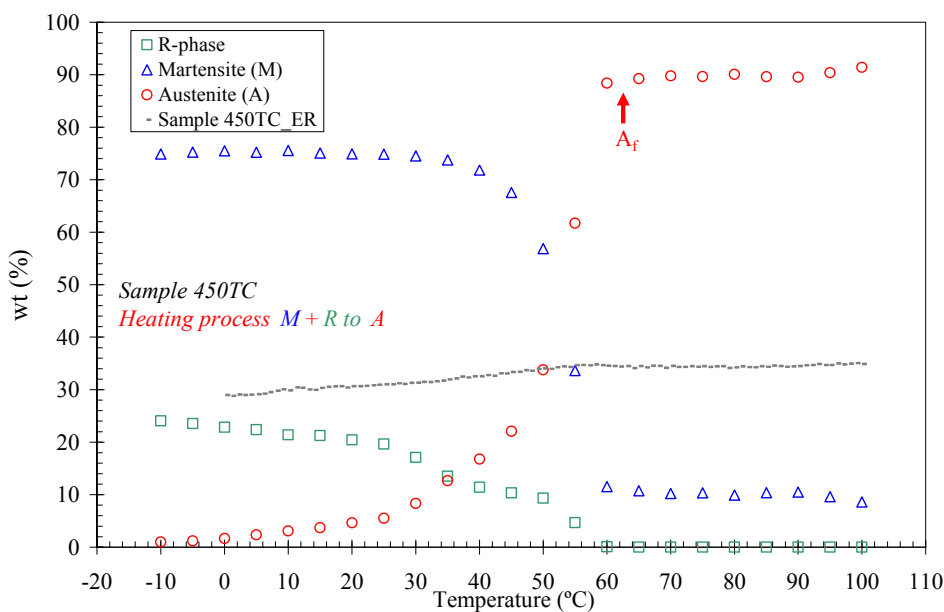


b)

Figure 4.3 Weight fraction evolutions in relation to temperature and compared with the ER measurements for a) sample 450 on cooling, b) sample 450 on heating.



c)



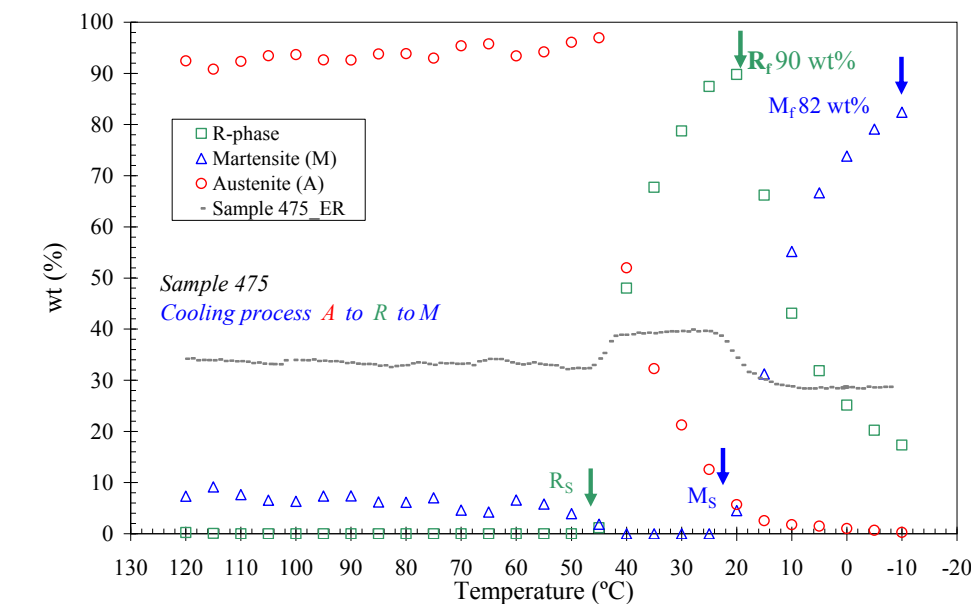
d)

Figure 4.3 Weight fraction evolutions in relation to temperature and compared with the ER measurements for c) sample 450TC₅₀ on cooling and d) sample 450T₅₀ on heating.

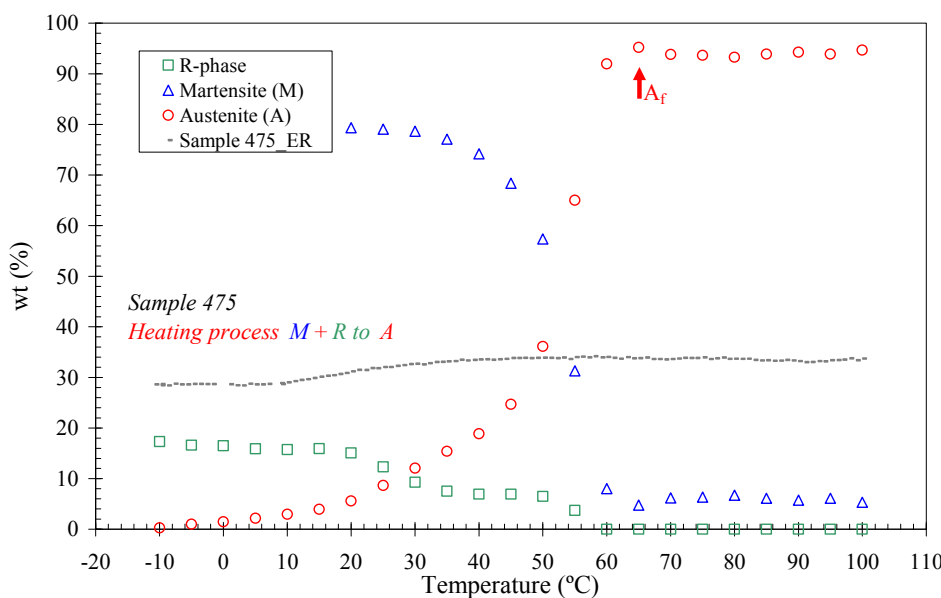
The transformation path of sample 450TC₅₀ is equal to the transformation path for the non-thermally cycled sample. The changes occur at about the same temperatures at which those transformations start or finish. Figure 4.3c shows that the transformation

from R to martensite ($R_f=M_s$) starts at 18°C, after which the austenite phase stops its transformation into martensite. The martensite phase reaches a 75wt% transformation at the end of the process with some residual R-phase and austenite phase. Figure 4.3d shows the three phases also involved in the heating process. The residual R-phase (24wt%) transforms simultaneously with the martensite phase into austenite. The austenite transformation finishes at 65°C. Figures 4.3c and 4.3d show that the wt% results and the ER measurements for sample 450TC₅₀ are the same as those previously described for sample 450. First, the increase in the resistivity values and the subsequent plateau is only due to the transformation of the austenite to R-phase. Second, the resistivity increase finishes when around 50% of the austenite has transformed into R-phase. Third, the R_f point found in the wt% diagrams in figure 4.3c corresponds with the end of the resistivity plateau. Finally, the end in the sharp decrease in the resistivity occurs when the wt% of R-phase is low.

Figures 4.4a and 4.4b show the weight fraction distribution for sample 475 and figures 4.4c and 4.4d show the same for sample 475TC₅₀ after 50 thermal cycles under no stress. The diagrams in figures 4.4a and 4.4b show that the transformation behaviour of sample 475 during cooling or heating is very similar to that of sample 450. The difference is that the maximum of R-phase is lower (90wt%) in sample 475 than in sample 450, but occurs at a higher temperature (20°C). Figures 4.4c and 4.4d show that the effect of the thermal cycling at zero stress on 475TC₅₀ samples is also similar to that on sample 450TC₅₀: the maximum wt% of the R-phase decreases to 87wt% (at 20°C) due to the increase in retained martensite, there being less austenite (3wt% less) that to transform into R-phase. The wt% distribution and the ER curves for samples 475 and 475TC₅₀ are also similar to those of samples 450 and 450TC₅₀.

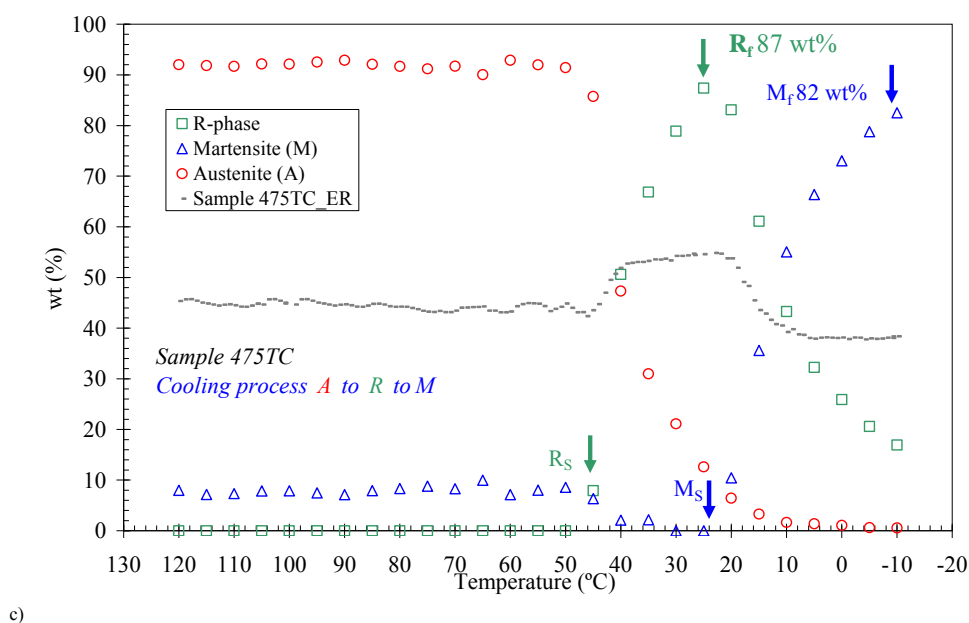


a)

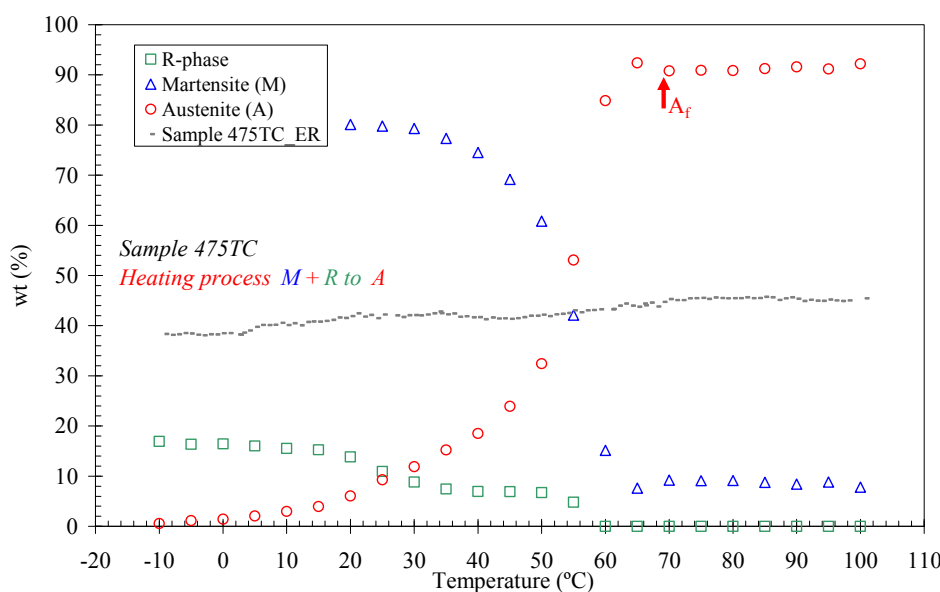


b)

Figure 4.4 Weight fraction evolutions in relation to temperature and compared with the ER measurements for a) sample 475 on cooling, b) sample 475 on heating.



c)



d)

Figure 4.4 Weight fraction evolutions in relation to temperature and compared with the ER measurements c) sample 475TC₅₀ on cooling and d) sample 475TC₅₀ on heating.

The picture is very different for samples 500 and 500TC₅₀. Figure 4.5a shows how the weight fraction for sample 500 evolves throughout the transformation range after heat treatment at 500°C and during the cooling process. Figure 4.5b gives the same information for the heating process.

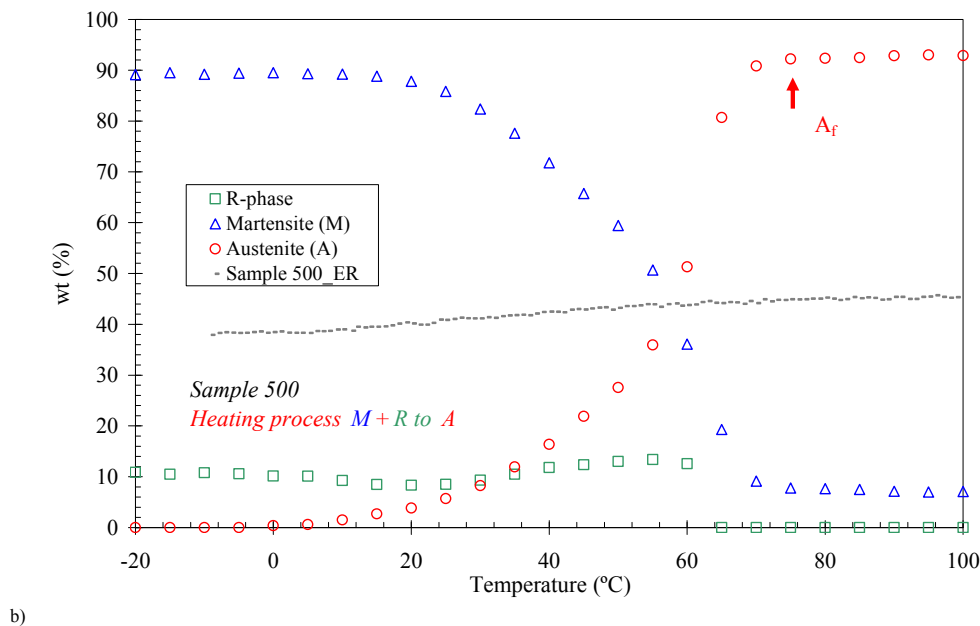
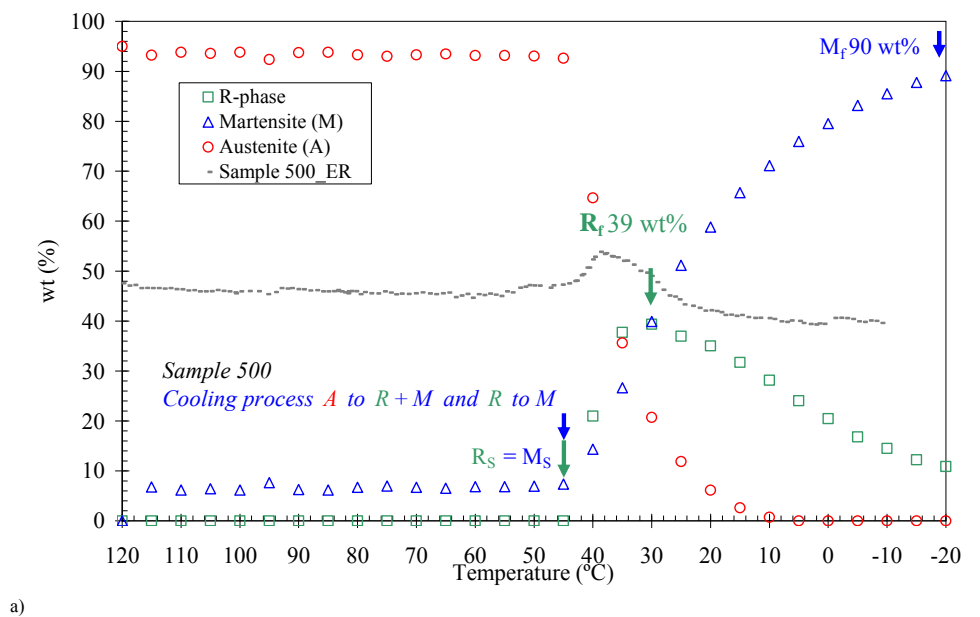
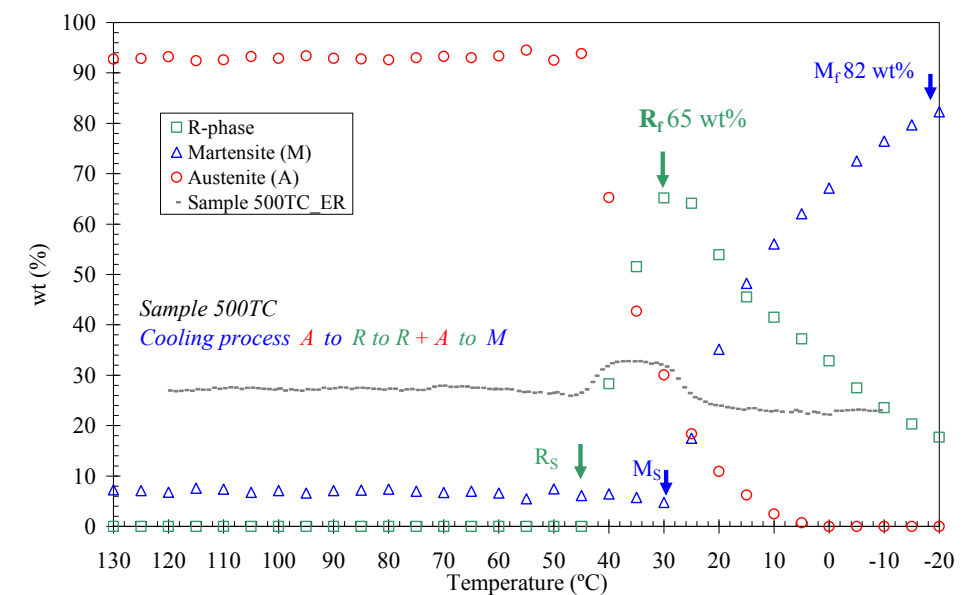
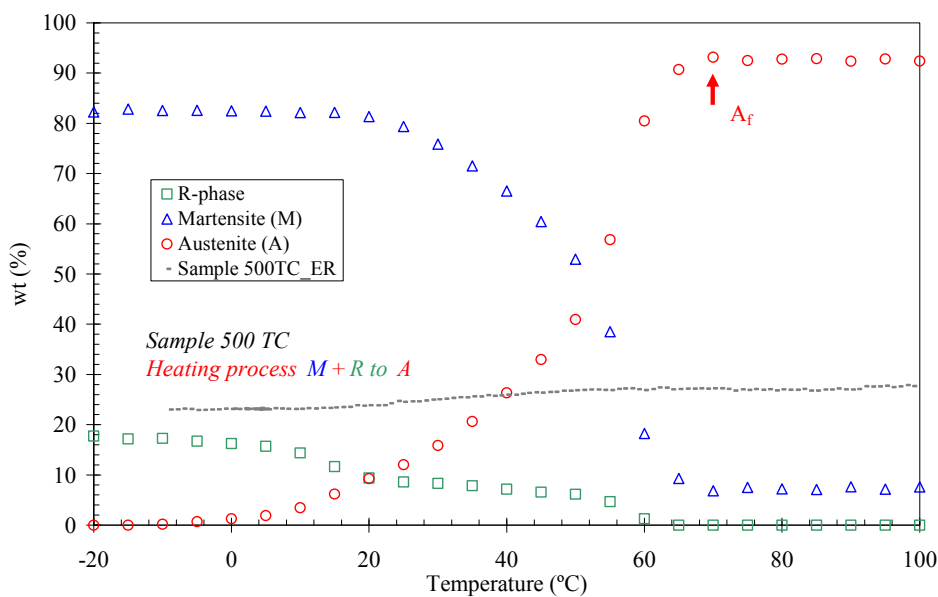


Figure 4.5 Weight fraction evolutions in relation to temperature and compared with the ER measurements for a) sample 500 on cooling, b) sample 500 on heating.



c)



d)

Figure 4.5 Weight fraction evolutions in relation to temperature and compared with the ER measurements for c) sample 500TC₅₀ on cooling and d) sample 500TC₅₀ on heating.

The first difference found in the phase transformation behaviour between sample 500 and 450 and 475 samples is that heat treatment at 500°C produces much less R-phase

than heat treatments at 450°C and 475°C; that is, 39 wt% at 30°C. This confirms that such heat treatment reduces the dislocation density introduced during previous cold work, although not entirely, which means that the presence of the R-phase in sample 500 is reduced, compared with samples 450 and 475. The second difference is that on cooling the austenite starts to transform into R-phase and martensite simultaneously ($45^{\circ}\text{C}=\text{R}_S=\text{M}_S$).

The third difference is that, while the R-phase is decreasing slightly, the martensite continues to increase at expense of the austenite phase and R-phase simultaneously. The R-phase starts to decrease transforming along with the austenite phase into martensite, showing that this heat treatment produces a multiple stage transformation process, where the B19' phase is formed not only from B2 in a continuous process, but also from the R-phase. At the end of the cooling process, there is the following wt% distribution: 90% for M, 10% for R and 0% for A. During the heating process, the martensite and the R-phase transform together into austenite, this process finishes at 75°C (see figure 4.5b).

Figure 4.5a compares the ER measurements with the wt% phase evolution for sample 500 and shows that the beginning of the ER resistivity hump (usually only associated with the R_S point [LIN, 1980]) corresponds with the beginning of the simultaneous transformation of the austenite phase into martensite plus R-phase ($\text{R}_S=\text{M}_S$). Therefore, for sample 500, the M_S is found at a different point than in samples 450 and 475 (see figures 4.3 and 4.4). Upon cooling, the R_f wt% corresponds with the end of the initial slight decrease in the ER hump. Moreover, the results show that the small temperature interval in the 500 ER curve between the end of the R-phase transformation and the beginning of the martensite transformation (see figure 4.1) was interpreted by [GOO, 1985] as a signal that the $\text{B2}\rightarrow\text{R}$ and the $\text{B2}\rightarrow\text{M}$ transformations could be simultaneous, fact that is confirmed by the XRD results presented here. For the heating process (see figure 4.5b), any sign of the transformation that occurs in the alloy can be found in the ER curve, as is the case for samples 450 and 475.

The effects of thermal cycling at zero stress on sample 500TC₅₀ are clearly shown in figures 4.5c and 4.5d. The first effect is that the transformation behaviour is clearly modified with the phases clearly separated: the austenite starts its transformation into R-phase at 45°C, and only when the R-phase transformation is finished does the martensite

transformation start ($R_f=M_s=30^\circ\text{C}$). Thus, the beginning of the martensite transformation has been delayed by thermal cycling at zero stress and it now coincides with the end of the R-phase transformation. Consequently, M_s decreases from 45°C (sample 500) to 30°C (sample 500TC₅₀). Austenite and R-phase simultaneously contribute to the transformation into martensite throughout the transformation process. Second, the R-phase develops because of the thermal cycling at zero stress and increases up to 65wt% (an increase of 27wt% compared with sample 500). The development of the R-phase can be attributed to the accumulation of dislocations in the parent crystals which, after a few transformation cycles delays the beginning of the martensite transformation and causes the R-phase to increase [MIY, 1986]b (see the wt% diagrams). Finally, when sample 500TC is heated, the R-phase (15wt%) and martensite (85 wt%) contribute to austenite transformation, which finishes at 73°C (see figure 4.5d). Figure 4.5c shows that once sample 500TC₅₀ has been thermally cycled, the beginning of the resistivity hump in the ER curve (R_s point) corresponds with the beginning of the R-phase in the wt% diagram. Moreover, it is important to remark that the M_s has been displaced until the end of the resistivity plateau. The wt% diagram shows that end of the R-phase transformation (R_f) corresponds again with the end of the plateau resistivity, as occurs in those samples with a highly developed R-phase (see figures 4.3 and 4.4). The decrease in the resistivity corresponds with the R-phase transformation to martensite. Finally, the development of the R-phase is reflected in the ER curves: the hump resistivity is increased by thermal cycling (see figure 4.1, samples 500 and 500TC), although this increase in resistivity (4%) cannot be correlated with the increase in wt% (27wt%).

The effects of heat treatment at 525°C and repeated thermal cycling at zero stress are shown in figures 4.6. Heat treatment at 525°C considerably reduces the presence of the R-phase (only 18 wt%). The resulting transformation behaviour for sample 525 is that the transformation from austenite to martensite starts at 45°C as the R-phase does (figure 4.6a). At the end of the cooling transformation the wt% distribution is 94% for M, 0% for A and 6% for R. On heating, the transformation to austenite finishes at 84°C with contributions from the R and M phases (figure 4.6b). Therefore, the highest heat treatment temperature does not entirely eliminate the presence of the R-phase. This shows that this heat treatment produces a simultaneous transformation process which

uses B2 to form the B19' and R-phase. The ER curve for sample 525 provides no information regarding these transformations but it does confirm that the R-phase transformations are the most important cause of the resistivity humps in the ER curves. The austenite transformation to martensite and back is hard to identify (see figures 4.6a and 4.6b).

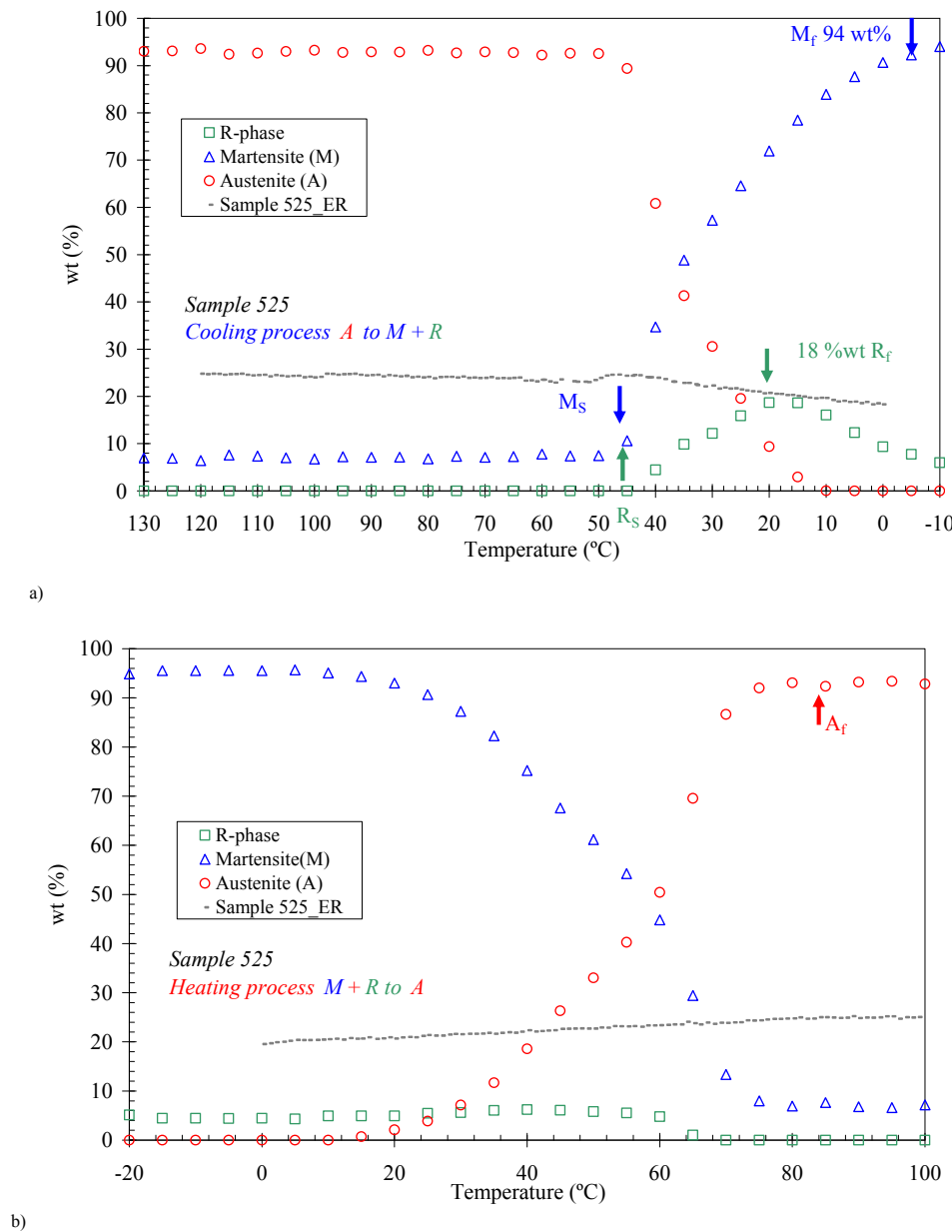


Figure 4.6 Weight fraction evolutions in relation to temperature and compared with the ER measurements for a) sample 525 on cooling, b) sample 525 on heating.

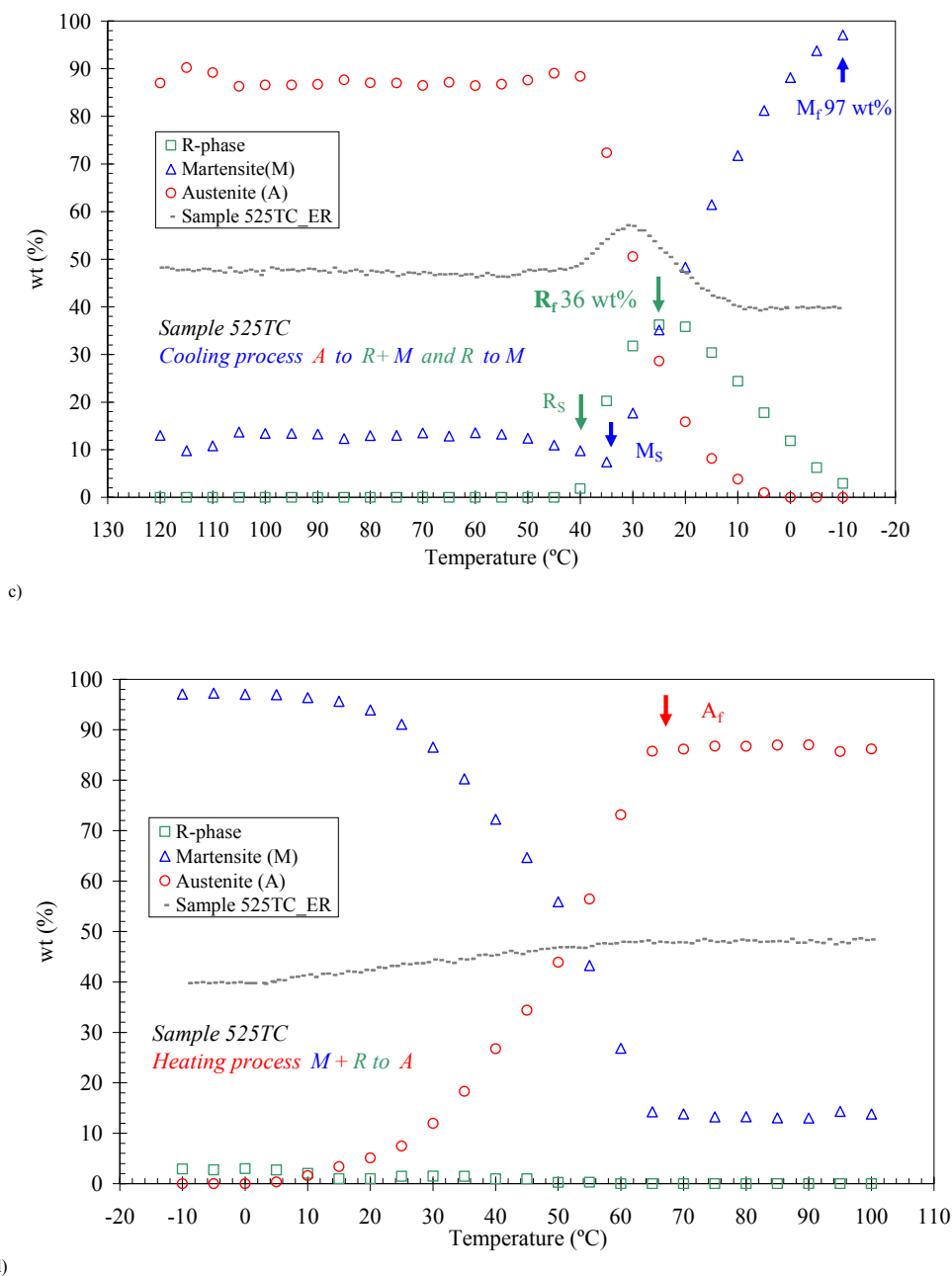


Figure 4.6 Weight fraction evolutions in relation to temperature and compared with the ER measurements for c) sample 525TC₅₀ on cooling and d) sample 525TC₅₀ on heating.

The effects of thermal cycling at zero stress on samples 525TC₅₀ (see figures 4.6c and 4.6d) in the phase transformation behaviour are very interesting. The transformation path for sample 525TC₅₀ is clearly modified by the increase in R-phase (18wt% of increase). The austenite starts its transformation into R-phase at 40°C and shortly after

begins to transform into martensite, resulting in a simultaneous transformation from austenite to R-phase plus martensite. The R-phase transformation finishes at 25°C, and then the austenite and the R-phase simultaneously contribute to the martensite transformation. The wt% distribution for the R-phase increased to 36wt% and the beginning of the martensite transformation is delayed ($M_S=35^\circ\text{C}$); both of which are the result of thermal cycling. In this case, thermal cycling at zero stress does not produce a separation of the transformation process as it does with sample 500TC₅₀. Finally, during the heating process the transformation into full austenite finishes at 70°C with contributions from the M phase (see figure 4.6d).

Comparing the wt% diagrams (figures 4.6c and 4.6d) with the ER results for sample 525TC₅₀ shows that the end of the R-phase transformation corresponds in the ER curve with the end of the little plateau in the resistivity hump, as does sample 500TC₅₀ (see figure 4.5c). The decrease in the resistivity corresponds with the R-phase transformation to martensite. Again, the M_S wt% corresponds with another point in the ER curve, which is different from its usual point [LIN, 1980]: M_S is found at the end of the sharp increase in resistivity.

Analyzing and comparing all the results exposed in this section 2, interesting conclusions can be done. Please consult section 4 of this chapter, summary and conclusions.

3 Effect of thermal cycling at zero stress on the Ti-Ni functional properties

3.1 Effect of heat treatment and thermal cycling on transformation temperatures

3.1.1 Effect of heat treatment on transformation temperatures

As seen from the results exposed in figure 4.1, the austenitic transformation temperatures are impossible to measure from the ER curves. Thus, these austenitic temperatures have to be obtained combining the results from *Af active* and XRD wt% diagrams methods. Table 4.1 shows the evolution of the austenitic temperatures with the

heat treatment temperature measured by A_f active and XRD for 450, 475, 500, and 525 samples.

<i>Sample</i>	$A_{f \text{ active, T-start movement}}$ (°C)	$A_{S \text{ active}}$ (°C)	$A_{f \text{ active}}$ (°C)	$A_{S \text{ XRD}}$ (°C)	$A_{f \text{ XRD}}$ (°C)
450	43	65	75	40	68
475	47	67	76	45	70
500	52	74	81	50	75
525	54	76	84	55	84

Table 4.1 Austenitic transformation temperatures for 450, 475, 500 and 525 samples measured by A_f active test and XRD wt% diagrams. The temperatures are in °C.

As seen in table 4.1, the very beginning of the movement of the sample during the A_f active test (T-start movement) and the A_S measured by XRD wt% diagrams ($A_{S \text{ XRD}}$) are similar ($A_{f \text{ active T-start movement}} \cong A_{S \text{ XRD}}$) but different of the $A_{S \text{ active}}$ values. This fact can be explained as follows. Meanwhile the values of $A_{S \text{ XRD}}$ are obtained from the phase transformation wt% diagram as the value when the reverse transformation begins to take place, the value of $A_{S \text{ active}}$ corresponds to that point at which the transformation takes place in a fast manner (the shape recovery is very fast when more than 60% of the transformation has been done, figure 3.3). Referring to the A_f temperature, the values calculated by these two methods are in reasonable agreement, taking into account that the $A_{f \text{ XRD}}$ values are considered as the maximum peak values; that is, the temperature at which the austenitic transformation is completely developed.

The martensitic and R-phase temperatures measured by ER using the tangent line method are shown in table 4.2a for the same samples. The transformation temperatures measured by XRD wt% diagrams are listed in table 4.2b. All the XRD temperatures are referred to the maximum wt% peak values of each transformation.

<i>Sample</i>	M_{fER} (°C)	M_{sER} (°C)	R_{fER} (°C)	R_{sER} (°C)	<i>Sample</i>	M_{fXRD} (°C)	M_{sXRD} (°C)	R_{fXRD} (°C)	R_{sXRD} (°C)
450	7	20	42	47	450	-5	18	18	45
475	13	22	41	48	475	-5	20	20	45
500	25	33	41	45	500	0	45	30	45
525	32	50	-	-	525	0	45	20	45

a)

b)

Table 4.2 Martensitic and R-phase transformation temperatures for samples 450, 475, 500 and 525 measured by a) ER and b) XRD wt% diagrams. The temperatures are in °C.

For the end of the martensitic transformation, the values measured by XRD are clearly lower than those measured by ER. Transporting each M_{fER} values of 450, 475, 500 and 525 samples to their corresponding XRD wt% diagrams, it is found that each of the M_{fER} temperature corresponds to that point at which martensitic transformation is already done near of or over 50wt%. Therefore, the point considered as M_f in the ER measurements by Lin and Kaplow [LIN, 1980] is not the real M_f . However, this point M_f defined by [LIN, 1980] could be used to indicate that the martensitic transformation has been done in more than 50%.

As seen, the results obtained by both methods are in well agreement for the martensitic start temperature (M_s) in case of heat treatment temperature under 500°C. Beyond this heat treatment temperature, the values are in clear disagreement due to the overlapping of the martensitic and R-phase transformations, which are not clearly shown in their ER curves (see figure 4.1). Therefore, as criterion for the initial and final points of the martensitic transformation, we proposed a **new interpretation of the ER curves** (figure 4.7). We take as a point for the end of the martensite transformation (M_f) that point at which the martensite transformation has been done in more than 50% ($M_{f50\%}$). This $M_{f50\%}$ point is usually over 0°C in annealed near equiatomic Ni-Ti, and

then, it is easy to measure by ER (as seen in figure 4.1). Regarding the initial temperature for the martensitic transformation, M_S , it is deduced from the explained in section 2 of this chapter that it has not a fixed point in the ER curves. The M_S position on the ER curve depends on the heat treatment temperature. Therefore, the ER results have to be combined with the XRD results. In any case, a hump resistivity of the ER curve followed by a long plateau can be taken to mean that the SMA has a transformation path clearly separated in two stages, and in this case, the M_S point is at the end of the plateau resistivity, as Ling and Kaplow published [LIN, 1980]. This is the case of 450 and 475 samples (see figure 4.7): the values of the M_S found by ER and by XRD are in well agreement. However, if there is a hump resistivity without a plateau as occurs in samples 500 and 525, this is a signal that the austenite transforms simultaneously to R-phase and martensite. In this case, the M_S temperature seems to be at the same point than R_S .

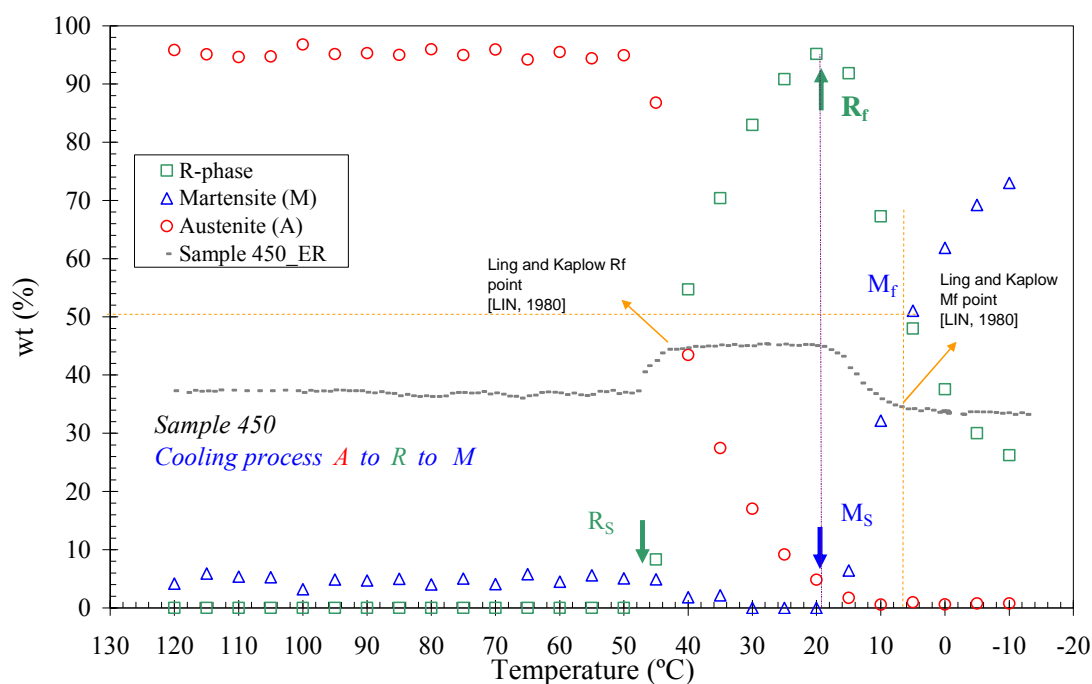


Figure 4.7 Comparison between martensite and R-phase transformation temperatures measured by ER and XRD. As seen, the point of the end of the martensitic transformation measured by ER corresponds to the point at which near of 50% of the martensite transformation is already done. The diagram also shows the R_f point by [LIN, 1980], which does not correspond with the real end of the R-phase transformation temperature measured by XRD.

Finally, the values of the beginning of the R-phase transformation (R_s) measured by both methods are in well agreement, as tables 4.2 show, excepting in the case of the sample 525, where the R-phase transformation is impossible to detect by ER measurements. Moreover, the values of the end of the R-phase transformation (R_f) are very different depending if they are calculated by ER or by wt%. As seen in figures 4.3 to 4.6, the R_f is at the end of the plateau resistivity. The R_f is not at the beginning of the resistivity plateau as published [LIN, 1980]. As this fact is repeated for each of the samples analyzed, independently of the heat treatment temperature applied, the R_f temperatures selected are those measured by XRD.

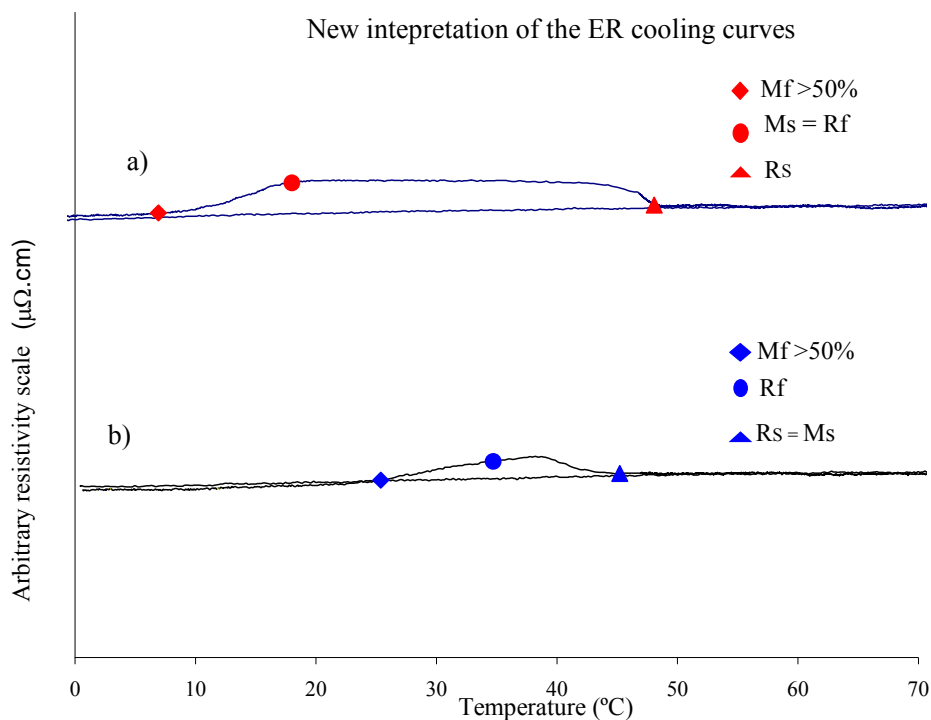


Figure 4.8 New interpretations of the ER curves depending of the shape of the ER curve for a) samples with a well-developed resistivity jump followed by a resistivity plateau and b) samples without plateau resistivity.

According to the findings above described, a new interpretation of the stress-free transformation temperatures measured by ER is proposed (figures 4.8). We thought that

this new interpretation of the ER curves really clarifies the ER measurements and its relation with the transformation temperatures in annealed near equiatomic Ti-Ni wires. Thus, in the case that the ER curve shows a well hump resistivity followed by a long plateau, the interpretation for the transformation temperatures is the one exposed in figure 4.8a (450 and 475 samples). If the ER curve does not show a resistivity plateau (sample 500), the new interpretation of the transformation temperatures is the one indicated in figure 4.8b. In the case that there is not jump resistivity in the ER curve (sample 525) is adequate to use another method to find the stress-free transformation temperatures.

To conclude, the transformation temperatures of the samples heat-treated are exposed in table 4.3:

<i>Sample</i>	$M_f 50\%$ (°C)	M_s (°C)	R_f (°C)	R_s (°C)	A_s (°C)	A_f (°C)
450	7	18	18	45	45	68
475	10	20	20	45	45	70
500	25	45	30	45	55	75
525	32	48	20	45	57	84

Table 4.3 Transformation temperatures depending on the heat treatment temperature received, according to the A_f active, XRD wt% diagrams and the new interpretation of the ER measurements proposed. The temperatures are in °C.

Analyzing the effect of the heat treatment on the austenitic transformation temperatures, the results show that both temperatures increase with the increase in the heat treatment temperature, in agreement with other authors [LIU, 1997]. For temperatures under 500°C, the values for both austenitic temperatures are very similar. Both martensitic temperatures increase their value with the increase in heat treatment temperature, and finally, the R_s temperature is very similar for all samples, and it

presents a stable behaviour that is independent of the heat treatment temperature performed, according to the results of [UCH, 2002].

3.1.2 Effect of thermal cycling at zero stress on transformation temperatures

According to the results exposed in section 3.1.1, the transformation temperatures after 50 thermal cycles are listed in table 4.4. The effect of repeated thermal cycling at zero stress on the transformation temperatures of samples 450TC₅₀ and 475TC₅₀ is that thermal cycling does not increase both martensitic transformation temperatures. However, both martensitic temperatures decrease considerably for samples 500TC₅₀ and 525TC₅₀ due to the development of the R-phase, which delays the martensitic transformation. The decrease for the austenite transformation is common to all samples.

<i>Sample</i>	<i>M_f50%</i> (°C)	<i>M_s</i> (°C)	<i>R_f</i> (°C)	<i>R_s</i> (°C)	<i>A_s</i> (°C)	<i>A_f</i> (°C)
450TC ₅₀	7	18	18	47	42	65
475TC ₅₀	10	20	20	47	44	68
500TC ₅₀	13	30	30	45	46	73
525TC ₅₀	16	35	25	45	48	78

Table 4.4 Transformation temperatures (°C) after 50 thermal cycles at zero stress, according to the *A_f* active, XRD wt% diagrams and the new interpretation of the ER measurements proposed.

3.2. Minimum number of thermal cycles at zero stress to develop the R-phase

As seen in section 2 of this chapter, 50 thermal cycles at zero stress have different effects depending on the heat treatment temperature performed on the sample prior to thermal cycling. The phase transformation behaviour considerably changes for samples 500TC₅₀ and 525TC₅₀, developing the R-phase and delaying the martensite transformation. In this section is studied the minimum number of thermal cycles at zero

stress that is necessary to apply to the Ti-Ni wire in order to achieve the changes in the phase transformation behaviour that have been found in section 2, that is, the development of the R-phase. The improvement of the SMA that we are looking for by thermal cycling at zero stress must include the minimum number of thermal cycles for each sample in order to save processing time.

Uchil et al. [UCH, 2002] defined the critical cycle as the cycle at which both, peak resistivity value and M_S temperature being constant, and it is considered as a sign that the R-phase is full developed and stable in the alloy. As discussed in section 2, the wt% diagrams (see figures 4.3 to 4.6) show that the position of the temperature measurements taken from the ER curves and used as a sign that the R-phase has developed are not the M_S temperature, as suggested by Uchil et al. These measurements correspond to the temperature for the end of the R-phase transformation (R_f), as all the wt% diagrams show. Therefore, in the next figure 4.9 is shown the evolution of the R_f temperature during 50 thermal cycles at zero stress for all samples. As seen, depending on the heat treatment temperature, the number of cycles at which the R_f temperature becomes stable is different. For samples 450TC₅₀ and 475TC₅₀ the R_f temperature slightly decreases and becomes stable (values around 17°C and 21°C respectively) from cycles 7 and 8 respectively. For sample 500TC₅₀ the R_f becomes stable from cycle twelve, and for sample 525TC₅₀, the cycle is the 25th.

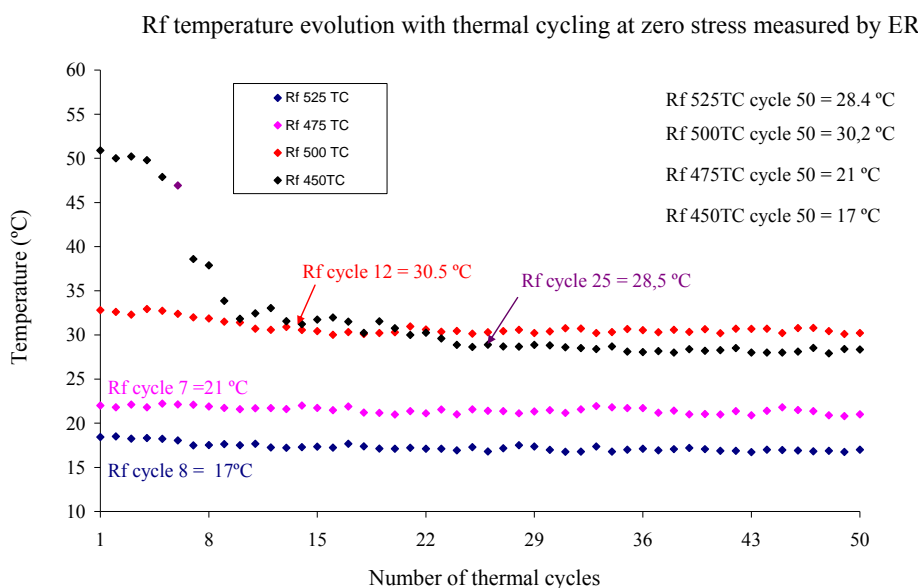


Figure 4.9 Evolution of the R_f temperature with thermal cycling at zero stress. The number of cycles at which is considered that the R-phase is developed it is indicated for each sample.

Then, recalling figure 4.2 and the comments referred to the evolution of the peak resistivity for each sample, it is possible to establish the critical cycle for each sample, that is, the cycle at which both, peak resistivity value and R_f temperature, being constant. As the critical cycle is reached, the phase transformation behaviour could be considered stable. The wire cannot change its phase transformation behaviour with further thermal cycling at zero stress. To illustrate that beyond the critical cycle the wire does not change its phase transformation behaviour, figures 4.10 display for 450TC₅₀ and 525TC₅₀ samples two different ER cycles (cycles 10-50 for sample 450TC₅₀, and cycles 30-50 for sample 525TC₅₀). As seen, no appreciable changes are detected between these ER cycles.

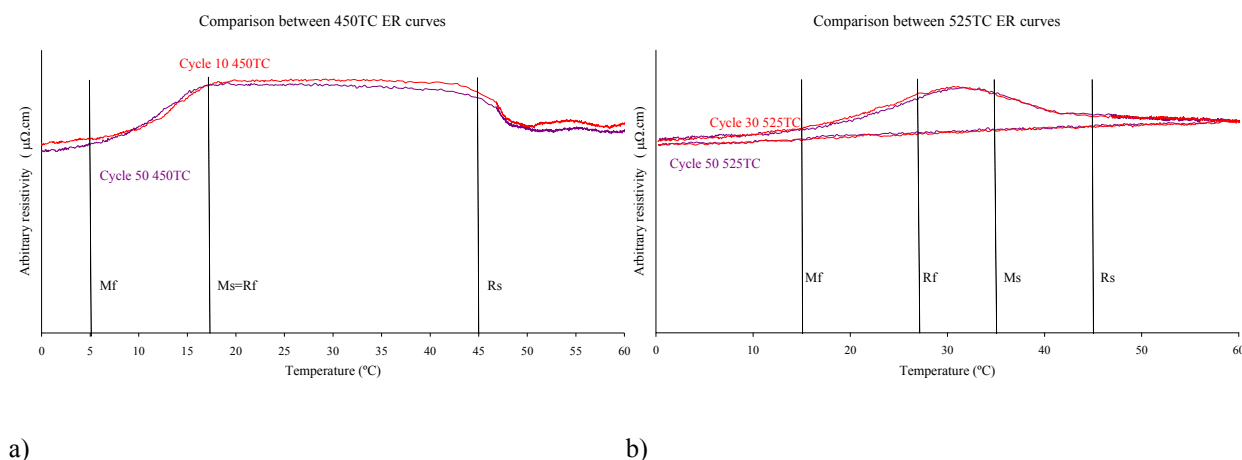


Figure 4.10 Different ER cycles for a) 450TC₅₀ and b) 525TC₅₀ samples.

From now, the number of thermal cycles at zero stress applied to 450, 475, 500 and 525 samples respectively are 8, 8, 12 and 25. These are their corresponding critical cycles. These samples are called 450TC, 475TC, 500TC, 525TC. The relationship between the application of a minimum number of thermal cycles at zero stress on the

wires and the possible improvement of the functional properties of these wires by this thermal cycling will be investigated in the next section. The analysis, then, will compare the functional properties of the samples thermally cycled at zero stress (450TC, 475TC, 500TC, 525TC) and the samples without thermal cycling (450, 475, 500, 525). Although the peak resistivity of 450TC₅₀ and 475TC₅₀ samples vary very slightly (figure 4.2) and all the results obtained since now indicate that thermal cycling at zero stress does not affect 450 and 475 samples, we found that their R_f temperature becomes stable further cycle 8 (figure 4.9). Therefore, 450 and 475 samples will be thermally cycled at zero stress during eight thermal cycles in order to find any difference between the functional properties of 450-475 samples and those of 450TC-475TC samples.

3.3 *Effect of thermal cycling on the stress-strain behaviour and on the apparent modulus*

It has been demonstrated that experimental determination of the modulus of elasticity of Ti-Ni SMA in conventional mechanical testing is dependent on a number of factors, including testing and previous thermal and mechanical treatment conditions of the specimen [LIU, 1998]. Measured values of the modulus of elasticity for near equiatomic Ni-Ti vary widely in the literature. Reported values of Young's modulus vary from 20 to 40 GPa for martensite, 20GPa for the R-phase [SIT, 2006] and from 40 to 90GPa for austenite [DUE, 1990], [SIT, 2006]. The martensite transformations, being a similar ordering condition and having a negligible volume change from the austenite, is expected to have a similar value for the modulus than that of the austenite. However, lower values of approximately one third of those of austenite have been measured. This is attributed to the high mobility of the twin boundaries, which renders the martensite vulnerable to deformation.

As seen, a significant difference between the values of the modulus for the 3 phases exists. Moreover, the modulus values are somewhat lower than expected, with the upper range being of the order of those aluminium and copper alloys. Near equiatomic Ti-Ni alloys, on the other hand, have ultimate strength similar to those of carbon steels and their Young's modulus is expected to be a similar order of that steels, which is around 200GPa. In addition, the variation of measurements is too large to be accounted for

experimental errors. The low consistency and poor reliability of the determination of elastic modulus by mechanical testing are believed to be due to the contribution of stress-induced martensitic transformation or martensite reorientation to the elastic deformation. The extra deformation associated to these processes during the elastic deformation causes the measurement of the elastic modulus to be lower than the true value. In addition, both, reorientation process and stress induced martensite are dependent on the heat treatment of the specimen and testing conditions [LIU, 1997] and [LIU, 1998].

As a consequence, as the measured values from the stress-strain curves are dependent on the testing conditions as well as specimen processing history, it is adopted the term **apparent modulus** instead modulus of elasticity, as proposed by [LIU, 1989].

<i>Sample</i>	$T < M_s$ (°C)	$R_f = M_s < T < R_s$ (°C)	$R_f < T < M_s = R_s$ (°C)	$R_s \leq T < A_f$ (°C)	$T > A_f$ (°C)
450	2; 8; 11; 15.5	19.5; 26; 32		40; 45; 50; 60; 70	82; 91; 97.5; 101
450TC	2; 8; 10.5; 15; 18	26; 32		40; 45; 50; 60	70; 80; 90; 99; 112
475	5; 11; 15; 20	25; 30; 35		40; 45; 50; 60; 70	80; 90; 100
475TC	5; 11; 14; 20	25; 30		40; 45; 50; 60; 70	80; 90; 100
500	15; 17; 19; 22; 25		36; 45	55; 60; 65; 70	80; 100
500TC	15; 20; 26	35; 45		55; 60; 65; 70	85; 100
525	10; 17; 20		23; 30; 40	50; 60; 65; 70; 80	90; 95
525TC	10; 20		30; 40	50; 60; 65; 70	80; 90; 95

Table 4.5 Selected temperatures for isothermal tension tests for all samples analyzed (°C).

A complete set of isothermal tension tests within the transformation temperature range were performed to compare the mechanical behaviour of the thermally cycled wires and the non-cycled ones. Table 4.5 presents the isothermal test temperatures for each sample. The temperature range is according to their transformation temperatures values (tables 4.3 and 4.4). A series of stress-strain profiles are obtained from

isothermal tension tests performed on the non-thermally and thermally samples. All isothermal tests were performed by imposing a strain, which ensured that a complete martensitic transformation took place (and that all the constitutive parameters could be obtained). The apparent modulus for each phase of the alloy (E_A , E_R and E_M) was measured from these stress-strain profiles. E_S was calculated from the slope of the curve corresponding to the deformation of the detwinned martensite for each test temperature.

3.3.1 Martensite state results

An example of strain-stress profiles at the fully martensite state (B19') from which E_M was obtained is presented in figures 4.11, which show the stress-strain curves at temperature $T < M_S$ for all samples. Each figure shows the stress-strain curve for sample non-thermally cycled and the one for the same sample but thermally cycled. Each stress-strain curve can be divided into three parts [LIU, 2000]. For samples 450, 475, 450TC and 475TC (figures 4.11a and 4.11b), the first part corresponds to the elastic deformation of B19', where the slope for the non-cycled sample is equal to the slope for sample thermally cycled and, thus, the apparent modulus for twinned martensite is similar for both samples. The obtained E_M average values for tension tests at $T < M_S$ for the 450TC thermally cycled sample is $E_{M450TC} = 20503 \text{ MPa}$, and for the non-thermally cycled sample it is $E_{M450} = 20808 \text{ MPa}$. The obtained E_M average for the 475TC thermally cycled sample is $E_{M475TC} = 20410 \text{ MPa}$, and for the non-thermally cycled sample it is $E_{M475} = 20433 \text{ MPa}$. The second part shows the deformation process by martensite orientation with a Lüders-like behaviour over a stress plateau, with equal values of stress plateau for samples 450-450TC and 475-475TC. In fact, for samples 475-475TC the value is the same for both (114 MPa). The Lüders-like deformation process finished at a tensile strain very slightly higher for sample 450 (5.19%) than for sample 450TC (4.94%). For samples 475 and 475TC the recoverable strain are practically the same for both (5.28% and 5.38% respectively).

The final deformation process (third part of the stress-strain curve) developed into a uniform stage with a rapid increase in the stress, showing the deformation of the fully oriented martensite, from which the apparent modulus for the detwinned martensite E_S is obtained. The average values of E_S obtained at $T < M_S$ are for samples thermally

cycled and non-thermally cycled, $E_{S\text{fromM450TC}} = 13407\text{MPa}$ and $E_{S\text{fromM450}} = 13490\text{MPa}$, and for the 475 samples they are $E_{S\text{fromM475}} = 12097\text{MPa}$ and $E_{S\text{fromM475TC}} = 13149\text{MPa}$.

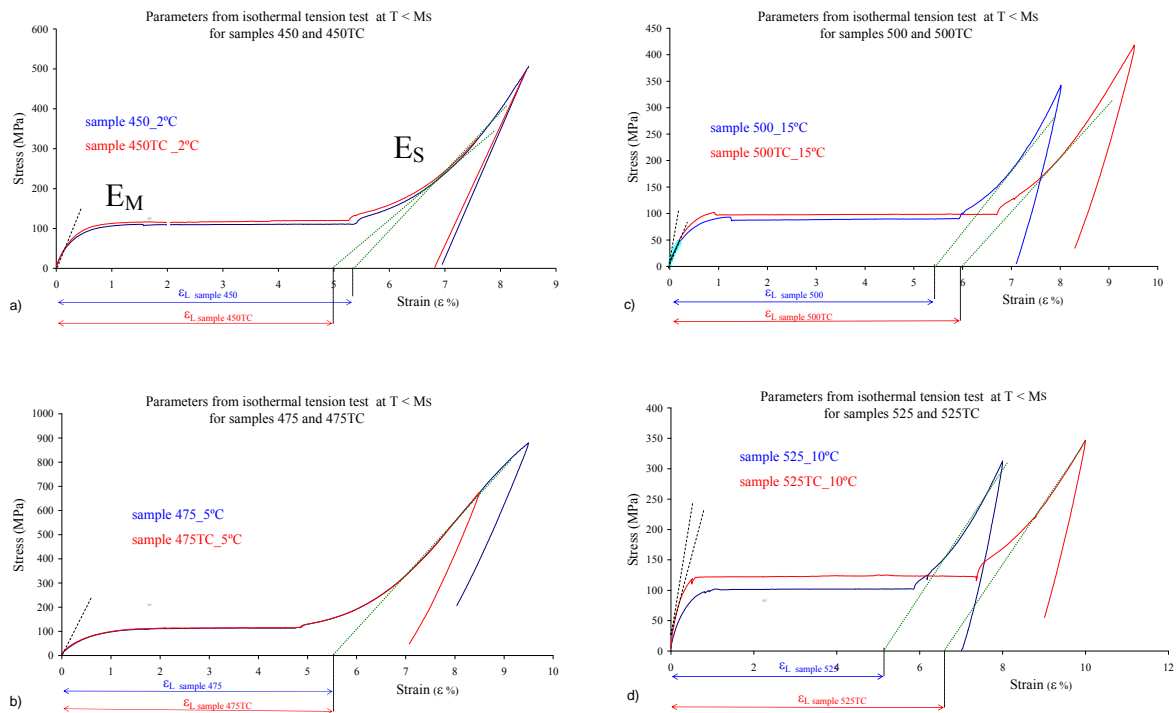


Figure 4.11 Stress-strain curves at full martensite state, comparing the non-thermally with thermally cycled behaviours for samples a) 450-450TC, b) 475-475TC, c) 500-500TC and d) 525-525TC. The slopes of the apparent modulus and the residual strains are indicated on each sample.

For samples 500-500TC and 525-525TC, the results are most interesting (figures 4.11c and 4.11d). For these samples, the first part of their curves corresponds to the elastic deformation of martensite, where the slopes for the non-cycled samples 500 and 525 are less pronounced than the slopes for samples 500TC and 525TC. The obtained E_M average values for tension tests at $T < M_s$ for the thermally cycled samples are $E_{M500TC} = 20116\text{MPa}$ and $E_{M525TC} = 22672\text{MPa}$. For the non-thermally cycled samples they are $E_{M500} = 19566\text{MPa}$ and $E_{M525} = 19303\text{MPa}$. The second part shows higher values of stress plateau for 500TC (100MPa) and 525TC (120MPa) samples than for 500 (94MPa) and 525 (88MPa) samples. At the onset of the Lüders-like deformation process, all samples show a stress drop. The Lüders-like deformation process finished at

tensile strains of 5.87% and 6.04% for samples 500TC and 525TC respectively, and 5.21% and 5.38% for samples 500 and 525 respectively. The average values of E_S obtained at $T < M_S$ are for non-thermally cycled samples $E_{S\text{from}M500}=10595\text{MPa}$ and $E_{S\text{from}M525}=7259\text{MPa}$. For thermally cycled samples they are $E_{S\text{from}M500\text{TC}}=11266\text{MPa}$ and $E_{S\text{from}M525\text{TC}}=8937\text{MPa}$.

3.3.2 R-phase state results

The samples can be divided depending on the heat treatment temperature as reaching the R-phase temperature. According to table 4.5, for 450-450TC, 475-475TC and 500TC samples, the test temperature range is $R_f=M_S < T < R_S$; for samples 500, 525 and 525TC is $R_f < T < R_S=M_S$. Therefore, the state of 450-450TC, 475-475TC and 500TC samples at the beginning of the test is full R-phase (see figures 4.3 to 4.5). However, the composition of 500, 525 and 525TC samples is a mixture of R-phase and martensite with low levels of R-phase. Therefore, the samples should be treated separately depending on their heat treatment temperature.

Samples 450 and 475 have a stress-strain curve with double plateau [LIN, 1981], [MIY, 1986]b, [SHA, 1995], [TOB, 1996] [SIT, 2006] and [DUE, 2006]. We use sample 475 as an example to explain the particular R-phase stress-strain behaviour. Figure 4.12 illustrates an enlarged portion of the initial state of the strain–stress curves at full R-phase state for sample 475. At first glance, the first part involves the elastic deformation of the R-phase. The plateau observed after is not a stress-induced plateau, but rather an R-phase reorientation plateau. We know this, because if R-phase was stress induced from the B2 phase, the plateau would increase in height with temperature (as seen in figure 4.12).

Between 20 and 35°C, both, R-phase re-orientation plateau and martensite plateau are developed during tension test. The R-phase reorientation plateau increases in height as temperature is decreased, even while the subsequent martensite plateau is increasing in height with temperature (as shows figure 4.12). As temperature is increased, the R-phase plateau becomes shorter and less pronounced. Based on the continuously changing rhomboidal angle and increased distortion during cooling [SIT, 2006], greater strain can be accommodated by rearranging the R-phase variants: the larger and

pronounced plateau should correspond when the R-phase is fully formed in the sample, as show figure 4.12 for sample tested at 20°C. The subsequent martensite plateau is increasing in height with temperature, because twin movement is easier when there is more thermal energy in the structure [DUE, 2006].

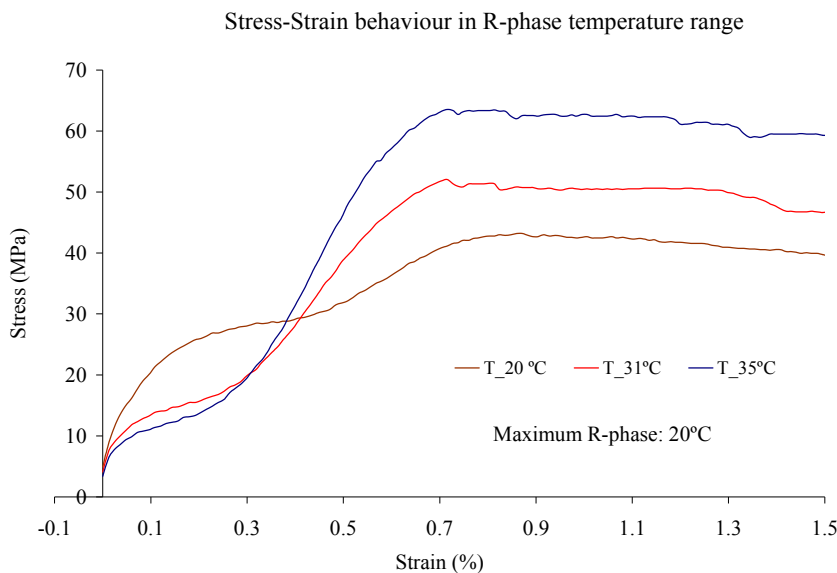


Figure 4.12 The particular R-phase stress-state behaviour for sample 475, where two plateaus are developed: the first one corresponds to the reorientation of the R-phase. The second one corresponds to the stress-induced martensite from R-phase, which increases with the temperature.

Relating the stress-strain values obtained for our samples heat-treated under 500°C, figure 4.13 presents the stress-strain curves obtained for thermally and non-thermally cycled samples 450-450TC and 475-475TC at initial R-phase state. Each curve can be divided into 5 parts.

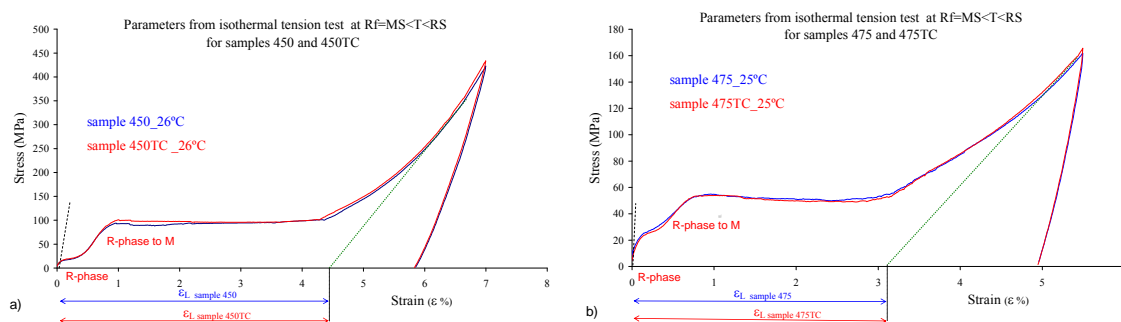


Figure 4.13 Stress-strain responses for a) 450-450TC and b) 475-475TC samples at full R-phase state.

The first part involves the elastic deformation of the R-phase, where it was found that the slopes are practically equal for thermally cycled and non-thermally cycled samples. This behaviour is reproduced in each test at temperatures between $R_f = M_S < T < R_S$ and only for these samples. The values of E_R obtained for the 450 samples ($E_{R450} = 19202 \text{ MPa}$ and $E_{R450TC} = 19735 \text{ MPa}$) and for 475 samples ($E_{R475} = 19757 \text{ MPa}$ and $E_{R475TC} = 19684 \text{ MPa}$) are very similar. After the reorientation of the R-phase (second step) a stress induced martensite is generated (third step), and then a second plateau is formed (fourth part). Finally, the further detwinning of the martensite occurs and the average value of E_S is obtained (fifth step). For 450 samples, the average values for the apparent modulus are $E_{S\text{from}R450} = 9979 \text{ MPa}$ and $E_{S\text{from}R450TC} = 9754 \text{ MPa}$. For 475 samples they are $E_{S\text{from}R475} = 7341 \text{ MPa}$ and $E_{S\text{from}R475TC} = 7638 \text{ MPa}$.

Figures 4.14 present the stress-strain results for thermally and non-thermally cycled samples heat-treated over 500°C . For sample 500 non-thermally cycled, the initial state of the samples at this test temperature ($R_f < T < M_S = R_S$) is a mixture of R-phase and martensite phase (see figure 4.5) However, 500TC sample presents an initial full R-phase state at these test temperature. Nevertheless, both profiles present similar behaviour; both curves do not present the double plateau, suggesting that the quantity of the R-phase developed by 500TC sample is not enough to promote a stress-strain curve with double plateau. Therefore, the curves showed in figures 4.14 can be divided into three parts [NG, 2006]. The first part involves the elastic deformation of the R-phase, where it was found that for sample 500TC the slope is more pronounced than for sample 500 (figure 4.14a). This behaviour is reproduced in each test at temperatures between $R_f < T < M_S = R_S$. Consequently, considerably higher values of E_R were obtained for the thermally cycled samples ($E_{R500TC} = 24139 \text{ MPa}$) than for the 500 samples ($E_{R500} = 21947 \text{ MPa}$). Then, after the stress-drop, the stress plateau indicating the $R \rightarrow B19'$ transformation is developed (second part). As shown in figure 4.14a, thermally cycled sample 500TC presents higher values for the stress plateau (102 MPa) and higher values of strain at the end of the stress plateau (6.3%) than sample 500 non-thermally cycled one (63.5 MPa and 5.6%). Finally, further detwinning of the martensite occurs and the average value of E_S is obtained. For the non-thermally cycled samples the average value is $E_{S\text{from}R500} = 7793 \text{ MPa}$ and for thermally cycled samples it is $E_{S\text{from}R500TC} = 11705 \text{ MPa}$.

Figure 4.14b shows that 525 and 525TC samples follow similar behaviour at this

temperature range ($R_f < T < M_s = R_s$) than samples 500. The difference between these samples 525-525TC and the 450-450TC, 475-475TC and 500TC samples is that 525-525TC samples have at this range of temperatures, a mixture of R-phase plus martensite before and after thermal cycling (see figures 4.6). For 525 samples, minor values of E_R are obtained ($E_{R525} = 19462 \text{ MPa}$) than for 525TC samples ($E_{R525TC} = 21318 \text{ MPa}$). Moreover, the thermally cycled sample 525TC presents higher values for the stress plateau (96 MPa), than the non-thermally cycled one (86 MPa). However, higher values of strain at the end of the stress plateau for sample 525 (6.2%) than for sample 525TC (5.2%) are found. The average value of E_S is little higher for thermally cycled samples: for non-thermally cycled samples the average value is $E_{S \text{ from } R525} = 6584 \text{ MPa}$ and for thermally cycled samples it is $E_{S \text{ from } R525TC} = 8709 \text{ MPa}$.

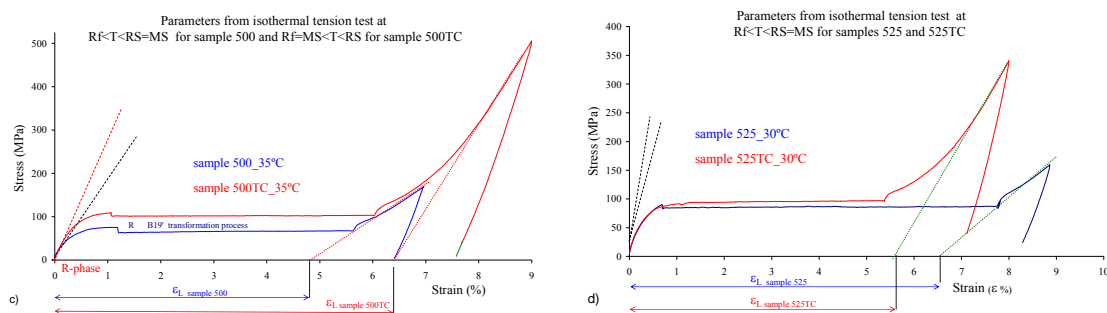


Figure 4.14 Stress-strain responses for a) 500-500TC and b) 525-525TC samples at R-phase plus martensite initial state.

3.3.3 Stress induced R-phase from austenite and R-phase initial state

With reference to $40^\circ\text{C} < T < 55^\circ\text{C}$ temperature test results, which are within the $R_s < T < A_f$ temperature test range, the stress-strain behaviour of the 450-450TC and 475-475TC samples are very different of 500 and 525 stress-strain behaviour. For 450-450TC and 475-475TC, at this range of temperatures, the initial structure of these alloys is a mixture of austenite and R-phase. Their stress-strain responses are characterized in

three stress-strain steps, as seen in figure 4.15a: a critical stress value to transform austenite to R-phase (stress-induced R-phase), a critical stress value to transform R-phase to martensite and finally, a critical stress value to finish the detwinning process of the martensite. Samples heat-treated at $T \geq 500^\circ\text{C}$ do not present this stress-strain behaviour, suggesting that the quantity of R-phase present in the alloy is not sufficient to develop the above explained stress-strain response. Comparing the stress-strain behaviour of samples thermally cycled and non-thermally cycled, no significant changes are found (figures 4.15b and 4.15c). However, it is important to remark that samples 450-450TC present higher stress plateaus than samples 475-475TC at the same test temperatures (40°C in figures 4.15b and c).

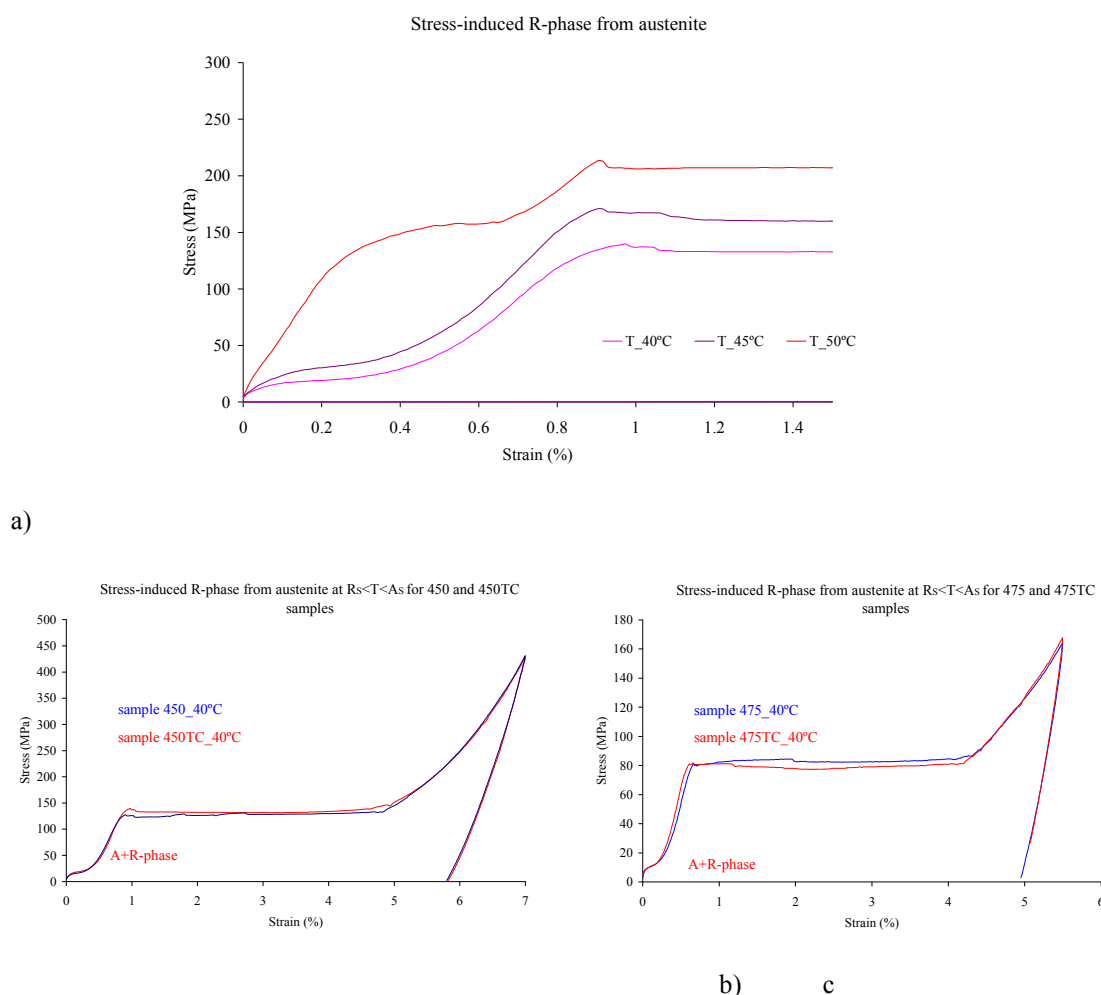


Figure 4.15 a) R-phase is stress induced from austenite: the stress plateau increases in height with temperature for sample 450, b) comparison between 450-450TC samples and c) comparison between 475-475TC samples.

3.3.4 Austenite state results

The stress-strain results at $T > A_f$ are different depending on the sample heat treatment temperature. All samples present an initial structure of full austenite at the beginning of the test. Figures 4.16 show the stress-strain profiles for samples 450-450TC and 475-475TC and figures 4.17 show those for the 500-500TC and 525-525TC samples. As seen, only 450-450TC and 475-475TC samples seem to develop the pseudoelastic behaviour. As an example of them, both samples 450-450TC (figure 4.16a) present the following explained stress-strain behaviour. The initial elastic deformation of austenite (B2) finishes with the transformation from B2 to martensite, and then, when the further detwinning of the martensite is finished, the reverse transformation begins (martensite-to-austenite) as the unloading of the sample begins, leading to recovery the strain. However, the fully transformation to austenite does not occur. The final segment of the unloading path does not reach zero macroscopic strain. Further tests at higher temperatures do not resolve this situation because a plastification process of the samples is observed. The same fact occurs for 475-475TC samples. The E_A average value for 450-450TC samples are similar to those for 475-475TC samples ($E_{A450} = 69014 \text{ MPa}$, $E_{A450TC} = 68006 \text{ MPa}$, $E_{A475} = 70185 \text{ MPa}$ and $E_{A475TC} = 68845 \text{ MPa}$).

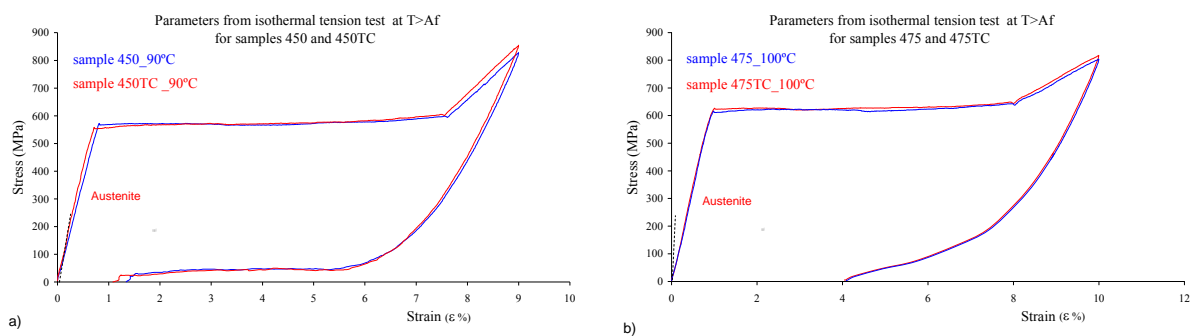


Figure 4.16 Stress-strain response at full austenitic state for samples a) 450-450TC and b) 475-475TC.

Figures 4.17 show an initial enlarged portion of the stress-strain profiles for 500-500TC and 525-525TC samples tested at 90°C , which also represents a full initial B2 state. The initial elastic deformation of B2 finishes with the transformation from

austenite to martensite. At this stage, it was found that the E_A average value obtained from tension test performed at $T > A_f$ was higher for sample 500 ($E_{A500} = 73809 \text{ MPa}$) than for sample 500TC ($E_{A500TC} = 70884 \text{ MPa}$). For samples 525, the E_A average value obtained from tension test performed at $T > A_f$ was higher for the thermally cycled sample 525TC ($E_{A525TC} = 72134 \text{ MPa}$) than for non-thermally cycled sample 525 ($E_{A525} = 69566 \text{ MPa}$).

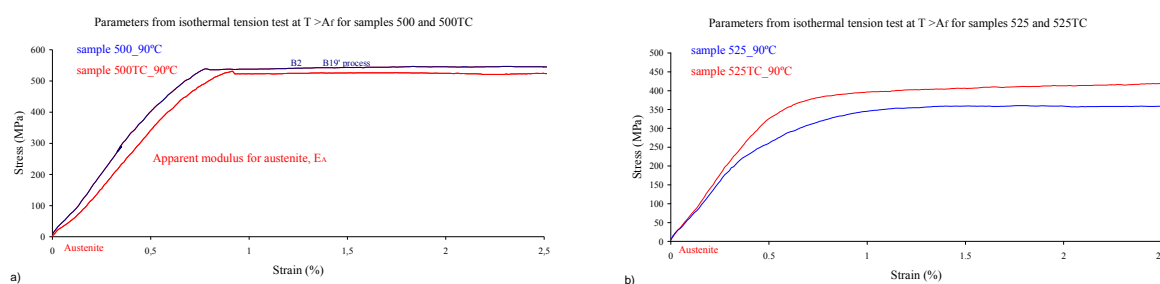


Figure 4.17 Stress-strain responses at full austenitic state for a) 500-500TC and b) 525-525TC samples.

3.3.5 Evolution of the apparent modulus with temperature

Figures 4.18a, b, c, and d plot the evolution of the apparent modulus through the full temperature range for the thermally cycled samples and for the non-thermally cycled samples. The influence of the heat treatment and thermal cycling at zero stress on the apparent modulus are discussed. For samples non-thermally cycled, the values of E_M , E_R , and E_A apparent modulus are represented by blue triangles. For samples thermally cycled, they are represented by red triangles. The apparent modulus for the detwinning path ($E_{S\text{from}M}$, $E_{S\text{from}R}$ and $E_{S\text{from}A}$) are represented by blue rhomboid for samples non-thermally cycled, and by red rhomboid for samples thermally cycled.

For all samples, the evolution of the apparent modulus for the loading part and the detwinning part of the stress-strain curve versus temperature are similar and independent of whether a prior thermal cycling is performed or not on the alloy as seen

in figures 4.18. The lowest value of the apparent modulus corresponds to martensitic (samples 500 and 525) or R-phase (samples 450 and 475). The apparent modulus reaches its maximum value for austenite phase. The relation between the E_A and E_M is around 3.5, value that is in agreement with values before published by [DUE, 1990], [LIU, 1998] and [SIT, 2006].

In addition, a range of temperatures exists from which it is possible to detect a change in the value of the apparent modulus that it is measuring. For all samples, the temperature range that occurs that change is compressed within $A_s \leq T < A_f$. We should note that the temperature at which begins the increase in the apparent modulus value coincides with the initial austenitic temperature (A_s) measured by the XRD diagrams (please, compare figures 4.3 to 4.6 with figures 4.18). In fact, the evolution of the apparent modulus versus temperature follows similar evolution than the austenite transformation in the wt% diagrams. Therefore, by increasing the test temperature from A_s , the value of the apparent modulus increases considerably as increases the austenite in the alloy.

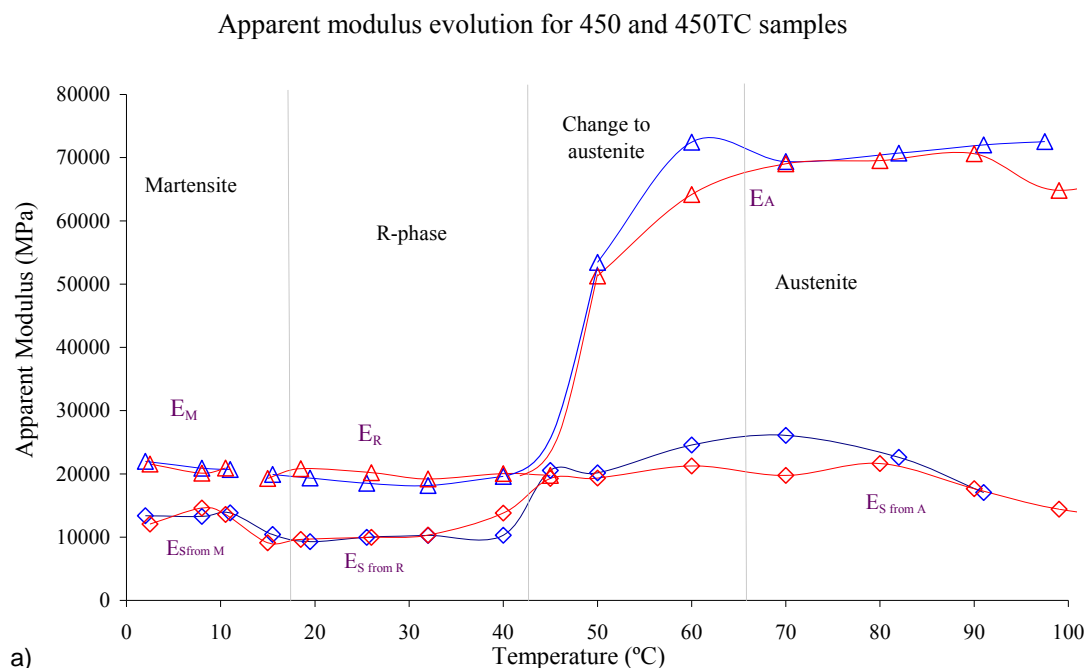
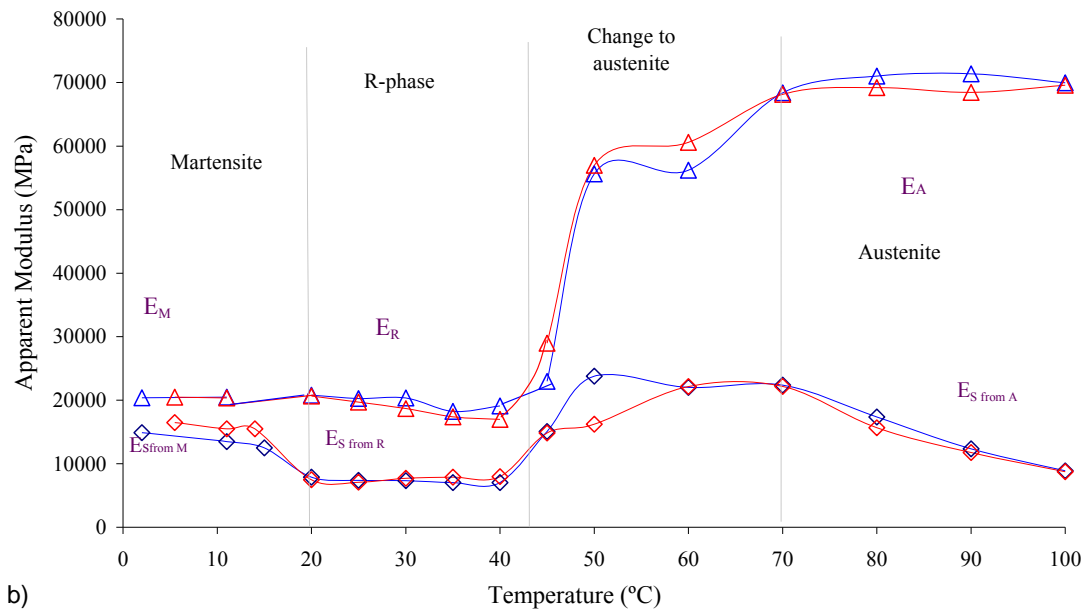


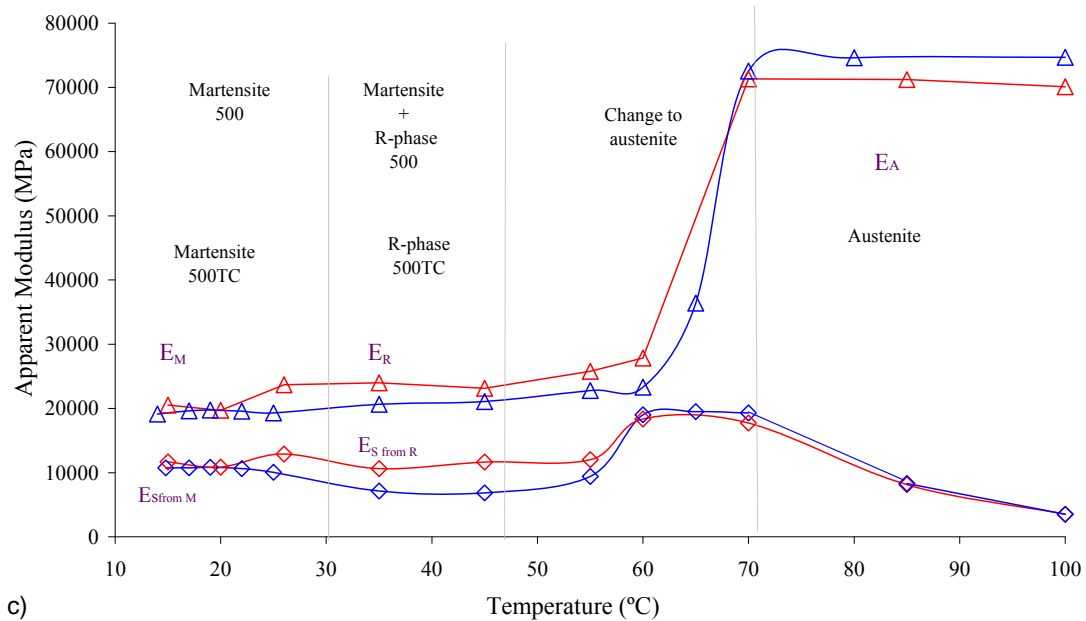
Figure 4.18a Evolution of martensite, R-phase, austenite and detwinned martensite apparent modulus versus temperature depending on the initial phase of the alloy for a) 450-450TC samples.

Apparent modulus evolution for 475 and 475TC samples



b)

Apparent modulus evolution for 500 and 500TC samples



c)

Figure 4.18b and c Evolution of martensite, R-phase, austenite and detwinned martensite apparent modulus versus temperature depending on the initial phase of the alloy for b) 475-475TC samples and c) 500-500TC samples.

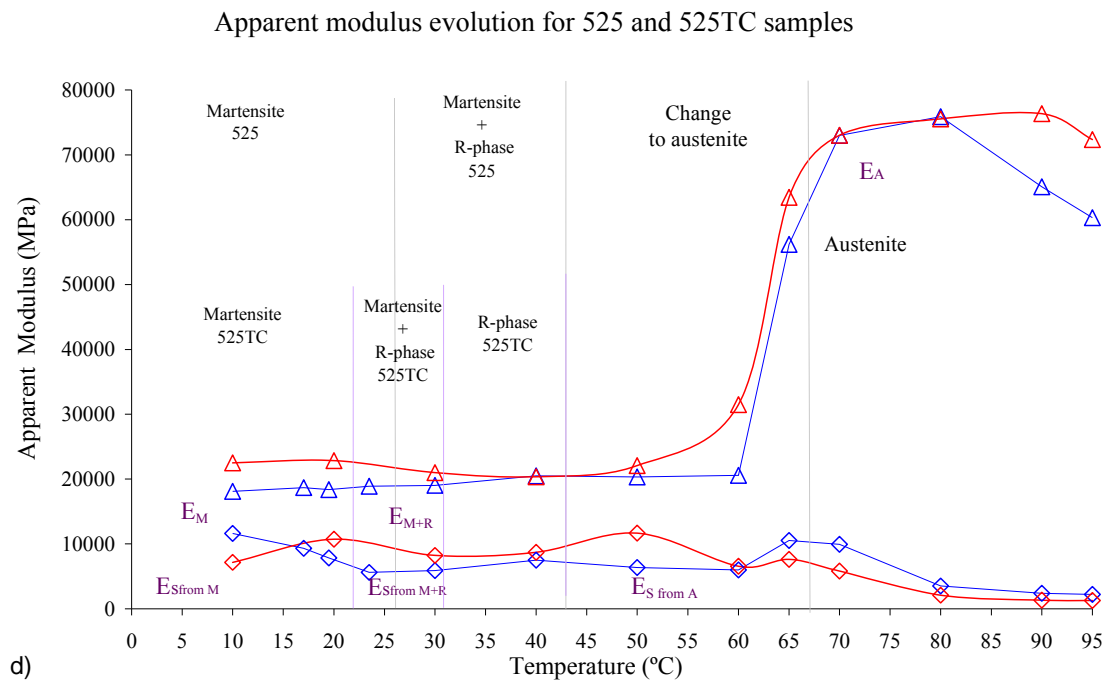


Figure 4.18d Evolution of martensite, R-phase, austenite and detwinned martensite apparent modulus versus temperature depending on the initial phase of the alloy for d) 525-525TC samples.

Taking into account the evolution of the apparent modulus with heat treatment temperature, we obtain that the values of E_M decrease slightly as increases heat treatment temperature. The higher is the heat treatment temperature, more complete is the mobility of the twin boundaries of the self-accommodated martensite. Therefore, an increase in the movement of the twin boundaries almost prohibits a pure elastic deformation of the martensite, making easy the contribution of martensite reorientation to the apparent elastic deformation.

Samples 450 and 475 present similar values for the apparent modulus for E_R . However, for this range of temperature (25-45°C) sample 500 present higher values of E_R than 450 and 475 samples. The reason is that sample 500 has a mixture of martensite and R-phase at this range of temperatures (25-40°C), according to figures 4.5 and 4.18c. Therefore, the measured apparent modulus of elasticity in this range of temperature has

a contribution of the two phases, martensite and R-phase, resulting in higher values of the apparent modulus for sample 500 than for samples 450 and 475.

Sample 525 maintains the value of the apparent modulus of martensite up to temperatures near of 40°C because the quantity of R-phase that this alloy has (figure 4.6) does not appreciably modify the value of the apparent modulus.

As seen in figures 4.18, the apparent modulus for the austenitic phase E_A slightly increases with increasing heat treatment temperature, reaching the maximum value of E_A for sample 500. As suggested by [LIU, 1998], the reason of this fact is the high homogenization of the matrix suffering by samples annealing near or over recrystallization temperature, which favours that the stress induced martensite transformation is only produced after the elastic deformation of the austenite. A homogenous matrix of austenite implies less martensite being formed during the initial stage of the deformation of the austenite, hence a higher apparent modulus of elasticity being measured. However, following this, higher values of E_A for sample 525 than for sample 500 are expected. The E_{A525} average value is lower than E_{A500} value. The reason may be the important reduction in the mechanical resistance with the increase in test temperature that samples 525 show.

Analyzing the evolution of the apparent modulus with thermal cycling at zero stress, we obtain that, for 450TC and 475TC samples, their E_M , E_R and E_A have not appreciable difference in value with the same modulus of the non-thermally cycled 450 and 475 samples. These results reinforce the suggested idea that thermal cycling at zero stress does not affect samples heat-treated at lower temperatures.

On the other hand, for 500TC and 525TC samples the values of their E_M and E_R modulus increase slightly with thermal cycling at zero stress, being the increase more important for the sample 525TC. These increases in E_M and E_R can be due to the transformation induced hardening through the repeating thermal stress free transformation cycles that these alloys may suffer for the martensite and R-phase state according to [LIN, 1994], [BRA, 2002] and [URB, 2010]c. Finally, analyzing the values of the apparent modulus at $T > A_f$ for non-thermally and thermally cycled 500-500TC and 525-525TC samples, the austenitic apparent modulus (E_A) decreases for samples 500TC thermally cycled and increases for 525TC samples (figures 4.18c and d). As seen in figure 4.17a, thermal cycling at zero stress promotes that the slope of the initial

part of the austenite stress-strain curve of sample 500TC can be less steep than that for sample 500. The introduction of dislocations by thermal cycling at zero stress in the sample 500TC can produce the loss of the initial homogeneity of the austenite matrix, promoting the softening of the austenite phase.

Conversely, for samples 525 and 525TC the E_A value is almost equal at temperatures near of 80°C. For sample 525, an increase in temperature (an increase of around 10°C) produces an important decrease in its E_A values, resulting in the softening of the austenite phase (figure 4.17b and figure 4.18d). A posterior increase in the alloy temperature results an indeed higher decrease in E_A . Thanks to thermal cycling at zero stress, sample 525TC does not suffer this rapid decrease in E_A (see figure 4.18d), maintaining the value of the apparent modulus of the austenite phase through the increase in temperature up to 90°C. That is, ten degrees more than sample 525.

Focusing on the last part of the stress-strain test, figures 4.18 plots the evolution of the apparent modulus for the detwinned martensite E_S versus temperature for samples thermally and non-thermally cycled (red and blue rhomboids respectively). First, it is worth noting that the values obtained for E_M , E_R , E_A are always higher than the E_S values for each test temperature. Following this, E_{SfromM} , E_{SfromR} , and E_{SfromA} values are found to decrease as increases the heat treatment temperature. This fact could have relation with the decrease in the critical stress for martensite reorientation as heat treatment temperature increases [LIU, 1999]c. As the same manner, a sample that has an increase in the critical stress for martensite reorientation due to thermal cycling at zero stress should present an increase in E_{SfromM} , E_{SfromR} , and E_{SfromA} . That is the fact that occurs in samples 500TC and 525TC, which present an increase in E_S respect to those of the non-thermally cycled samples 500 and 525 (figures 4.18c and d). However, samples 450TC and 475TC samples did not present any appreciative change in E_S respect to those of 450 and 475 respectively.

Consequently, thermal cycling at zero stress seems to optimise the alloy microstructure: the apparent modulus for martensite, R-phase and detwinned martensite are higher for the thermally cycled samples 500TC and 525TC than for the non-thermally cycled samples. These improvements are achieved without

permanent strain of the martensite phase. However, for samples 450 and 475TC no improvements seem to be achieved.

3.4 *Effect of thermal cycling on maximum residual strain*

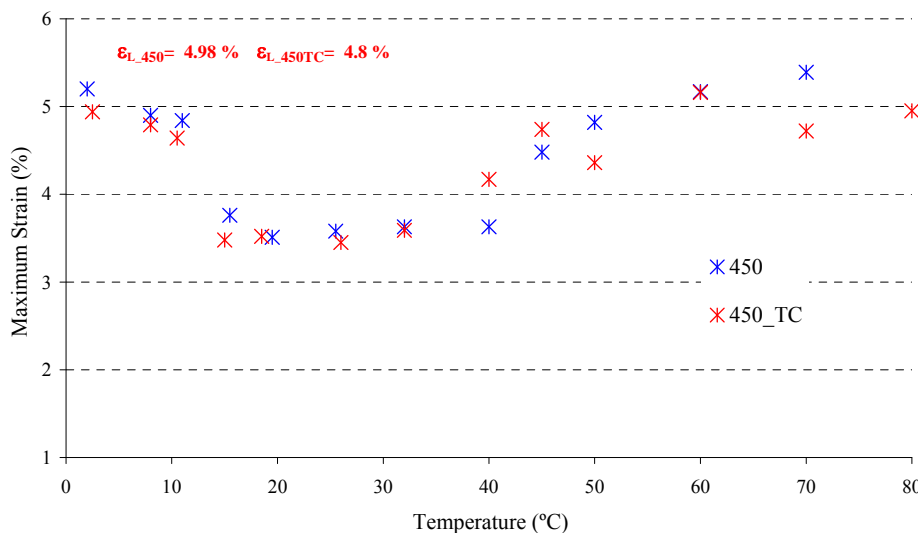
The maximum residual strain ε_L is obtained from the stress-strain curves for each temperature after unloading, and it is measured as the remaining deformation that can be totally recovered after heating the sample above A_f . The evolution of ε_L with temperature is illustrated in figures 4.19a, 4.19b, 4.20 and 4.21 for samples 450-450TC, 475-475TC, 500-500TC and 525-525TC respectively, where the obtained ε_L is represented by blue cross for samples non-thermally cycled and by red cross for samples thermally cycled. The average value of residual strain in martensite range is added in each figure, in order to exemplify the capacity of each sample to show the shape memory effect in function of the heat treatment temperature and the thermal cycling at zero stress. As seen in figures 4.19, 4.20 and 4.21 as the heat treatment temperature is increased, the residual strain increases as well: the higher the annealing temperature the more complete is the mobility of the twin boundaries and thus the shape memory effect.

The analysis of the effect of thermal cycling at zero stress is divided depending on the sample heat treatment temperature. The reason is the different results that present samples heat-treated over 500°C and those heat-treated at $T < 500^\circ\text{C}$.

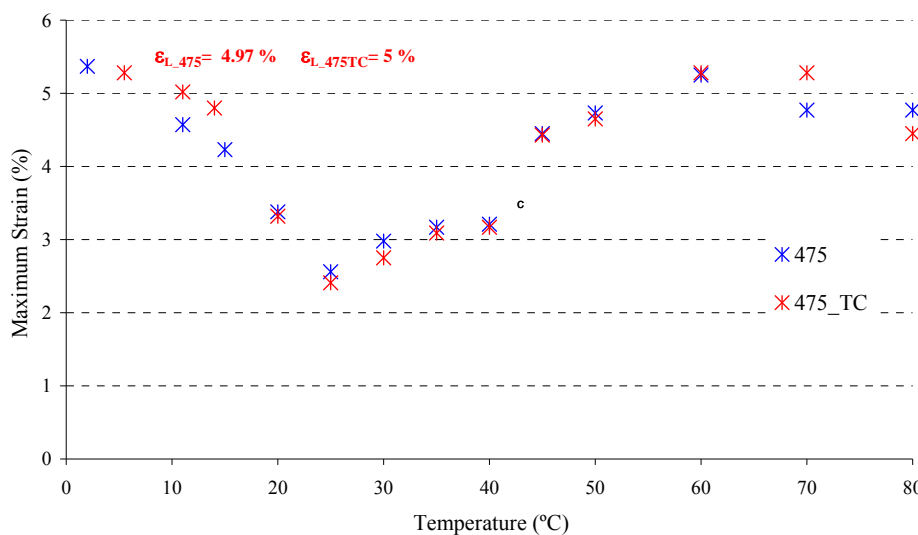
Figures 4.19a and b show that samples 450-450TC and 475-475TC have similar evolution of the residual strain with temperature and no influence of thermal cycling at zero stress on their shape memory effect is detected. All samples have similar ε_L at martensitic temperature range ($T < 18^\circ\text{C}$). The evolution of the ε_L with temperature shows that residual strain has the highest values when martensite range ($T < 18^\circ\text{C}$) or full austenitic range ($T \cong 65^\circ\text{C}$) is reached (near of 5%). The minimum values correspond to values where the R-phase is full developed ($T \cong 25^\circ\text{C}$). Figure 4.19a shows that samples 450 have better ε_L (3.51%) than samples 475 (2.56%) in R-phase range. Moreover, as figures 4.10 show, the plateau strain is longer for the 450 samples, giving better

recovery properties for these samples 450. On the other hand, for temperatures $T > 80^\circ\text{C}$ these sample show a near superelasticity behaviour.

Evolution of the Residual Strain with Temperature



a)



b)

Figure 4.19 Maximum residual strains for a) 450-450TC and b) 475-475TC samples.

Comparing the evolution of ε_L for samples 500 and 500TC, figure 4.20 shows that sample 500TC has a higher ε_L than sample 500 until $T \cong 60^\circ\text{C}$ is reached. The decrease in ε_L that sample 500 shows at temperatures between $25^\circ < T < 55^\circ\text{C}$, sample 500TC does not present. Inside this range, sample 500 presents a mixture of martensite and R-phase, fitting the minimum value of the residual strain with the maximum distribution of R-phase in the alloy (35°C). On the other hand, not only 500TC samples show a longer detwinning process than 500 samples and this behaviour is repeated in each isothermal tension test performed under $T < 60^\circ\text{C}$, but also samples 500TC present a well separate transformation path on cooling (figure 4.5c). Both facts suggest that, the hardening process and the modification of the phase transformation behaviour due to thermal cycling at zero stress cause the increase in ε_L , thus improving the shape memory effect for this sample 500TC. Finally, as the temperature increases, the austenite phase increases in the alloy, and the values for both specimens at $T \cong 60^\circ\text{C}$ become similar. Outside this range ($T > 80^\circ\text{C}$), this parameter is not constant but a function of temperature.

However, for 525 and 525TC samples (figure 4.21) the evolution of the residual strain with temperature is a little different from the others samples analyzed. These 525 and 525TC samples do not present a decrease in the residual strain between $20^\circ < T < 45^\circ\text{C}$ as did 450, 450TC, 475, 475TC and 500 samples. In fact, samples 525 present a slightly increase in ε_L during the increase in temperature. ε_L starts to decrease as the temperature reaches or overpass the austenite condition. The very little quantity of R-phase that has this sample 525 seems to avoid the decrease in residual strain that those samples with well-developed R-phase have (as occurs in 450 and 475 samples) or that those samples that show a mixture of R-phase plus martensite (as occurs in 500 samples). The influence of thermal cycling at zero stress on 525 samples could reinforce this assumption: the cycling produces a reduction in the values of ε_L for sample 525TC (excepting for full martensite state), as seen in figure 4.21. For sample 525TC, the quantity of R-phase is increased but the transformation process is not well-separated (figure 4.6c). As increasing the quantity of R-phase, the initial condition of the alloy is not as pure martensite as for 525 sample is, resulting in a decrease in ε_L values for

sample 525TC. In any case, the shape memory effect (martensite condition) of both, 525 and 525TC samples, is the highest of all samples analyzed.

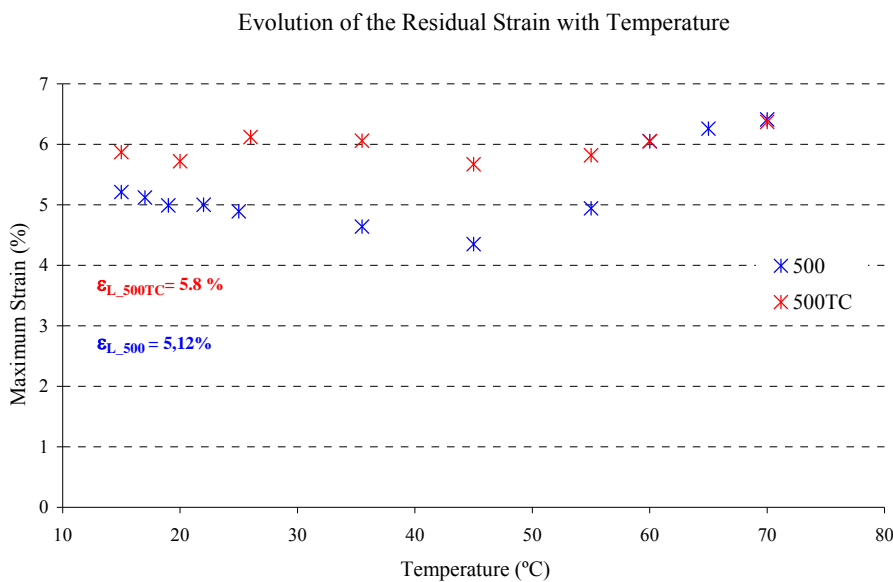


Figure 4.20 Maximum residual strains for 500 and 500TC samples.

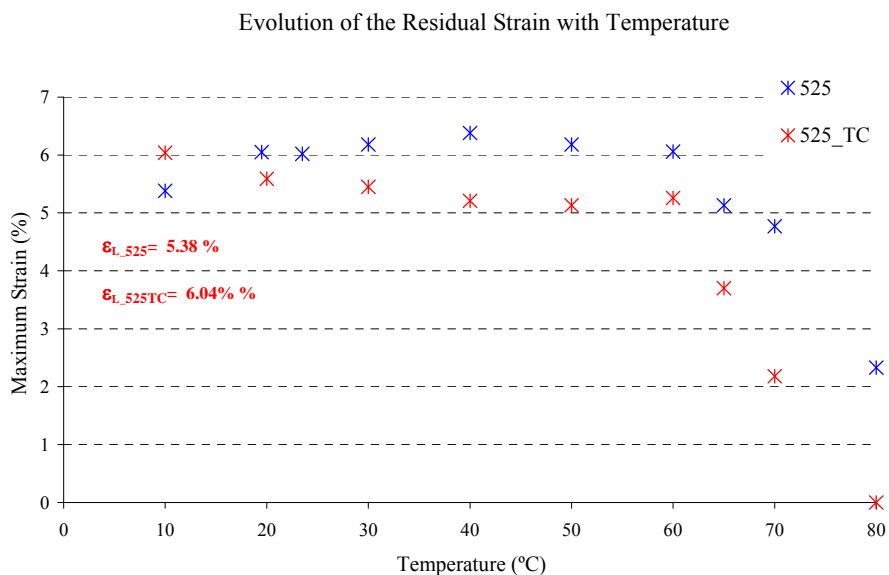


Figure 4.21 Maximum residual strains for 525 and 525TC samples.

3.5 *Effect of thermal cycling on the overall thermomechanical behaviour of Ni-Ti SMA wires: critical stress-temperature diagrams*

To compare the mechanical behaviour of the thermally cycled samples and that of the non-cycled samples, figures 4.22 and 4.23 show the complete critical stress-temperature diagrams for the non-cycled samples and for the thermally cycled samples. The critical stress-temperature diagram shows the evolution of the critical transformation stress required to induce martensitic transformation versus temperature depending on the initial state of the alloy: σ_S^{CR} , σ_F^{CR} and σ_{RtoMS}^{CR} and σ_{RtoMF}^{CR} . The stress influence coefficients that represent the relationship between stress and temperature ($C=d\sigma/dT$) for each phase are plotted. The stress influence coefficients are the stress temperature coefficient C_M for the beginning and end of the martensite transformation; C_R for the beginning and end of the R-phase transformation and C_A for the beginning and end of the austenite transformation. Moreover, we should establish others coefficients to difference the special transformations that has the SMA alloy depending of its initial state (R plus M, A plus R). These stress temperature coefficients are $C_{M\text{ from }R}$ for the transformation to martensite from R-phase and $C_{A\text{ to }R}$ for the transformation from austenite to R-phase.

The full critical stress-temperature diagrams were deduced from the stress-strain responses from isothermal tension tests (see table 4.5) and from constant stress test at selected stress values (table 4.6 shows the selected constant stress used). The reason to perform those constant stress tests is to complete the critical stress-temperature diagram because isothermal tension tests do not allow the extraction of stress-temperature dependence values higher than $T > A_f$ in samples 475-475TC, 500-500TC and 525-525TC. These alloys have to show the pseudoelastic behaviour at these temperatures, however, a process of plastic deformation of these alloys prior to the transformation process was obtained. Therefore, a complete set of constant stress tests are conducted within different ranges of stresses and by varying the temperature from lower than M_f to higher than A_f . Before each constant stress test, the SMA wire was at full martensitic state to avoid mixtures of phases at the beginning of the test that could interfere with the results. The results are already included in their respective final critical stress diagrams.

<i>Sample</i>	<i>Constant stress applied</i> (MPa)
475	103.7; 116.7; 128.6
475TC	103.7; 116.7; 128.6
500	78; 91; 103.7; 116.7; 128.6
500TC	78; 91; 103.7; 116.7; 128.6
525	91.9; 103.7; 128.6
525TC	91.9; 103.7; 128.6

Table 4.6 Constant Stress values for samples 475-475TC, 500-500TC, and 525-525TC.

The legend to interpret the symbols of the critical stress–temperature diagrams is:

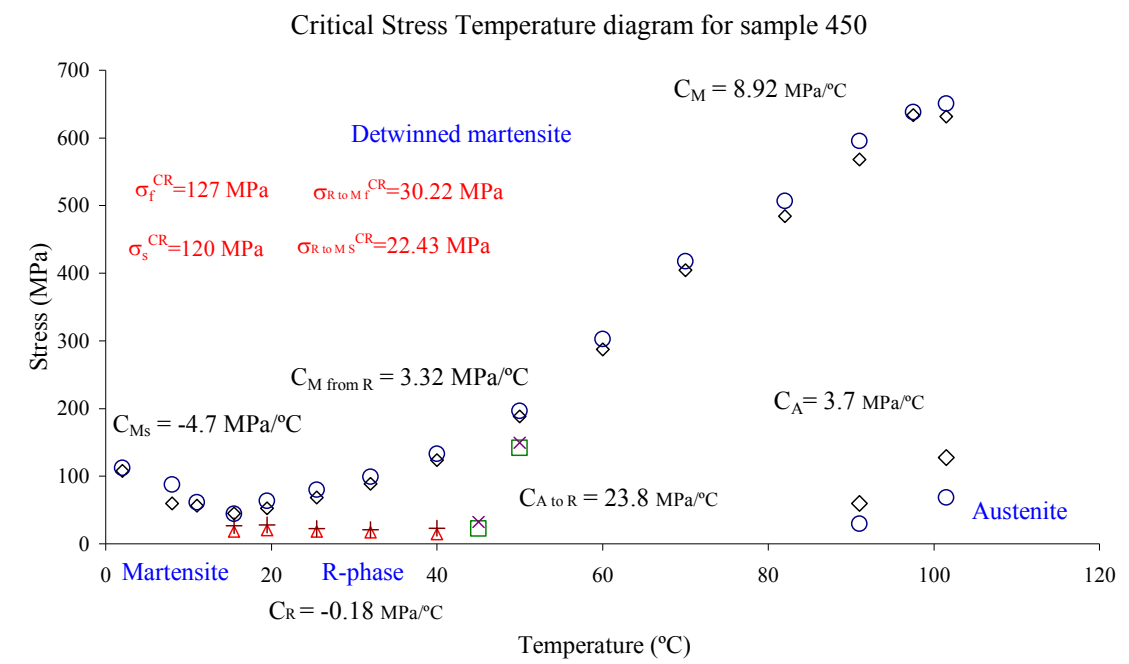
- Stress to finish transformation process from Martensite, R-phase or Austenite to detwinned martensite
- ◇ Stress to start transformation process from Martensite, R-phase or Austenite to detwinned martensite
- Stress to start transformation process from Austenite to R-phase
- × Stress to finish transformation process from Austenite to R-phase
- △ Stress to start transformation process from R-phase to Martensite
- ⊕ Stress to finish transformation process from R-phase to Martensite

Figures 4.22 show for 450-450TC and 475-475TC samples a similar evolution for the critical stress to induce martensite transformation with temperature: up to temperatures $T < R_f$ ($T \cong 20^\circ\text{C}$), the relationship between stress and temperature is no longer constant, as Tanaka, Liang–Rogers and Brinson models predicted ([TAN, 1986], [LIA, 1990] and [BRI, 1993]). In fact, critical stress values tends to increase as the temperature decreases; regardless of whether the sample has been thermally cycled or not, in accordance with De la Flor's model [DFO, 2006]. Therefore, the stress temperature coefficients (C_{MS}) delimiting the detwinned martensite region are negatives for the non-cycled sample and for the thermally cycled sample (see figures 4.22). For temperatures between $R_f < T < 90^\circ\text{C}$ the evolution of the critical stress to induce martensite transformation values is linear, and follows the Clausius-Clapeyron equation.

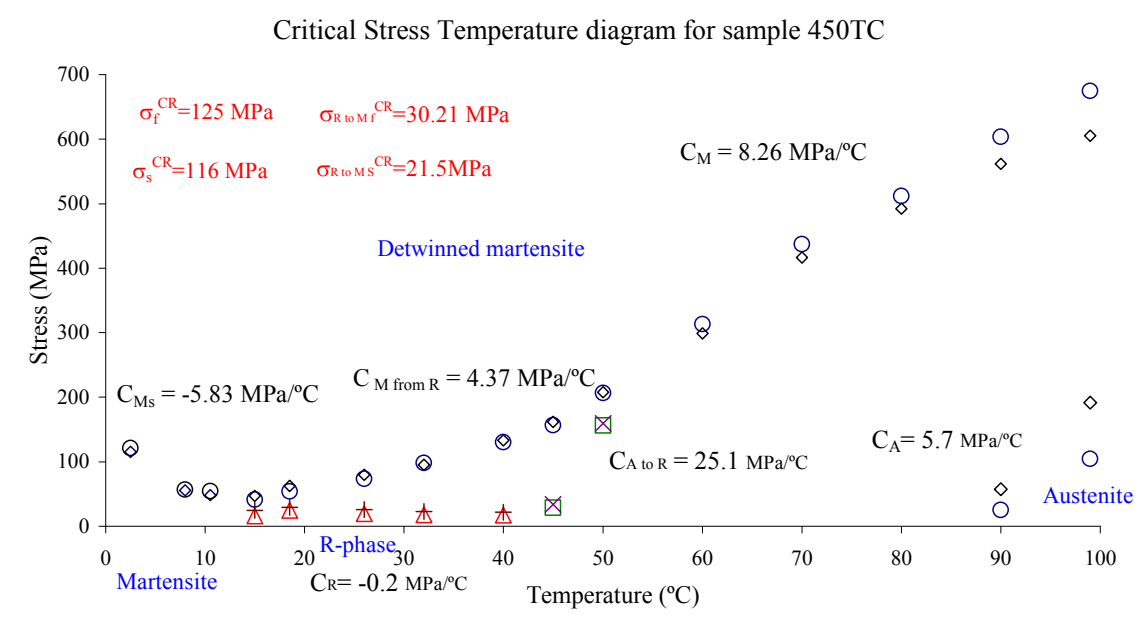
However, two different linear regions can be detected for all samples: $R_f < T < 50^\circ\text{C}$ and $50 < T < 90^\circ\text{C}$. The stress temperature coefficients are divided depending on the origin of the martensite. The influence of the stress with temperature is notably higher for the stress-induced martensite formed from austenite (C_M) than the stress-induced martensite formed from R-phase ($C_{M \text{ from R}}$).

The evolution of the critical stress to induce martensite transformation from R-phase is again no longer constant for all samples (σ_{RtoMS}^{CR} and σ_{RtoMF}^{CR}): critical stress values tends to increase as the temperature decreases; regardless of whether the sample has been thermally cycled or not. The stress-temperature coefficient for the R-phase formed from austenite has the highest values for all samples ($C_{R \text{ from A}}$), and the values found are in agreement with those found by [MIY, 1988], [TOB, 1994] and [SIT, 2006].

Focusing the analysis on the values of the critical stresses for samples 450 and 450TC (figures 4.22a and 4.22b), and initially focusing the analysis on the martensitic range ($T < M_s = R_f$), no appreciably difference can be observed between thermally cycled sample 450TC and non-thermally cycled sample 450. In fact, both present almost the same critical stresses for the initial and final values for martensite transformation (σ_S^{CR} , σ_F^{CR}).

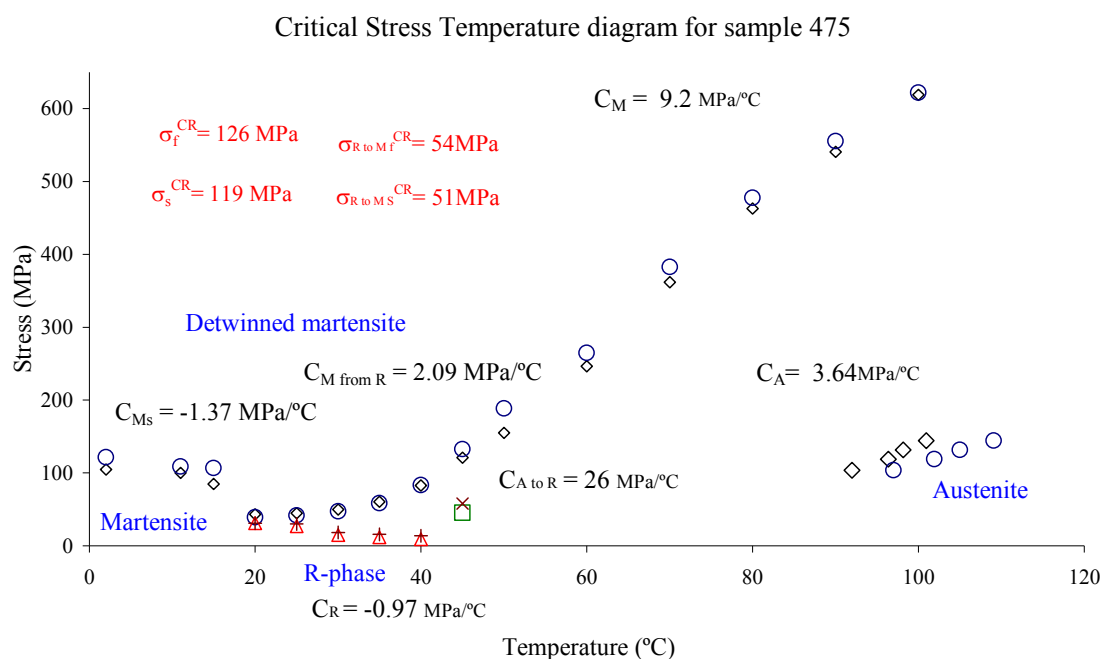


a)

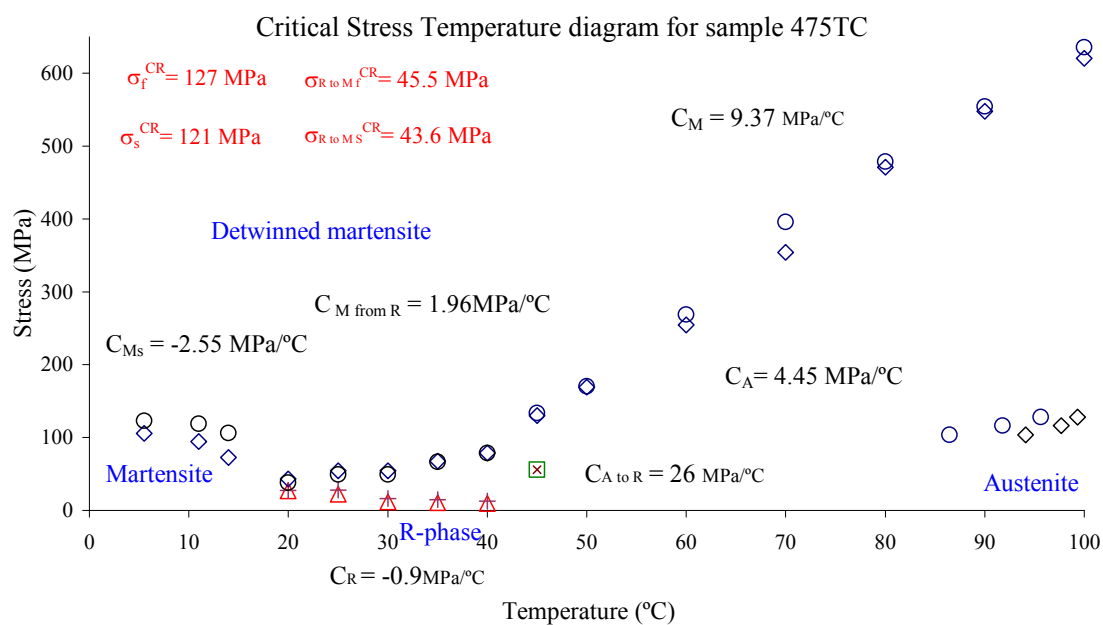


b)

Figure 4.22a and b Critical Stress Temperature diagram for a) 450 sample, b) 450TC sample.



c)

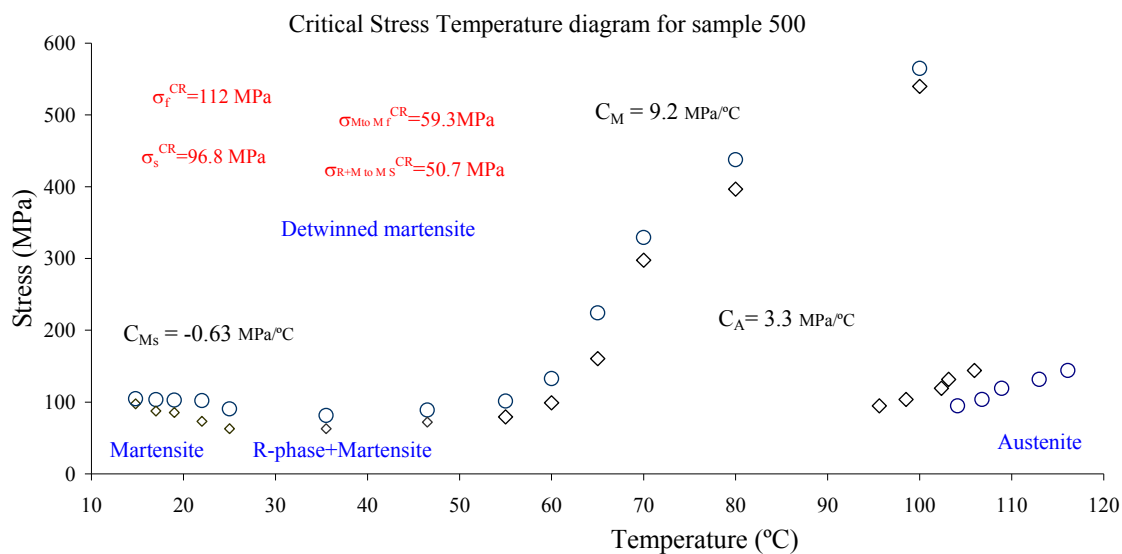


d)

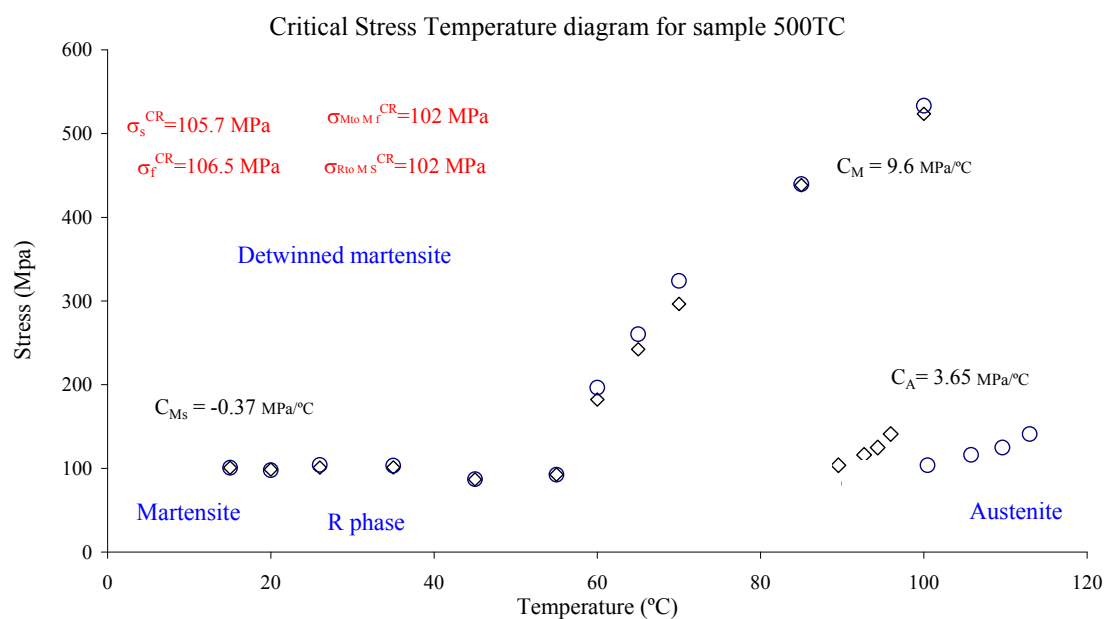
Figure 4.22c and d Critical Stress Temperature diagram for c) 475 sample and d) 475TC sample.

Same situation occurs for the R-phase temperature range ($R_f = M_s < T < 40^\circ\text{C}$), where by increasing the temperature the transformation process is performed in two steps (figure 4.13, σ_{RtoMS}^{CR} and σ_{RtoMF}^{CR}), presenting the thermally cycled sample similar values of the critical transformation stress required to induce martensite from R-phase than the 450 samples. Raising the temperature ten degrees ($40 < T < 50^\circ\text{C}$), the initial structure of the samples 450 and 450TC is a mixture of austenite and R-phase (see figure 4.3). Then, the transformation process is performed in three steps, as show in figure 4.15: a critical stress value to transform austenite to R-phase, a critical stress value to transform R-phase to martensite and a critical stress value to finish the detwinning process of martensite. By ever increasing the temperature, the initial structure of the alloy should be fully austenite, and the transformation process is pseudoelastic as illustrates figure 4.16. All tension test profiles for 450TC samples at $T > A_f$ showed similar values of the stress plateau than 450 samples, resulting in similar values of stress to start the martensitic to austenite transformation in the pseudoelastic process. Similar conclusions about the evolution of the critical stresses and the comparison between samples thermally cycled and non-thermally cycled can be done for 475-475TC samples, as can be deduced from figures 4.22c and d, excepting that samples 475-475TC do not present the pseudoelastic behaviour. Therefore, thermal cycling at zero stress (8 thermal cycles) does not affect the behaviour of the as-received alloy if it is heat treated under $T < 500^\circ\text{C}$, showing similar stress-temperature relationship the samples thermally cycled at zero stress than those samples non-thermally cycled.

Figures 4.23 show the evolution for the critical stress with temperature for 500 and 500TC samples (4.23a and 4.23b) and for 525 and 525TC samples (4.23c and 4.23d). Regarding the evolution of the stress with temperature for 500-500TC samples, the critical stress-temperature graphs clearly show that the relationship between critical stress and temperature is linear and follows the Clausius-Clapeyron equation for temperatures approximately between 55°C and 100°C . On the other hand, at temperatures $T < 55^\circ\text{C}$, the relationship between stress and temperature changes: for both samples 500-500TC the stress-temperature ratio is no longer constant, as occurs for samples 450-450TC and 475-475TC: critical stress tends to increase as the temperature decreases, regardless of whether the sample has been thermally cycled or not.

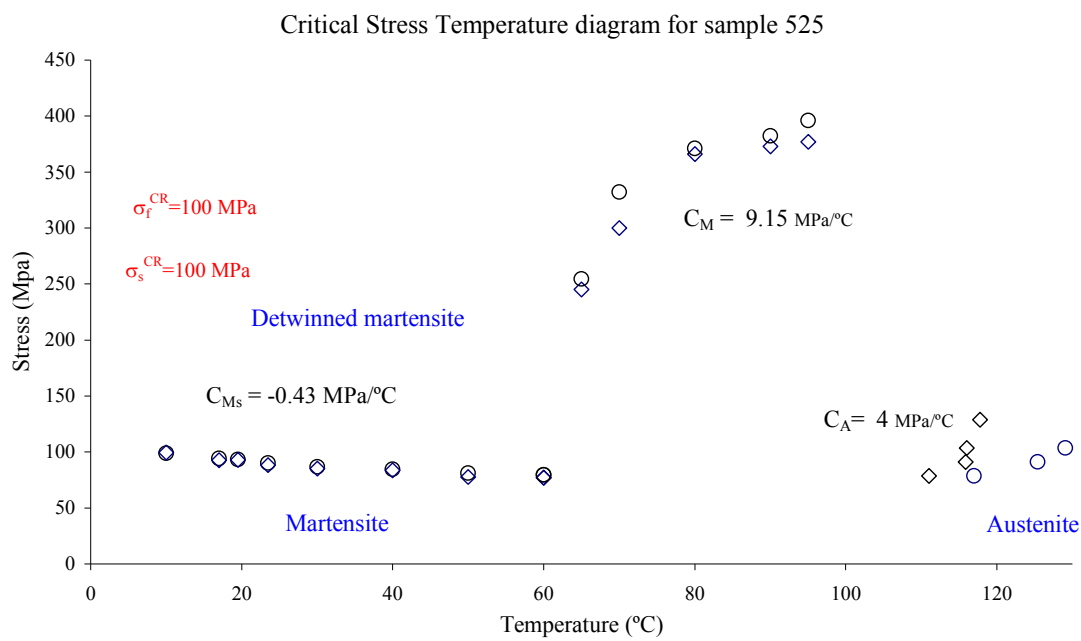


a)

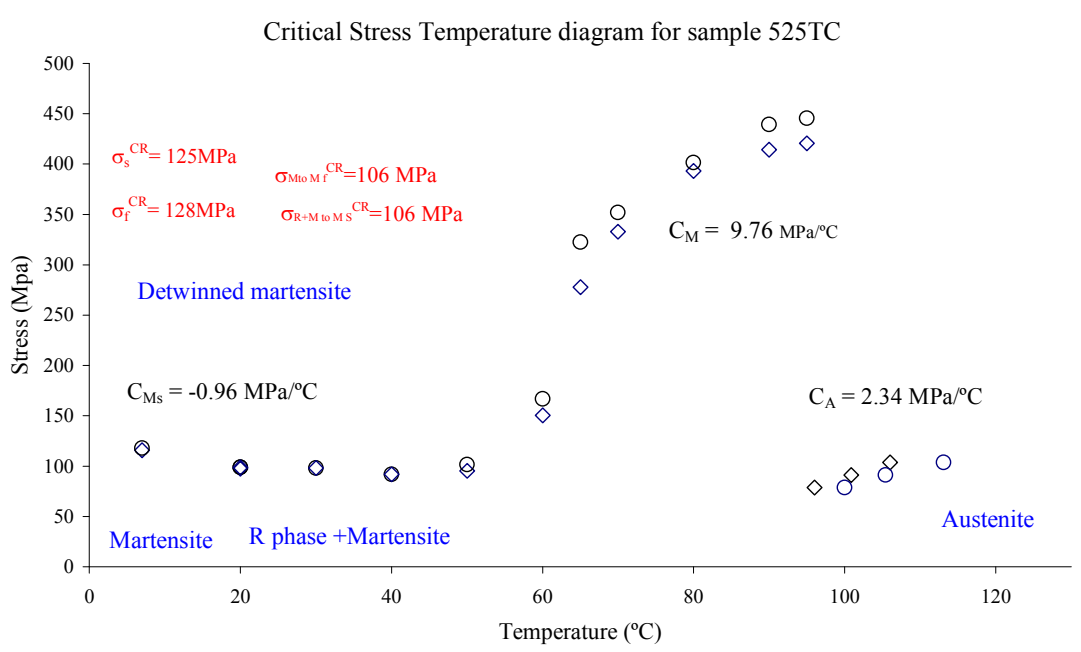


b)

Figure 4.23a and b Critical Stress Temperature diagram for a) 500 sample, b) 500TC sample.



c)



d)

Figure 4.23c and d Critical Stress Temperature diagram for c) 525 sample and d) 525TC sample.

Therefore, the stress temperature coefficients (C_{MS}) delimiting the detwinned martensite region are negative for the non-cycled samples and for the thermally cycled samples (see figures 4.23a and b). Comparing the linear transformation zone of these samples 500-500TC, the results show that the effect of thermal cycling is that, the linear transformation region is stretched for sample 500TC considerably in comparison with that of non-cycled sample 500. The martensitic transformation region is also narrowed considerably, shortening the transformation rate. For the non-linear transformation zone ($T < 55^\circ\text{C}$), because of thermal cycling, the martensite transformation region lines of sample 500TC are displaced toward higher levels of stress than sample 500.

Analysing the values of critical stresses of samples 500 and 500TC up to temperatures $T < 55^\circ\text{C}$, it is found that critical stress values increase as the temperature decreases (σ_S^{CR} , σ_F^{CR}). For temperatures between $55^\circ\text{C} < T < 100^\circ\text{C}$ the evolution of the critical stress values is linear, and for $T > 100^\circ\text{C}$ the evolution becomes slightly curved, suggesting a process of plastic deformation of the alloy prior to the transformation process. Comparing the behaviour of samples 500 and 500TC, and initially focusing the analysis on the martensitic range ($T < 30^\circ\text{C}$ for both samples), the first difference that can be observed is that thermally cycled sample 500TC has higher values of start critical stresses than sample 500 (σ_S^{CR} , see Figures 4.23a and 4.23b). The second difference is that sample 500TC presents almost the same critical stresses for the initial and final values ($\sigma_S^{CR} = 105.7 \text{ MPa}$, $\sigma_F^{CR} = 106.5 \text{ MPa}$). Therefore, to finish the detwinning process and to start the deformation of fully oriented martensite no increase of stress is measured (i.e. figure. 4.23b).

As for R-phase temperature range ($R_S < T < A_S$ for sample 500TC, $M_S = R_S < T < A_S$ for sample 500), thermally cycled sample presents again higher values of critical transformation stress required to induce martensite from R-phase ($\sigma_{R \text{ to } M}^{CR} = 102 \text{ MPa}$) than 500 samples ($\sigma_{R \text{ to } M}^{CR} = 50.7 \text{ MPa}$). As discussed before, all tension test profiles for 500TC samples at $T < A_S$ showed higher values of stress plateau than 500 samples, resulting in higher values of stress to start the martensitic transformation process for samples thermally cycled than for samples non-thermally cycled (figure 4.14a).

Thus, **the introduction of dislocations by thermal cycling at zero stress that develops the R-phase in sample 500TC improves its mechanical properties.** The

alloy shows an **improvement in the shape memory effect, in the value of the E_M and E_R apparent modulus and in the critical transformation stresses (σ_S^{CR} , σ_F^{CR} and $\sigma_{R \text{ to } M}^{CR}$)**.

Figures 4.23c and 4.23d show the evolution for the critical stress with temperature for 525 and 525TC samples. Up to temperatures $T < 60^\circ\text{C}$, critical stress values increase as the temperature decreases for sample 525; for temperatures between $60^\circ\text{C} < T < 80^\circ\text{C}$ the evolution of the critical stress values is linear, and for $T > 80^\circ\text{C}$ the evolution becomes curved, suggesting a process of plastic deformation of the alloy prior to the transformation process. However, for sample thermally cycled, the temperature range where the critical stress values increase as the temperature decreases is reduced near of 5°C ($T = 55^\circ\text{C}$). For temperatures between $55^\circ\text{C} < T < 80^\circ\text{C}$ the evolution of the critical stress values is also linear, and for $T > 80^\circ\text{C}$ the evolution becomes curved as for 525 sample. The delaying of the martensite transformation due to the thermal cycling in sample 525TC can be responsible of this change in this range of temperature. Sample 525 present similar critical stresses for the initial and final values (σ_S^{CR} , σ_F^{CR}). Same fact occurs for sample 525TC. Therefore, to finish the detwinning process and to start the deformation of fully oriented martensite no increase of stress is measured for both samples (i.e. figures. 4.23c and 4.23d).

Comparing the behaviour of samples 525 and 525TC the mainly difference that can be observed is that **thermally cycled sample 525TC has higher values of critical stress than sample 525** (see figures 4.23c and 4.23d). For 525TC R-phase temperature range ($35^\circ\text{C} < T < A_S$), this thermally cycled sample presents values of critical stress required to induce martensite from R-phase higher ($\sigma_{R \text{ to } M}^{CR} = 106\text{MPa}$) than those for sample 525 in the same range of temperatures ($\sigma_S^{CR} = 86\text{MPa}$). As discussed before, all tension test profiles for 525TC samples at $T < A_S$ showed higher values of stress plateau than did 525 samples, resulting in higher values of critical stress to start the martensitic transformation process for samples thermally cycled than for samples non-thermally cycled.

Comparing the effect of heat treatment temperature on the critical stress values of 450, 475, 500 and 525 samples, a decrease in σ_S^{CR} and σ_F^{CR} as increasing the heat treatment temperature occurs, showing the lowest values of critical stresses those

samples heat-treated at 500 and 525°C. This reduction in critical stress values is linked with the reduction in dislocation density due to the increase in heat treatment temperature.

Regarding to the effect of thermal cycling at zero stress in samples heat treated at $T \geq 500^\circ\text{C}$, the increase in σ_S^{CR} that suffer samples 500TC and 525TC results from the dislocation generated during thermal cycling. Repeated stress-free thermal cycling through the transformation zone improves the critical stress of the **500TC and 525TC** samples. In fact, sample 525TC achieved critical stress values similar to those of samples 450 and 475 after 25 thermal cycles at zero stress. Therefore, thermal cycling at zero stress improves the mechanical properties of 500TC and 525TC samples. These alloys **show an improvement in the critical transformation stresses (σ_S^{CR} , and σ_R to M^{CR}), in the E_M and E_R apparent modulus and in the shape memory effect.**

4 Summary and conclusions

The main objective of this thesis was to establish the relationships between the changes in Ti-Ni phase transformation behaviour caused by thermomechanical processes, especially in the R-phase range, and the functional properties of the Ti-Ni shape memory alloys. Establishing these relationships should allow us to find appropriate thermomechanical processes to substantially improve the Ti-Ni functional properties.

To reach the main objective of this thesis, the first step of this thesis was to study experimentally how repetitive thermal cycling at zero stress through the full transformation range changes the phase transformation behaviour and develops or stabilizes the R-phase, depending on the temperature applied in the previous heat treatment.

To achieve this objective, the study used different sets of Ti-Ni wires with Ti-rich chemical composition (49.33at%Ni-50.67at%Ti). One set was heat treated at temperatures of 450, 475, 500 and 525°C. This was done for one hour before quenching the set in water to obtain different levels of R-phase in different transformation paths,

whereas the other set had the same heat treatment followed by repeated thermal cycling at zero stress to investigate the changes in the wires phase transformation behaviour because thermal cycling at zero stress. The number of thermal cycles at zero stress applied to each sample was 50. The study then used the experimental techniques of electrical resistivity and XRD weight fraction diagrams to analyze how heat treatment and thermal cycling affect the phase transformation behaviour of these samples. Comparing these two experimental techniques we have clarified the interpretation of the electrical resistivity measurements, regardless of whether there is an R-phase in the alloy or not, but also we obtained valuable information about the SMA dynamic transformation behaviour between austenite, R-phase and martensite.

In the second part of chapter four, by calculating the mechanical parameters that define the shape memory properties of these alloys, we analyzed and determined how the evolution of the phase transformation behaviour with heat treatment and subsequent thermal cycling at zero stress influenced the SMA functional properties. We compared the mechanical parameters of samples that had been heat-treated and thermally cycled at zero stress and those of samples that had been heat treated and non-thermally cycled

The comparison paid special attention to the R-phase transformation zone and its parameters in order to detect a possible improvement in the SMA's functional properties as a result of applying a minimum number of thermal cycles at zero stress to the Ti-Ni wires. We used the tension test results to obtain and analyze the critical stress-temperature diagrams for non-thermally cycled samples and for thermally cycled samples. Table 4.7 summarizes the parameters obtained.

The main conclusions derived from this chapter are:

(i) ER curves are very effective at detecting the R-phase in Ti-Ni SMAs. However, **to detect simultaneous transformations, the ER curves should be analyzed in detail together with the XRD results** because these transformations are not revealed in the ER curve alone. Moreover, none of the samples analyzed showed any significant jump in resistivity throughout the heating process, which suggests that the R-phase transformation is the most important cause of change in the ER curves' resistivity values. Therefore, the results have to be deduced using XRD. In any case, **a**

jump resistivity in the ER curve followed by a long plateau can be taken to mean that the SMA has a transformation path which is clearly separated into two stages and that, in this case, is $R_f=M_S$. However, a jump resistivity without a plateau indicates that the austenite transforms simultaneously to R-phase and martensite.

(ii) For samples with R-phase before thermal cycling (450 and 475) and for samples with R-phase after thermal cycling (450TC₅₀, 475TC₅₀, 500TC₅₀ and 525TC₅₀) **the end of the R-phase transformation (R_f) always corresponds to the end of the resistivity plateau that is formed after the sharp increase in the resistivity curve.** Ling and Kaplow [LIN, 1980] considered this point to be M_S in the ER curve. Our results show that this point is, in fact, the end of the R-phase transformation (R_f) and that it only corresponds to M_S in some cases. Consequently, **we propose a new interpretation of the ER curves that takes into account the shape of the ER curve measured for the sample** (figures 4.8).

(iii) It is found that the **R-phase increases after thermal cycling at zero stress** for the sample 500TC, which was heat treated at 500°C and thermally cycled. Moreover, for this sample 500TC, thermal cycling at zero stress **produced a well separated two stage transformation on cooling**; that is, the increase in the dislocation density due to thermal cycling increases the R-phase, thus retarding the martensite transformation and eliminating the simultaneous transformation that had the sample 500 non-thermally cycled. **However, the R-phase does not reach 100wt%**, in fact, it only reaches 65wt%. For sample 525, thermal cycling increases the R-phase to 36wt% after 50 thermal cycles, but does not increase it to 100wt% and does not separate the transformation process. Therefore, it can be said that for heat-treated samples that generate small quantity of R-phase, **thermal cycling at zero stress causes R-phase to develop beyond a certain number of thermal cycles at zero stress but only up to a certain saturation level, which depends on the initial presence of the R-phase.** Moreover, if the initial R-phase is almost inexistent, as occurs with sample 525, repeated thermal cycling cannot fully modify the transformation behaviour (or separate the transformation process).

(iv) **On the basis of the constitutive parameters and the critical stress-temperature diagrams** obtained, it is possible to establish that the most **effective way**

to use a near equiatomic Ti-rich Ni-Ti wire is to heat-treat the sample at temperatures equal to or greater than 500°C for one hour before quenching the sample in water. Then, the sample has to be thermally cycled at zero stress prior to use to achieve the best shape memory properties (12 cycles for 500 samples and 25 cycles for 525 samples).

(v) **Due to repeated thermal cycling at zero stress**, 500TC and 525TC wires experience a hardening process that improves their mechanical and functional properties. The **apparent modulus** for martensite and R-phase for the load process E_M and E_R , the apparent modulus measured for oriented martensite E_S , and the **shape memory effect** are improved with respect to the corresponding values for non-thermally cycled SMA, 500 and 525 samples (Table 4.7).

The following interesting conclusions can be drawn from the analysis of how heat treatment and thermal cycling at zero stress influence the phase transformation behaviour:

(vi) The ER and XRD results show that the transformation behaviour for this 49.33Ni at% - 50.67Ti at% SMA changes dramatically when the heat treatment temperature reaches 500°C, and again when the temperature is above 500°C. Samples annealed at $T < 500^\circ\text{C}$ retain a high density of dislocations, which leads to a well developed R-phase. Samples annealed at $T \geq 500^\circ\text{C}$ produce a little or almost no R-phase because of the considerable decrease in defects and dislocations in the matrix caused by heat treatment.

(vii) The ER and XRD results show that the transformation path for samples heat-treated at $T < 500^\circ\text{C}$ leads to a well-separated two-stage transformation on cooling ($B2 \rightarrow R \rightarrow B19'$) with a well-developed R-phase. It also shows that there is no temperature interval between the end of the R-phase transformation and the beginning of the martensite transformation; that is, $R_f = M_s$.

(viii) The XRD quantification shows that the transformation path for samples heat-treated at $T > 500^\circ\text{C}$ results in a simultaneous transformation on cooling ($B2 \rightarrow R + B19'$) and a very poor quantity of R-phase. It also shows that there is no

temperature interval between the beginning of the R-phase and the beginning of the martensite transformation; that is, $R_S = M_S$.

(ix) On heating, all samples presented a simultaneous transformation of the martensite and R-phase to austenite phase ($B19'+R \rightarrow B2$), which confirms that during heating the R-phase is not an intermediate phase. The fact that this simultaneous transformation is not detected by the ER measurements may be due to the poor quantity of R-phase that the alloy has to transform into austenite.

(x) The XRD diagrams for all the samples show that the beginning of the transformation to martensite (M_S) corresponds to different points in the ER curves depending on the quantity of the R-phase that the alloy develops during the heat treatment or during thermal cycling at zero stress. Therefore, the ER curves should be combined with the XRD results to ascertain at which point the martensite transformation starts in the ER measurements.

(xi) The results published by [UCH, 2002] state that when the M_S attains fixed values, the R-phase is considered to have developed during repeated thermal cycling at zero stress. If we compare these results with those described in (ii.) and (x.), we can deduce the following: the temperature that is taken from the ER curves and that indicates that the R-phase has developed is not the M_S temperature. Instead, this temperature seems to be the same temperature as the one at the end of the R-phase transformation (R_f), as all of the wt% diagrams suggest.

(xii) The ER curves of the samples heat-treated under 500°C show no effect on the transformation behaviour after thermal cycling at zero stress. The remaining high dislocation density resulting from the heat treatment, along with the increase in the internal stress field due to transformation, may act as an obstacle to the movements of the martensite interfaces and interfere with the transformation process, thus increasing the (non-transformed) martensite retained at the end of each thermal cycle. This may be responsible for the increase in retained martensite and the corresponding decrease in austenite and R-phase wt% found.

Property	450	450TC	475	475TC	500	500TC	525	525TC
Residual strain or shape memory strain (%)	4.98	4.8	4.97	5	5.12	5.8	5.38	6.04
Apparent modulus on load (MPa)								
E_M	20808	20503	20433	20410	19566	20116	19303	22672
E_R	19202	19735	19757	19684	21947	24139	19462	21138
E_A	69014	68006	70815	68845	73809	70884	69566	72134
Apparent modulus for detwinning martensite (MPa)								
Initial B19'	13490	13407	12097	13149	10595	11266	7259	8937
Initial R	9979	9754	7341	7638	7793	11705	6584	8709
Critical Stress (MPa)								
σ_S^{CR}	120	116	119	121	96.8	105.7	100	125
σ_F^{CR}	127	125	126	127	112	106.5	100	128
$\sigma_{R \text{ to } MS}^{CR}$	22.43	21.5	51	43.6	50.7	102		106
$\sigma_{R \text{ to } Mf}^{CR}$	30.22	30.21	54	45.5	59.3	102		106

Table 4.7 Summary of the mechanical properties of the samples analyzed.

CHAPTER 5

IMPROVEMENT OF THE TWO WAY SHAPE MEMORY EFFECT BY THERMAL CYCLING AT ZERO STRESS PRIOR TO TRAINING



CHAPTER FIFTH:

IMPROVEMENT OF THE TWO WAY SHAPE MEMORY EFFECT BY THERMAL CYCLING AT ZERO STRESS PRIOR TO TRAINING.

Introduction

1 Influence of heat treatment and thermal cycling at zero stress on the constant stress training method

<i>1.1 Influence of heat treatment temperature and thermal cycling at zero stress on the training parameters</i>	197
<i>1.2 Influence on the transformation temperatures during training</i>	202
<i>1.3 Influence on the two-way memory strain obtained</i>	205
<i>1.4 Quantification of the effect of constant stress training on the phase transformation behaviour and on the activation temperatures</i>	210
1.4.1 Analysis of the TWSME strain-temperature curves by constant load method	210
1.4.2 Analysis by ER	212
1.4.3 Weight fraction diagrams after 30 TWSME thermal cycles	214
1.4.4 Activation temperatures	225
<i>1.5 Relationships between the TWSME macroscopic behaviour and the changes in the phase transformation behaviour</i>	227

2 Influence of the heat treatment and thermal cycling on isothermal tensile deformation below M_f training method

<i>2.1 Influence of heat treatment temperature and thermal cycling at zero stress</i>	
---	--

<i>on the training parameters</i>	233
2.1.1 Samples 500it and 500TCit	233
<u>2.1.1.1 Influence on the two-way memory strain obtained</u>	239
2.1.2 Samples 525it and 525TCit	240
<u>2.1.2.1 Influence on the two-way memory strain obtained</u>	242
2.1.3 Samples 450it and 475it	243
2.3 <i>Influence of the isothermal training on the TWSME activation temperatures and on the phase transformation behaviour.</i>	247
2.3.1 500it and 500TCit samples	251
2.3.2 525it and 525TCit samples	255
2.3.3 475it and 450it samples	259
2.3.4 Activation temperatures	262
2.4 <i>Relationships between the TWSME macroscopic mechanical behaviour and the phase transformation behaviour</i>	263
3 Summary and conclusions	267

Introduction

To date, various training procedures have been discovered and investigated in effort to develop a TWSME of both, high magnitude and stability ([SAB, 1974], [PER, 1984] and [LIU, 1990]). Recently, one of the best improvements of the TWSME was performed by Wada et al. [WADA, 2008]b, who found that an adequate pre-strain of the SMA wire in martensite phase improves the TWSME and decreases the plastic strain accumulated during posterior training at constant stress. This method of training

(*Combined cycling: pre-strain and thermal cycling under constant stress*, chapter 2, section 3.1) allows to introduce an optimum amount of prior to training dislocations, creating preferentially oriented martensite which are rearranged by the posterior training at constant stress. This combination of methods results in the increase in the two-way memory strain obtained. However, it introduces large permanent strains in the alloy in martensitic state.

To avoid this important problem, **we think that the dislocations introduced in the alloy by thermal cycling at zero stress can play an important role during the development of the TWSME.** The most important advantage is that thermal cycling at zero stress does not produce any permanent deformation in the alloy.

As seen in chapter four, an adequate application of thermal processes, that is, heat treatment temperature and a minimum number of thermal cycles at zero stress, has a large impact on the mechanical and functional properties of the 500TC and 525TC samples. There are improvements in their apparent module for the martensite and the R-phase, in their apparent module for the reoriented martensite, in their critical stresses that transform twinned martensite into reoriented martensite and in their shape memory effect. Therefore, heat treatment plus thermal cycling at zero stress prior to use can be considered a way of improving the microstructure of the alloy because the process not only avoids permanent deformation in the martensite phase, but also gives good yield strength in the austenite phase. Therefore, **we will train the wires which have been heat treated and thermally cycled at zero stress to investigate a possible improvement of the two-way shape memory effect. The training procedures and training parameters, the two-way memory strain obtained and the change in the transformation temperatures and the phase transformation behaviour will be analyzed looking for an improvement of these TWSME important parameters. This is our first objective of this chapter.**

The TWSME is a particular SMA functional property since the material is able to remember a geometrical shape at high temperature, above austenite finish temperature (A_f) and another shape at low temperature, below martensite finish temperature (M_f). During repeated heating and cooling the material changes its shape, through a hysteresis loop, between a hot shape, linked with austenite phase and a cold shape, linked to the

martensite phase. These training procedures involve repeated deformation and transformation between the austenite and martensite, producing a dislocated structure. This structure creates an anisotropic stress fields, which favours the formation of the preferentially oriented martensite variants, resulting in a macroscopic shape change between the phase transformation temperatures. Therefore, **it is important to know how the thermomechanical cycling that involves the training procedures affects and changes the phase transformation behaviour of the Ti-Ni wires.**

Experimental studies of the thermomechanical response and phase transformation behaviour of trained Ti-Ni wires are reported using the electrical resistance of the Ti-Ni wire as a feedback for strain in actuator applications, taking advantage of the observed linear dependence of the electrical resistance with the strain. However, the results are often very difficult to understand and interpret: different published opinions have been reported about the influence of the R-phase in the development of the TWSME [POZ, 1999], [WUX, 2000], [UCH, 2002]b. Then again, quite complicated electrical responses in thermomechanical tensile tests were reported. In order to clarify the phase transformation behaviour of a trained Ti-Ni SMA, Turenne et al. [TUR, 2000] reported a qualitative understanding of the TWSME obtained from XRD patterns. However, quantitative analysis focused on relating the trained Ti-Ni wire phase transformation behaviour with the TWSME macroscopic properties through the complete temperature transformation range are still far from complete.

To achieve **the second objective of this chapter**, that is, **how the thermomechanical cycling that involves the training procedures affect the phase transformation behaviour of the Ti-Ni wires**, the effects of the TWSME training on the Ti-Ni phase transformation behaviour are quantified by X-ray diffraction. This XRD analysis may clarify first, the possible improvement of the TWSME by repeated thermal cycling at zero stress prior to training, and, secondly, if the R-phase is developed or not by thermomechanical cycling and its influence in the TWSME development. The results are compared with those obtained by electrical resistivity measurements in order to clarify the electrical resistance behaviour of a trained Ti-Ni SMA.

To attain these two above mentioned objectives, 450, 475, 500, 525, 500TC and 525TC wires are used. We use two samples that did not show any improvement in their

mechanical properties after thermal cycling at zero stress and that presented an initial full developed R-phase after heat treatment (450 and 475 samples); we also use samples that showed little or almost non-existent R-phase in their initial transformation path (500 and 525 samples), and finally, we use samples that had developed the R-phase after thermal cycling at zero stress and that showed an improvement in their mechanical properties after thermal cycling at zero stress (500TC and 525TC samples). As can be seen, a wide variety of mechanical and phase transformation behaviours are used in this experimental study.

Two different TWSME trainings, that is, thermal cycling under constant stress and isothermal tensile deformation under martensite state, are performed on each set of samples as described in chapter 3. Lately, by weight fraction is quantified the evolution of the phase transformation behaviour due to these two TWSME training for all trained samples and the results are correlated with the macroscopic TWSME behaviour (strain-temperature behaviour) of each sample.

1 Influence of heat treatment and thermal cycling at zero stress on the constant stress training method

1.1 Influence of heat treatment and thermal cycling at zero stress on the training parameters

First, an analysis of the parameters obtained during the training, that is, the austenite strain, the martensite strain, and the recovery strain, is presented. The samples trained by constant stress are called: 475cs, 500cs, 500TCcs, 525cs and 525TCcs.

The process to choose the adequate value of training stress (σ_{tr}) for each sample is described in chapter 3, section 3.6.1. To know the optimal number of training cycles to apply (n), 20 thermal cycles under constant stress are performed on each of the above-mentioned samples. The value of the constant stress applied to each sample is the same that the value of the corresponding training stresses. As a criteria, the optimum number of training cycles is associated with training conditions that should minimize the permanent strain and maximizes the martensite strain that the alloy may develop

through the constrained cooling during the TWSME training ([STA, 1992], [WAD, 2005], [WAD, 2008]). Therefore, the training cycle at which the maximum value of ε_m is given will indicate to us the optimum number of training cycles that we should apply to each sample.

Figures 5.1 show the evolution of austenite strain (represented by full circles), martensite strain (represented by stars) and recovery strain (represented by rhomboids) during 20 thermal cycles under constant stress for sample 475cs (figure 5.1a), for 500cs and 500TCcs samples (figure 5.1b) and for 525cs and 525TCcs samples (figure 5.1c). Samples non-thermally cycled have the blue colour and the red colour is for samples thermally cycled.

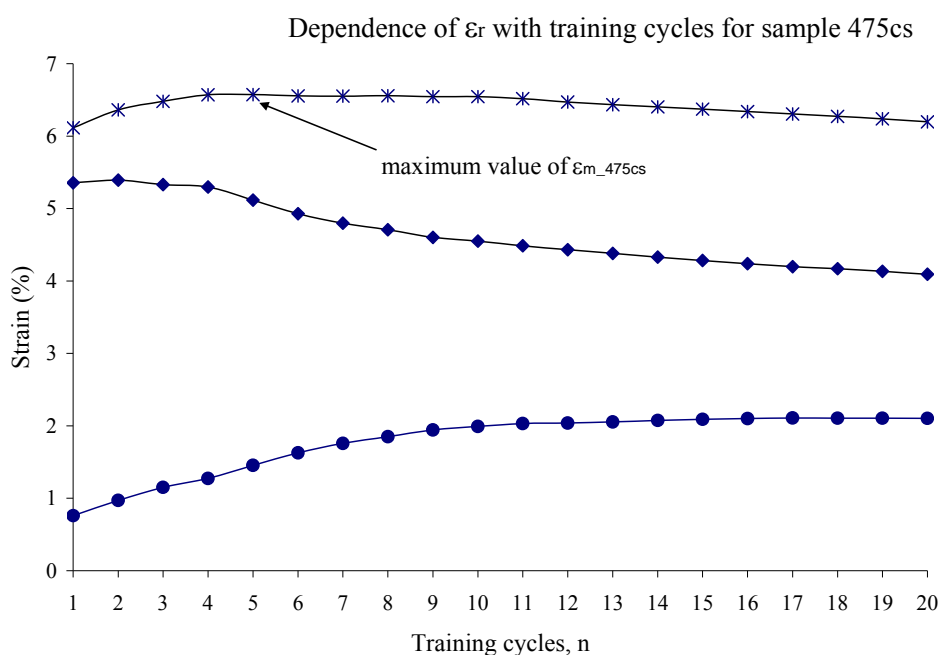
As seen in figures 5.1, a continuous growth of austenite or irreversible strain (ε_a) is produced for all samples during thermal cycling at constant stress. When the cyclic temperature reaches the A_s temperature transformation, this increase in irreversible strain, (or the gradual elongation of the specimen during cycling) is attributed to the increase in the dislocation density corresponding to strain and transformation induced hardening. The strain hardening is beneficial since it increases the flow stress. On the other hand, high dislocation density regions serve as nucleation sites for the martensite plates during cooling [VHU, 1991]. However, the resulting internal friction hinders the evolution of direct and reverse transformations causing variations in transformation temperatures and reduction in the alloy stability.

Moreover, an increase in martensite strain (ε_m) is also done during cycling. This evolution of the ε_m with cycling could be attributed to the permanent flow related to the dislocation movement and to the reorientation of the martensite variants. This second mechanism explains the more important increase in martensite strain comparatively to austenite strain, which results in a net increase in the recovery strain ($\varepsilon_r = \varepsilon_m - \varepsilon_a$). Turenne et al. published evidence about the increase in dislocation density and following stabilization, and the initial reorientation of the martensite variants during thermal cycling under constant stress by XRD patterns [TUR, 2000].

However, as seen in figures 5.1, different trends for the five cases of heat treatment temperature and/or posterior thermal cycling at zero stress are observed. Sample annealed at 475°C suffers an increase in ε_m (the maximum value of ε_m is reached after 5

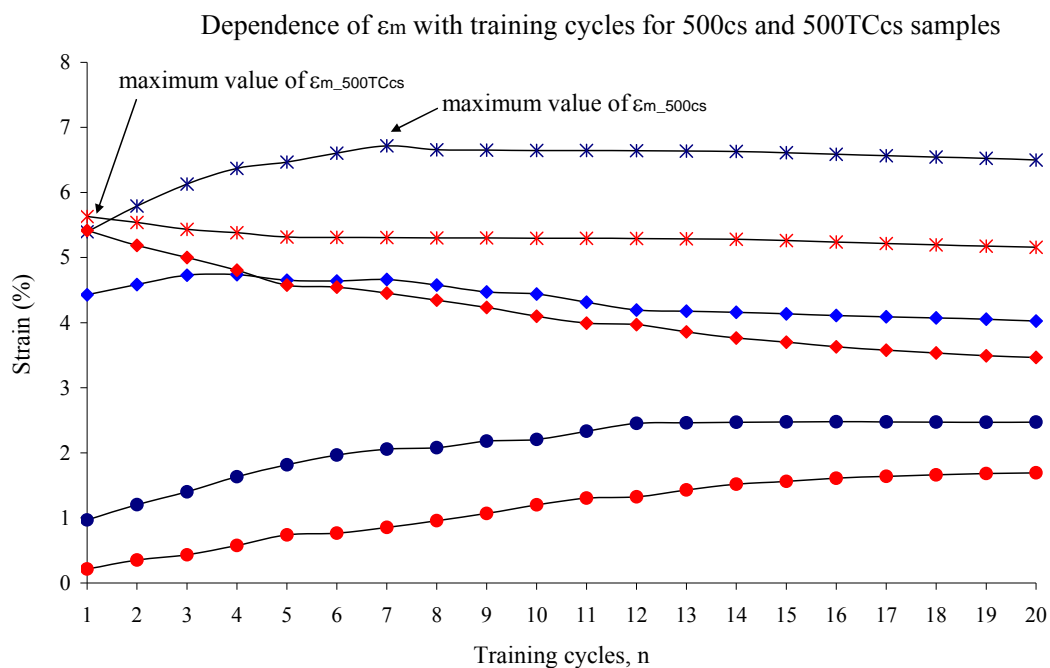
cycles, $\epsilon_m=6.6\%$), that represents an almost constant or even slightly decrease in recovery strain due to the increase in ϵ_a until the fifth cycle. Subsequent cycling is accompanied by an increase in ϵ_a and by slightly decrease in ϵ_m obtaining a gradual decrease in recoverable strain.

The results also show that samples analyzed in Figure 5.1b (500cs and 500TCcs samples) behave completely differently between them during thermal cycling at constant stress. After four cycles sample 500 presents an increase in martensite strain, reaching its maximum value after seven training cycles ($\epsilon_m=6.7\%$). This increase in ϵ_m is accompanied by an increase in ϵ_a (as 475cs sample did). After eight cycles, the austenite and martensite strains vary slightly.

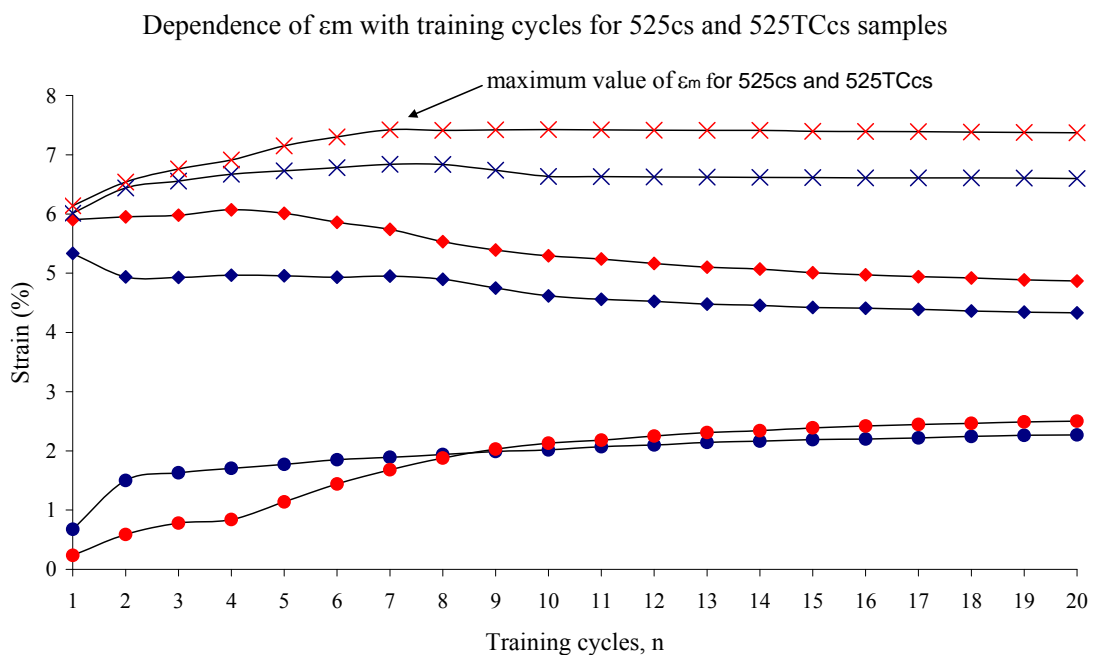


a)

Figure 5.1a Evolution of the strain in martensite, the irreversible strain and the recovery strain with constant stress training for a) 475cs samples.



b)



c)

Figure 5.1b and c Evolution of the strain in martensite, the irreversible strain and the recovery strain with constant stress training for b) 500cs and 500TCcs samples and c) 525cs and 525TCcs samples.

Applying the same training parameters, sample 500TCcs behaves very different of sample 500cs, as can be seen in figure 5.1b. The ε_m and, consequently, the ε_r reach their maximum at first training cycle ($n=1$). With further training, the ε_r decreases not only because of the increase in ε_a , but also because of the notably decrease in ε_m . Focusing on the evolution of the martensite and austenite strains, ε_m gives fairly constant values after the fifth training cycle, whereas ε_a is still rising after the fifth training cycle, resulting in a net decrease in the recovery strain (ε_r) around 1.95% after 20 thermal cycles under constant stress. Notably, thermally cycled sample 500TCcs accumulated lower irreversible strain (1.7%) than 500cs (2.5%) at the end of the 20 cycles. This lower accumulation of irreversible strain (ε_a) may indicate that the density of the dislocations introduced by training is higher for the non-thermally cycled sample 500cs than for thermally cycled 500TCcs.

Samples 525cs and 525TCcs have similar evolution of the ε_m between them (figure 5.1c) because the maximum value of ε_m is done after 7 cycles, but sample 525TCcs shows a greater capacity for developing higher ε_m with similar irreversible strain (ε_a), resulting in higher values for the total recovery strain ε_r at the end of 20 thermal cycles.

As seen, prior thermal cycling at zero stress seems to have serious influence on the evolution of the strains during thermal cycling at constant stress: sample 500TCcs shows faster ε_m reorientation process than 500cs sample and, sample 525TCcs shows higher capacity of martensite reorientation than sample 525cs.

The martensite reorientation capacity for a specific heat treatment condition can be estimated from the extension of the martensite plateau in the stress-strain curve as published by [LIU, 1990] and [SCHE, 1998]. As obtained in chapter four, samples 500TC and 525TC have longer martensite plateau than samples non-thermally cycled 500 and 525, please see table 4.7. Thus, **it is possible to say that the dislocations introduced in the alloy microstructure by prior thermal cycling at zero stress [MIY, 1986] could be favourably involved in the martensitic reorientation process due to thermal cycling under constant stress** (which is an essential factor for obtaining a substantial ε_{tw}), thus helping the formation of preferentially oriented martensite.

Following the analysis of the evolution of the strains, the next steps are first, to train the samples according to the training parameters exposed in table 5.1 and, secondly, to analyze the evolution of the transformation temperatures during the TWSME training. Table 5.1 plots the optimal constant stress training parameters for each sample.

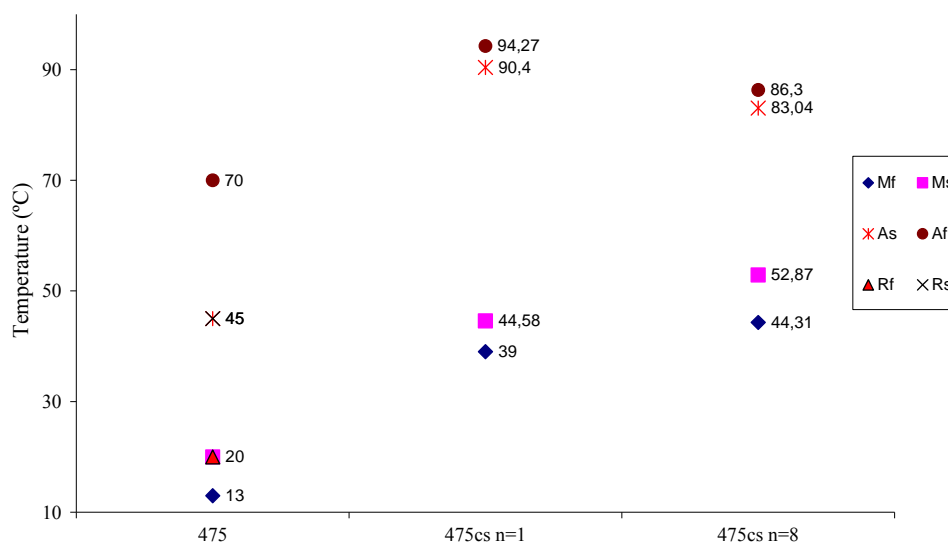
<i>Samples</i>	<i>Training stress, σ_r</i> (MPa)	<i>Training cycles, n</i>
475cs	104	6
500cs	104	8
500TCcs	104	2
525cs	72	8
525TCcs	72	8

Table 5.1 Training parameters.

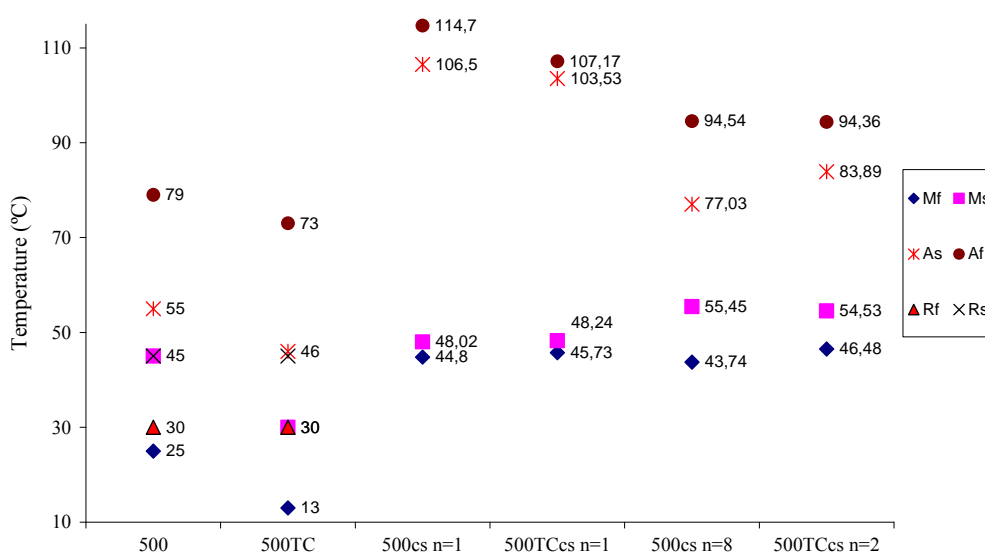
1.2 Influence on the transformation temperatures during training

The evolution of the transformation temperatures during training in all samples can be measured using the strain-temperature profiles obtained during training. The transformation temperatures were determined using the applied loading method (figure 3.4). Since these temperatures are measured under stress, the Clausius-Clayperon relation predicts that they should be different from those obtained by ER under no stress or XRD and they cannot be taken as real transformation temperatures. However, the results provide valuable information about temperature evolution from cycle to cycle and serve as an indication of how the transformation temperatures of the trained sample change in relation with the untrained material. Figure 5.2 shows the evolution of the transformation temperatures during training for the first and last training cycle according to the number of training cycles exposed in table 5.1, together with the transformation temperatures of the untrained 475, 500, 500TC, 525 and 525TC samples (initial reference values). For all samples, there is a high increase in martensitic temperatures during the direct transformation (A to M) in the first training cycle, but M_s

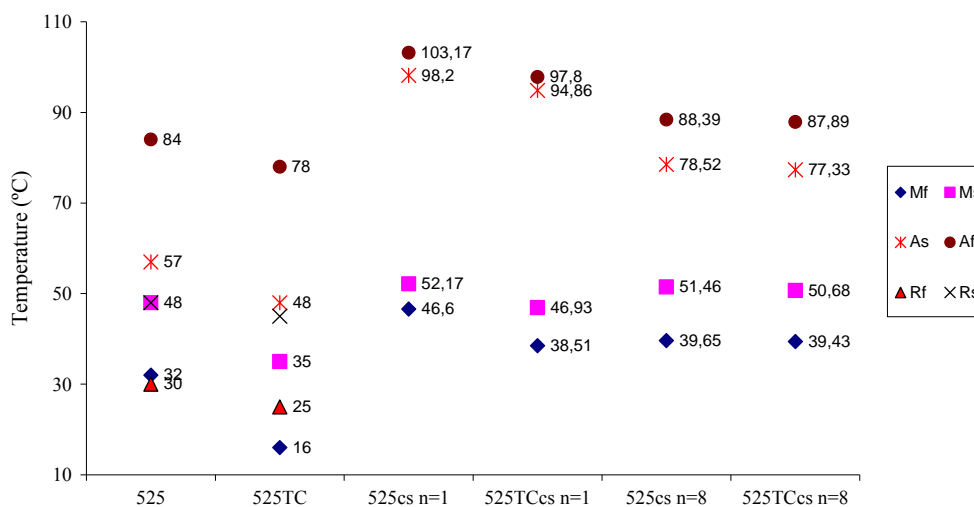
and M_f increase very slightly with further training. Such variations suggest that thermal cycling influences strongly the martensite transformation. These increments in M_s and M_f indicates an easier formation of martensite plates due to the increasing number of dislocations favouring the formation of the martensite variants that are preferentially oriented with respect to the deformation direction [STA, 1988], [TUR, 2000], [LAH, 2004].



a)



b)



c)

Figure 5.2 Evolution of the transformation temperatures during constant stress training for samples a) 475cs b) 500cs and 500TCcs, and c) 525cs and 525TCcs.

This increase in M_S for all samples may also produce R-phase transformation to disappear: in neither sample, it is possible to detect any contribution of the R-phase transformation strain in the strain-temperature profiles throughout training. Therefore, the training stress applied to all samples seems to be high enough to suppress the R-phase transformation during training in accordance with the findings of [POZ, 1999]. In fact, all first training cycle martensite temperatures are similar or higher than the initial R-phase temperature. This detail is independent of the previous heat treatment and thermal cycling at zero stress applied. However, this point has to be clarified by the XRD analysis.

The slightly increase in martensitic temperatures that is done after the first training cycle for all samples can be in relation with the martensite reorientation process. Therefore, as the increase in martensitic temperature is being lower, the full reorientation of the martensite may be attained. To reinforce the idea that a relationship between the increase in M_S temperature and the martensite reorientation exists, figure 5.2b shows that both, sample 500cs non-thermally cycled prior training and sample 500TCcs thermally cycled prior training, reached similar M_S temperatures, but after

different number of training cycles. This situation suggests as the figure 5.1b showed, that sample 500TCcs reaches the full reorientation of the martensite in two training cycles.

Figures 5.2 also show for all samples that, after an initial rise, both austenitic temperatures decrease considerably in the subsequent training cycles. [LIU, 2000]b published that the internal stress field created during the training has the same direction as the oriented martensite and that it is the responsible for the noticeable modification in austenitic temperatures: the internal stress fields create resistance to the austenite transformation, thus both austenitic temperatures increases in the first training cycle. With further training, a decrease in austenitic temperatures is shown for all samples (see figures 5.2) revealing an easier reverse phase transformation (M to A).

Comparing all samples, the lowest decrease in austenitic temperatures is done by sample heat treated at 475°C. After heat treatment, the remaining dislocations in the 475 sample structure do not favour martensite-austenite transformation. The remaining dislocations interacting with the dislocations created during thermal cycling at constant stress. This situation does not occur with samples heat treated at 500°C and 525°C, where the decrease in austenitic temperatures is continuous during all thermomechanical cycling. As a resulting of the change in transformation temperatures the hysteresis (the net difference between A_f and M_f) is stretched heavier for those samples that have received higher temperature of heat treatment and higher number of training cycles, that is, samples 500cs, 525cs and 525TCcs.

1.3 *Influence on the two-way memory strain obtained*

To measure the two-way memory strain (ϵ_{tw}) developed by constant stress training, all samples underwent a further thermal cycling under no-load for thirty cycles (called TWSME thermal cycling). Figure 5.3 illustrates the spontaneous shape changes in the length of the wires. As can be seen, thermally cycled samples 500TCcs and 525TCcs develop higher ϵ_{tw} values than samples non-thermally cycled 500cs and 525TCcs, despite the more important initial presence of R-phase on the samples thermally cycled. Sample 475cs has a very poor TWSME behaviour because its martensite activation temperatures are far from room temperature, as it shows its TWSME hysteresis loop

(figure 5.3). Therefore, we analyze those samples that have activation temperatures near room temperature after training procedures because they have interest from the point of view of usual actuator applications, as occurs with samples 500cs, 500TCcs, 525cs and 525TCcs.

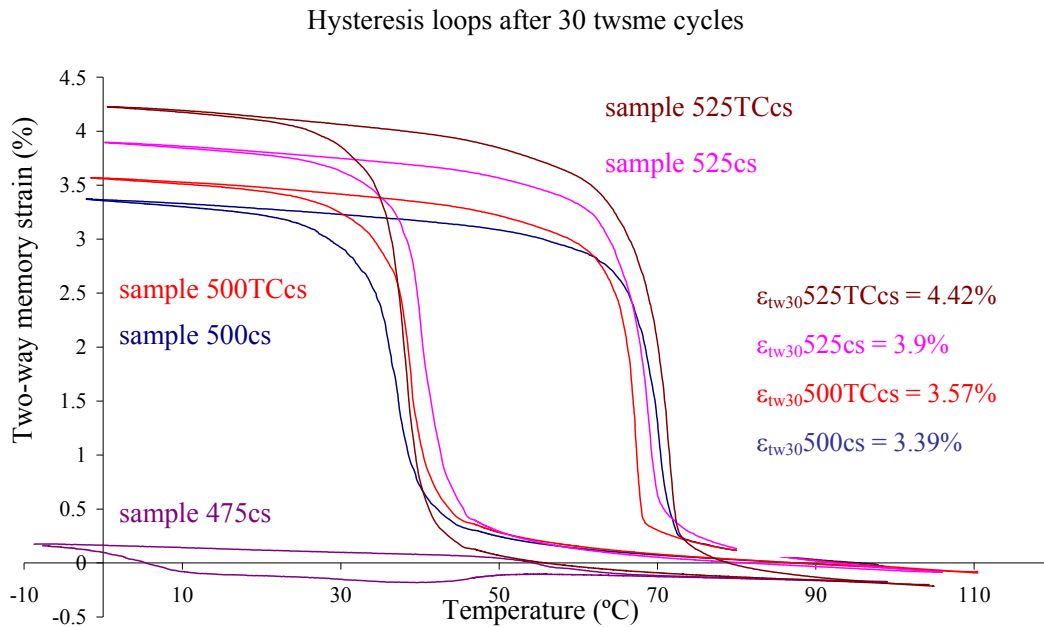


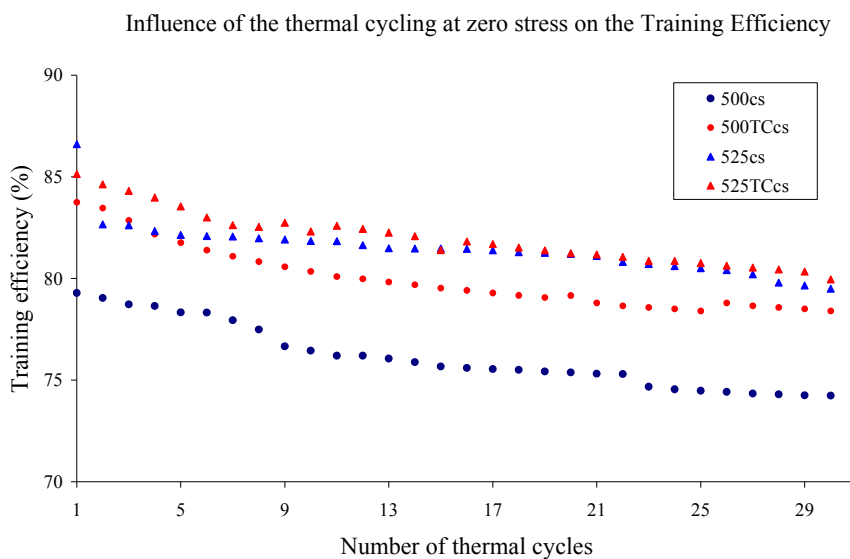
Figure 5.3 Two-way shape memory strain after 30 TWSME thermal cycles for all samples analyzed.

The orientation of the martensite variants is supported by the generated dislocation structure, which is improved with ongoing training (increase in martensite strain, as figures 5.1 show). The oriented martensite reaches to a saturation value, indicating the end of the training. Taking into account the irreversible strain, the recovery strain could give to us an indication of the magnitude of the orientation capacity of the sample after training. [LIU, 1999] observed that the recovery strain exhibits a near proportionally with the obtained two-way memory strain: the magnitude of the recovery strain indicates the amount of martensite variants that is actually oriented. In other words, the evolution of the recovery strain during training is a direct consequence of the evolution of the martensite strain and austenite strain, and thus, the TWSME that can be developed by the sample. As a result, Liu et al. proposed the ratio $\epsilon_{tw} / \epsilon_r$, called training efficiency “ η ”, which is defined as the ratio of the two-way memory strain to the

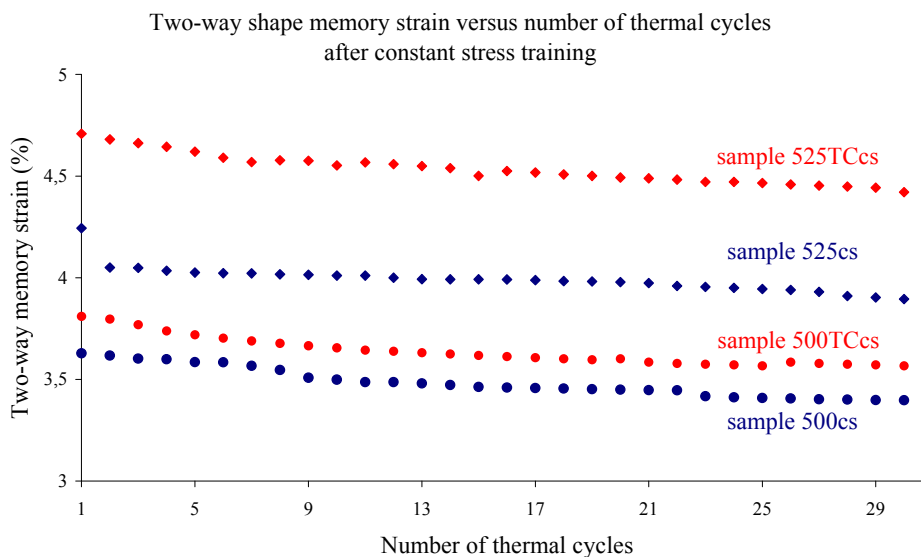
recovery strain (measured at the last training cycle). The obtained training efficiency results are shown in figure 5.4a for all trained samples. In addition, figure 5.4b shows the ε_{tw} values for 500cs, 500TCcs, 525cs and 525TCcs samples recorded during 30 TWSME thermal cycles. As seen in figure 5.4a, samples 525cs and 525TCcs initially present the highest training efficiency (86.6% and 85.13% respectively) according to the values of two-way memory strain and the recovery strain obtained. However, sample 525cs has higher decrease in training efficiency (7.11%) than sample 525TCcs (5.18%) and both samples 500 (5%). Moreover, sample 525cs non-thermally cycled presents a very fast decrease up to the second thermal cycle, producing that, after 30 TWSME thermal cycles, both samples 525 had similar values for the training efficiency (79%). On the other hand, sample thermally cycled 500TCcs (78.4%) always presents higher training efficiency than the respective non-thermally cycled sample 500cs (74.2%). Although the lost in training efficiency is similar between samples 500 (5%), we should remember that the number of training cycles applied to sample 500TCcs was only two. Therefore, it is possible to say that **thermal cycling at zero stress prior to training produces an improvement in the training efficiency.**

We studied the case that the number of training cycles applied to sample 500TCcs was the same than sample 500cs [URB, 2010]b (8 training cycles). Under this situation, sample 500TCcs developed lower two-way memory strain than sample 500cs (0.15% less).

To explain the decrease in training efficiency caused by the decrease in two-way memory strain values, figure 5.4b shows the ε_{tw} values recorded during these 30 TWSME thermal cycles. As seen, all samples show a little degradation of the ε_{tw} during these 30 thermal cycles, which is attributed to changes in the microstructure caused by TWSME thermal cycling. These changes are due to the partial relaxation of the stress field formed during training procedure as published by [SCHE, 1998], [LIU, 1999] and [WAN, 2003], causing a slightly degradation of the two-way memory strain.



a)



b)

Figure 5.4 a) Evolution of the training efficiency versus number of TWSME thermal cycles and b) Evolution of the two-way shape memory strain versus number of TWSME thermal cycles.

From the results exposed in figure 5.4b and figure 5.5, we discuss the origin of the small decrease that is produced in the ϵ_{tw} . Figure 5.5 shows the loss of martensite strain, the increase in austenite strain and the resulting decrease in ϵ_{tw} after 30 TWSME thermal cycles for all samples. As seen, the loss of ϵ_{tw} is principally due to the loss of the capacity of the reorientation of the martensite strain and not for the increase in

austenite strain. During training, a dislocation pattern has been developed, as well a compatible stress-field. Since during the stress free thermal cycles a different internal stress field is present, the energetically most favoured distribution of dislocations can be changed as well. Therefore, the decrease in martensite strain could be motivated by the rearrangement and/or annihilation of the dislocations created by training. These processes may change the dislocation pattern that has been created during the training cycles being most intensive on the beginning of the TWSME thermal cycling.

Therefore, the results presented in figures 5.4 and 5.5 are in agreement with those of [SHE, 1998], [LIU, 1999] and [WAN, 2003]. Between samples, 500cs and thermally cycled 500TCcs present similar decrease in ε_{tw} , meanwhile sample 525cs present a decrease in ε_{tw} slightly higher than thermally cycled 525TCcs (0.06%) after 30 TWSME thermal cycles.

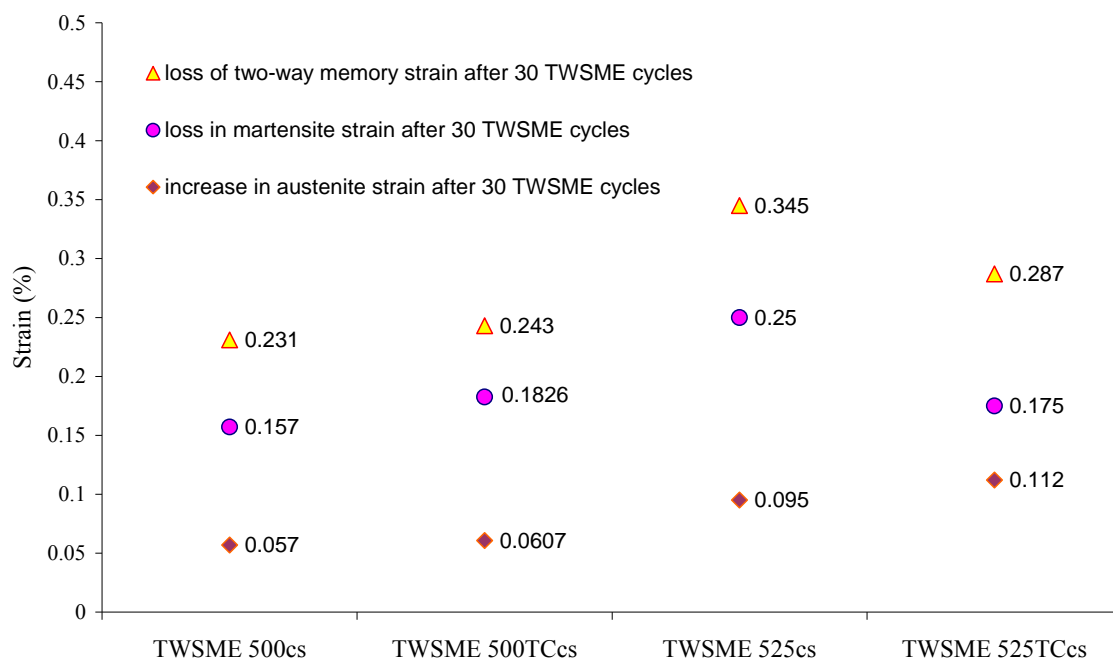


Figure 5.5 Loss of martensite strain, increase in austenite strain and decrease in ε_{tw} after 30 TWSME thermal cycles for 500cs, 500TCcs, 525cs and 525TCcs samples.

To elucidate why the samples thermally cycled have higher ε_{tw} than samples non-thermally cycled, next section presents an analysis of the changes in the phase transformation behaviour due to constant stress training.

1.4. Quantification of the effect of constant stress training on the phase transformation behaviour and on the activation temperatures

To determine the temperatures at which the two-way memory effect is activated, the transformation temperatures are measured after training for all trained samples. The change in the transformation temperatures is studied using three methods: 1) by applying the applied loading method using the TWSM strain-temperature curves; 2) by taking ER measurements under no load and 3) by the wt% diagrams. The results can be very different depending on the method used. For this reason, firstly, we will expose the results obtained by each experimental method and later, we will compare all results obtained. On the one hand, the strain-temperature curves (see figure 5.3) are useful to determine the evolution of the activation temperatures during the TWSME thermal cycling, that is, during the real application of the trained wire. However, these curves reveal nothing about the presence of the R-phase. On the other hand, we use the ER measurements because they are useful to show the appearance or disappearance of the R-phase during cooling and/or heating, although, the martensitic transformations shown by ER measurements are much less obvious [LAI, 2004]. These ER measurements are taken after 30 TWSME thermal cycles. These problems are overcoming using the wt% diagrams obtained from the XRD patterns of trained samples after 30 TWSME thermal cycling. These wt% diagrams help to clarify the phase transformation behaviour and the activation temperatures of the trained samples.

1.4.1 Analysis of the TWSME strain-temperature curves by applied loading method

Figure 5.6 shows the evolution of the activation temperatures versus the number of TWSME thermal cycles for all trained samples. The temperatures are plotted for the first and last TWSME thermal cycling. The activation temperatures obtained are within

room temperature for the cold shape of the wire (martensite, 28°C) and around 80°C for the hot shape of the wire (austenite). All transformation temperatures decrease respect to those measured during training (see figures 5.2b and c). The decrease of these temperatures at the beginning of the TWSME application could be attributed to the establishment of the dislocation structure formed during training [TUR, 2000]. Further TWSME thermal cycling, the austenite temperatures tend to decrease, and the martensite temperatures tend to increase slightly or keep almost constant for all trained samples, narrowing the temperature interval. The decrease in austenite temperatures and the increase in martensite temperatures can be linked with the partial relaxation of the stress field formed during the training procedure as a consequence of the TWSME thermal cycling [LIU, 1999], [WAN, 2003]. This partial relaxation of the microstructure makes the transformation be easier to produce in thermal cycle 30 than in thermal cycle 1, as suggest the changes in these activation temperatures. The R-phase transformation is not shown in any strain-temperature curve analyzed, suggesting that the training procedure eliminates the R-phase due to the important increase in M_S temperature during training.

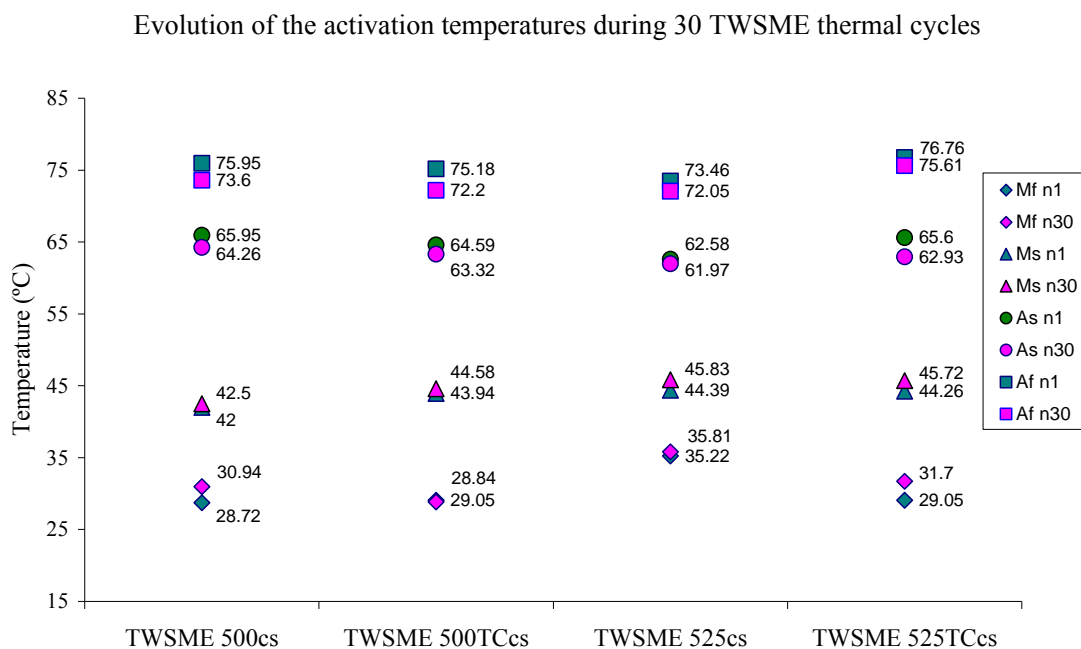


Figure 5.6 Evolution of the activation temperatures with TWSME thermal cycling measured applied loading method.

1.4.2 Analysis by ER

Figures 5.7a (samples 500cs-500TCcs) and 5.7b (samples 525cs-525TCcs) show the ER profiles corresponding to the untrained samples and to the trained samples, respectively. Figures 5.7 also show the increase in resistivity values ($\Delta\rho$) resulting from the transformation process from austenite to a possible R-phase. The ER analysis shows that an important change in the phase transformation behaviour and in the transformation temperatures occurs. The ER results measured for the trained samples 500cs, 500TCcs, 525cs and 525TCcs (the upper curves in figure 5.7a for samples 500cs and 500TCcs, and the second and fourth curve in figure 5.7b for samples 525cs and 525TCcs respectively) show how the training procedure changes the electrical resistivity response of the trained SMA wires. Regarding the cooling part of the ER profiles for trained samples 500cs and 500TCcs, figure 5.7a shows a resistivity cup at 53°C for sample 500cs and at 49°C for sample 500TCcs. According to the values given by Wu et al. [WUK, 2006] the considerable $\Delta\rho$ may indicate the existence of the R-phase regardless of the training process applied. This large increase in the resistivity values suggests a simultaneous transformation process from B2 to R-phase plus B19' between 53°C to 20°C for sample 500cs and, between 49°C to 20°C for sample 500TCcs. Moreover, figure 5.7a shows that resistivity drops considerably during the heating process, which indicates clearly the reverse transformation to austenite (this drop does not occur in the profiles for untrained samples 500 and 500TC). The fact that the decrease in resistivity is considerable for both trained samples 500, suggests that R-phase transformation may also be present during the heating process. Thus, the ER results suggest that the R-phase transformation is not suppressed by the training procedure: the R-phase presence seems to increase in the direct transformation process and is developed in the reverse transformation process, in accordance with Uchil et al. [UCH, 2002]b.

Figure 5.7b shows the resistivity curve as a function of temperature after heat treatment (sample 525), after thermal cycling, (sample 525TC) and after constant stress training (525cs and 525TCcs). This figure also shows for each sample the increase in resistivity value ($\Delta\rho$) resulting from the transformation from austenite to R-phase. These

$\Delta\rho$ values may also indicate the existence of the R-phase, as occurs with samples 500cs and 500TCcs.

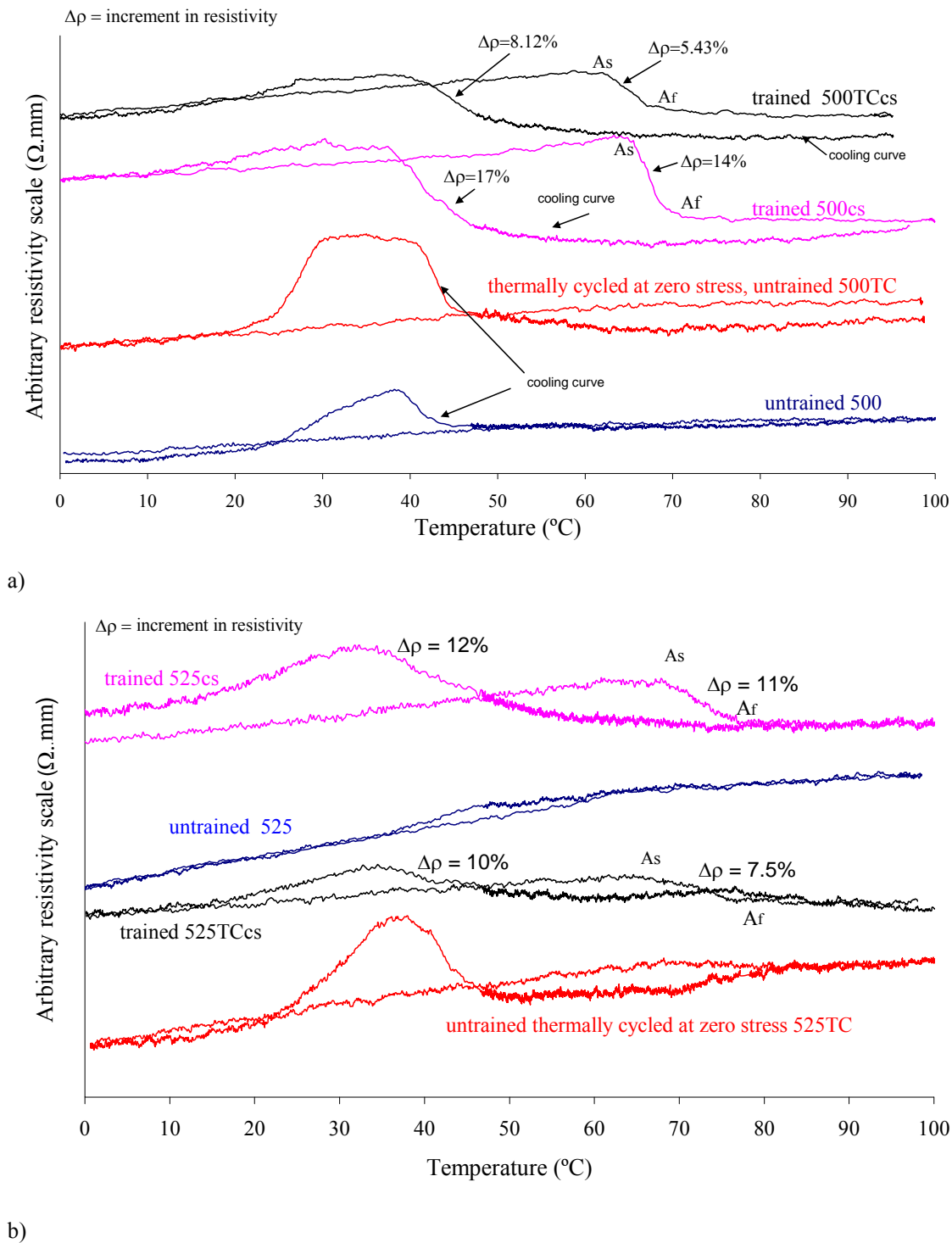


Figure 5.7 Constant stress training effect on ER curves for samples a) 500cs and 500TCcs and b) 525cs and 525TCcs.

Thus, for sample 525cs, with no R-phase before training, the constant stress training seems to develop the R-phase showing now an austenite \leftrightarrow R-phase plus martensite transformation path in both the cooling and the heating process.

To conclude, all ER curves seem to mark clearly the austenitic temperatures during the heating process. Moreover, the martensite and the R-phase seem to transform together from austenite. Therefore, to make a better analysis of the change in transformation temperatures and phase transformation behaviour of these samples due to constant stress training, we will combine the ER measurements and those obtained by the wt% diagrams to obtain the activation temperatures, as we did in chapter four.

1.4.3 Weight fraction diagrams after 30 TWSME thermal cycles

Following the analysis made by applied loading method and ER, the effects of constant stress training on samples phase transformation behaviour and activation temperatures are now discussed by wt% diagrams. They are calculated from a quantitative analysis of the XRD powder patterns using the Rietveld method and the software TOPAS. The evolution of the phase transformation behaviour after constant stress training for 500cs, 500TCcs, 525cs and 525TCcs and 475cs samples is shown in figures 5.8 to figures 5.12. The results are given for each trained sample as the % percent of the weight fraction (wt%) of each phase present in the sample as a function of temperature and through the completed temperature transformation range. The shape of the corresponding electrical resistivity curve is added in each diagram to correlate the ER measurements with the wt% results.

The effects of the constant stress training on sample 500cs are clearly shown in figures 5.8a and b. The transformation behaviour of the trained sample is clearly modified respect to the untrained sample (figure 4.5): during cooling, untrained sample 500 has lower level of R-phase (38wt%) than the trained sample 500cs (46wt%). During heating, the quantity of R-phase is also increased up to 18wt% for the trained sample 500cs (12wt% for sample 500cs). Then, the R-phase does not disappear in the cooling and the heating part of the process after training. In fact, the quantity of the R-phase has been increased due to training.

The transformation process during the direct transformation is as following. During cooling, the martensite and the R-phase evolve together from austenite being the transformation simultaneous ($R_S=M_S=50^\circ\text{C}$), as occurs in the untrained sample 500. This simultaneous transformation has been advanced respecting to the untrained sample 5°C (see figure 4.5a). Therefore, the R-phase appears and is promoted due to training and it evolves together with martensite in the cold shape of the wire. When the R-phase transformation ends ($R_f=35^\circ\text{C}$), reaching a maximum level of 46wt% at 35°C , then, the martensite is formed from austenite plus R-phase, as seen in figure 5.8a. At 25°C the austenite reaches the 0wt%. At this temperature, the wt% of martensite is equal to 61wt%. This point can be considered as $M_{f50\%}$ temperature (as we defined in chapter 4). From this point, the martensite is formed only from contribution of the R-phase. Then, at the end of the cooling process there is less martensite (79wt%) and more residual R-phase (21wt%) in sample 500cs than in sample 500.

The heating process for sample 500cs is done with contribution of martensite and R-phase that transform into austenite ($A_S=40^\circ\text{C}$). The R-phase transformation starts to transform into austenite in a little quantity but enough to affect the ER curve. Therefore, we can define the temperature $R_{S\text{-heating}}$ as the temperature where the R-phase transforms to austenite during the heating process [HE, 2006]. This temperature is 60°C for sample 500cs. At the end of this transformation process, $A_f=75^\circ\text{C}$, there is 82wt% of austenite with little wt% of retained martensite (6wt%) and R-phase (12wt%). In agreement with [WAD, 2005], we can say that this poor quantity of retained martensite observed over A_f temperature seems to make impossible that it could be the mechanism responsible of the TWSME.

As seen in figure 5.8a, comparing the wt% results with the ER measurements for sample 500cs, the beginning of the resistivity hump in the ER curve corresponds well with the beginning of the simultaneous transformation of the austenite into R-phase and martensite in the wt% diagram. The end of the ER increase corresponds with the complete R-phase transformation. The following transformation from austenite and R-phase to martensite promotes a slight decrease in resistivity.

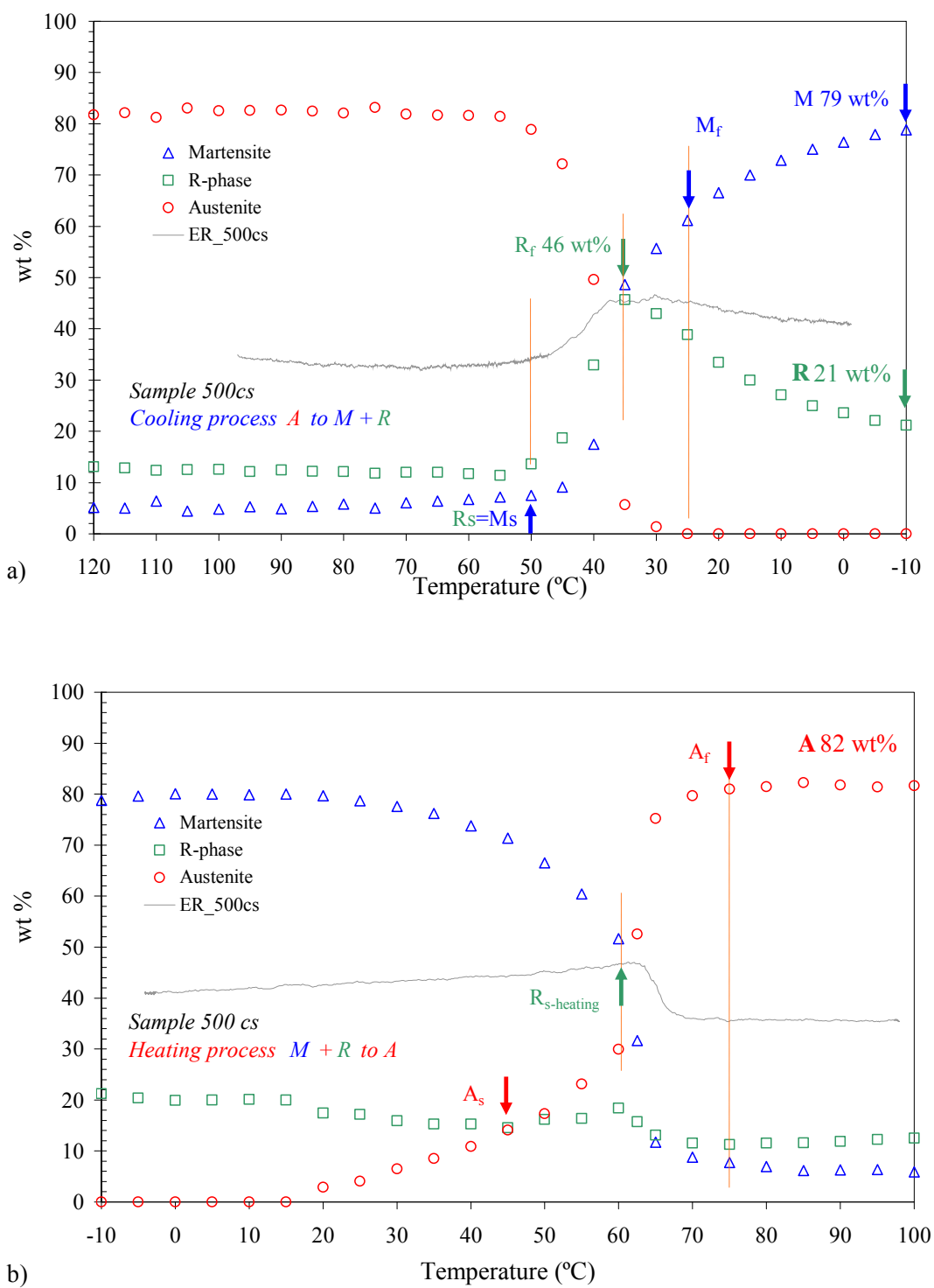


Figure 5.8 Evolution of the phase transformation behaviour due to training for samples 500cs during a) cooling and b) heating. The ER measurements have been added on the diagrams.

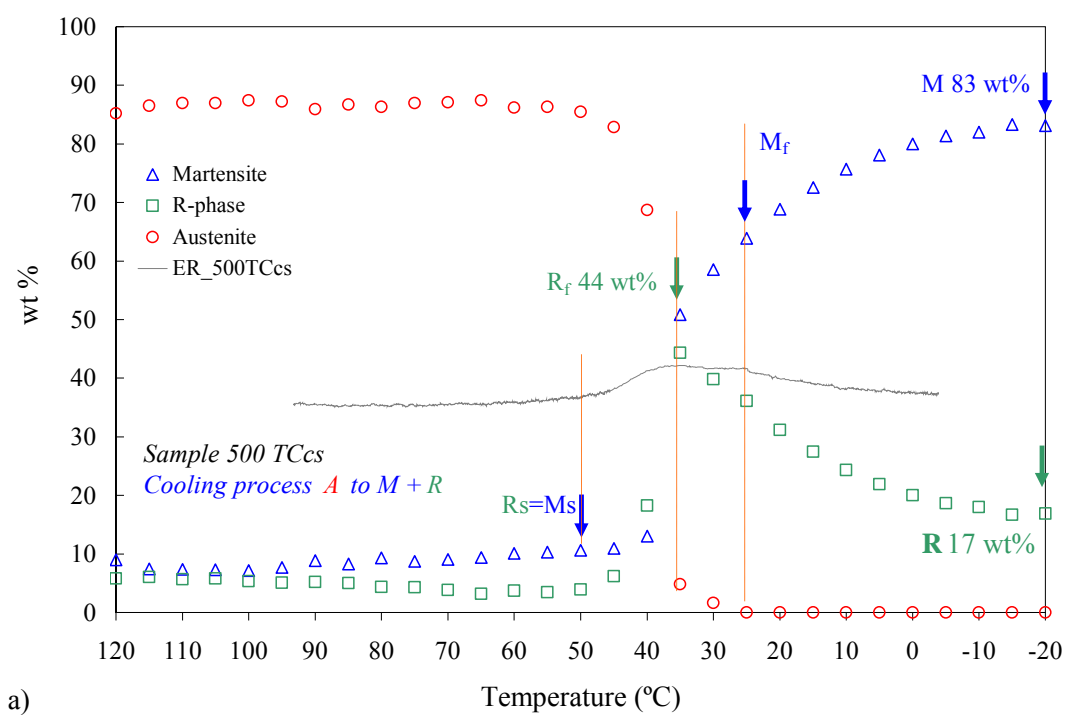
During heating (see figure 5.8b) occurs that the beginning of the decrease in resistivity corresponds well with the point at which the R-phase starts to transform into austenite (around 60°C). The end of the ER decrease coincides well with the end of R-phase and martensite transformation into austenite ($A_f=75^\circ\text{C}$). Therefore, the decrease in resistivity values seems to indicate the temperature at which the R-phase contributes to the austenite transformation ($R_{S\text{-heating}}$).

Comparing the experimental results for sample 500cs non-thermally cycled and those for sample 500TCs, thermally cycled at zero stress prior to training, we see that both have similar phase transformation path and similar transformation temperatures. However, some interesting differences are found (see figures 5.9a and b).

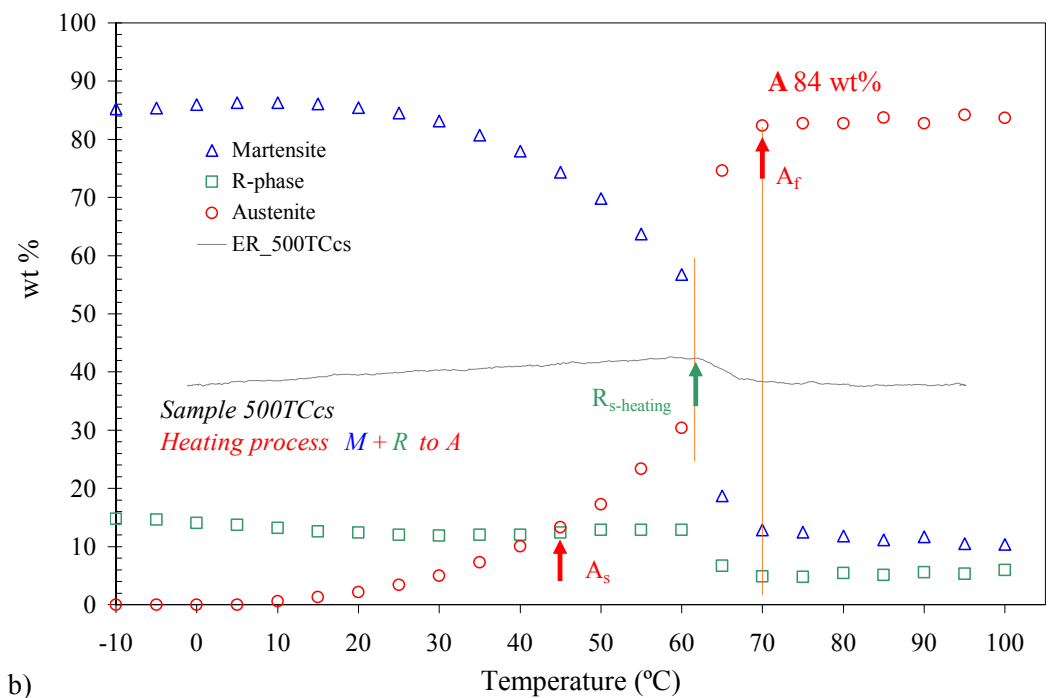
We have to notice that untrained sample 500TC has the phase transformation clearly separate in two steps (A to R to M, see figure 4.5c and d) because of the thermal cycling at zero stress. Therefore, constant stress training eliminates this separation between martensite and R-phase, promoting that martensite and R-phase evolve together after training and advancing the martensite transformation in 15°C. The second difference is that during cooling, although sample 500TC has a level of R-phase prior to training near of 61wt%, this training process did not increment this R-phase for sample 500TCs. In fact, this training reduces its R-phase wt% up to 44wt% in the cooling part of the process. This wt% value for sample 500TCs is very close to that of sample 500cs (figures 5.8a and 5.9a). Finally, in the heating part of the process, the R-phase is promoted by training up to 13wt% but in less quantity than in sample 500cs.

At the end of the cooling process, the 500TCs transformation to martensite reaches 82wt% with less residual R-phase than sample 500cs (4wt% less). The heating process for sample 500TCs is done with contribution of martensite ($A_s=40^\circ\text{C}$) and R-phase ($R_{S\text{-heating}}=60^\circ\text{C}$) that transforms into austenite. At the end of heating process, $A_f=70^\circ\text{C}$, there is a distribution of 84wt% for austenite with a little wt% of martensite (10wt%) and R-phase (6wt%).

As seen in figure 5.9a and b and comparing the wt% results with the ER measurements for sample 500TCs during the cooling and the heating process, the same remarks that we have been exposed for sample 500cs can be done for sample 500TCs.



a)



b)

Figure 5.9 Evolution of the phase transformation behaviour due to training for samples 500TCcs during a) cooling and b) heating. The ER measurements have been added on the diagrams.

The effects of constant stress training on sample 525cs are clearly shown in figures 5.10a and b. The transformation behaviour is clearly modified: although there is almost non-existent R-phase in the beginning of the training for this sample 525 (figure 4.6a), the constant stress training effectively promotes the R-phase in the cooling and the heating part of the process. During cooling, the quantity of the R-phase has been increased up to 46wt%; during heating, the quantity of R-phase is increased up to 19wt% (65°C). The transformation path in figure 5.10a indicates that the martensite and R-phase evolve together from austenite being the transformation simultaneous ($R_S=M_S=50^\circ\text{C}$), as occurs in the untrained samples 500 and 525, and in the trained samples 500cs and 500TCcs. This simultaneous transformation has not been advanced respecting to the untrained sample 525. The R-phase reaches its maximum level at 35°C (R_f), as seen in figure 5.10a. Therefore, the R-phase appears and is promoted due to training and it evolves together with martensite in the cold shape of the wire. When the R-phase transformation ends ($R_f=35^\circ\text{C}$), the austenite also reaches its 0wt%. At 35°C, the wt% of martensite is equal to 54wt%. This point can be considered as $M_{f50\%}$ temperature. From this point, the martensite is transformed thanks to R-phase. Then, at the end of the cooling process sample 525cs has less martensite (88wt%) than sample 525 (94wt%) and there is more residual R-phase (12wt%) in sample 525cs than in sample 525 (6wt%). The heating process for sample 525cs is done with contribution of martensite that transforms into austenite ($A_S=45^\circ\text{C}$). Around 65°C, we have a transformation to R-phase, as occurs in samples 500cs and 500TCcs ($R_{S\text{-heating}}=65^\circ\text{C}$). At the end of transformation process, there is a distribution of 84wt% of austenite (the untrained sample 525 had 93wt%) with a little wt% of residual martensite (4wt%) and R-phase (12wt%). Once more, there is a very little quantity of retained martensite over A_f temperature for this sample 525cs, as occurs for samples 500cs and 500TCcs.

Comparing the experimental results for sample 525cs non-thermally cycled and sample 525TCcs (figures 5.11a and 5.11b), it is possible to say that although sample 525TCcs has higher level of R-phase before training (36wt%) than sample 525cs, this training promotes less R-phase in sample 525TCcs (43wt%) than in sample 525cs (46wt%). After training and TWSME thermal cycling, both samples have similar quantity of R-phase, as occurs in samples 500cs and 500TCcs.

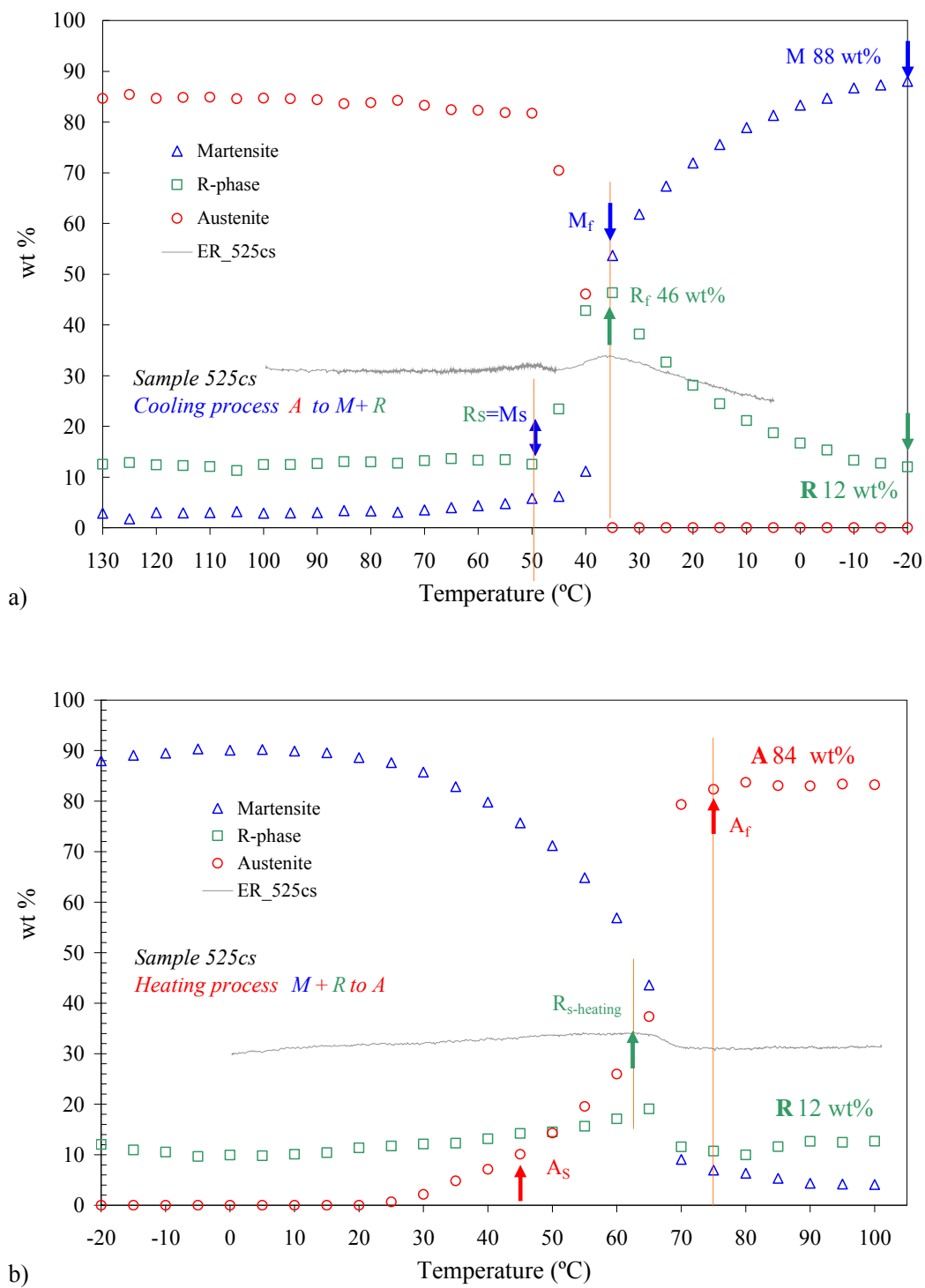


Figure 5.10 Evolution of the phase transformation behaviour due to training for samples 525cs during a) cooling and b) heating. The ER measurements have been added on the diagrams.

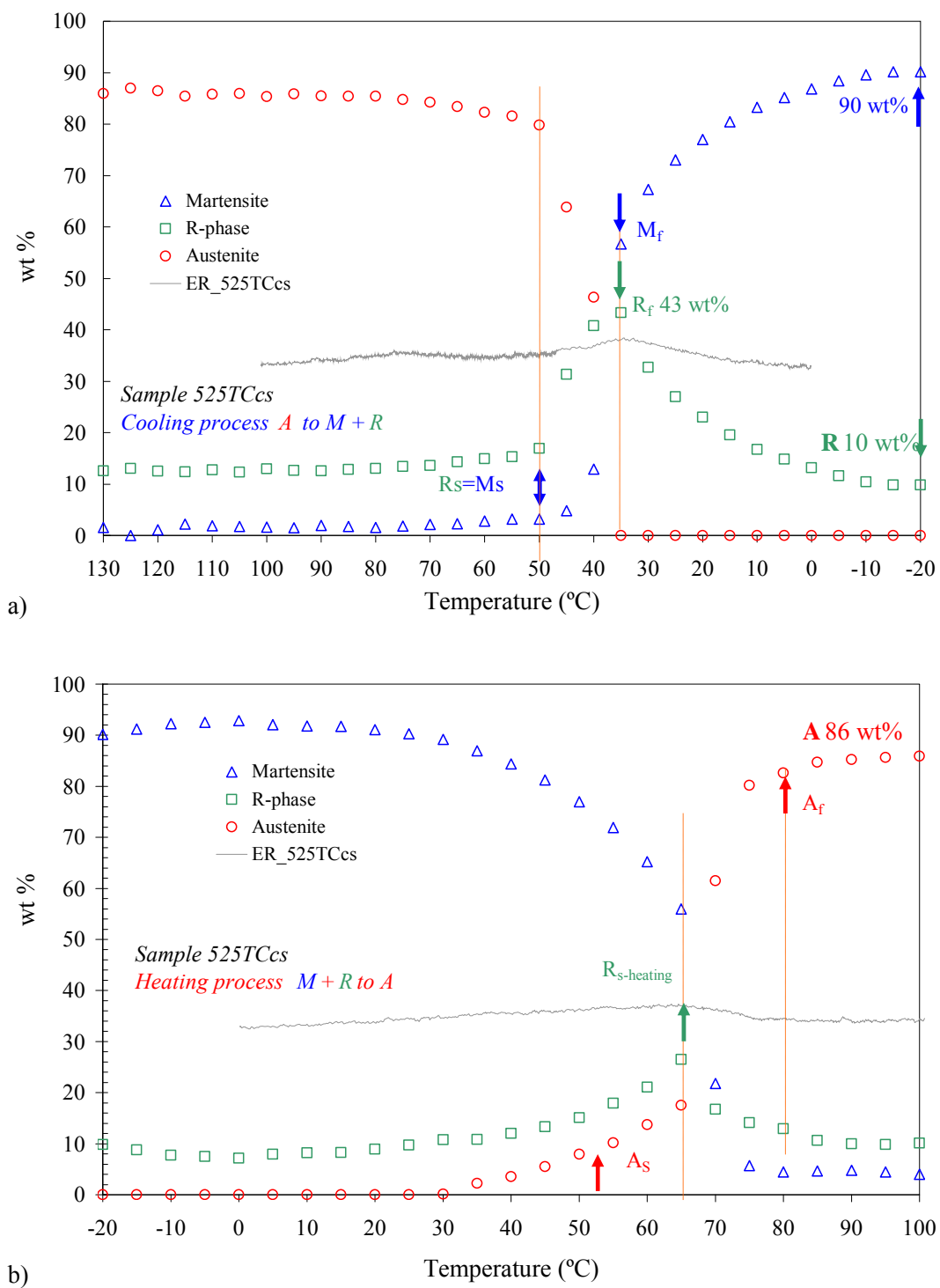


Figure 5.11 Evolution of the phase transformation behaviour due to training for samples 525TCcs during a) cooling and b) heating. The ER measurements have been added on the diagrams.

In the case of sample 525TCcs, the beginning of the martensite transformation is advanced respect to one of the untrained sample 525TC (around 15°C), thus eliminating the slightly separation of the phase transformation behaviour that thermal cycling at zero stress produced in sample 525TC. At the end of the cooling process, it is found an important difference with sample 525cs: the distribution of wt% for martensite is slightly higher (90wt%) for sample 525TCcs than for sample 525cs.

The heating process for this sample 525TCcs is done as sample 525cs did. The austenite transformation finishes at 80°C, as seen in figure 5.11b, and non-retained martensite is observed above austenite finish temperature. As seen in figures 5.10 and 5.11, and comparing the wt% results with the ER measurements for samples 525cs and 525TCcs, similar remarks can be done than those did for samples 500cs and 500TCcs.

Regarding of sample 475cs, which has not only an R-phase full developed due to heat treatment temperature, but also, the thermal cycling at zero stress applied (8 cycles) has not discernible effect on it, figures 5.12a and 5.12b show the effect of constant stress training and posterior TWSME thermal cycling on its phase transformation behaviour. We remember that its two-way shape memory effect is almost inexistent ($\epsilon_{tw}=0.37\%$, figure 5.3). Figure 5.12a shows the results for the cooling process. The first and main difference that is possible to appreciate respect to samples 500cs and 525cs is that training has not been eliminated the two step transformation that had the 475 untrained sample (figure 4.4a). In fact, this training not only kept its original two stage transformation path (A to M to R), but also the martensitic transformation has been delayed 15°C respect to the untrained one ($M_s=5^\circ\text{C}$ for 475cs). Moreover, the 475cs R-phase temperature interval is wider than one of 475 sample: the temperature interval of the R-phase transformation is 45°C for sample 475cs and for sample 475, it is 25°C. Therefore, training under constant stress promoted the R-phase transformation, but this is a cost to displace the martensitic transformation to values near of 0°C. At -30°C, the martensitic transformation reached only 65wt% of transformation. This explains the poor two way memory strain produced at room temperature. During heating (figure 5.12b), its phase transformation is similar to those explained for samples 500 and 525, but this sample has the austenitic transformation early than those samples ($A_s=30^\circ\text{C}$ and $A_f=60^\circ\text{C}$). The austenite reaches a distribution of 67wt% at the end of the heating

process. These results make the sample 475cs not very useful for TWSME applications near room activation temperatures.

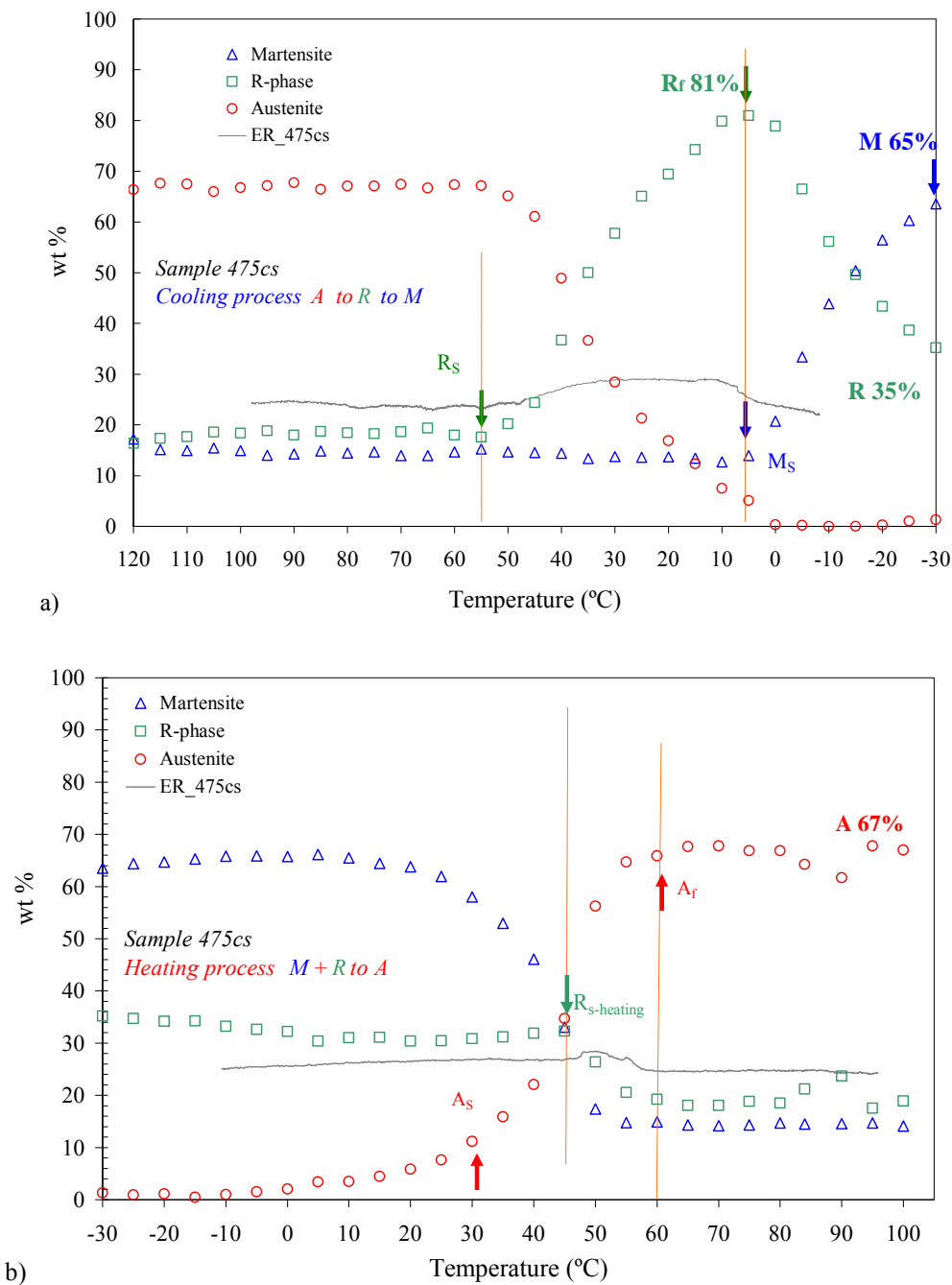


Figure 5.12 Evolution of the phase transformation behaviour due to training for sample 475cs during a) cooling and b) heating. The ER measurements have been added on the diagrams.

The ER measurements added to figures 5.12a and b are in good agreement with the wt% diagrams. As seen, the 475cs ER curve on cooling is similar to that of 475 untrained sample (see figure 4.1); nevertheless sample 475cs has the resistivity plateau longer than that of 475, with an increase in resistivity that marks the beginning of the R transformation. At the end of the wide resistivity plateau, the R_f transformation is finished, giving to the martensite transformation the opportunity to transform. However, during heating the ER curve presents a little decrement in resistivity that match well with the austenite transformation in the wt% results. This decrement in resistivity did not appear in the resistivity curve of the sample 475 (figure 4.1).

Concerning the changes that constant stress training produces on the phase transformation behaviour of the samples analyzed, it can be concluded that **to develop a substantial two way memory strain is necessary that the training promotes in the SMA sample a phase transformation path characterized by a simultaneous transformation of the austenite to R-phase plus martensite during cooling**. To achieve this transformation path, training has to increase the martensite transformation temperature and promoting that the R-phase evolving together with martensite phase during all the heating and cooling process. The kind of sample suitable to promote this above explained convenient phase transformation behaviour and then, to develop substantial two way memory strain is the one which is heat treated at temperatures equal to or greater than 500°C (500 and 525 samples).

Secondly, as seen in the wt% diagrams, the increase in the dislocation density in the matrix by constant stress training permits certain development of the R-phase for those samples non-thermally cycled before training (500cs and 525cs). However, we have seen that for sample thermally cycled prior training 500TCcs, its R-phase decreases a little respecting to the untrained sample 500TC. Similar situation occurs for sample 525TCcs, which suffers an increase in R-phase lower than that for non-thermally cycled 525cs. In any case, all samples have similar distribution of R-phase after training and TWSME thermal cycling. Therefore, **the R-phase does not disappear with thermomechanical cycling** as Pozzi et al. suggested in [POZ, 1990]. In fact, it is present in all trained samples. To explain the development of the R-phase due to thermomechanical training, Uchil et al. [UCH, 2002]b suggests that the dislocations created by thermomechanical training may form the nucleation site for the martensite

phase or they may pin down the motion of the martensite plates depending on their density or interaction. Pining down the motion of the martensite plates paves the way to the formation of the R-phase during thermomechanical cycling. Therefore, the density of dislocations that remains after heat treatment in sample 475cs makes difficult the mobility of the martensite plates, promoting the development of the R-phase by training. Samples with a initial low density of dislocations after heat treatment (500 and 525 samples) and samples with a initial density of dislocations that are developed by thermal cycling at zero stress (500TCcs and 525TCcs samples), seem to have the optimal conditions to permit the motion of the martensite plates needed to obtain substantial TWSME.

The reasons why the samples thermally cycled present higher two-way memory strain than those samples non-thermally cycled will be discussed in section 1.5.

1.4.4 Activation temperatures

To conclude the analysis of the activation temperatures, a summary of the activation temperatures obtained by each of the different experimental methods used is listed in table 5.2a for samples 500 and in table 5.2b for samples 525.

We present the ER and XRD measurements combined as we established in chapter 4. As seen, all temperatures measured by different methods are in reasonable agreement and they are in an affordable range for TWSME industrial applications. We should remark that the A_S temperature measured by the applied loading method (strain-temperature curve) is almost equal than those that we found by wt% called $R_{S\text{-heating}}$.

In general, we can say that for trained samples non-thermally cycled (500cs and 525cs samples) the M_S is similar and the M_f is higher than those of the untrained samples 500 and 525. For trained samples thermally cycled 500TCcs and 525TCcs both martensitic temperatures increase larger respect to the original samples 500TC and 525TC. The R-phase transformations of trained samples have been advanced around 5°C respect to the untrained ones. Respecting to the austenitic activation temperatures, all trained samples have slightly lower or very similar temperatures than those of the untrained samples.

That means first, that the transformation temperature interval is stretched by the constant stress training and posterior TWSME thermal cycling, being more grand this stretching for samples thermally cycled prior to training than for samples non-thermally cycled prior to training. Secondly, the transformation temperatures of the untrained samples can be taken as a reference to know how can result the activation temperatures of the same samples after training.

	Activation Temperatures (°C) Sample 500cs/sample 500TCcs		
	<i>Temperatures of untrained samples 500/500TC</i>	<i>Applied loading 500cs/500TCcs</i>	<i>Combination of ER and XRD 500cs/500TCcs</i>
M _{f50%}	25 / 13	31 / 29	25 / 25
M _S	45 / 30	42.5 / 44.6	50 / 50
R _f	30 / 30		35 / 35
R _S	45 / 46		50 / 50
A _S	55 / 46	64 / 63	40 / 40
R _{S-heating}			60 / 60
A _f	79 / 73	73.5 / 72.2	75 / 70

a)

	Activation Temperatures (°C) Sample 525cs/sample 525TCcs		
	<i>Temperatures of untrained samples 525/525TC</i>	<i>Applied loading 525cs/525TCcs</i>	<i>Combination of ER and XRD 525cs/525TCcs</i>
M _{f50%}	32 / 16	35.8 / 31.7	35 / 35
M _S	48 / 35	45.8 / 45.7	50 / 50
R _f	30 / 25		35 / 35
R _S	45 / 47		50 / 50
A _S	57 / 48	62.5 / 63	45 / 45
R _{S-heating}			65 / 65
A _f	84 / 78	72.5 / 75.6	80 / 80

b)

Table 5.2 Activation temperatures measured by different methods for a) 500cs-500TCcs and b) 525cs-525TCcs samples.

1.5 Relationships between the TWSME macroscopic behaviour and the changes in the phase transformation behaviour

In this section, the relationship between the macroscopic mechanical behaviour of the Ti-Ni wire after constant stress training (that is, the obtained two-way memory strain) and the phase transformation behaviour of the alloy is presented. We try to clarify first, the improvement of the two-way shape memory strain by thermal cycling at zero stress and second, the role of the R-phase in the TWSME.

As seen in this section and in chapter four of this thesis, the selection of the heat treatment temperature has a strong influence on the properties of the alloy: the heat treatment temperatures 500°C and 525°C permit to obtain a material with a lower initial dislocation density. If a thermal cycling at zero stress is applied to these samples, the level of the dislocations increased: the accumulation of dislocations in parent crystal promotes the development of the R-phase in the cooling part of the phase transformation process, as seen in chapter four. Moreover, the temperature of the martensite transformation decrease because of thermal cycles at zero stress (see tables 5.2a and 5.2b). The reason of these temperature decreases lies on the stress field introduced by the dislocations, which depress all the temperature transitions: the dislocations generated during cycling interfere with the transformation process and increase the degree of under-cooling required for the transformation to proceed.

The mechanism to obtain TWSME through thermomechanical cycling lies in developing reminders of the desired cold shape (known as dislocation arrangement) in the austenite phase by repeating the transformation cycle between the martensite phase and the austenite phase with the application of an external stress [LUO, 2007]. These dislocation arrangements create an anisotropic stress field in the matrix of austenite, which guides the nucleation growth of the martensite variants towards the preferred orientations in relation to the deformation adopted in the training procedure. The changing microstructure appears to assist the martensitic transformation resulting in a decrease of the required under cooling. On the other hand, maximum TWSME is generated due to optimum density of dislocations and magnitude of internal stress [WAD, 2008]. A low initial density of dislocations in the alloy due to the application of an adequate annealing temperature allows introducing new dislocations easily by

thermomechanical cycling and therefore to develop a substantial TWSME, as seen in the above sections.

Nevertheless, **the effects of repeated thermal cycling at zero stress and the effects of thermomechanical training at constant stress are opposite if each process is applied separately to the Ti-Ni alloy. The first one makes that the dislocation arrays interfere with the transformation accommodation mechanism thus reducing the martensite transformation temperature. The second one, through the introduction of dislocations that act as a nucleation sites for martensite plates, assists the martensite transformation.** Therefore, how to explain that samples thermally cycled prior to training develops higher TWSME than those samples non-thermally cycled?

As published by Miyazaki et al. [MIY, 1986], if thermal cycling at zero stress is applied to a previous pre-strain 49.8%Ni SMA, M_S increased with the pre-strains from 4.66% to 11.8%, and M_S was almost constant when the pre-strain was as high as 22.8%. When no pre-strain was induced, a decrease in M_S was observed. It is found that the degree of change in M_S depends upon the amount of pre-strain and that the effects of conventional thermal cycling at zero stress (decrease in M_S) are suppressed by the previous work hardening (pre-strain). Then, if the pre-strain is small, new dislocations may be generated or existing dislocations may be rearranged by thermal cycling at zero stress such that the transformation gradually becomes easier. However, in a strongly work hardened condition, dislocations will find it very difficult to move during thermal cycling and thus M_S changes a little.

Joining the effects of thermal cycling at zero stress and constant stress training, it may be possible **to suppose that the existing dislocations introduced by thermal cycling at zero stress (developing the R-phase) are rearranged by constant stress training, facilitating the nucleation growth of the martensite variants towards the preferred orientations in relation to the deformation adopted in the training procedure.** Accordingly, the thermal cycling dislocations with the new dislocations introduced by training, both help to built the anisotropic stress field in the matrix of austenite that is necessary to make possible the reorientation of the martensite variants.

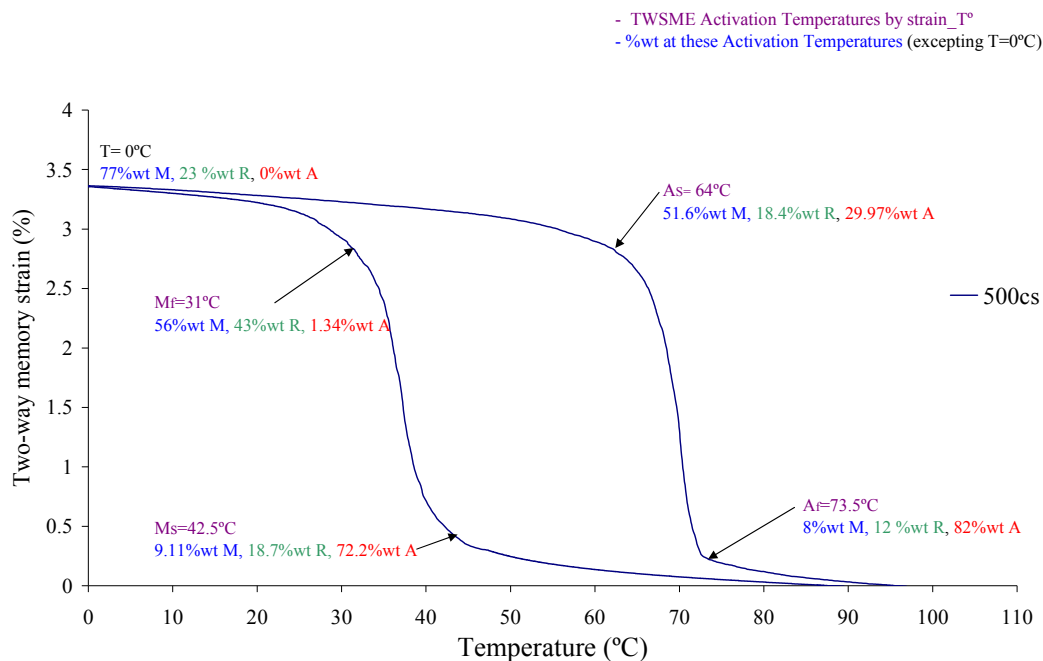
Thus, for samples thermally cycled the process of reorientation of the martensite is easier, as it has been experimentally demonstrated (figure 5.1).

On the other hand, the recoverable strain associated with the austenite \leftrightarrow martensite transformations is the most important contribution to the two-way memory strain [LIU, 1990]. Then, as more the microstructure transforms from participating austenite to martensite, the greater the formation of preferentially oriented martensite variants, and thus larger the martensite strain will be, resulting in higher two-way memory strain. From this words is deduced that **as higher is the increment in R-phase by thermomechanical training respect to the initial distribution of the R-phase in the alloy, a reduced amount of motion of the martensite plates can be generated due to training**. Then, lower the formation of preferentially oriented martensite variants, and thus shorter the martensite strain will be, resulting in lower values of two-way memory strain.

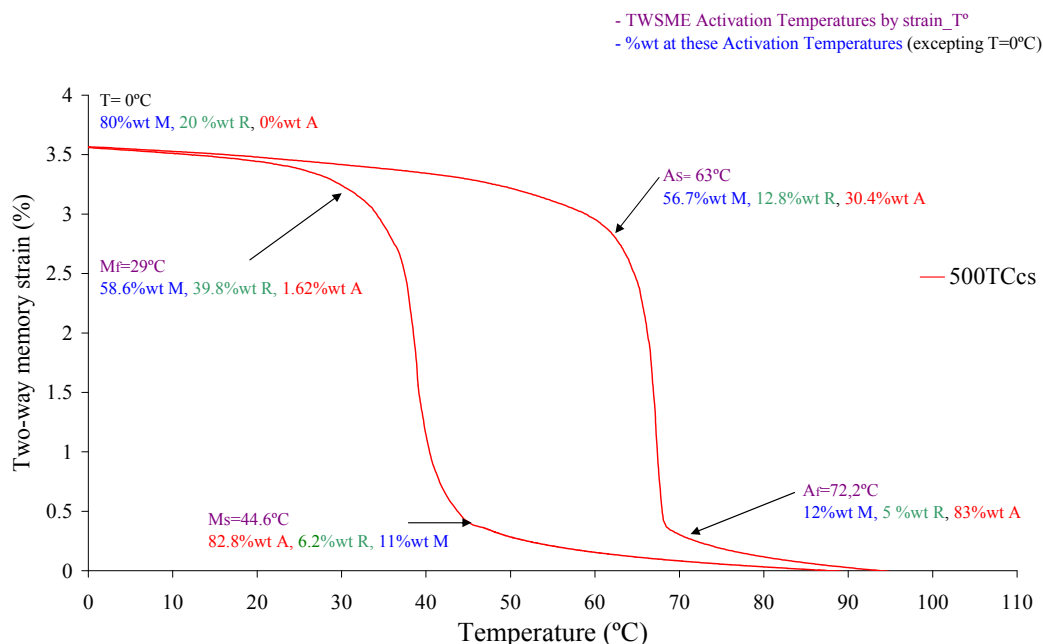
For that reason, trained samples 500cs and 525cs non-thermally cycled have a microstructure as not as favourable for the martensite-austenite transformations as the trained thermally cycled samples 500TCcs and 525TCcs have (see figures 5.8 to 5.10). The responsible of this is the development of the R-phase in samples non-thermally cycled during training, which is much larger than in thermally cycled alloys. Therefore, trained samples non-thermally cycled generate lower two-way memory strain than samples thermally cycled. To verify all the above referred, the relationship between the macroscopic behaviour of the TWSME sample and its phase transformation behaviour after training is shown in figures 5.13. To make the analysis easy, the activation temperatures according to the applied loading method (tables 5.2) and the wt% distribution at these activation temperatures are reported in these figures 5.13.

Analyzing the heating and cooling transformations that show all figures 5.13, it is very important to remark that **the wt% distribution follows well the TWSME hysteresis loop**. Then, the wt% evolution with temperature reflects well the macroscopic TWSME behaviour for all the alloys analyzed (strain-temperature behaviour). Moreover, the following differences between samples are found. Focusing on the heating process, that is, from the cold to the hot shape of the samples, figures 5.13 show that the sample which has the highest two-way memory strain is the sample

which has the highest availability of martensite at a temperature A_S , that is, sample 525TCcs (65.2wt%). In opposition, the sample which has the lowest two-way memory strain is sample 500cs with a distribution of 51.6wt% of martensite at A_S .

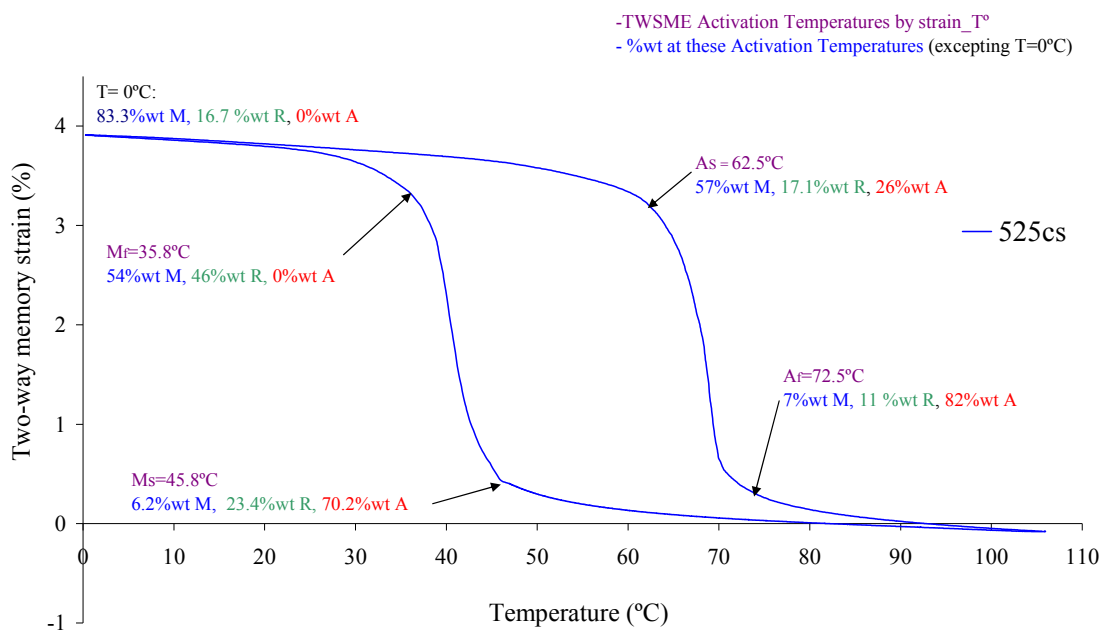


a)

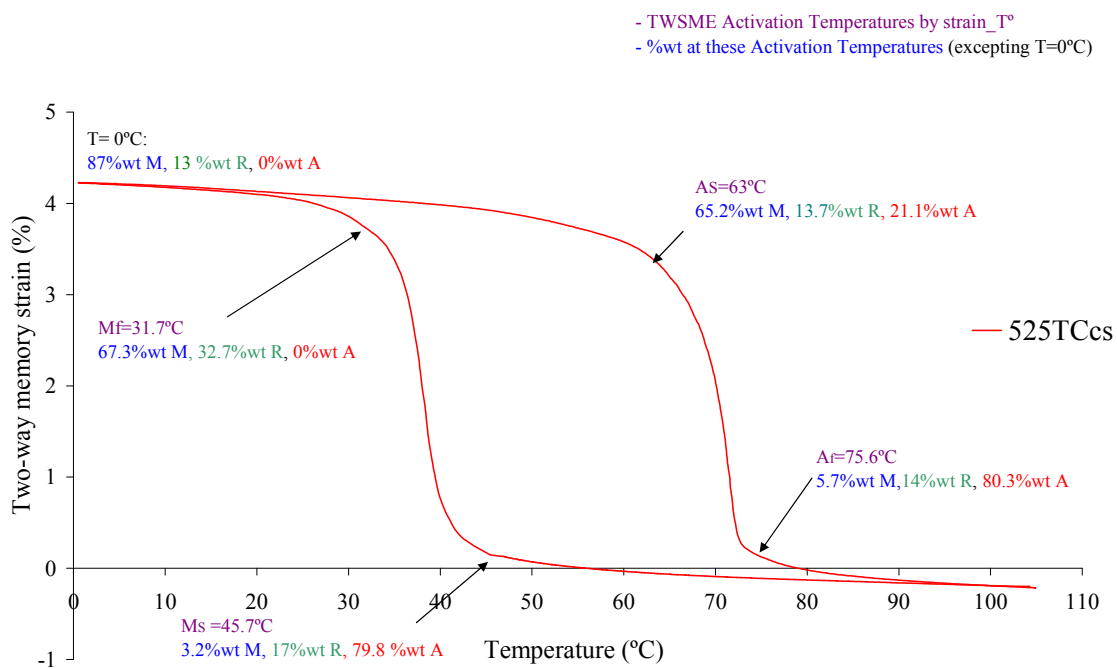


b)

Figure 5.13 Relationship between the macroscopic two-way memory strain and the phase transformation behaviour for a) 500cs and b) 500TCcs samples



c)



d)

Figure 5.13 Relationship between the macroscopic two-way memory strain and the phase transformation behaviour for c) 525cs and d) 525TCcs samples.

It is important to note that R-phase participates in the transformation to hot shape of the sample, although in a poor quantity. Then, samples thermally cycled 500TCs and 525TCs not only have higher distribution of martensite, but also have lower distribution of R-phase than samples non-thermally cycled at temperature A_S . Finally, the retained martensite (non transformed martensite) at the end of the heating process, varies from 12wt% to 5.7wt% depending on the sample. According to [WAD, 2008], we think that the retained martensite is not the responsible mechanism to produce the generation of TWSME.

Focusing on the initial activation temperature to recovery the cold shape of the alloys (M_S), the simultaneous transformation from austenite to martensite plus R-phase begins with further wt% distribution of martensite for samples thermally cycled. At M_S temperature, samples 500TCs and 525TCs have more austenite and less R-phase (82.8wt% and 79.8wt% for austenite and 6.2wt% and 17wt% for R-phase, respectively) to transform to martensite than their respective samples non-thermally cycled 500cs and 525cs (72.2wt% and 70.2wt% for austenite and 18.7wt% and 23.4wt% for R-phase). As less quantity of R-phase has the alloy at the beginning of the cold transformation, the possibility of martensite formation increases, allowing development a longer martensite transformation strain. In fact, samples thermally cycled have longer transformation to the cold shape, as it is determined by their martensitic temperature interval (table 5.2).

Then, the hypothesis that we make about the dislocations introduced by previous thermal cycling at zero stress are rearranged by the constant stress training, thus helping the formation of preferentially oriented martensite, seems to be certainly true.

The next step is to study the isothermal training.

2 Influence of the heat treatment and thermal cycling on isothermal tensile deformation below M_f training method

The second part of this section presents the results obtained for isothermal tensile deformation under M_f training for trained samples 450it, 475it, 500it, 500TCit, 525it and 525TCit. We used the term “it” to differentiate these samples from those trained by constant stress training.

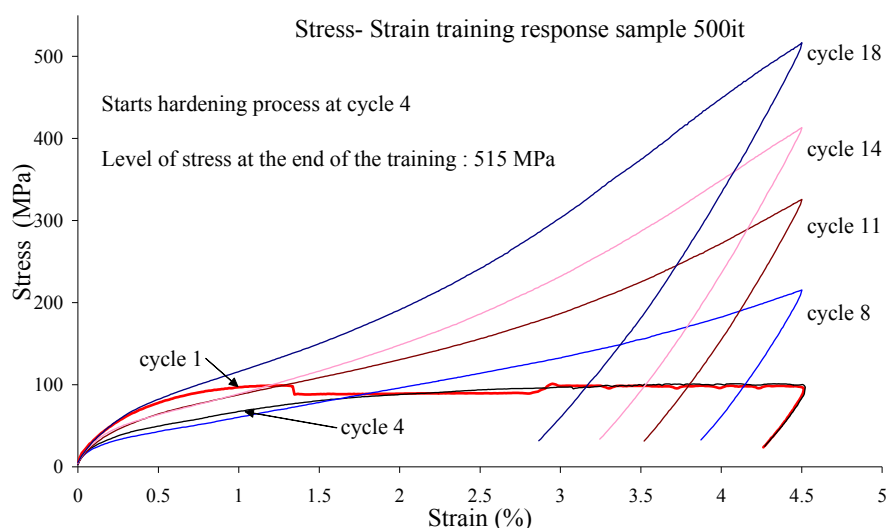
2.1 *Influence of heat treatment and thermal cycling at zero stress on the training parameters*

2.1.1 Samples 500it and 500TCit

Figure 5.14 summarizes the effect of the isothermal training procedure on the stress-strain response. Specifically, figure 5.14a shows the non-thermally cycled trained sample 500it and figure 5.14b shows the thermally cycled trained sample 500TCit. Both figures show the profiles for the first training cycle, several intermediate training cycles, and the last training cycle. The following observation can be made for both samples regarding the effect of the training on the stress-strain response. When the number of the training cycles increases, a hardening of the material is observed, resulting in a large stress level, together with a decrease in the stress for the onset of the reorientation. The effect of the training is a high slope of the reorientation plateau after 18 training cycles for sample 500it and after 33 training cycles for sample 500TCit. This hardening process is due to the formation of a dislocation structure [LIU, 1990], that benefits the two-way shape memory behaviour of the material. As shown in figure 5.14a, the hardening process of the alloy is faster when the material is non-thermally cycled prior to training: after only four training cycles sample 500TCit starts the hardening process. In comparison, sample 500TCit starts to show this effect much later, after twelve training cycles.

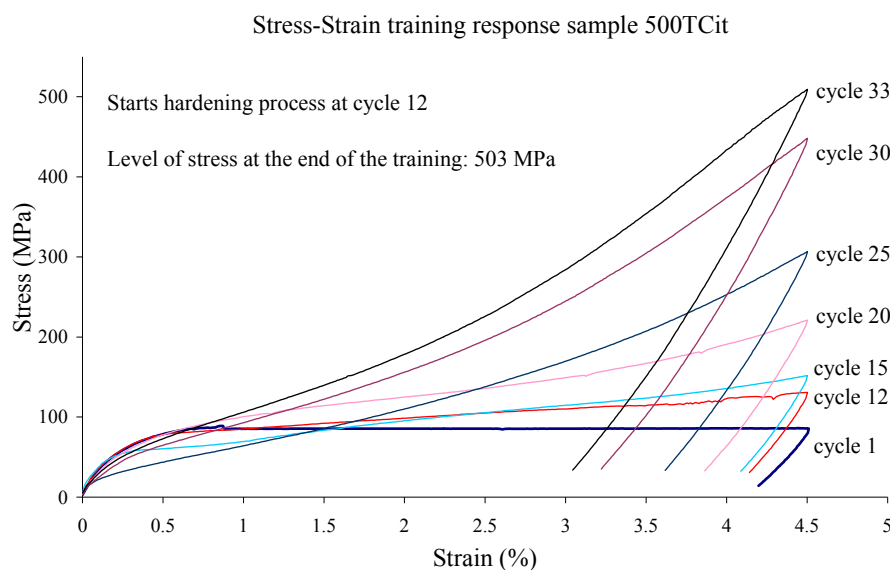
Figures 5.15a and 5.15b give for samples 500it and 500TCit the increasing two-way memory strain during training (ε_{tw_tr}) and the accumulated plastic strain (ε_p) versus the number of training cycles. Regarding the growth of ε_{tw_tr} during training, both figures clearly show that the ε_{tw_tr} appears when the hardening process starts and increases

when the number of training cycles also increases. In fact, the ε_{tw_tr} is non-existent in sample 500it before the fourth training cycle and for sample 500TCit, the ε_{tw_tr} is non-existent before the twelfth training cycle. In particular, figure 5.15a (500it) shows that ε_{tw_tr} increases from 0.37% (the initial value at the fourth training cycle) to 3.35% after 18 cycles. For sample 500TCit, figure 5.15b shows that ε_{tw} increases from 0.24% (the initial value at the twelfth training cycle) to 2.6% after 33 cycles. The training is considered finished when five consecutive values of ε_{tw_tr} measured during training are constants (n=18 for 500it, n=33 for 500TCit). It is important to note that the level of the final stress at the end of the training is practically the same for both samples. To clarify this, figure 5.16 shows the evolution of the final stress level versus the number of training cycles for both samples. Similar stress level values are found for both samples, suggesting that the dislocation arrangements introduced by training achieve a certain saturation level regardless of the number of training cycles. Once the saturation level of dislocations is reached, the alloy reaches its maximum value of ε_{tw} , and the two-way shape memory behaviour cannot be further improve by applying additional training cycles. Therefore, the maximum value of ε_{tw} is associated with a certain level of stress and certain level of dislocation arrangements, and not with the number of training cycles.



a)

Figure 5.14a Stress–Strain responses during isothermal training for a) sample 500it



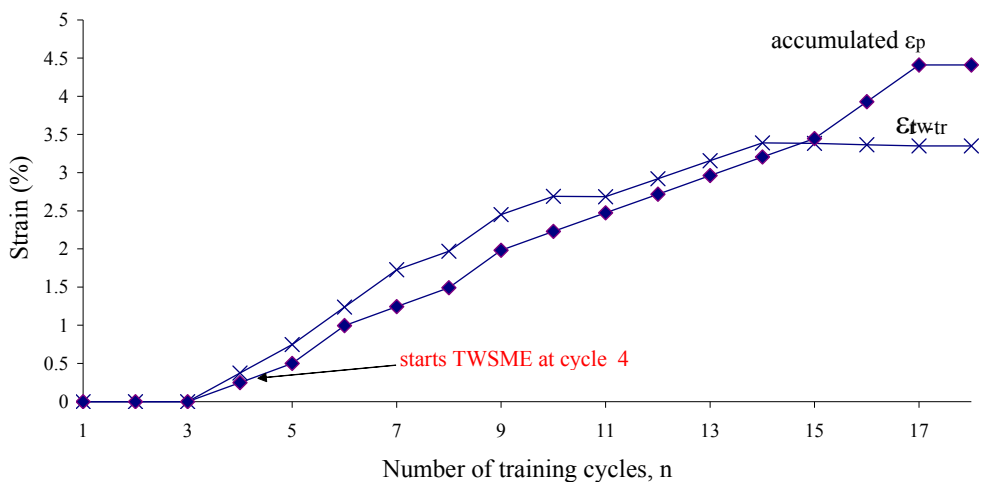
b)

Figure 5.14b Stress–Strain responses during isothermal training for b) sample 500TCit.

Figure 5.15 (a and b) also shows that the accumulated ϵ_p at the end of the training has the same value for both samples. The accumulated ϵ_p for thermally cycled sample 500TCit is 4.36% and for sample 500it it is 4.40 %. This fact reinforces the idea that the maximum value of ϵ_{tw} is associated with a certain level of stress and certain level of dislocation arrangements, and not with the number of training cycles.

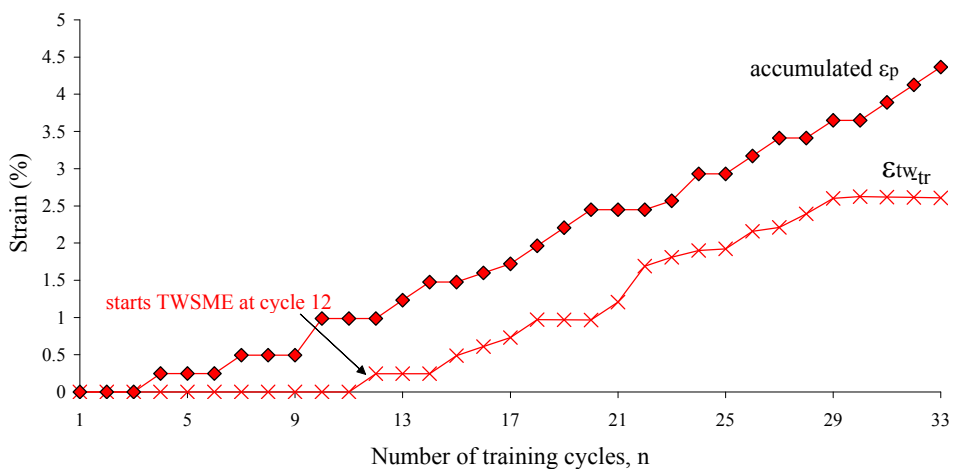
An important conclusion we reach: the thermally cycled 500TCit sample seems to be more resistant to the introduction of dislocations by isothermal training when same training parameters are applied to both samples. Therefore, further training cycles (almost twice as many) are needed to start the formation of the dislocation structure in order to reach a substantial but fairly constant value of ϵ_{tw-tr} in the thermally cycled sample. To study the sample 500TCit disadvantage, other immediate consequences of the training we should analyze. These are firstly, the progressive and obvious decrease in the initial critical stress for slip (σ_s^{CR}) during training and, secondly, the appreciable change in the slope of the initial elastic part of the stress-strain curve, which as well indicates the change in the apparent modulus (E_{load}) as the training proceeds. These changes are also accompanied by the change in the values of the apparent modulus for the deformation of the oriented martensite (E_{reor}).

Strain evolution during isothermal training for sample 500it



a)

Strain evolution during isothermal training for sample 500TCit



b)

Figure 5.15 Permanent strain and two-way memory strain evolution for a) sample 500it and b) sample 500TCit.

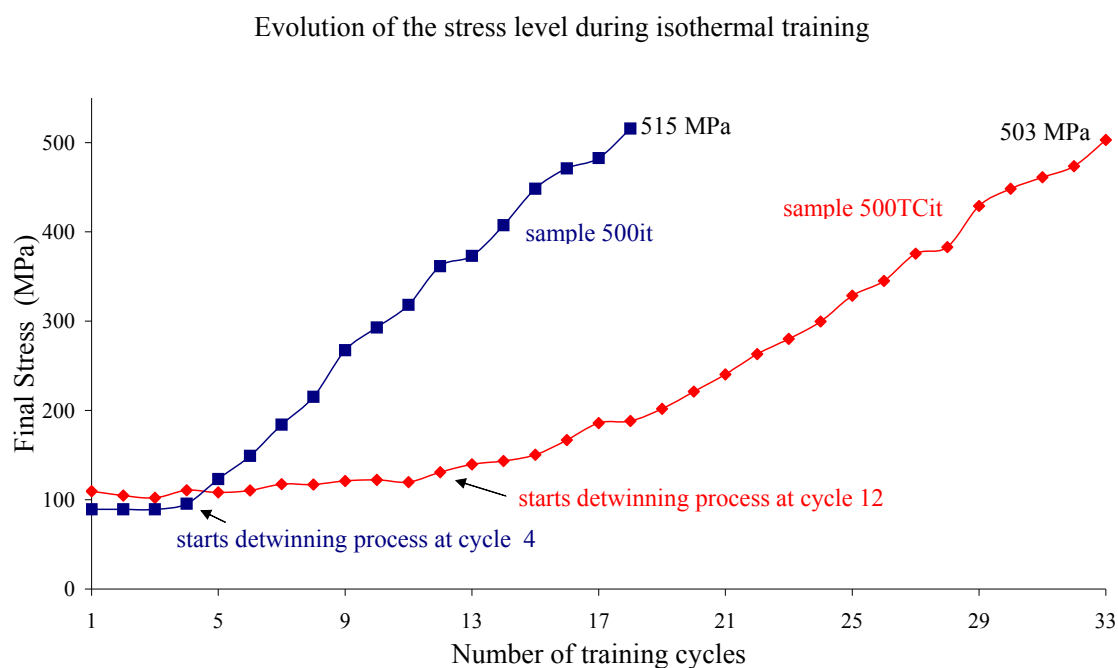


Figure 5.16 Evolution of the level of stress at the end of each isothermal training cycle: comparison between samples 500it and 500TCit.

Isothermal training has as main deformation mechanism the martensite variant reorientation in the direction of the applied stress. As the training proceeds, a reconfiguration of martensite twins takes place, more martensite variants are aligned in the stress direction, and then, it becomes easier to reorient all the martensite variants. Then, the stress needed for the onset of the reorientation process (σ_S^{CR}) decreases as the number of cycles increases [LIU, 1999]. This decrease is less pronounced for sample 500TCit, as seen in figure 5.14, because this sample initially presents higher σ_S^{CR} than sample 500it (see table 4.7).

On the other hand, figure 5.17 shows the apparent modulus for the initial linear part of the curve and the apparent modulus for the reoriented martensite (E_{reor}) versus the number of training cycles. The initial values of the apparent modulus are according with those considered appropriate for the apparent modulus of the martensite. As can be appreciated in figure 5.17, the E_{load} for sample 500it starts to decrease heavily from cycle fourth, however, for sample 500TCit its E_{load} starts to decrease heavily from cycle twelve. These decreases in E_{load} coincide with the training cycle at which the two-way

memory properties appear in each sample. As the values of the E_{load} decrease, the apparent modulus for the reoriented martensite increases. Both, E_{load} and E_{reor} , reach progressively a coincident value as the training proceeds. Comparing the results in the figure 5.15 with those in figure 5.17, the values of both modules are almost equal when the number of training cycles is high enough to produce a stable value of the two-way memory strain measured during training. The decrease in the value of apparent modulus on load suggests that pure thermal martensite variants disappears as training advances until that all martensite is reoriented martensite. Then, both modules have the same value because the structure of the sample is composed by the same type of martensite: reoriented martensite.

As seen, the modulus evolution shows that sample 500TCit is more resistant to the reorientation of the martensite variants than sample non-thermally cycled 500it: the decrease in critical stress and E_{load} confirms that sample 500TCit reaches lately the appropriate dislocation structure to produce the two-way memory properties.

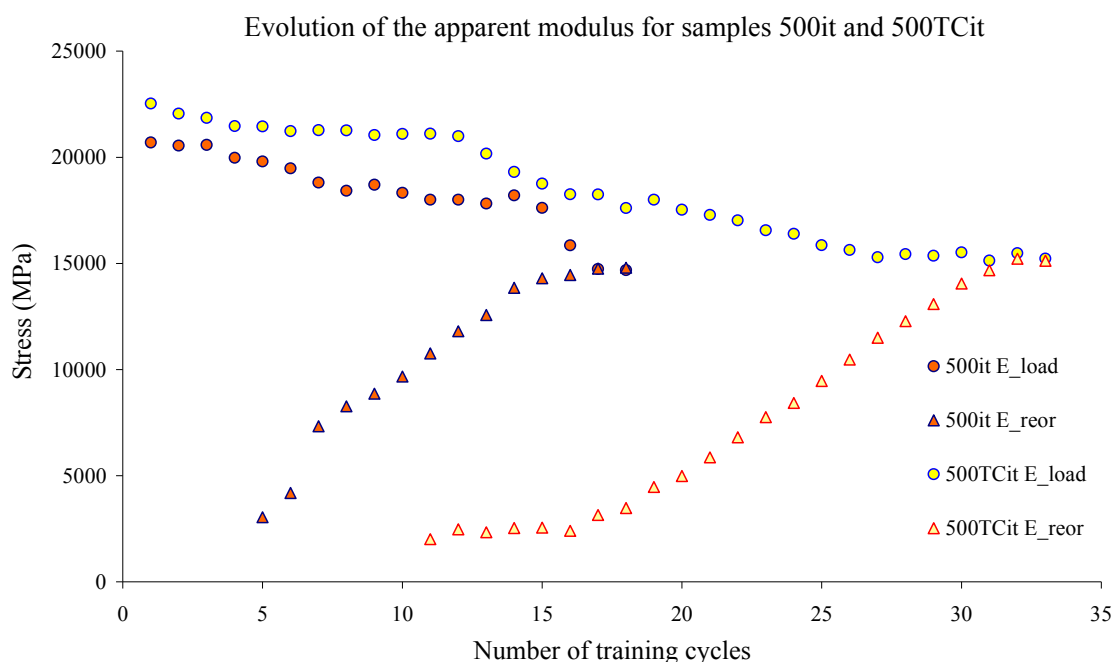


Figure 5.17 Evolution of the apparent modulus for the initial elastic portion of the stress-strain curves (E_{load}) and evolution of the apparent modulus of the reoriented martensite (E_{reor}) with number of training cycles for 500it and 500TCit trained samples.

2.1.1.1 Influence on the two-way memory strain obtained

Two-way memory strain values for both samples were measured after isothermal training. To obtain the values of ϵ_{tw} , 500it and 500TCit underwent a further thermal cycling under no-load for thirty cycles (TWSME thermal cycling). Figure 5.18 shows the evolution of ϵ_{tw} during TWSME thermal cycling for both samples. The maximum ϵ_{tw} for sample 500it is 3.85% and the maximum ϵ_{tw} for sample 500TCit is 3.12%. This shows that thermally cycled sample 500TCit develops lower ϵ_{tw} values than those of 500it (about 0.7% of difference). Despite this, the evolution of ϵ_{tw} during TWSME thermal cycling is similar for both samples and there is a continuous loss of the two-way memory strain, which, after 30 thermal cycles is 0.2% for both samples, as occurs with samples trained by constant stress training (see figure 5.4b).

By now, it can be said that applying a prior thermal cycling at zero stress work against the development of the two-way memory behaviour by isothermal training. However, more analysis are needed to elucidate the reasons of the above results, because the effect of isothermal training on sample thermally cycled 525TCit is exactly the opposite: 525TCit needs lower number of training cycles to develop a significant ϵ_{tw} than sample 525it.

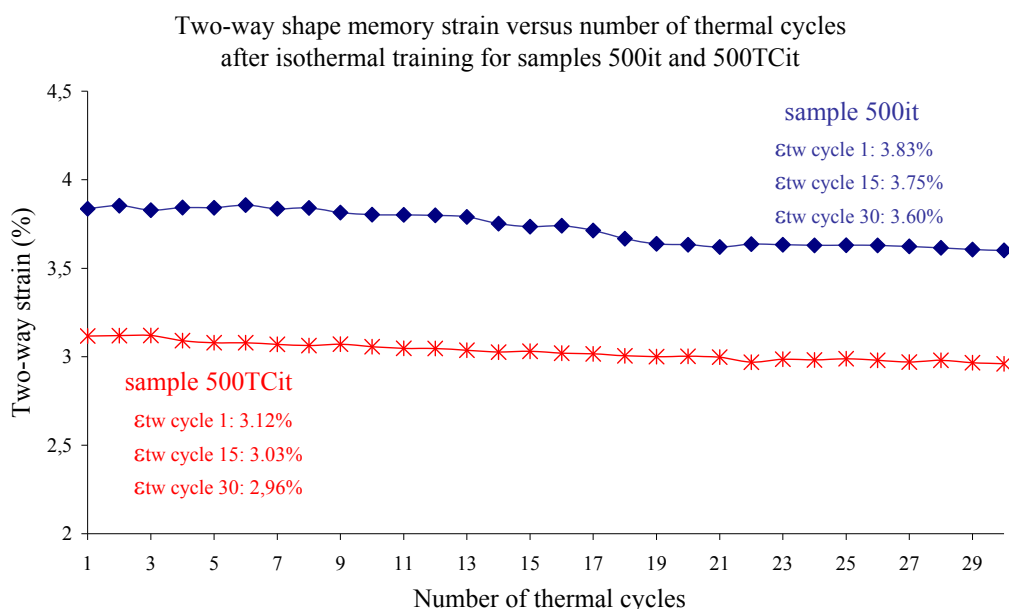


Figure 5.18 Evolution with TWSME thermal cycling of the two-way memory strain obtained by isothermal training for samples 500it and 500TCit.

2.1.2 Samples 525it and 525TCit

Figure 5.19 shows the effect of isothermal training on both samples 525it and 525TCit, namely a high slope of the reorientation plateau of the stress-strain curve after 20 training cycles for sample 525it and after 16 training cycles for sample 525TCit. This is because of the hardening process of the material, which is caused by the formation of a dislocation structure, as occurs with samples 500. This hardening process is slightly faster when material 525 is thermally cycled prior to training. Both samples show two-way memory properties from the first training cycle, but sample 525it develops more slowly these properties than sample 525TCit. In addition, the accumulated ϵ_p at the end of isothermal training for thermally cycled sample 525TCit is similar (6.8%) than sample 525it (7%), as occurs with trained samples 500.

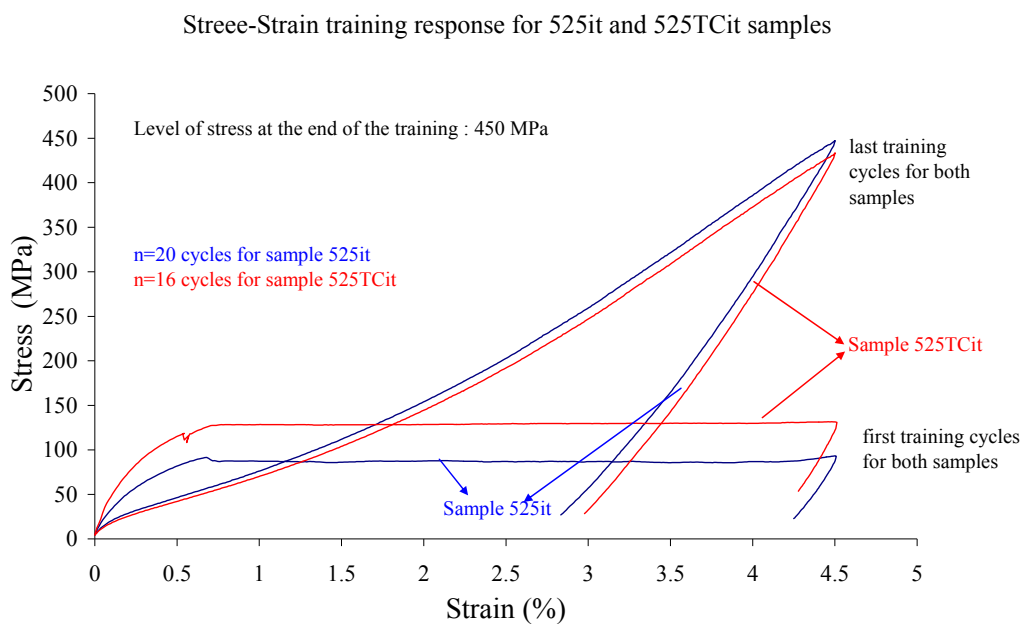


Figure 5.19 Effect of isothermal training on the stress-strain-response for 525it and 525TCit samples.

However, it is important to note that the level of stress (see figure 5.19) is the same for both samples at the end of training but lower than those required for trained samples 500it-500TCit. Consequently, we can say that, after the results obtained for 500it, 500TCit, 525it and 525TCit samples, **the level of stress necessary to obtain the maximum two-way memory strain is independent of the prior thermal cycling**

applied to the sample and the number of training cycles performed. The dislocation arrangements introduced by training attain a certain saturation level, regardless of the number of training cycles. Then, the two-way shape memory behaviour cannot be further improved by applying additional training cycles.

In figure 5.20, the apparent modulus for the initial linear load part of the curve (E_{load}) and the apparent modulus for the reoriented martensite (E_{reor}) are plotted versus the number of training cycles for trained samples 525it-525TCit. As can be appreciated in figure 5.20, the values of the E_{load} start to decrease heavily from the very first training cycle according to the apparition of the two-way memory properties for both samples. However, the decrease in E_{load} is more pronounced for sample 525TCit than for sample 525it according to the fact that this sample 525TCit reaches the TWSME in less training cycles. Again occurs that E_{reor} and E_{load} reach similar values when the number of training cycles is higher enough to produce a stable value of the two-way memory strain measured during training (as samples 500it-500TCit did).

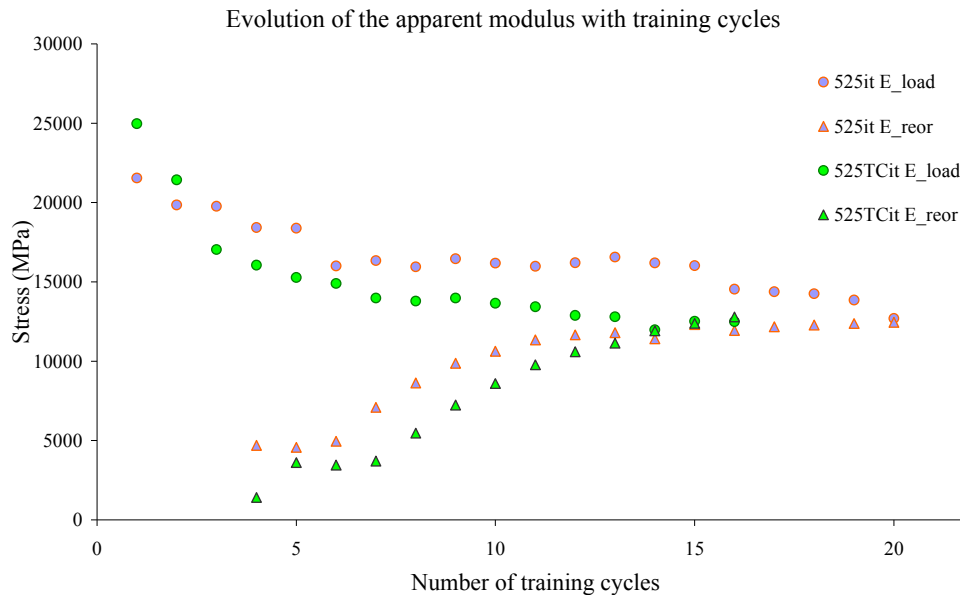


Figure 5.20 Evolution of the apparent modulus for the initial elastic portion of the stress-strain curves (E_{load}) and evolution of the apparent modulus of the reoriented martensite (E_{reor}) with number of training cycles for trained 525it and 525TCit samples.

2.1.1.2 Influence on the two-way memory strain obtained

Two-way memory strain values for both samples were measured after isothermal training. Figure 5.21 shows the evolution of ϵ_{tw} during TWSME thermal cycling for both samples. The maximum ϵ_{tw} for sample 525it is 5.11% and the maximum ϵ_{tw} for sample 500TCit is 5.2%. This shows that thermally cycled sample 525it develops slightly lower ϵ_{tw} values than those of 525TCit. The evolution of ϵ_{tw} during TWSME thermal cycling is worst for sample non-thermally cycled: its ϵ_{tw} decrease 0.31% meanwhile sample 525TCit has a decrease in two-way memory strain of 0.23% during TWSME cycling. Similar fact occurs due to constant stress training: sample thermally cycled has a minor decrease in ϵ_{tw} than sample non-thermally cycled (see figure 5.4b). Therefore, the dislocation introduced in the alloy microstructure by prior thermal cycling at zero stress seems to help a little the process of 525TCit training.

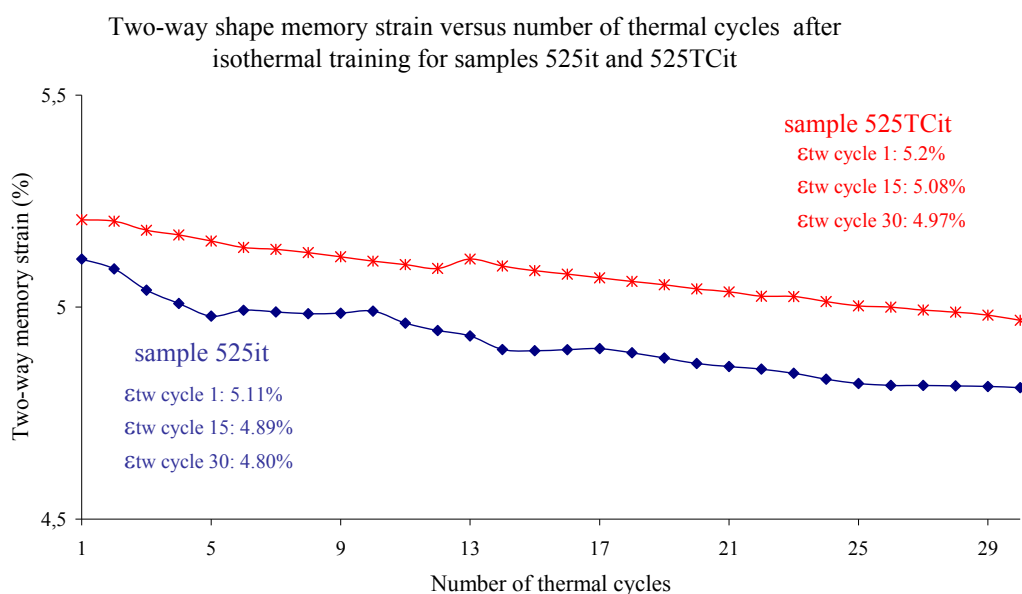


Figure 5.21 Evolution with thermal cycling of the two-way memory strain obtained by isothermal training for samples 525it and 525TCit

However, we will see that the results obtained for samples 450it and 475it are very different from those obtained for samples 500it and 525it.

2.1.3 Samples 450it and 475it

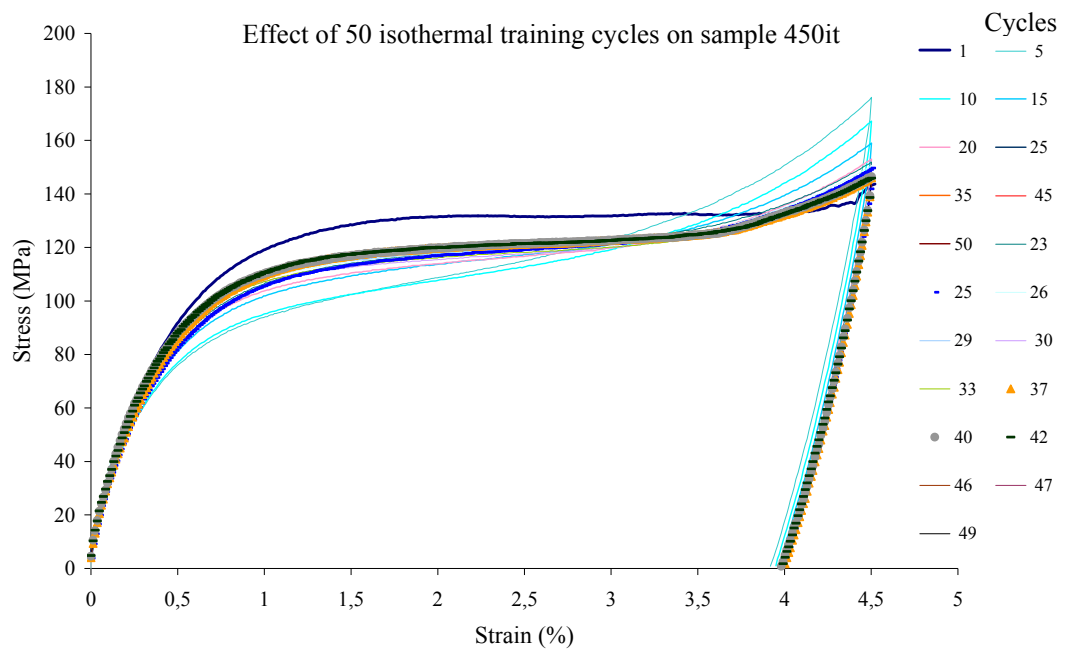
Figures 5.22a and 5.22b summarize the effect of isothermal training procedure on the stress-strain response for samples 450it and 475it. Both figures show the profiles for the first training cycle, several intermediate training cycles and the last training cycle. The following observation can be made for both samples regarding the effect of training on their stress-strain response: as seen in both figures 5.22 neither sample develops the TWSM properties, in fact, **both samples stabilize their one-way shape memory properties through the application of this isothermal training.**

In agreement with De La Flor et al. [DFO, 2009], **we define a performance criteria that can be considered as indicative of stabilized behaviour:** various constitutive parameters extracted from the stress-strain curves are measured. They are the **shape memory strain (the recoverable strain ϵ_{sm} useful in shape memory applications); the critical transformation stress to induce martensitic transformation (σ_S^{CR}), the apparent modulus for the initial elastic portion of the stress-strain curves (E_{load}) and the apparent modulus of the reoriented martensite (E_{reor}) versus number of training cycles.** To determine whether a sample had reached a steady behaviour, the average value and the standard deviation of these parameters over ten successive cycles were calculated. A sample was considered stable when the standard deviation value was under 5% and this condition was repeated for at least five consecutive values.

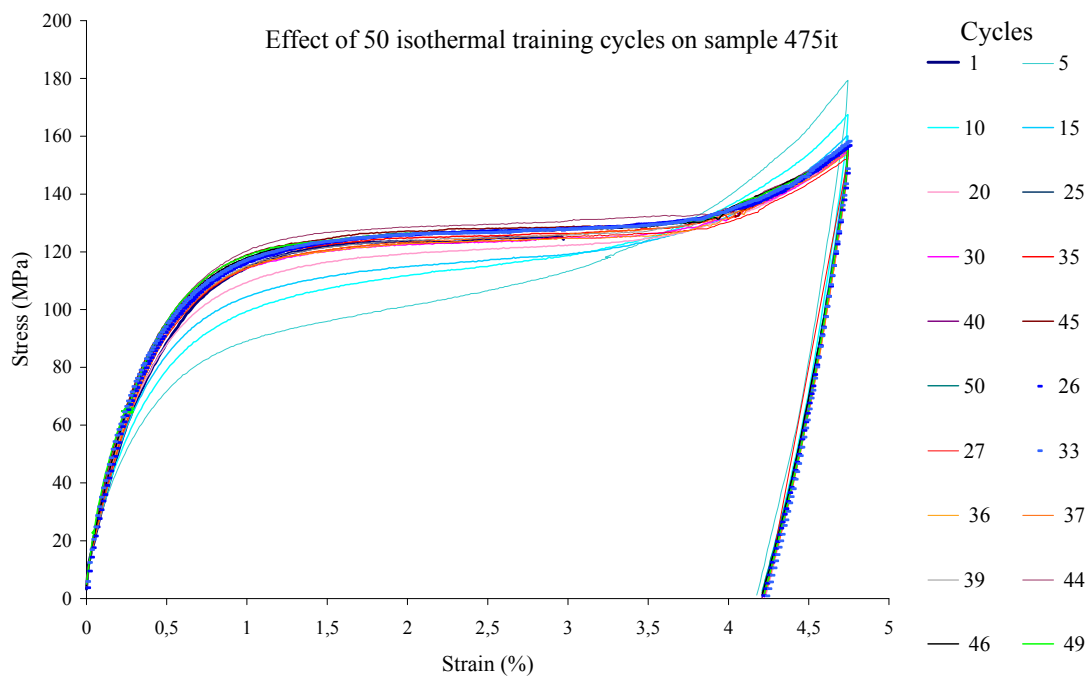
Firstly, also of note in figures 5.22 is that, the shape memory strain remains almost constant during training for both samples ($\epsilon_{sm}= 3.85\%$ for sample 450it and $\epsilon_{sm}= 4.2\%$ for sample 475it), thus indicating that the strain imposed for the cyclic training is not high enough to produce plasticity effects in both samples. The residual strain after heating is nearly zero for both samples, thus indicating that there is no degradation of the shape memory effect during 50 training cycles.

Analyzing other important parameters, the next figure 5.23 shows the critical transformation stress to induce martensitic transformation (σ_S^{CR}) and the final level of stress at the end of the training cycle versus the number of training cycles performed for samples 450it and 475it. As seen, both samples present the same evolution and similar values for both quantities: during the initial fifth training cycles, as final level of stress

increases, the critical stress decreases. This initial process is followed by an increase in the σ_S^{CR} and a decrease in the level of final stress.



a)



b)

Figure 5.22 Effect of isothermal training on the stress-strain-response for samples a) 450it and b) 475it.

This respective increase in σ_S^{CR} and respective decrease in the level of stress finish at cycle 36 for sample 450it and at cycle 26 for sample 475it. Afterwards, both, critical stress and final level of stress tend to reach a fairly stable value. For sample 450it, the value of σ_S^{CR} at cycle one is $\sigma_S^{CR}_1=124.94\text{MPa}$, at 36th cycle it is $\sigma_S^{CR}_{36}=111.32\text{ MPa}$ and for the last 50th cycle it is $\sigma_S^{CR}_{50}=110\text{MPa}$. For sample 475it the value of the σ_S^{CR} at cycle one is $\sigma_S^{CR}_1=117.44\text{MPa}$, at 26th cycle it is $\sigma_S^{CR}_{26}=117.84\text{ MPa}$ and for the 50th cycle it is $\sigma_S^{CR}_{50}=119.64\text{MPa}$. As seen, both samples suffer a stabilization of their shape memory behaviour and do not develop TWSME.

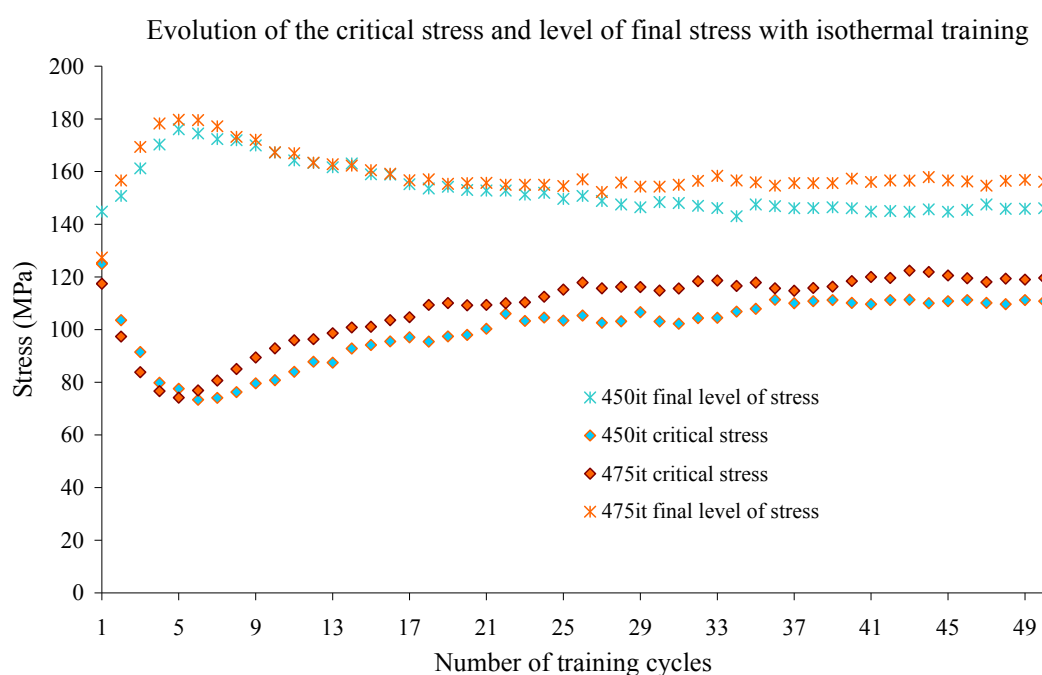


Figure 5.23 Evolution of the critical stress to induce martensitic transformation and evolution of the level of final stress to reach the imposed strain during training with number of training cycles for 450it and 475it samples.

Another fact to comment regarding figure 5.23 is that the final level of stress not only follows the reverse evolution that follows the critical stress, but also the final level of stress does not increase as increases the number of training cycles, as occurs with trained samples 500it-500TCit and 525it-525TCit. The values of the final stress turn into stable values at the same training cycles than values of the critical stress.

Finally, we analyze in figure 5.24 the evolution of the apparent modulus for the initial linear load part (E_{load}) of the curve and for the reorientation process (E_{reor}) versus number of training cycles for both samples. The values and the evolution of both modules are very similar between samples 450it and 475it. Moreover, the evolution of the E_{load} follows similar trend to the evolution of the critical stress (see figure 5.23). Initially, the E_{load} decreases up to the fifth cycle, and then increases up to the cycle 25. Further cycling, this parameter presents an almost stable value for both samples. The apparent modulus for the reoriented martensite increases at the beginning of cycling, and then, when the E_{load} starts to increase, the E_{reor} becomes to decrease, reaching a fairly stable value after 25 training cycles. The values of E_{reor} are always considerably inferior to those for the E_{load} and they are lower than those for trained samples 500it-500TCit and 525it-525TCit.

The stabilization of both, apparent modulus and critical stresses, could be explained by the assumption that the effect of isothermal training on samples heat-treated under 500°C is the stabilization of certain configuration of martensite twins instead of TWSME structure.

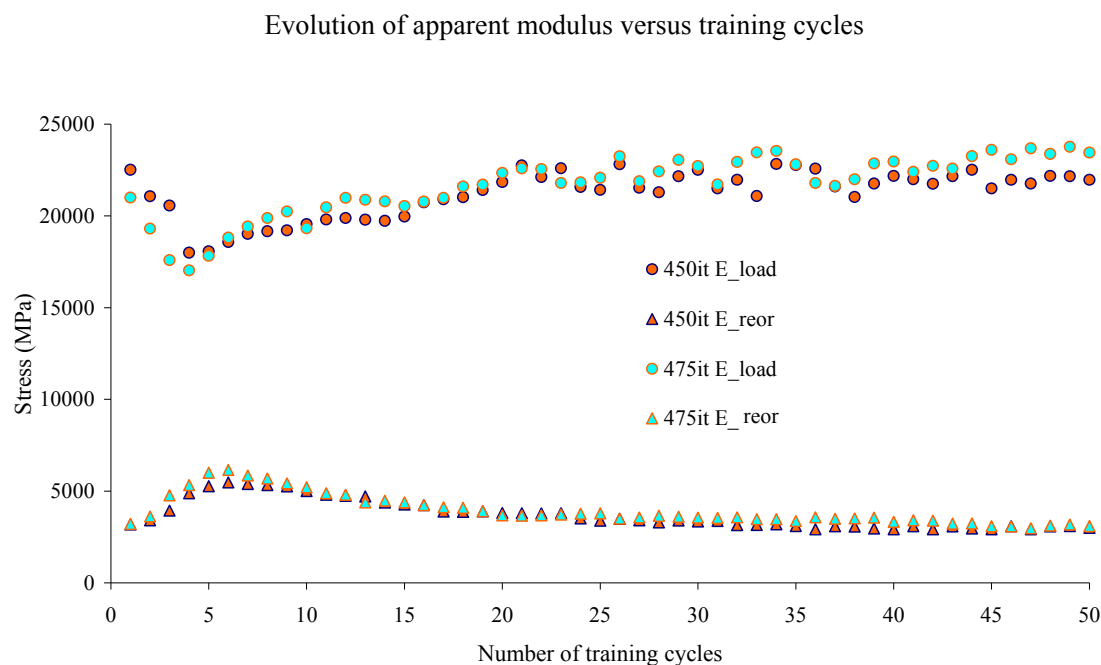


Figure 5.24 Evolution of the apparent modulus for the initial elastic portion of the stress-strain curves (E_{load}) and evolution of the apparent modulus of the reoriented martensite (E_{reor}) with number of training cycles for 450it and 475it samples.

In figures 5.22, 5.23 and 5.24 it should be pointed out that for all the parameters analyzed, the most important variation occurred during the initial 1-10 cycles and less significantly from the 10th cycle onwards. All the figures also show how, as the cycling proceeds, all the parameters stabilize. However, although the shape memory strain stabilize after 8 cycles, and the modulus (E_{load} and E_{reor}) stabilize after 25 cycles in 450it and 475it samples, the critical stress stabilizes around cycle 36 for sample 450it and around 26 for sample 475it. Therefore, the criterion that can be considered as indicative of stabilized behaviour, as it is expected, is the critical stress at the onset of the martensitic transformation.

2.3 Influence of the isothermal training on the phase transformation behaviour and on the TWSME activation temperatures

The transformation temperatures for all trained samples are measured after TWSME thermal cycling to determine the temperatures at which the two-way memory effect is activated. The change in the transformation temperatures is studied using 3 methods: 1) by applying the applied loading method; 2) by taking ER measurements and 3) by wt% diagrams from the XRD results. The results are complementary and very similar, helping understanding of the transformation behaviour of the samples after isothermal training.

Figure 5.25 shows the TWSME hysteresis loops after 30 thermal cycles for each trained sample, from which are obtained the temperatures applying the applied loading method. Figure 5.26 shows the changes in the transformation temperatures for the first and last thermal cycling for all trained samples analyzed. By comparing the transformation temperatures for the untrained samples 500, 500TC, 525 and 525TC (see figures 5.2a and b, first and second columns), with the transformation temperatures at TWSME thermal cycle 1, it can be seen that isothermal training decreases a little the M_S transformation temperatures for samples non-thermally cycled, but it increases M_S appreciably for samples thermally cycled (M_S suffered a previous decrease due to thermal cycling at zero stress in these samples). In any case, after isothermal training, all martensitic temperatures are similar between samples and their values are independent of the previous thermal cycling at zero stress that has been applied.

Moreover, all martensitic temperatures are around room temperature for all samples. The final austenite temperature (A_f) decreases for all trained samples, being this decrease higher for samples non-thermally cycled 500it and 525it than for samples thermally cycled 500TCit and 525TCit. The R-phase transformation is not shown in these profiles, and this suggests that isothermal training diminishes the R-phase because of the important increase in M_s temperature.

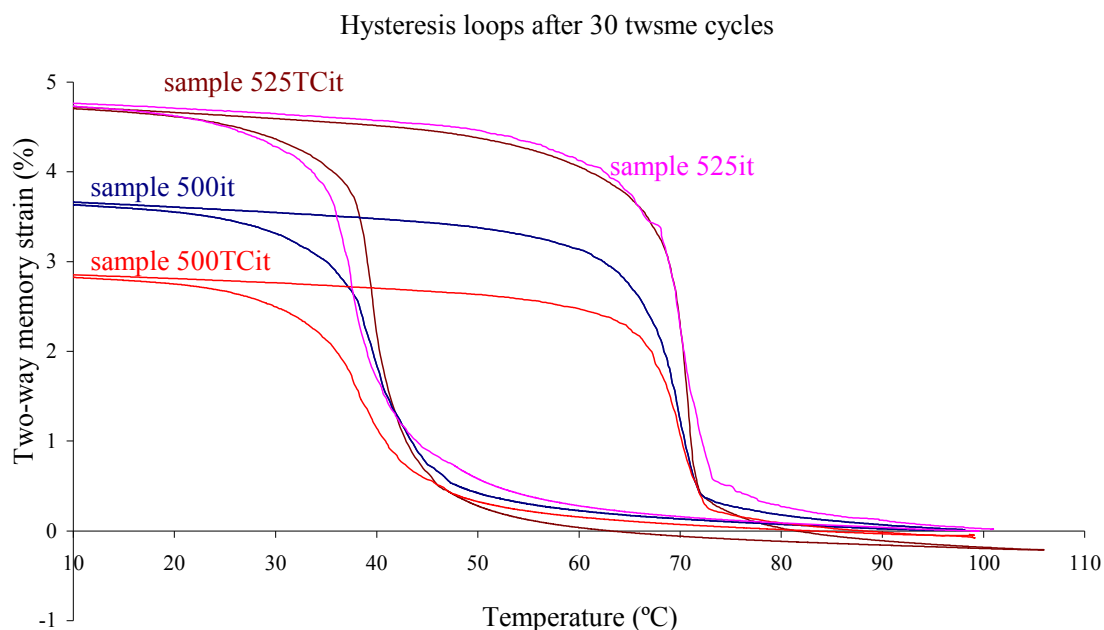


Figure 5.25 Hysteresis loops after 30 TWSME thermal cycles.

Figure 5.26 also indicates the values of the activation temperatures after 30 TWSME thermal cycles. The results show that the hysteresis loop of the transformation is narrowed due to TWSME thermal cycling. After 30 TWSME thermal cycles, the martensitic temperatures are increased and the austenitic ones decreased, suggesting that the transformation is being easier as increasing the number of TWSME thermal cycles. Between samples 500it-500TCit and 525it-525TCit, thermally cycled ones 500TCit and 525TCit have minor variation in activation temperatures with TWSME thermal cycling.

In any case, these results will be analyzed in more detail with the help of the ER measurements and the wt% diagrams.

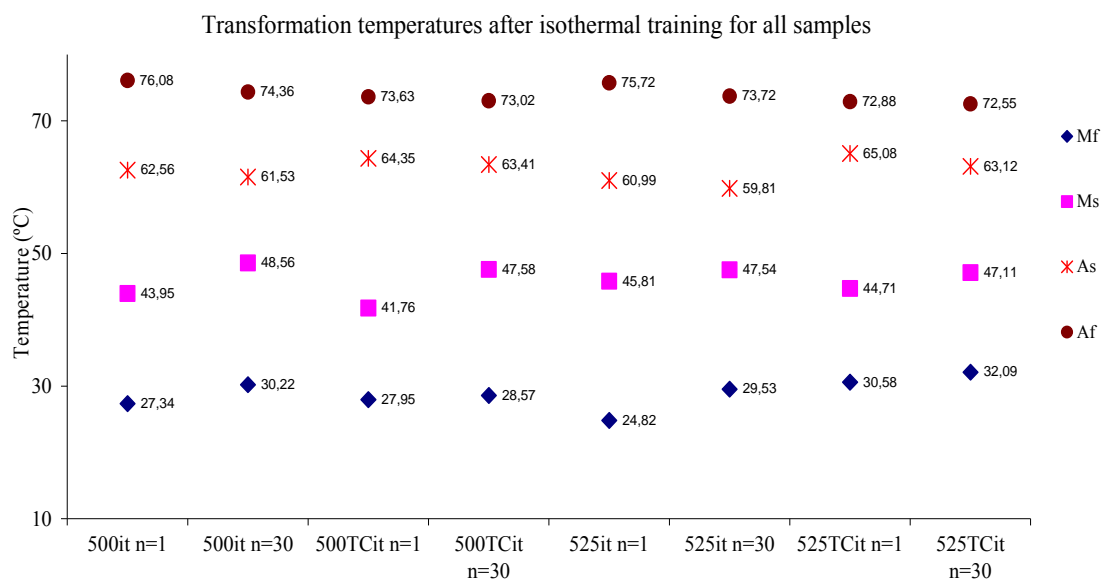
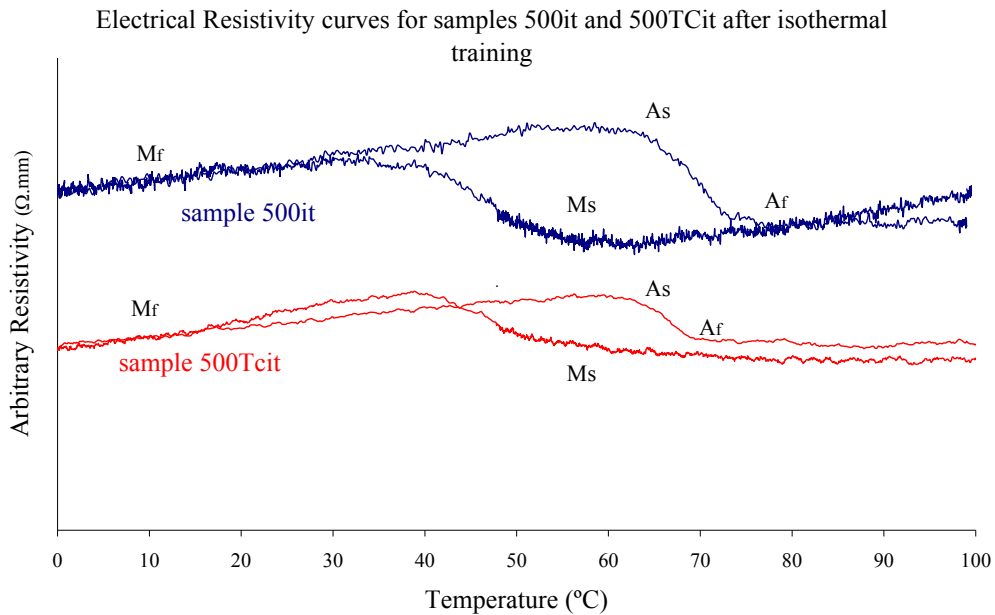


Figure 5.26 Evolution of the transformation temperatures measured by applied loading method with TWSME thermal cycling for all samples analyzed. The values are given for the first and last TWSME thermal cycle.

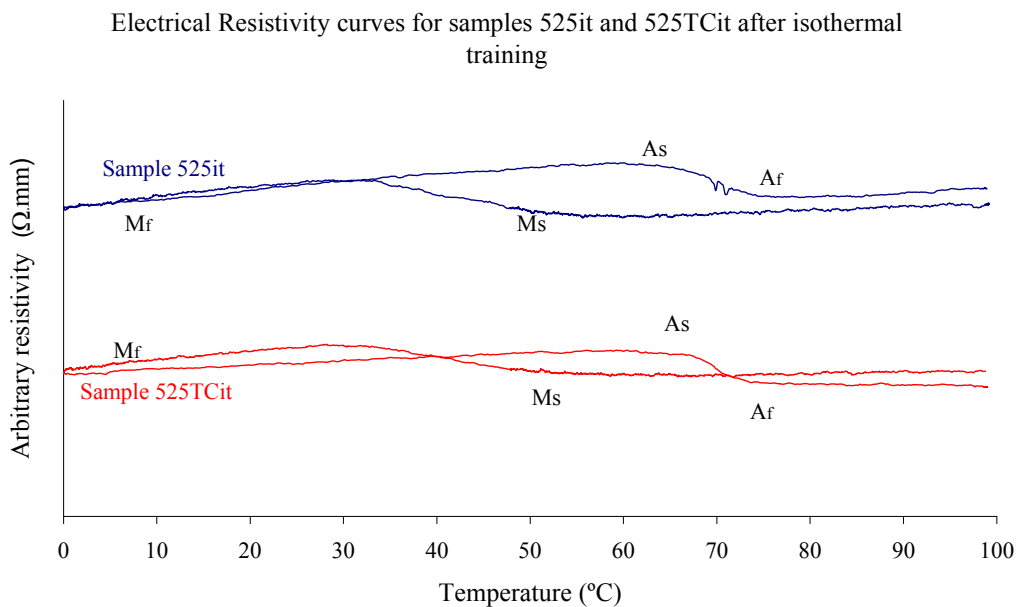
Figures 5.27a and 5.27b show the ER profiles for trained samples 500it-500TCit and 525it-525TCit respectively obtained after 30 TWSME thermal cycles. The cooling part of the ER profiles shows the possible situation of the M_f temperature (about 11°C for samples 500it-500TCit and about 5°C for samples 525it-525TCit) and the M_s temperature (about 50-55°C) for all trained samples. The ER curves show a more important decrease in M_f temperature that the one suggested by the applied loading method, resulting in a higher martensitic temperature interval using ER measurements than using applied loading method to calculate the activation temperatures. During cooling, the increase in resistivity values is near of 7% for 500it-500TCit samples and near of 9% for 525it-525TCit samples. This indicates that the level of R-phase is not as evident as it is in samples trained by constant stress training.

During heating, figures 5.27a and b show a drop in resistivity indicative of the transformation to austenite (this does not occur in untrained samples). This occurs at an austenite temperatures lower than the austenite temperatures of the untrained samples.

In any case, the values of the austenite temperatures measured by ER are similar to those measured by applied loading method for 500it-500TCit and 525it-525TCit samples. However, we should accurately compare these results with the XRD results.



a)



b)

Figure 5.27 Isothermal training effects on ER curves for samples a) 500it and 500TCit and b) 525it and 525TCit.

Following the analysis of the activation temperatures made by applied loading method and ER, the effects of isothermal training on the phase transformation behaviour and activation temperatures are now discussed by quantitative analysis derived from XRD powder patterns using the Rietveld method and the software TOPAS. The evolution of the phase transformation behaviour after isothermal training is shown in figures 5.28 to 5.33 for samples, 500it, 500TCit, 525it, 525TCit, 475it and 450it respectively. The results are given for each sample as the % percent of the weight fraction (wt%) of each phase present in the sample as a function of temperature and through the full temperature transformation range. The shape of the corresponding electrical resistivity curve is added in each diagram to correlate the ER measurements with the wt% results.

2.3.1 500it and 500TCit samples

The effects of isothermal training on sample 500it are shown in figures 5.28a and 5.28b. The transformation behaviour of this trained sample is little modified respect to the untrained sample 500 (figure 4.5). In the cooling part of the process, the trained sample 500it has equal level of R-phase (37.8%wt) than the untrained sample 500 (38wt%), but this sample 500it has lower level of R-phase than sample 500cs trained by constant stress (46wt%, figure 5.8). Then, the R-phase does not disappear due to isothermal training, but its evolution is modified. During cooling, the martensite and the R-phase evolve together from austenite being the transformation simultaneous ($R_S=M_S=50^\circ\text{C}$), as occurs in the untrained sample 500 and in the constant stress trained sample 500cs. This simultaneous transformation has been advanced respecting to the untrained sample 5°C . When the R-phase transformation ends ($R_f=40^\circ\text{C}$), reaching a maximum level of 37.8wt%, the martensite is formed from austenite plus R-phase. At 20°C the austenite reaches the 0wt%. At this temperature, the wt% of martensite is equal to 67wt%. From this point, the martensite is formed only from the contribution of the R-phase. Then, at the end of the cooling process sample 500it has lower martensite (83.6wt%) than the untrained sample 500, but it has more martensite than the constant stress sample 500cs (79wt%). Sample 500it has more residual R-phase (16.4wt%) than sample 500, but less than sample 500cs (21wt%).

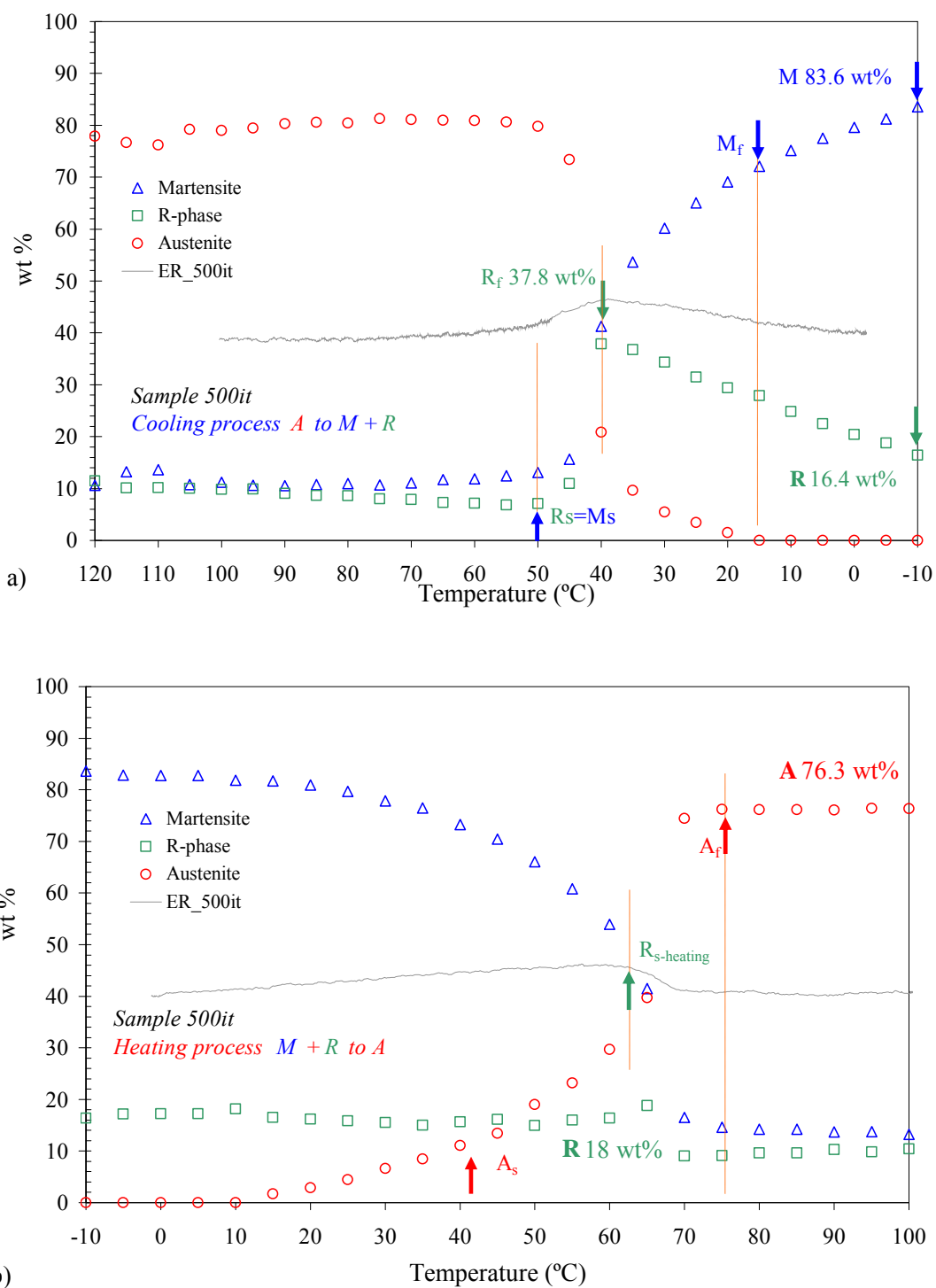


Figure 5.28 Evolution of the phase transformation behaviour due to training for samples 500it during a) cooling and b) heating. The ER measurements have been added on the diagrams.

In the heating process, the R-phase is promoted: the quantity of R-phase is increased up to 18wt% for trained sample 500it. This wt% of R-phase is increased respect to that of the untrained one (12wt% for sample 500, figure 4.5a). Similar values of R-phase are found for sample 500cs (figure 5.8). This heating process is done with contribution of martensite and R-phase that transforms into austenite ($A_S=40^\circ\text{C}$). The R-phase transformation starts to transform into austenite in a little quantity but enough to affect the ER curve. The temperature $R_{S\text{-heating}}$ is around 65°C for this sample 500it. At the end of transformation process, $A_f=75^\circ\text{C}$, there is a 76.3wt% of austenite with a little wt% of retained martensite (13wt%) and R-phase (10wt%).

As seen in figures 5.28a and b, comparing the wt% results with the ER measurements for sample 500it on cooling, the beginning of the resistivity hump in the ER curve corresponds well with the beginning of the simultaneous transformation of the austenite into R-phase and martensite in the wt% diagram. The end of the ER increase corresponds with the complete R-phase transformation. The following transformation from austenite and R-phase to martensite has non influence on the ER curve. During heating occurs that the beginning of the decrease in resistivity values of the ER curve corresponds well with the point at which martensite has transformed in more than 50wt% in austenite, as well with the point at which the R-phase starts to transform into austenite (around 65°C). The end of the ER decrease coincides well with the end of R-phase and martensite transformation into austenite ($A_f=75^\circ\text{C}$).

The experimental results for trained sample 500TCit are shown in figures 5.29a and 5.29b. We found that although untrained sample 500TC has the phase transformation clearly separate in two steps because of thermal cycling at zero stress (figures 4.5c and 4.5d), isothermal training eliminates the separation between martensite and R-phase, promoting that martensite and R-phase evolve together, advancing the martensite transformation around 15°C .

During cooling, this training reduces the level of the R-phase that sample 500TC had before training from 65wt% to 46.7wt% (figure 5.29a). Sample 500TCit had slightly higher quantity of R-phase than sample 500TCcs (44wt%, figure 5.9a). In the heating part of the process, the R-phase is slightly promoted by training up to 17wt%, as occurs in 500it, 500cs and 500TCcs samples.

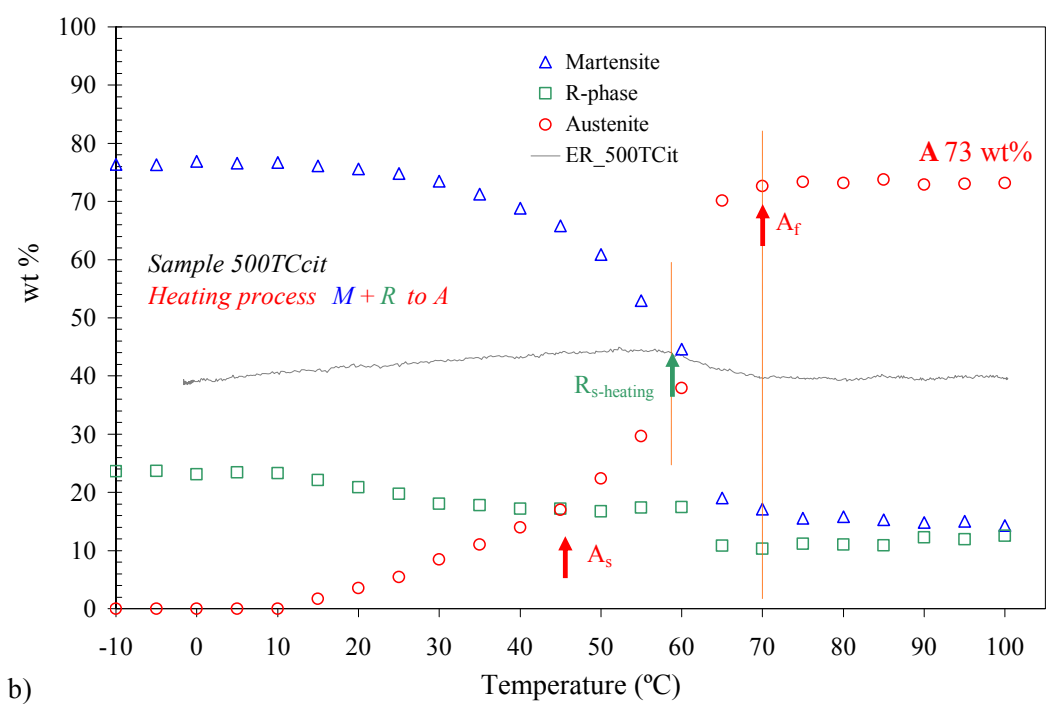
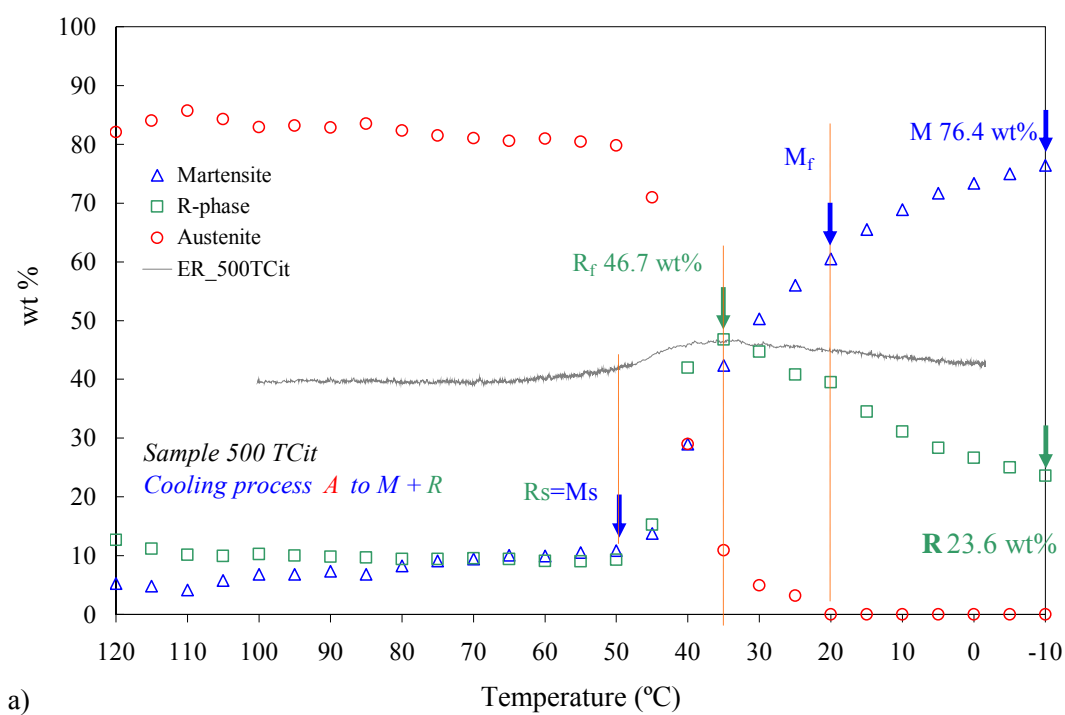


Figure 5.29 Evolution of the phase transformation behaviour due to training for samples 500TCit during a) cooling and b) heating. The ER measurements have been added on the diagrams.

During cooling, the austenite transforms to R-phase and martensite at 50°C, being the transformation equal to sample 500it. At the end of the cooling process, it is found that the transformation to martensite reaches a distribution of 76.4wt% (less than sample 500it) and that this sample 500TCit has a quantity of residual R-phase lower than sample 500it (5wt% less). The heating process for sample 500TCit is done with contribution of martensite and R-phase ($R_{S\text{-heating}}=65^{\circ}\text{C}$, $A_S=40^{\circ}\text{C}$) that transforms into austenite. At the end of transformation process, $A_f=70^{\circ}\text{C}$, there is a distribution of 73wt% of austenite with a little wt% of martensite (14.5wt%) and R-phase (12wt%). As seen in figures 5.29 and comparing the wt% results with the ER measurements for sample 500TCit, same trends can be done than those done for 500it trained sample.

2.3.2 525it and 525TCit samples

The effects of isothermal training on sample 525it are shown in figures 5.30a and 5.30b. The transformation behaviour is clearly modified: although sample 525 has almost non-existent R-phase in the beginning of training, isothermal training effectively promotes the R-phase in the cooling and the heating part of the process for this sample 525it. In fact, the quantity of the R-phase is increased up to 40.5wt% for sample 525it (the constant stress training increased the R-phase up to higher values, 46wt%). During heating, the quantity of R-phase is increased up to 25wt% (around 65°C).

The phase transformation behaviour results in the fact that martensite and R-phase evolve together from austenite being the transformation simultaneous ($R_S=M_S=55^{\circ}\text{C}$), as occurs in the untrained sample 525 (figure 4.6) and in 500it and 500TCit trained samples (figures 5.28 and 5.29). This simultaneous transformation was advanced respecting to the untrained sample 525 near of 10°C. The R-phase reaches its maximum level at 40°C (R_f), as seen in figure 5.30a. Therefore, the R-phase appears and is promoted due to isothermal training for this trained wire. This increase in R-phase that samples 525it and 525TCit show, it is a big difference respect to samples 500it and 500TCit, where isothermal training does not increase the level of the R-phase of these samples.

At 35°C the wt% of austenite is 0wt%. From this point, the martensite is transformed thanks to R-phase. Then, at the end of the cooling process, there is slightly less

martensite (90wt%) and more residual R-phase (10wt%) for sample 525it than for the untrained sample 525 (94wt% for M and 6wt% for R). The heating process is done with contribution of martensite that transform to austenite ($A_S=55^\circ\text{C}$). Around 65°C we have an austenitic transformation from R-phase, as occurs in samples 500it and 500TCit ($R_{S\text{-heating}}=65^\circ\text{C}$). At the end of transformation process, $A_F=80^\circ\text{C}$, there is a distribution of 77wt% of austenite (the untrained sample has 93wt%) with a little wt% of martensite (3wt%) and R-phase (19wt%).

Concerning the effects of isothermal training on sample 525TCit (figures 5.31a and 5.31b), it is possible to say that although sample 525TC (figure 4.6) had higher level of R-phase before training (36wt%) than sample 525, isothermal training promotes similar level of R-phase for sample 525TCit (40wt%) than for sample 525it (37.8wt%) (see figures 5.30 and 5.31). In the case of sample 525TCit, the martensite transformation is advanced respect to the martensite transformation of the untrained sample 525TC (around 15°C), eliminating the slightly separation of the phase transformation behaviour that thermal cycling at zero stress produced in the phase transformation behaviour of this sample 525TCit (as constant stress training did with sample 525TCcs). At the end of the cooling process, the distribution of wt% for martensite is equal to 90wt% for sample 525TCit and it is the same for sample 525it.

The heating process for sample 525TCit is the same as for 525it sample. The martensite transformation into these two phases finishes at 80°C , as seen in figure 5.31b. As seen in figure 5.31a and 5.31b and comparing the wt% results with the ER measurements for sample 525TCit, similar remarks can be done than those did for sample 525it.

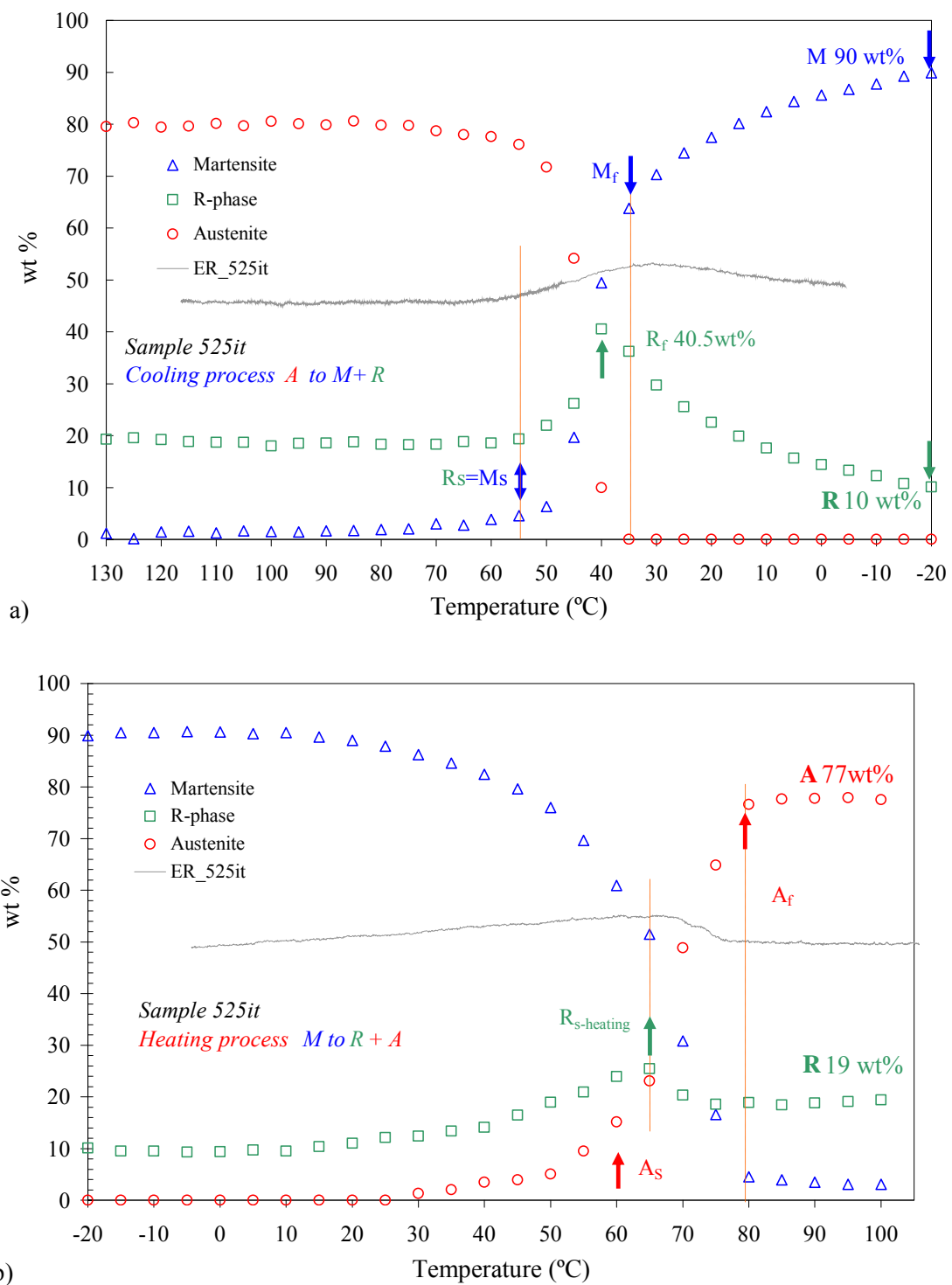


Figure 5.30 Evolution of the phase transformation behaviour due to training for samples 525it during a) cooling and b) heating. The ER measurements have been added on the diagrams.

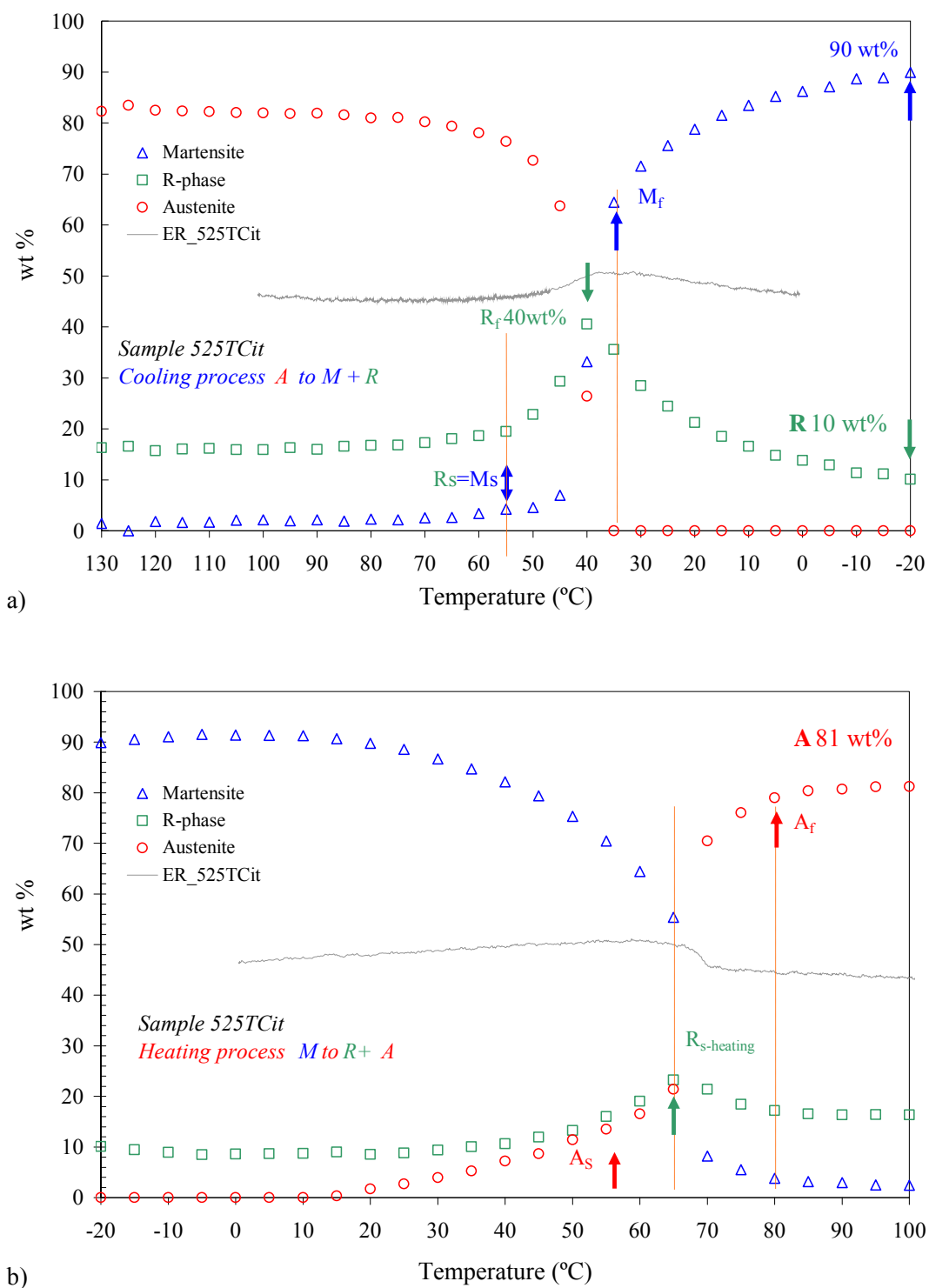


Figure 5.31 Evolution of the phase transformation behaviour due to training for samples 525TCit during a) cooling and b) heating. The ER measurements have been added on the diagrams.

2.3.3 475it and 450it samples

Since isothermal training is far to produce TWSME on samples 450it and 475it, we expect different results about the effect of isothermal training on their phase transformation behaviour. Figure 5.32a shows the cooling process for 475it phase transformation behaviour after 50 isothermal training cycles. We can say that the effects of isothermal training are similar to those produced by constant stress training on the phase transformation behaviour of this sample (figure 5.11-figure 5.32). The first and main difference that is possible to appreciate respect to samples 500it and 525it is that training did not eliminate the two-step transformation of the untrained sample 475. The training not only maintains its original transformation path (A to M to R), but also the martensitic transformation has been delayed 10°C respect to the untrained one ($M_S=10^\circ\text{C}$ for 475it). Therefore, isothermal training displaces the martensitic transformation to values near of 0°C. At -30°C the martensitic transformation reached only 56wt% of transformation. Moreover, the 475it R-phase temperature interval is wider than one of the 475 sample: the temperature interval of the R-phase transformation is 40°C for sample 475it and for sample 475 it is 25°C.

During heating (figure 5.32b), the phase transformation is similar to those explained for samples 500it and 525it, but this sample 475it has the austenitic transformation earlier than these samples ($A_S=30^\circ\text{C}$ and $A_f=60^\circ\text{C}$). The austenite reaches a distribution of 57wt% at the end of the heating process. At the end of the cooling and heating processes, the values of wt% for martensite and austenite phase are indeed lower than those measured after constant stress training for this sample (figure 4.11).

The ER measurements added to figures 5.32a and 5.32b are in good agreement with the wt% diagrams. **As seen, the ER curve on cooling is similar to the original one** (see figure 4.1), which an increase in resistivity that marks the beginning of the R transformation is followed by a wide resistivity plateau. At the end of the plateau, the R_f transformation is finished, giving to martensite the opportunity to transform. During heating, the ER curve does not present any increment in resistivity; therefore, it is difficult to extract any conclusions from it, as occurs with the untrained sample 475.

Next figures 5.33 show the results for sample 450it after 50 isothermal training cycles. As seen, the same remarks made for sample 475it are possible to do for sample

450it. To comment that during cooling, the M_s is indeed nearest to zero degrees than for 475it sample. The subsequent transformation for sample 450it is almost equal to that of sample 475it.

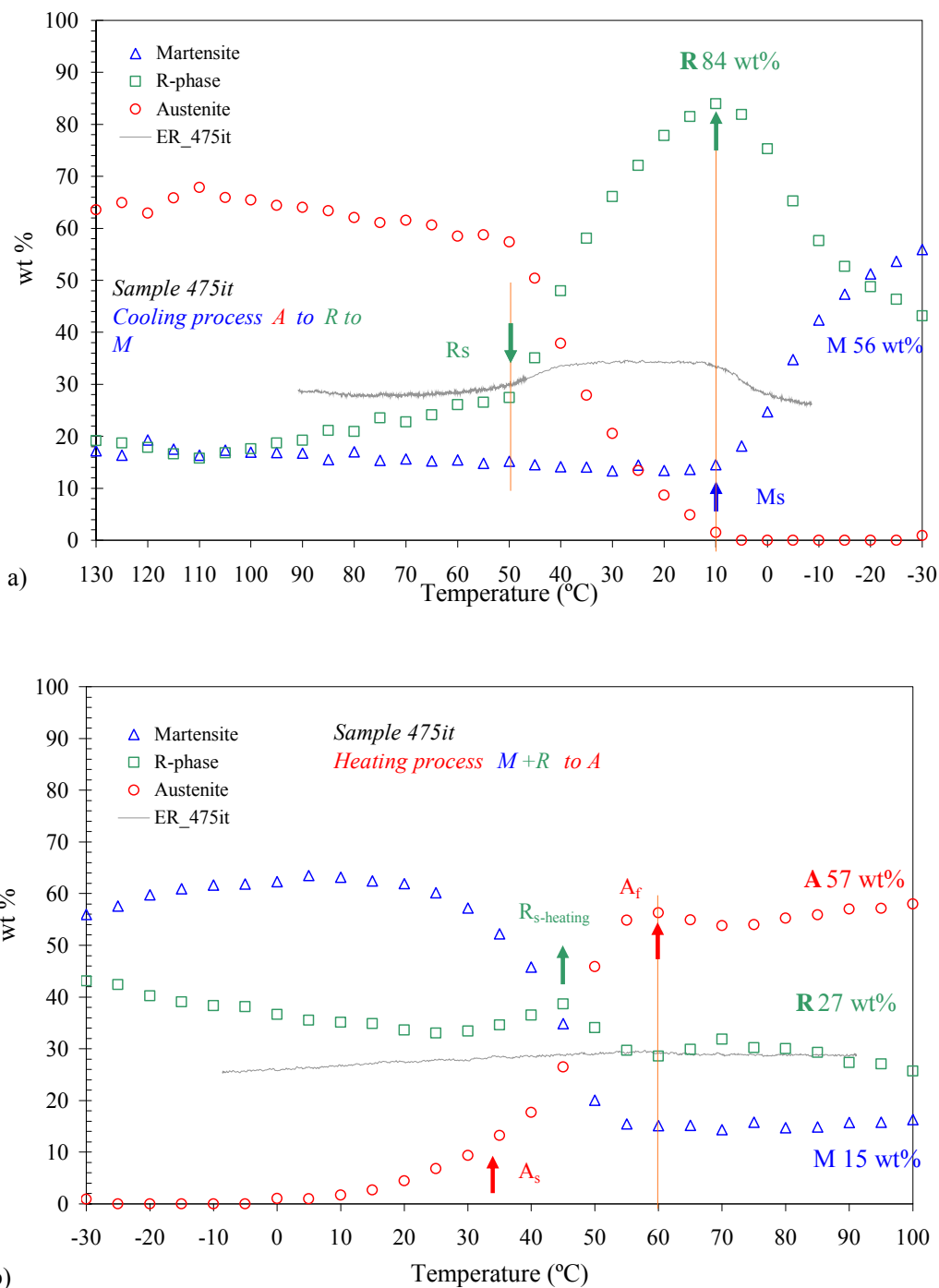


Figure 5.32 Evolution of the phase transformation behaviour due to training for samples 475it during a) cooling and b) heating. The ER measurements have been added on the diagrams.

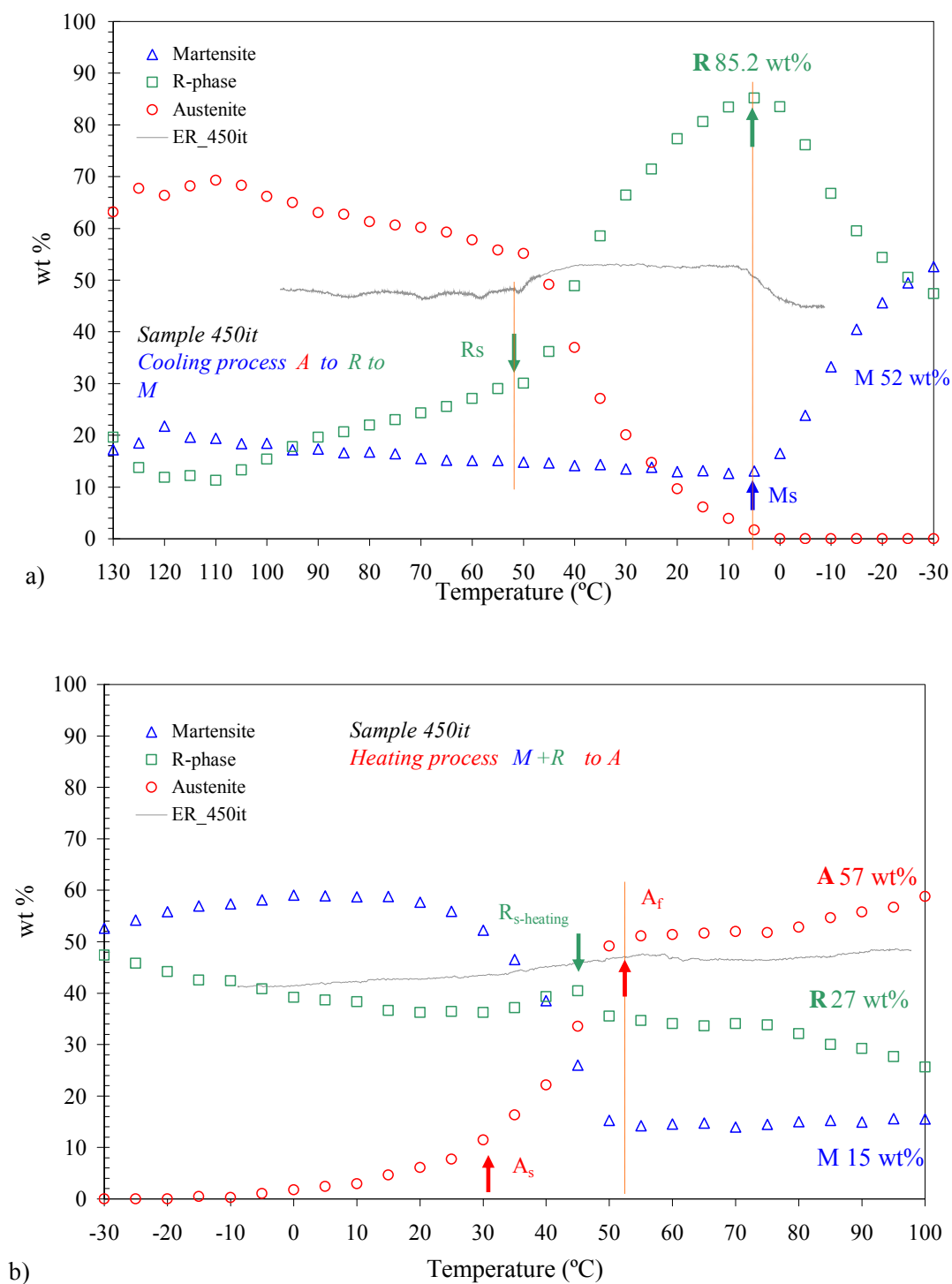


Figure 5.33 Evolution of the phase transformation behaviour due to training for sample 450it during a) cooling and b) heating. The ER measurements have been added on the diagrams.

2.3.4 Activation temperatures

To conclude the analysis of the activation temperatures, a summary of the activation temperatures is listed in tables 5.3a and 5.3b for samples 500 and 525, respectively. As seen, all methods used to measure the activation temperatures after isothermal training are in reasonable agreement for all temperatures. Similar remarks than those did for the activation temperatures found after constant stress training are possible to make for these temperatures measured after isothermal training.

	Activation Temperatures (°C) sample 500it/sample 500TCit		
	<i>Temperatures of untrained samples 500/500TC</i>	<i>Applied loading 500it/500TCit</i>	<i>Combination of ER and XRD 500it/500TCit</i>
	$M_{f50\%}$	25 / 13	30 / 28
M_S	45 / 30	48.5 / 47.5	50 / 50
R_f	30 / 30		40 / 35
R_S	45 / 46		50 / 50
A_S	55 / 46	61.5 / 63	40 / 40
$R_{S\text{-heating}}$			65 / 65
A_f	79 / 73	74.5 / 73	75 / 70

a)

	Activation Temperatures (°C) sample 525it/sample 525TCit		
	<i>Temperatures of untrained samples 525 / 525TC</i>	<i>Applied loading 525it/525TCit</i>	<i>Combination of ER and XRD 525it/525TCit</i>
	$M_{f50\%}$	32 / 16	29 / 32
M_S	48 / 35	47.3 / 47.1	55 / 55
R_f	30 / 25		40 / 35
R_S	45 / 47		55 / 55
A_S	57 / 48	60 / 63	55 / 55
$R_{S\text{-heating}}$			65 / 65
A_f	84 / 78	73.5 / 72.5	80 / 80

b)

Table 5.3 Activation temperatures measured by different methods for a) 500it-500TCit and b) 525it-525TCit samples.

2.4 Relationships between the phase transformation behaviour and the obtained two-way memory strain

Figures 5.34 show the relationship between the macroscopic mechanical behaviour of the Ti-Ni wire after isothermal training (the obtained two-way memory strain versus temperature), and the phase transformation behaviour obtained after isothermal training by XRD. The activation temperatures according to the strain-temperature curve (tables 5.3) are indicated on each curve. Moreover, the corresponding wt% distribution for each activation temperature is listed on the figures. Initially, as occurs with samples trained by constant stress method, **the wt% distribution follows well the strain-temperature hysteresis loop, reflecting that the wt% corresponds well with the macroscopic TWSME behaviour of the alloys.**

The following differences between all samples are found. Analyzing the transformation from the cold to the hot shape of the samples, figures 5.34 show that the sample with the highest two-way memory strain is the sample with the highest availability of martensite to transform into austenite at temperatures A_S , that is, samples 525TCit and 525it (64.5wt% and 61wt% respectively). In opposition, the sample with the lowest two-way memory strain of all is the sample 500TCit with a martensite distribution of 44.6wt% at temperature A_S .

Focusing on the activation temperature to recovery the cold shape of the alloys (M_S), the simultaneous transformation from austenite to martensite plus R-phase starts at similar temperature for all samples, but again, with more austenite wt% distribution for samples 525it-525TCit than for samples 500it-500TCit. At M_S temperature, samples 525TCit and 525it present slightly more austenite (76.3wt% and 76.1wt% respectively) to transform to martensite than samples 500it and 500TCit (73.4wt% and 70.9wt% of A respectively).

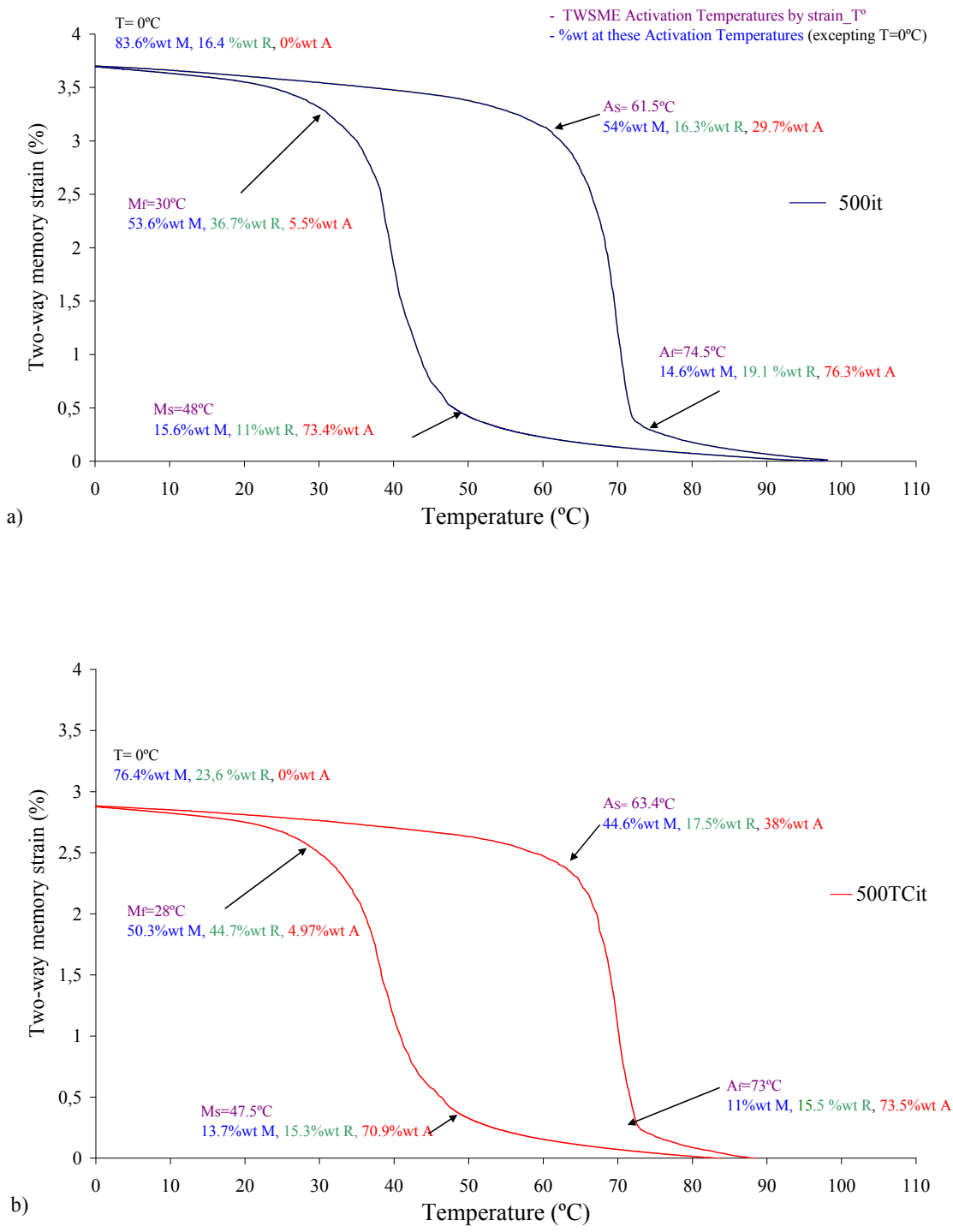


Figure 5.34a and b Relationship between the macroscopic two-way memory strain and the phase transformation behaviour for a) 500it sample, b) 500TCit sample.

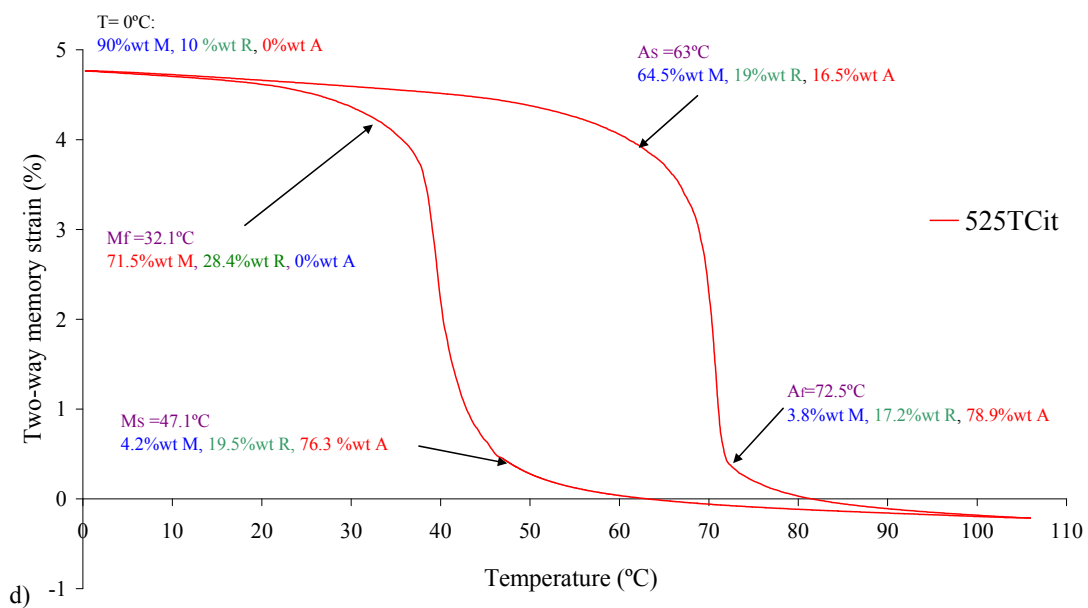
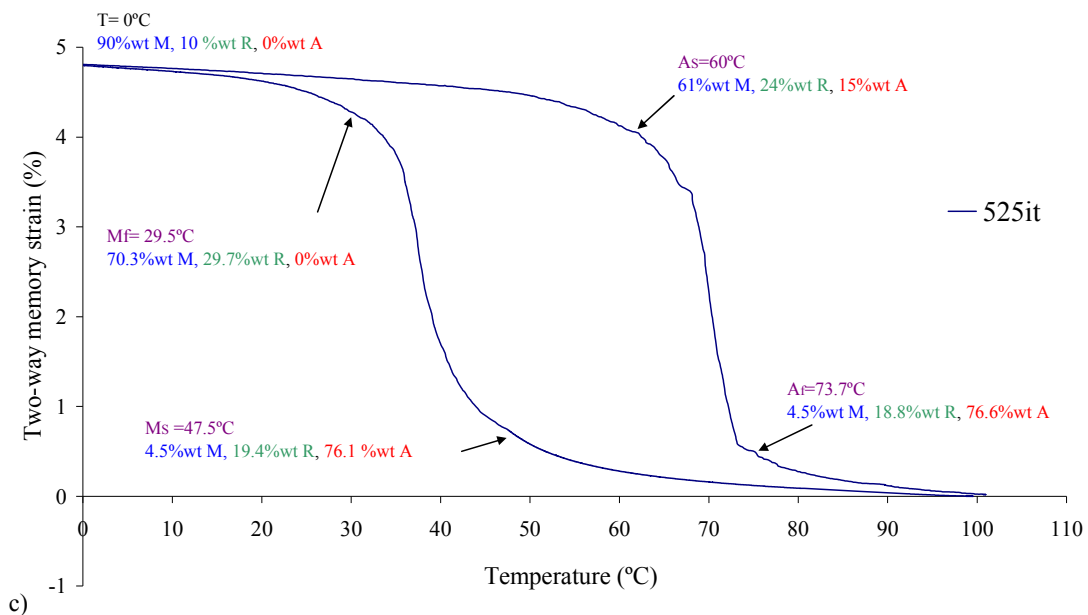


Figure 5.34c and d Relationship between the macroscopic two-way memory strain and the phase transformation behaviour c) 525 it and d) 525TC it sample.

Once all the %wt diagrams have been analysed, it seems that, as occurs with constant stress training, **to develop a substantial two-way memory strain by isothermal training, it is necessary that this training promotes in the sample a phase transformation path characterized by a simultaneous transformation of austenite to R-phase plus martensite during cooling.** To achieve this, this training has to increase the martensite transformation temperature and to produce that the R-phase evolves together with the martensite during all TWSM process. For a second time, the kind of sample suitable to promote this above explained convenient phase transformation behaviour is the sample heat treated at temperatures equal to or greater than 500°C. As seen in all the wt% diagrams, the increase in dislocation density by isothermal training permits certain development of the R-phase for those samples that have little quantity of R-phase before training (500it and 525it). However, we have seen that for samples thermally cycled prior to isothermal training (500TCit and 525TCit samples) the R-phase decreases a little respect to that of the untrained samples thermally cycled (500TC and 525TC samples). In any case, the R-phase does not disappear; the R-phase is present in all trained samples analyzed.

Afterwards, we consider that the selection of an adequate heat treatment temperature and the application of thermal cycling at zero stress prior to training have larger influence on isothermal training than on constant stress training. **Due to the higher initial dislocation density that samples 450 and 475 have after heat treatment (R-phase totally developed), the introduction of the necessary dislocations to develop TWSME is difficult or impossible. The result of the isothermal training on these samples is the stabilization of the one-way shape memory behaviour.**

For samples heat-treated at temperatures equal to or greater than 500°C, isothermal training develops the TWSME, however, thermal cycling at zero stress has different effects depending on the heat treatment temperature. Thermal cycling at zero stress allows to sample 525TCit developing the TWSM state in shorter number of training cycles than sample 525it, developing similar two-way memory strain. Nevertheless, thermal cycling at zero stress seems to stop the development of the adequate structure in 500TCit sample. Sample 500TCit not only spends 15 training cycles more than 500it to develop the TWSME, nevertheless, sample 500TCit develops lower two-way memory strain than sample 500it (figures 5.34a and b).

We search the reason of this disagreement in the effect of thermal cycling at zero stress on isothermal training in the initial structure of the untrained samples 500TC. Sample 500TC has two stage transformation behaviour on cooling and then, lowest martensitic temperatures. Samples 500, 525 and 525TC do not have two-step transformation behaviour on cooling, resulting in higher martensitic temperatures than sample 500TC (see tables 5.3). As seen, isothermal training has to produce an overlapping of martensite and R-phase promoting that both phases evolving together during the TWSME process. An increase in martensitic temperatures is essential to obtain this above commented structure. Therefore, isothermal training has to overcome the separation of the phase transformation behaviour that has sample 500TC. As a resulting, more training cycles are necessary to obtain the same favourable TWSME dislocation structure in sample 500TCit than in the others samples (please consult figures 5.22, 5.23 and 5.24 where is possible to see the slow evolution of the two-way memory strain during training and the apparent modulus versus number of training cycles for this sample). As a resulting of this, samples 500TCit generate lower two-way memory strain than samples 500it non-thermally cycled.

3 Summary and conclusions

The effects of heat treatment and posterior repeated thermal cycling at zero stress on two different trainings procedures to develop TWSME in Ti-Ni SMA wire have been presented. The influences on the training parameters, two-way memory strain, phase transformation behaviour, and transformation temperatures have been widely analyzed depending on the training methods used: thermal cycling under constant stress or isothermal tensile deformation under M_f .

The first section of this chapter discussed the results obtained for samples 475, 500, 525, 500TC and 525TC trained by thermal cycling under constant stress. It also presented an in-depth analysis of the main parameters obtained during training (permanent strain, strain in the martensite state, and recovery strain). After this, this chapter presented the two-way memory strain that was obtained and its evolution with thermal cycling before finally analyzing and discussing the evolution of the TWSME

activation temperatures after constant stress training. Following this, the resulting phase transformation behaviour was analyzed by ER and XRD for all the trained samples after constant stress training and the results of this analysis were correlated with the macroscopic TWSME behaviour (strain-temperature behaviour) of each sample. The second part of Chapter 5 presented the results obtained for the isothermal tensile deformation under M_f training in the same order as the results for the constant stress training. The following are the main conclusions of this chapter:

(i) **The improvement in TWSME is found by applying a heat treatment prior to training at a temperature equal to or greater than 500°C. This is followed by repeated thermal cycles at zero stress to develop the R-phase (12 cycles for sample 500TCs and 25 cycles for sample 525TCs) and training the sample by constant stress training.** After this complete sequence of processes, the TWSME is improved because the training efficiency and the two-way memory strain increase and the permanent strain decreases during training.

(ii) **The dislocations introduced by thermal cycling at zero stress seem to be rearranged by constant stress training.** Thus, in thermally cycled samples, not only is the process of reorienting the martensite easier than in non-thermally cycled samples, but also the increment of R-phase is little or non-existent, as has been experimentally demonstrated. Therefore, **samples that are thermally cycled prior to training generate higher two-way memory strain** than non-thermally cycled samples (0.6% higher).

(iii) **The two-way memory strain values attained for the 500TCs and 525TCs samples** are higher than the values published by other authors for similar materials, composition, and training. For example, Scherngell et al. [SCHE, 2002] obtained a two-way strain of around 2.8% and Prader et al. [PRA, 1997] obtained a two-way memory strain of 2.6%. We obtained a maximum value of the two-way memory strain of **4.8% for the 525TCs samples and 3.8% for the 500TCs samples.**

(iv) **The changes produced in the phase transformation behaviour by TWSME trainings** indicate that **to develop a substantial two-way memory strain, the training needs to promote a phase transformation path in the sample that is characterized by a simultaneous transformation of the austenite to the R-phase**

plus martensite. To achieve this kind of transformation path, training has to increase the martensite transformation temperature and to make the R-phase and the martensite evolve together throughout the TWSME process. The best samples for obtaining this useful phase transformation behaviour (the simultaneous transformation from austenite to R-phase plus martensite) are those that are heat treated at temperatures equal to or greater than 500°C. These heat treatment temperatures ensure that samples are obtained with a low dislocation density and similar phase transformation behaviour to those samples subjected to constant stress training or isothermal training. Consequently, the development of TWSME properties in these samples is fast and effective.

(v) **The analysis of the effect of the aforementioned thermomechanical processes on the evolution of the phase transformation behaviour has led to the finding of an important variety of behaviours** for this commercial SMA. These behaviours vary according to the heat treatment temperature, thermal cycling at zero stress, and the training method applied. **For TWSME applications**, the appropriate process is heat treatment at a temperature equal to or greater than 500°C, followed by repeated thermal cycling at zero stress and then constant stress training. **For one-way applications**, the appropriate heat treatment temperatures are 450 and 475°C. These samples are suitable for one-way memory effect applications because they are very stable during mechanical cycling at M_f . Sample 450 becomes stable after almost 36 isothermal cycles under M_f and sample 475 becomes stable after almost 26 isothermal cycles under M_f .

(vi) We should note that **the shape memory behaviour of the as-received (non-heat treated) material has been improved.** The number of isothermal cycles needed to obtain stable one-way shape memory behaviour is lower for the 450 and 475 samples than for the as-received material. The as-received sample needs almost 50 isothermal cycles to reach stable behaviour [DFO, 2009]. Moreover, the values of the critical stress are always higher for the 450 and 475 samples than for the as-received material (almost 50MPa higher)

Moreover, this chapter draws the following conclusions regarding the effects of TWSME training on Ti-Ni phase transformation behaviour and the role of the R-phase in the development of the TWSME:

(vii) For samples heat-treated at $T > 500^{\circ}\text{C}$, both trainings have the same effect on the phase transformation behaviour of these samples (i.e. an increase in martensite transformation temperatures). For samples heat-treated at $T < 500^{\circ}\text{C}$ both trainings have the same effect on the phase transformation behaviour of these samples (i.e. a decrease in the martensite transformation temperatures and an increase in the temperature interval of the R-phase). Therefore, it can be seen that these effects are only dependent on the heat treatment temperature applied to the Ti-Ni wire and are not dependent on the type of training applied.

(viii) In samples with an initial full-developed R-phase (the 450 and 475 samples), the trainings do not develop the TWSME. The initial high dislocation density, and thus, the high quantity of R-phase presented by these samples reduces the mobility of the martensite plates. Consequently, the necessary change in the phase transformation behaviour is not produced by training. In fact, training produces the opposite effect; that is, the martensite temperature decreases and the interval of the R-phase transformation increases, thus impeding the development of the TWSME in the 450 and 475 samples.

(ix) Samples non-thermally cycled prior to training 500cs and 525cs and samples thermally cycled prior to training 500TCcs and 525TCcs develop similar distributions of R-phase after training. This means that the net increase in R-phase is superior for those samples that are non-thermally cycled prior to training (500cs and 525cs). Thus, **training seems to rearrange the dislocations introduced by thermal cycling at zero stress, thus improving the mobility of martensite and limiting the increase in R-phase.**

A comparison of the trainings gives the following conclusions:

(x) The results suggest that to obtain the best SMA performance, that is, to obtain a substantial two-way memory strain together with a minimum final irreversible strain and TWSME activation at room temperatures, the Ti-Ni wire should be trained by thermal cycling under constant stress.

(xi) Isothermal training developed the largest two-way memory strain but the irreversible strain generated during this training is higher than that generated by constant stress training.

The next step is to measure the work production of the improved samples.

CHAPTER 6

WORK PRODUCTION OF THE IMPROVED

Ti-Ni WIRES



CHAPTER SIX:

WORK PRODUCTION OF THE IMPROVED Ti-Ni WIRES

Introduction

1	Operating mode	275
2	Work production of samples 500TCcs	276
3	Work production of samples 525TCcs	284
4	Comparison between samples	289
5	Quantification of the changes in phase transformation behaviour due to thermomechanical cycling	296
6	Summary and conclusions	302

Introduction

In recent years, there has been growing interest in the use of near equiatomic Ti-Ni SMA as smart materials for a variety of applications [HUM, 2001]. When applied in actuators, the SMA is subjected to thermal cycling under a given load across the transformation range, this process generally being referred to as thermomechanical cycling. The actuator is thermally cycled under a constant load and, in contrast to TWSME thermal cycling, the cooling and the heating are performed under constant stress. The actuators are expected to perform the desired operation repeatedly without any deterioration in their strain response. However, it is known that thermal cycling under external constant stress changes the transformation temperatures and the phase transformation behaviour. Moreover, it accumulates an irreversible strain that changes the hot and cold shape of the sample. Nevertheless, studies have shown that these changes are

quite significant during the initial few cycles and that the material tends to stabilize with further thermal cycling [PER, 1984], [WAY, 1990], [TUR, 2000], [MIL, 2001] and [BRA, 2001]. Evidence for this can be found in the microscopic reproducibility and stability of the martensite transformation path after these few initial cycles [STA, 1992]c.

It is known that the formation of oriented martensite creates significant macroscopic strain and that the formation of self-accommodated martensite creates little macroscopic strain. At different stress levels, the microstructure of martensite is different, oriented martensite forms at high stress level, self-accommodated martensite forms at low stress level, and partially oriented martensite forms at intermediate level. Therefore, the formation of different structures of martensite at different stress levels causes variation in the transformation strain [WUX, 2003]. All this reveals a very important trend. **When Ni-Ti wire has to work against low levels of stress**, it is important to **orient its martensite variants prior to work** in order to maximize the work production of the Ni-Ti wire. In this way, the Ti-Ni wire will produce the highest possible macroscopic strain under low levels of stress because the oriented martensite path is already generated in the alloy. This oriented martensite path can be achieved if the sample is trained using TWSME methods prior to work [STA, 1992]c. Moreover, Stalmans et al. found that after a sufficient number of training cycles, the martensite formation path is stabilized in such way that it hardly changes when resisting stresses are applied in subsequent transformation cycles. Hence, it seems that TWSME trained samples are highly resistance to the formation and growth of variants that are different from those developed by training, meaning that the trained SMA can withstand considerable forces during cooling [STA, 1992]c.

Miller et al. [MIL, 2001] found that training a Ni-Ti wire (50 training cycles at 300MPa) prior to thermomechanical cycling increases considerably its transformation strain when it is working at stresses equal to or lower than those used for training. When the trained samples are subjected to thermal cycles under constant stresses between 50 to 300MPa, their transformation strain increases depending on the initial cold working condition of the sample, the annealing temperature and the opposing stress applied. As the applied stress overpass the training stress (300 MPa) the improvement in the transformation strain is only achieved by those samples with low initial cold working.

Posterior studies reaffirmed the convenience to train the sample to obtain the highest transformation strain. Likewise, Liu et al. [LIY, 2004] proposed several

recommendations for obtaining the best performance in a Ti-Ni wire: “**prior to work, train the SMA to have a TWSME, and preferentially, use the wire under tension**”. He suggests that this method will fully use the capacity of the SMA wire by uniformly distributing the deformation and recovery strain.

This last chapter of this thesis is dedicated to determine the work capacity of our trained wires, as the above-referred idea suggested [LIY, 2004]. The wires used will be those that had been heat treated at a temperature equal to or greater than 500°C, followed by repeated thermal cycling at zero stress and then trained by constant stress training. These wires will be called improved wires. All the improved wires will be analyzed to determine the changes caused by this thermomechanical cycling in the work production, recovery strain, transformation temperatures and phase transformation behaviour. The process will be repeated for the non-improved (non-thermally cycled) samples and then the results for both the non-improved and the improved samples will be compared. Furthermore, we used XRD to quantify the phase transformation behaviour of the samples after the thermomechanical work production.

The level and the stability of the work production generated by the samples during 50 working cycles under different applied stresses would be considered as criteria of the material performance.

1 Operating mode

As Liang et al. [LIA, 1992] proposed the operating parameters for an SMA actuator are the maximum travel distance and the work generated by the actuator. In addition, the basic design parameters include the selection of the SMA material, the initial length of the SMA wire, the cross-section area, and the initial state of the SMA, that is, its initial recovery strain and residual strain (or austenite strain).

Based on the results given by the TWSME improvement (chapter 5), several samples thermally cycled and then, trained by constant stress training method (500TCs and 525TCs) of 200mm long and a 1mm of diameter were thermally cycled under constant tensile stresses of 29, 41, 68, 104 and 128MPa during 50 cycles and through the full

transformation range. Trained samples 500cs and 525cs (same length and diameter) were also thermally cycled under the following constant tensile stresses, 29, 41, 68 and 104MPa. The main elements of the experimental bench are exposed in chapter 3.

The direct output from the thermal cycling under constant load recorded by the data acquisition system is represented by hysteresis loops of total strain versus temperature. Two strains will be recorded when the sample returns to the hot shape and to the cold shape but an external tensile force is applied on heating and on cooling, respectively. We call these strains austenite strain (ε_a) and martensite strain (ε_m). Other result calculated from the data recorded is the work production performed by these samples. The work output is presented as the work production calculated by the general equation:

$$W_n = (\sigma \cdot A \cdot \varepsilon_r) \quad [J] \quad (\text{eq. 6.1})$$

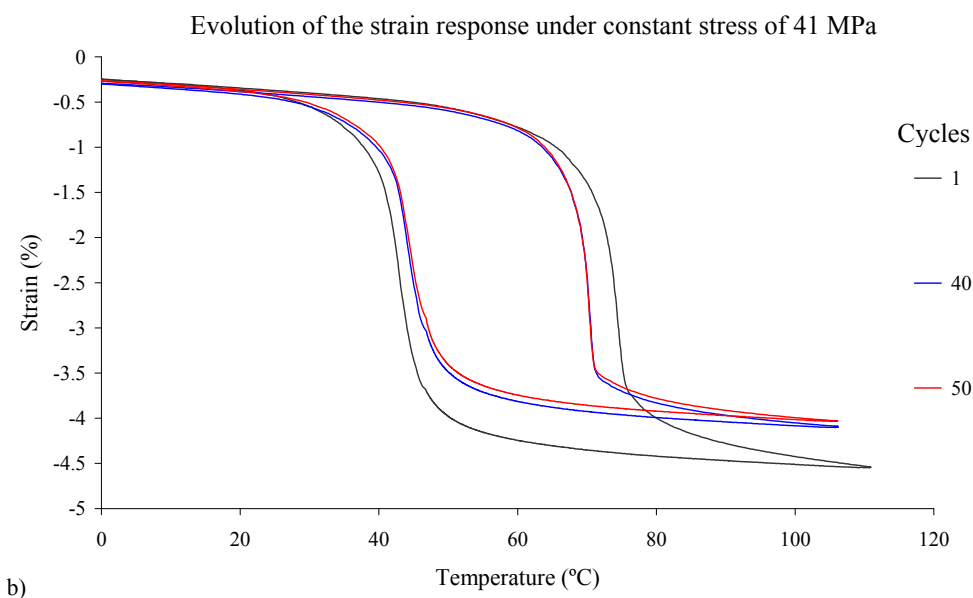
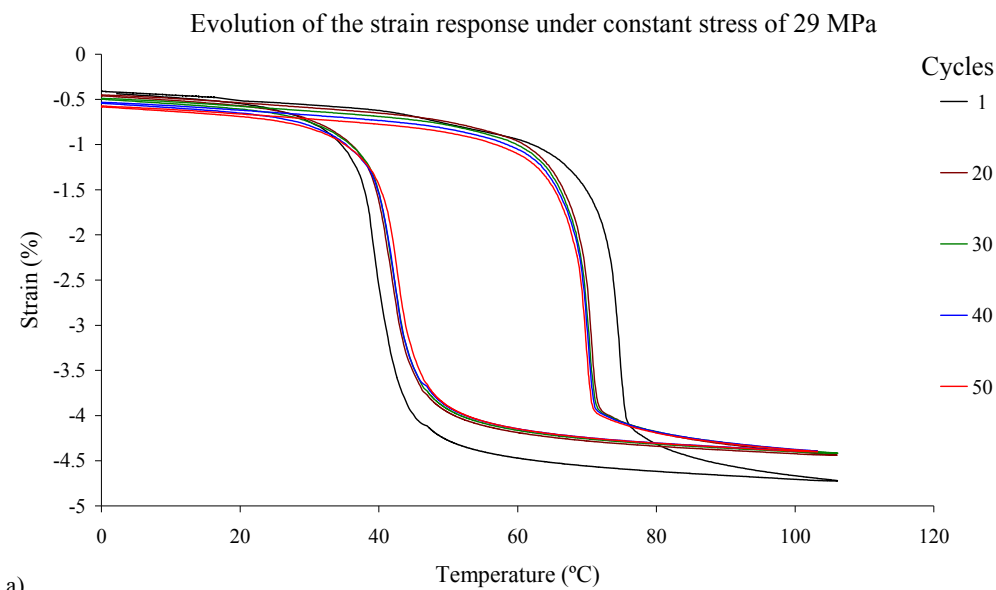
Where n is the number of the working cycle at which the work is calculated, σ is the opposing stress (MPa), A is the cross section area of the wire (0.7854mm^2) and ε_r is the recovery strain measured in mm ($\varepsilon_r = \varepsilon_m - \varepsilon_a$). Since the cooling process is assisted by the applied stress, other authors call the recovery strain SATWME (stress assisted two-way memory effect [CON, 1990]). The ε_r is recorded for a reference length of 50mm. The direct output from this equation will be the evolution of the work production of each sample versus the number of working cycles and depending on the value of stress applied.

2 Work production of samples 500TCcs

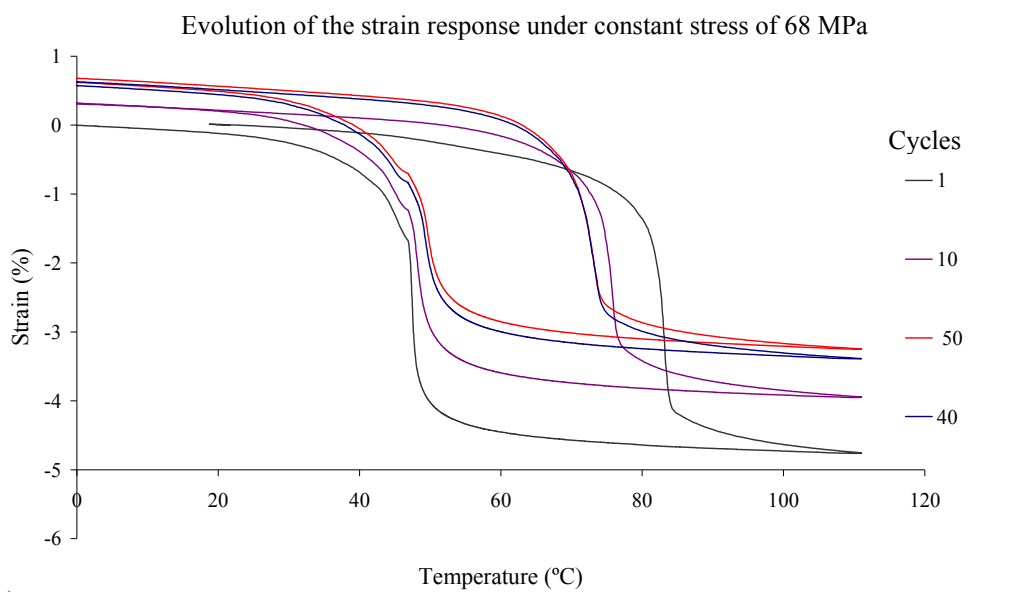
Several trained samples 500TCcs were subjected to 50 thermal cycles under different values of constant stresses. These samples are named as follows: 500TC₂₉, 500TC₄₁, 500TC₆₈, 500TC₁₀₄, and 500TC₁₂₈; where the samples sub index denote the value of the constant opposing stress during the thermomechanical cycling. The initial state of the samples prior to thermomechanical training and after the TWSME training is the next. These samples have an austenite strain and a recovery strain of around 0.6% and 5.2% respectively.

Figures 6.1 represent the hysteresis loops of total strain in function of temperature for all samples at selected cycles during all the process. From these figures the work production, the recovery strain and the transformation temperatures are measured in function of the number of cycles and the level of the stress applied. As show figures 6.1, since there is a displacement against a force during cooling, the trained samples can withstand considerable opposing stresses. As seen, the hysteresis is reduced and the austenite strain is incremented as the opposing stress is increased for all samples.

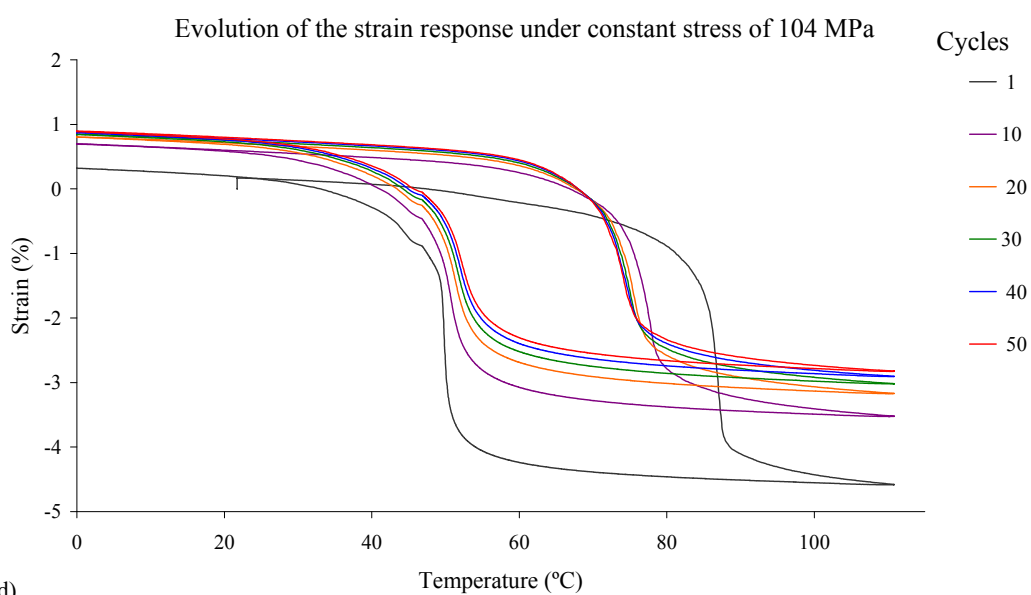
Figure 6.2 shows the evolution of the work production of the wire calculated by equation 6.1 versus number of thermal cycles and in function of the level of stress applied. From this figure 6.2, several important conclusions can be deduced. First, an increase in work production with the increase in the level of stress is measured, with no sample buckling for these stress values and number of working cycles. Second, a slightly decrease in work production exits through thermomechanical cycling for samples 500TC₂₉ and 500TC₄₁. As the stress applied increases, the decrease in the work production of the samples increases (500TC₁₀₄ and 500TC₁₂₈ samples). However, the major part of this decrease in work production is given during the initial part of the cycling. In fact, samples 500TC₂₉ and 500TC₄₁ show a fairly stable behaviour from cycle 10, followed by sample 500TC₆₈. This decrease in work production and its influence on sample applicability will be analyzed in more detail in section 4.



Figures 6.1a and b Evolution of the strain-temperature response versus number of thermal cycles and depending on the stress level applied for sample 500TCs: a) 29MPa and b) 41MPa.



c)



d)

Figures 6.1c and d Evolution of the strain-temperature response versus number of thermal cycles and depending on the stress level applied for sample 500TCcs: c) 68MPa and d) 104MPa.

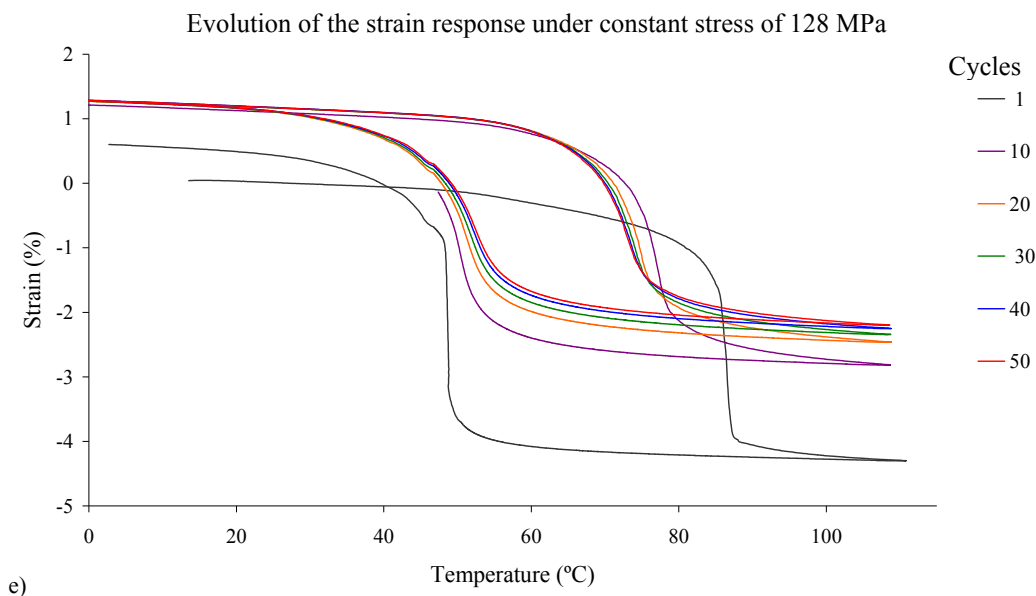


Figure 6.1e Evolution of the strain-temperature response versus number of thermal cycles and depending on the stress level applied for sample 500TCcs: e)128MPa.

The average work production and the relative increase in work production respect to the relative increase in the level of stress (in %) are calculated for each sample (figure 6.3). As seen, the best relation between recovery strain and opposing stress is the one that shows sample 500TC₆₈, which obtains an increase in work production of around 78.85% with an increment in stress of 27MPa respect to sample 500TC₄₁ (figure 6.3). As seen, further increment in opposing stress does not produce an increment in work production as higher as is produced in other samples (i.e. 500TC₁₂₈, 17.64%). These results indicate to us that the Ti-Ni wires give the best work performance, that is, the best relation between recovery strain and work production for a range of stresses of around 30-100MPa. However, we need to discuss other parameters as the decrease in recovery strain during cycling, to decide which sample presents the best work performance.

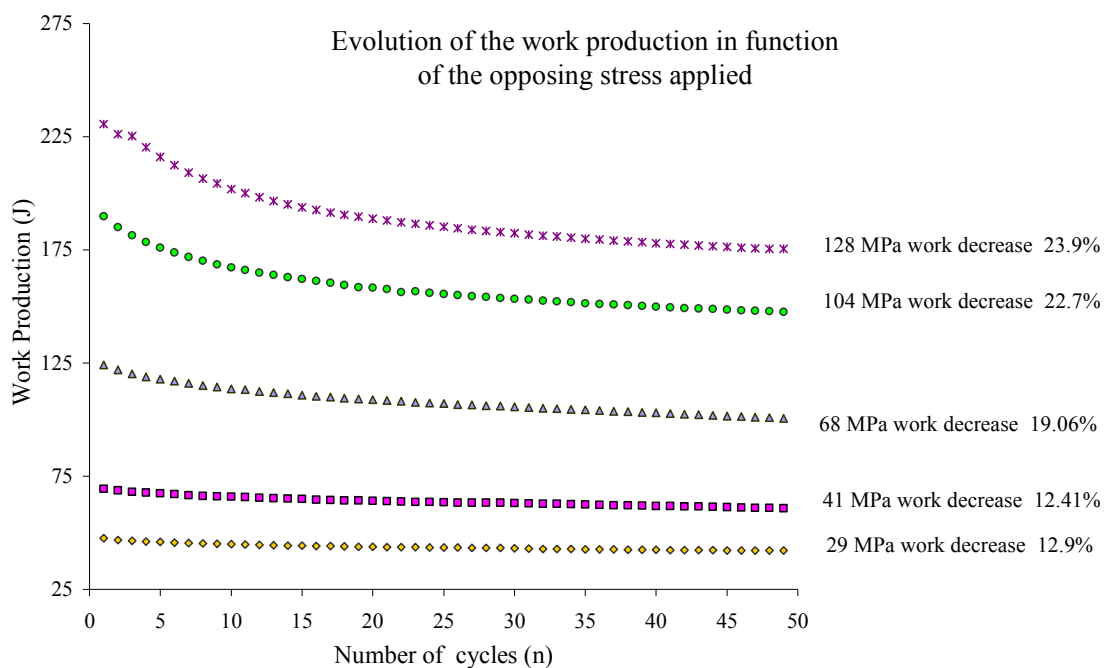


Figure 6.2 Work production evolutions in function of the level of the stress and the number of working cycles for samples 500TCs. The decrease in work production for each sample is also indicated in the figure.

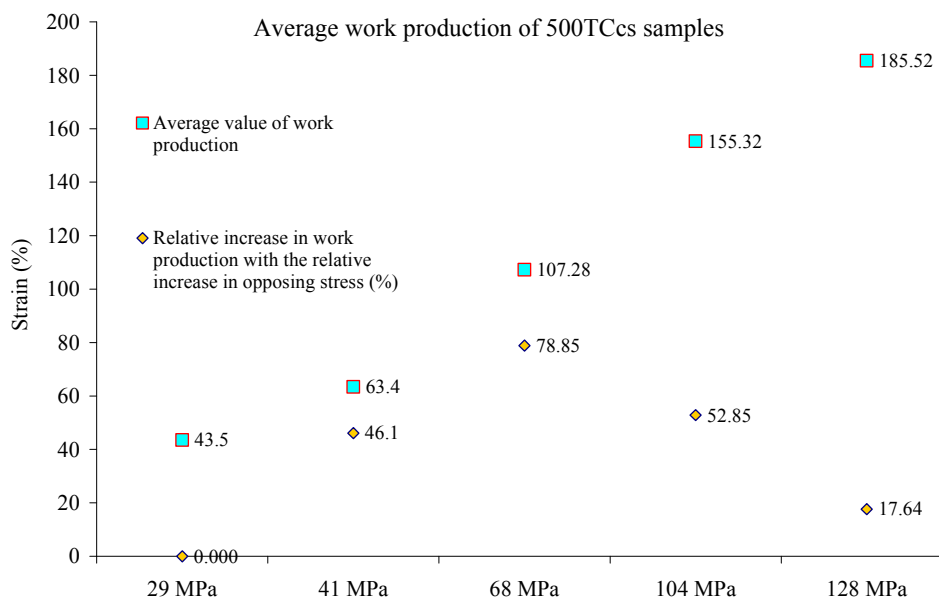


Figure 6.3 Average work production versus level of stress applied (magenta spots). The increase in work production respect to the relative increase in stress is indicated in the figure (yellow spots).

Figure 6.4 exposes the evolution of the recovery strain with thermomechanical cycling for all samples 500TCcs. The decrease in recovery strain is calculated as the difference between the first given value of the recovery strain at cycle 1 ($n=1$) and the last given value of the recovery strain ($n=50$). From the equation 6.1, it is obvious that the responsible of the decrease in work production is the decrease in recovery strain during cycling (pink circles in figure 6.4), which is produced due to the increase in irreversible strain, that is, the austenite strain. The most important decrease in recovery strain is produced at the beginning of the thermomechanical process. The maximum decrease in recovery strain is for those samples working at stresses equal to or greater than training stress, that is, 500TC₁₀₄ and 500TC₁₂₈ samples.

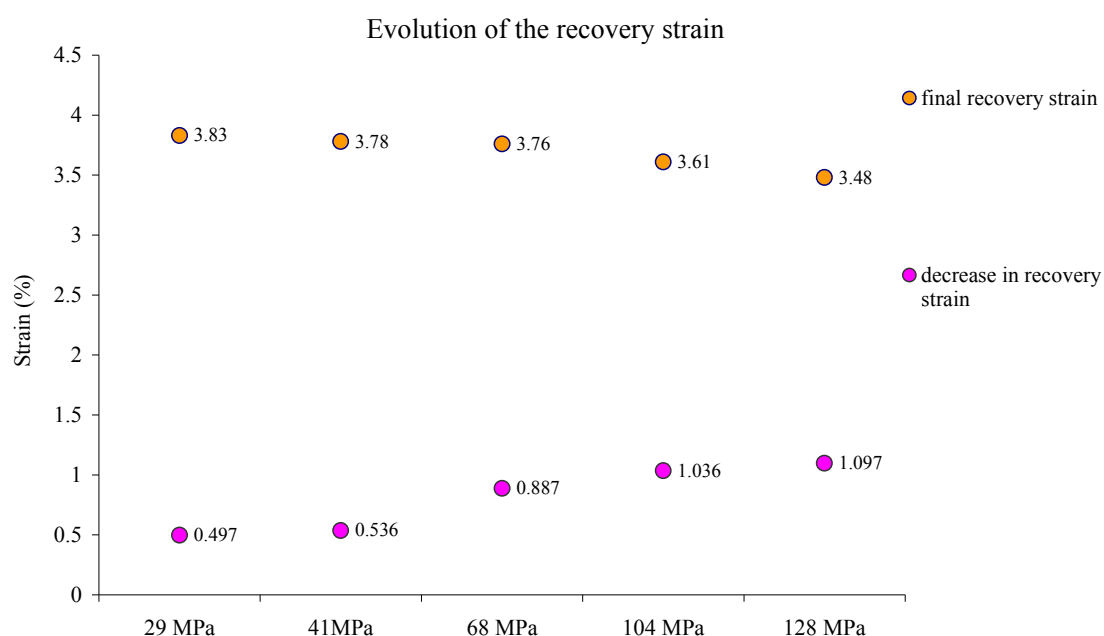


Figure 6.4 Evolution of the recovery strain with thermomechanical cycling for 500TCcs samples.

To extend our analysis, the evolution of the activation temperatures versus the number of cycles and the level of stress has been measured. The method used is the applied loading method (chapter 3). This method is highly recommended for real actuator design [ABE, 2004]. The reason is that real load values are applied to simulate

conditions in practice. This will help to ensure that the activation temperatures measured are of value in the development of the work production.

Figure 6.5 displays the evolution of the activation temperatures for the first and last working cycles in function of the level of the stress applied. As the level of stress increases, the martensitic (M_S) and austenitic (A_S) initial temperatures increase (blue colour points). The increase in M_S is higher (near of 5°C) in those samples that work at high level of stresses. This increase in M_S could be attributed to an increase in the facility to form the martensite plates, which are preferentially oriented with respect to the deformation direction during working. With cycling, all specimens present a very slightly decrease in M_F (red points) and this decrease is focused in the initial ten working cycles. The highest decrease in M_F is for sample 500TC₁₂₈. From cycle 10, all martensitic temperatures attained fairly stable values. The entire initial A_S temperatures decrease from 10°C (sample 500TC₂₉) to 17°C (samples 500TC₁₀₄ and 500TC₁₂₈) as seen in figure 6.5. The final austenitic temperature A_F behaves in a similar way, but the decrease is minor (from 8 to 14°C for the same samples) than for the A_S temperature. The decrease in the austenitic temperatures are produced in the first ten working cycles, revealing that the austenitic transformation is being easier as the work proceeds.

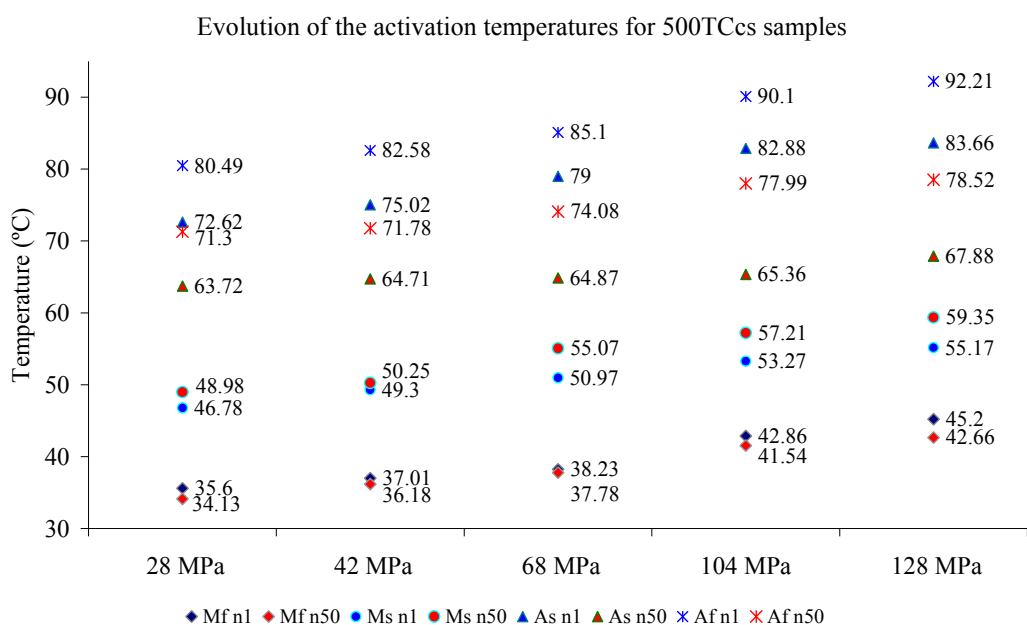


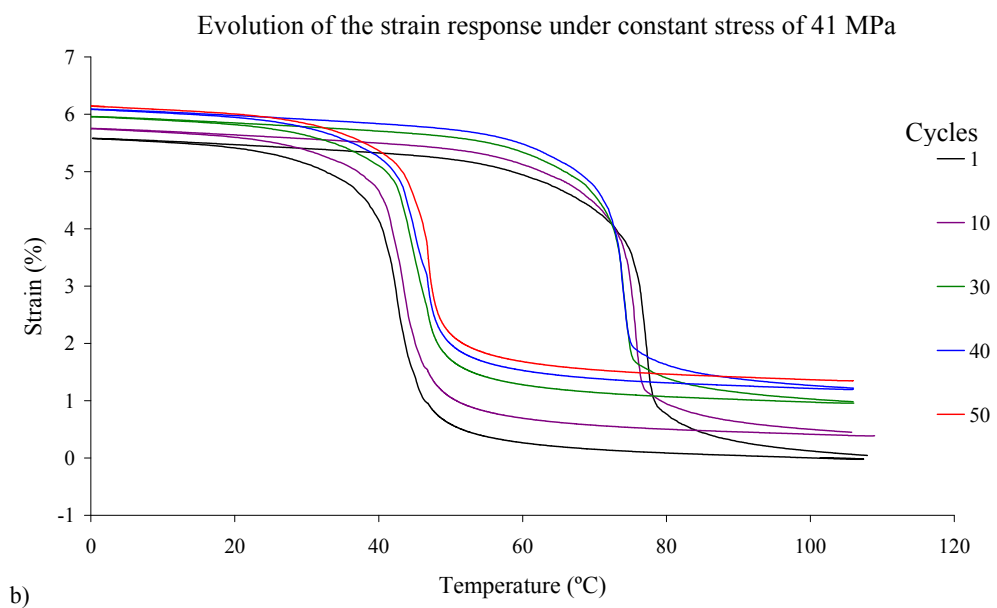
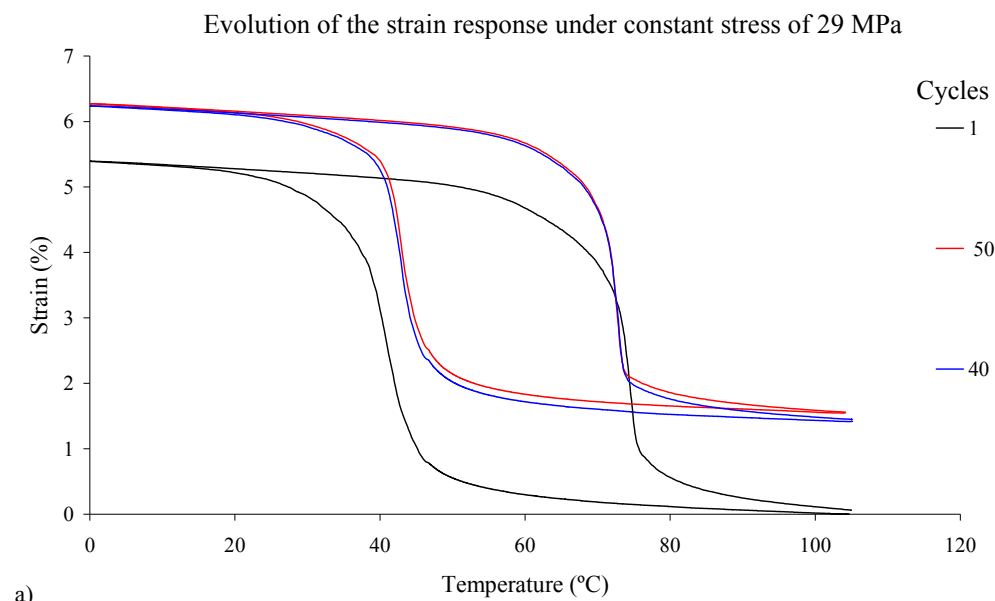
Figure 6.5 Evolution of the activation temperatures with working cycles. The values listed here are for the first (blue colour) and the last (red colour) working cycles.

3 Work production of samples 525TCcs

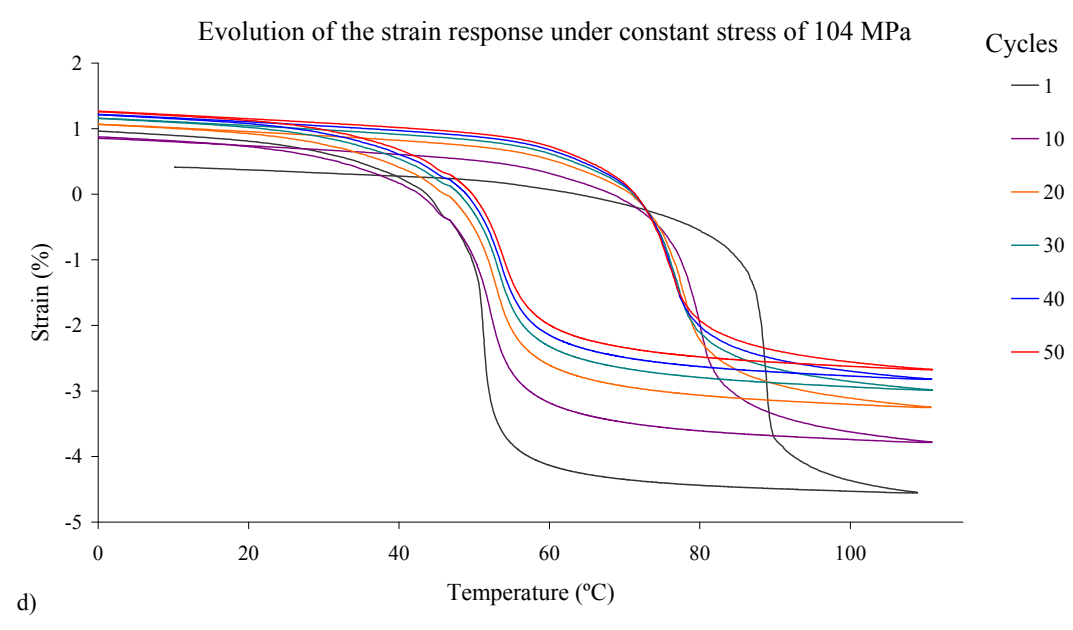
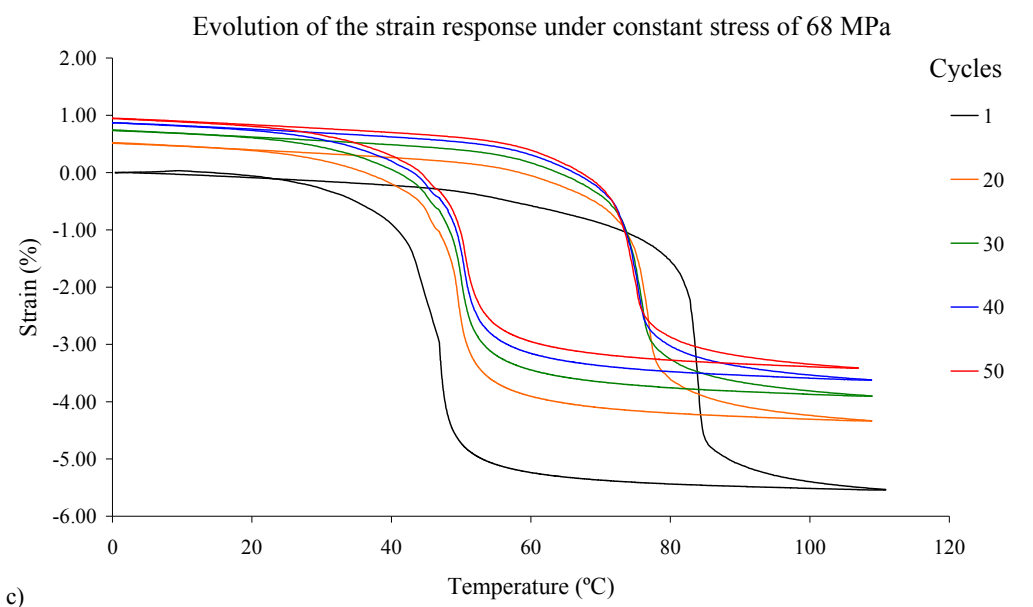
Several trained samples 525TCcs were subjected to 50 thermal cycles under different constant stresses. These samples are named as following: 525TC₂₉, 525TC₄₁, 525TC₆₈, and 525TC₁₀₄. After TWSME training, these samples have values of initial martensite and austenite strains near of 5.5% and 1.85% respectively. Figures 6.6 represent the hysteresis loops of the recovery strain in function of temperature for all samples at selected cycles during all the process. From these figures the work production, the recovery strain and the activation temperatures are measured in function of the number of cycles and in function of the level of the stress applied. As occurs with samples 500TCcs, the trained samples 525TCcs can withstand considerable opposing stresses.

Figure 6.7 shows the evolution of the work production calculated by equation 6.1 versus number of thermal cycles for each sample 525TCcs. The evolution of the work production with working cycles for samples 525TCcs is similar to that measured for samples 500TCcs. The work production values are according to the decrease in hysteresis with cycling that figure 6.6 shows. The most stable feature is shown by samples 525TC₂₈ and 525TC₄₁.

The average work production and the relative increase in work production (in %) respect to the relative increase in the level of stress are shown in figure 6.8 for samples 525TCcs. As seen, the best relation between recovery strain and the level of stress is shown by sample 525TC₆₈, which obtains an increase in work production of around 61% with an increment in stress of 27MPa respect to sample 525TC₄₁ (figure 6.8).



Figures 6.6a and b Evolution of the strain-temperature response versus number of thermal cycles under different stress values for samples 525TCcs: a) 29MP and, b) 41MPa.



Figures 6.6c and d Evolution of the strain-temperature response versus number of thermal cycles under different stress values for samples 525TCs: c) 68MP, and d) 104MPa.

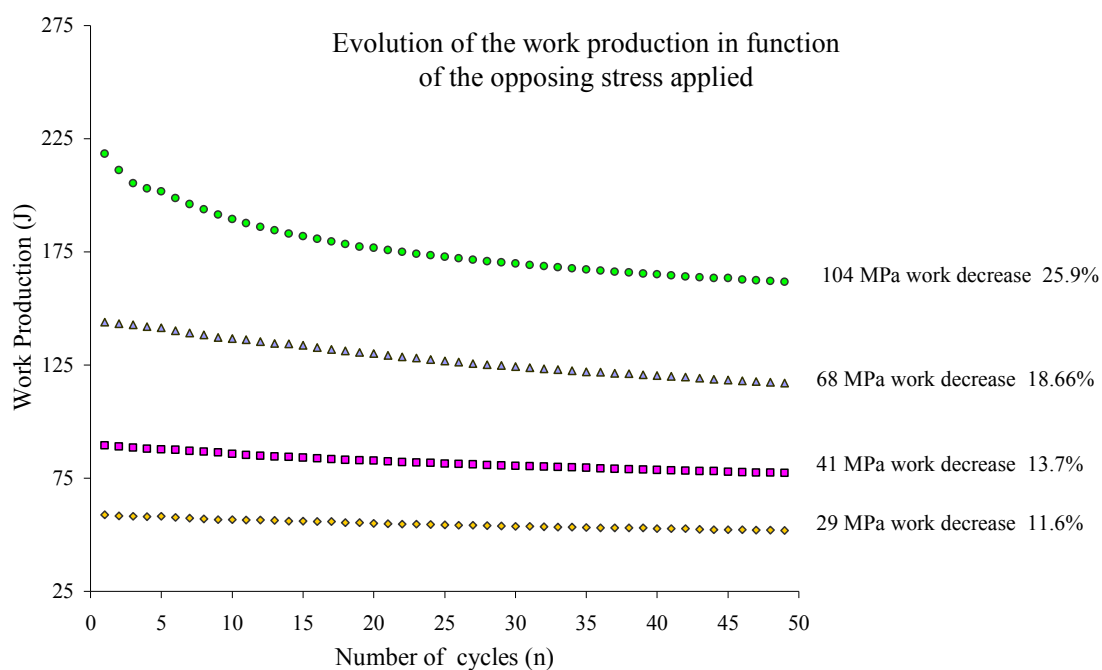


Figure 6.7 Evolution of the work production in function of the stress applied and the number of working cycles for samples 525TCcs. The decrease in work production (%) is also indicated in the figure.

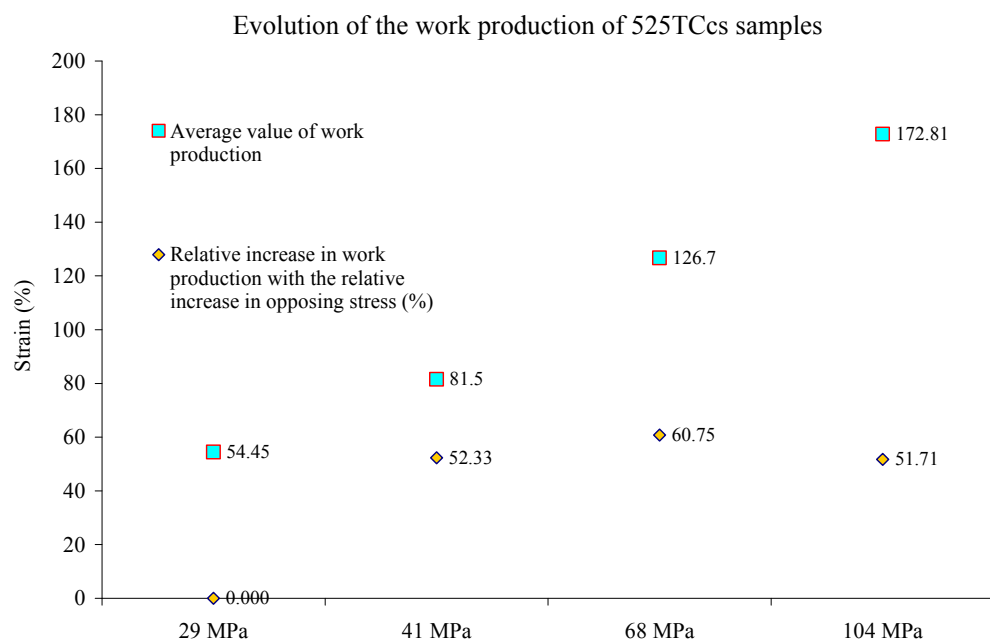


Figure 6.8 Average work production versus level of stress applied for samples 525TCcs. The increase in work production respect to the relative increase in opposing stress is indicated in the figure.

Figure 6.9 shows the evolution of the recovery strain with cycling and with the level of stress. As occurs with 500TCs samples, the responsible of the decrease in work production is the decrease in recovery strain during cycling. From the results obtained for 500TCs and 525TCs samples, the decrease in recovery strain with the increase in the stress level and number of working cycles that occurs in these samples can be explained by the plasticity emergence interfering with the martensite transformation as suggested by [BIG, 1996].

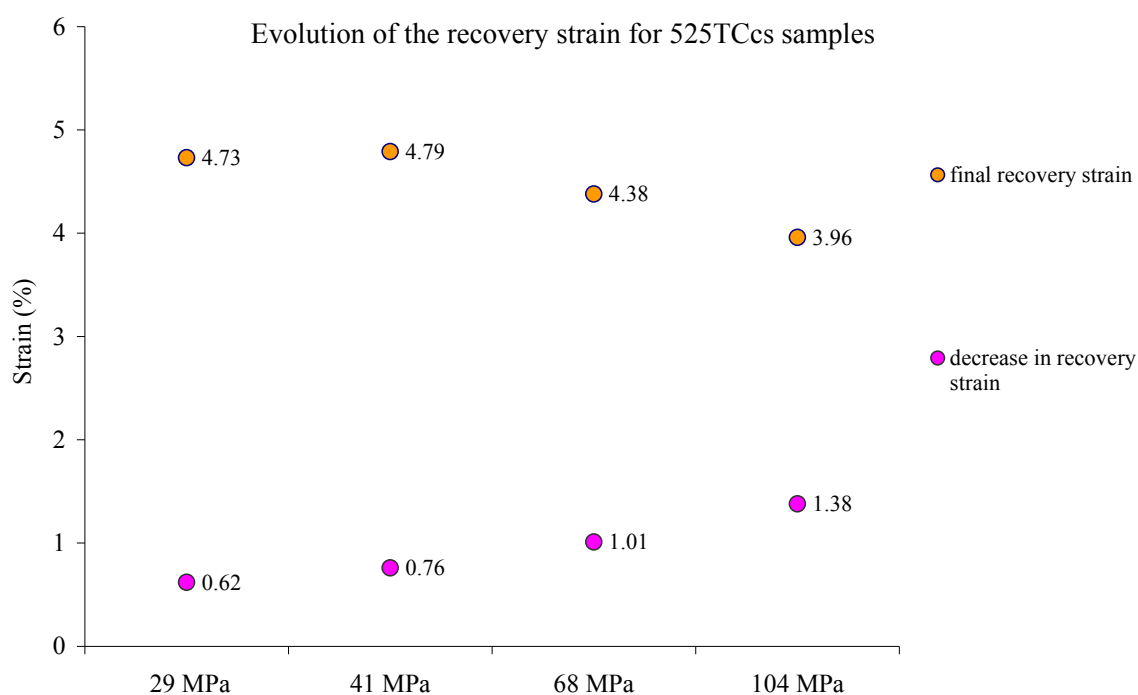


Figure 6.9 Evolution of the recovery strain during thermomechanical cycling for samples 525TCs.

The evolution of the activation temperatures versus the number of working cycles using the applied loading method is shown in figure 6.10. The evolution of the transformation temperatures is similar than those explained for 500TCs samples.

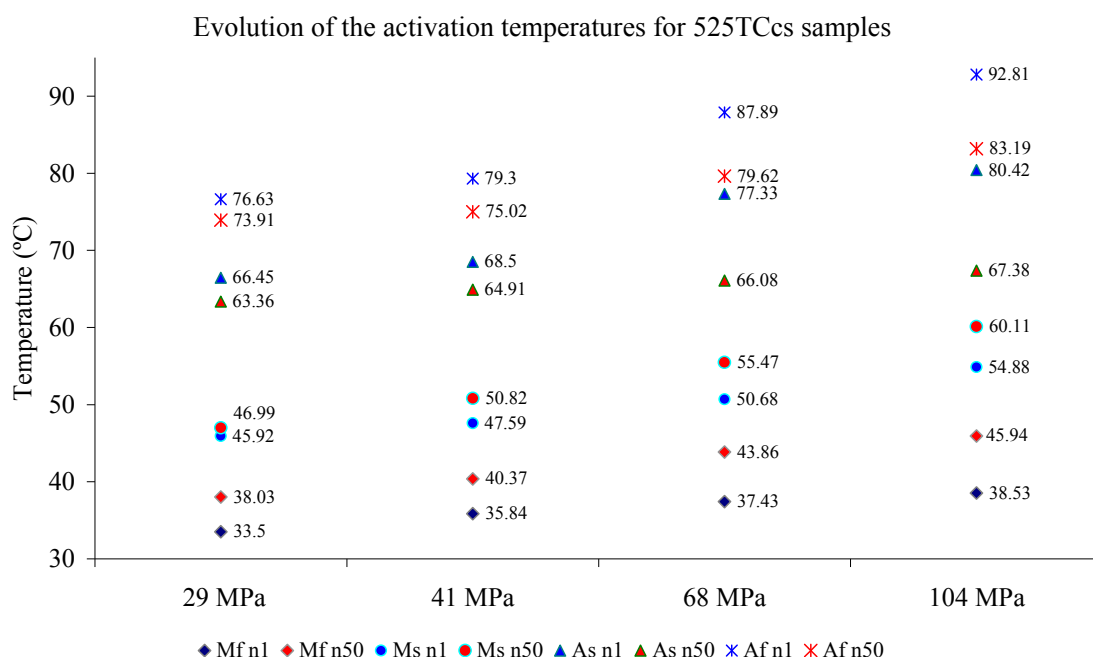


Figure 6.10 Evolution of the activation temperatures with working cycles for samples 525TCcs. The values listed here are for the first (blue colour) and the last (red colour) working cycles. The decrease in the activation temperatures with cycling is higher as is the working stress applied.

4 Comparison between samples

A comparative analysis between 500TCcs and 525TCcs samples will be helpful to elucidate which samples show the best mechanical behaviour under thermomechanical cycling. The criteria performance is the level and stability of the work production generated by the samples.

Following this comparative study, a second comparative analysis is done. We compare the work production of non-improved trained samples, that is, non-thermally cycled prior to TWSME training (500cs and 525cs), and the work production of the improved trained samples.

Table 6.1 shows the results for samples 500TCcs and 525TCcs depending on the value of the opposing stress applied. We include the results obtained for samples 500TCcs and 525TCcs when these samples are working at zero stress (TWSME samples).

The differences between 500TCs and 525TCs samples are:

a) Sample 525TC₂₉ has slightly higher average work production than sample 500TC₂₉ (11MPa) because its recovery strain is larger than that for 500TC₂₉ sample. Both samples present a decrease in work production, being this decrease focused on the initial ten cycles for 500TC₂₉ sample and along the cycling for sample 525TC₂₉. Although sample 525TC₂₉ presents higher recovery strain than sample 500TC₂₉ (0.9% more), the decrease in recovery strain is minor in sample 500TC₂₉ than in sample 525TC₂₉ (0.13% less). Concerning the decrease in temperature interval with cycling, both samples present equal decrease in their corresponding temperature interval (7.3°C). Therefore, it is possible to say that both samples present similar properties under constant stress cycling.

b) The analysis of 525TC₄₁ and 500TC₄₁ samples results reports similar conclusions than the above ones. 525TC₄₁ has higher average work production than sample 500TC₄₁ (18.2MPa) because sample 525TC₄₁ has higher recovery strain than sample 500TC₄₁ during all cycling (0.86% more). However, the net decrease in recovery strain is higher for sample 525TC₄₁ than for sample 500TC₄₁ (0.23% more). Regarding the decrease in temperature interval with cycling, both samples present similar decrease in their corresponding temperature interval (10°C for sample 500TC₄₁ and 9°C for sample 525TC₄₁).

c) 500TC₆₈ and 525TC₆₈ samples have an important increase in the work production respect to that produced by samples 500TC₄₁ and 525TC₄₁. Sample 525TC₆₈ has higher average work production and very slightly lower decrease in work production than sample 500TC₆₈, however, the initial decrease in work production for sample 500TC₆₈ is 7.86%, and for sample 525TC₆₈ is 4.64%. Sample 525TC₆₈ has higher recovery strain (0.74%) than sample 500TC₆₈. Regarding the decrease in temperature interval with cycling, this is around 15°C for sample 525TC₆₈, and it is 10°C for sample 500TC₆₈. Therefore, both samples present different mechanical performances under constant stress of 68MPa, because although sample 525TC₆₈ have lower decrease in work production than sample 500TC₆₈, sample 500TC₆₈ has minor decrease in temperature interval than sample 525TC₆₈.

d) Sample 525TC₁₀₄ has higher average work production than sample 500TC₁₀₄ (17.5MPa). Moreover, the decrease in work production is similar for both samples. Regarding the values for the recovery strain, sample 525TC₁₀₄ has higher decrease in recovery strain than sample 500TC₁₀₄ at cycle 50 (0.35% more). Regarding the decrease in temperature interval with cycling, the cycling again affects sample 525TC₁₀₄ (17°C) more than sample 500TC₁₀₄ (11°C). Therefore, we think that, given both similar work decrease, sample 500TC₁₀₄ shows better mechanical performance than sample 525TC₁₀₄ due to the minor decrease in recovery strain and in temperature interval that this sample 500TC₁₀₄ developed.

e) **Others interesting trends** can be made from the results exposed in table 6.1. Firstly, all entire working samples 500TCs and 525TCs have greater recovery strain values than the TWSME samples. This occurs for all cases of stress and number of working cycles, excepting for the cases of samples 525TC₆₈ and 525TC₁₀₄ at cycle 50. This fact can be explained as follows. Since the martensite strain is assisted by the applied stress during the cooling part of the working cycling (SATWME), the efficiency of dislocations in the formation of oriented martensite variants is higher as higher is the stress applied, being the values of martensite strain the largest when the samples are working under stress [BIG, 1996], [MIL, 2001] and [WAD, 2008]. Therefore, the samples develop better mechanical properties if they work under certain values of constant stress than if they work under free stress conditions. However, an important limitation exists; the level of the opposing stress cannot permit the material buckling.

f) Moreover, for samples 525TCs, the values of the recovery strain for cycle 1 increase as the stress increases up to 41MPa. Beyond this value of stress, the recovery strains decreases a little for 525TC₆₈ and 525TC₁₀₄ samples. For samples 500TCs the recovery strain increases with the stress up to 68MPa and then, the recovery strain given in cycle 1 by this sample 525TC₆₈ is similar to those given by 525TC₁₀₄ and 525TC₁₂₈ samples in cycle 1. Therefore, it occurs a process of saturation of the recovery strain of the sample, which depends on the heat treatment temperature and value of the stress applied. Consequently, **optimum ranges of working stress can be defined for these samples.**

CRITERIA OF THE MATERIAL PERFORMANCE	TWSME 500TC_{cs}	TWSME 525TC_{cs}	500TC₂₉	525TC₂₉	500TC₄₁	525TC₄₁	500TC₆₈	525TC₆₈	500TC₁₀₄	525TC₁₀₄
<i>Work average (J)</i>	-	-	43.5	54.45	63.4	81.5	107.28	126.7	155.32	172.81
<i>Decrease in work production (%) cycle 10</i>			6.58	3.54	4.84	3.45	7.86	4.64	14.11	12.31
<i>Decrease in work production (%) cycle 50</i>			12.9	11.57	12.41	13.72	19.06	18.66	22.27	25.9
<i>Recovery strain (%) cycle 1</i>	3.77	4.78	4.4	5.34	4.32	5.56	4.65	5.39	4.62	5.34
<i>Recovery strain (%) cycle 10</i>	3.65	4.55	4.1	5.16	4.09	5.37	4.06	5.14	4.24	4.68
<i>Recovery strain (%) cycle 50</i>	3.56	4.42	3.83	4.73	3.78	4.79	3.76	4.38	3.61	3.96
<i>(n 30 for TWSME samples)</i>										
<i>Activation temperature interval cycle 1 (A_f-M_f) (°C)</i>	46.13	45.06	44.89	43.13	45.57	43.46	46.87	50.46	47.24	54.28
<i>Activation temperature interval cycle 10 (A_f-M_f) (°C)</i>	44.7	44.16	38.99	41.48	38.31	40.31	38.73	42.85	37.31	44.43
<i>Activation temperature interval cycle 50 (A_f-M_f) (°C)</i>	43.2	43.9	37.17	35.88	35.6	34.65	36.3	35.76	36.45	37.25

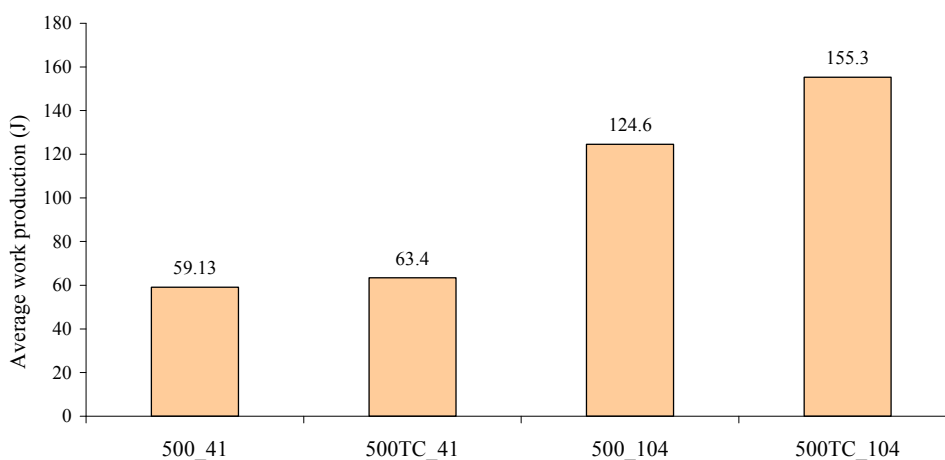
Table 6.1 Comparison between samples.

To validate the results obtained by 500TCcs and 525TCcs samples during working, the same thermomechanical cycling applied to samples 500TCcs and 525TCcs will be applied to samples 500cs and 525cs, which were non-thermally cycled prior to training by constant stress. Then, the average work production and the average recovery strain between the improved samples and the non-improved samples are compared. Figures 6.11 show the results for samples 500cs and 500TCcs. Figures 6.12 show the results for samples 525cs and 525TCcs. Figure 6.13 shows the initial recovery strain and the initial austenite strain that have these sample after TWSME training and before thermomechanical work.

The results in figures 6.11a and 6.12a show that samples thermally cycled prior to TWSME training (improved wires) produce higher work than samples non-thermally cycled prior to TWSME training (non improved wires). This fact is produced because the recovery strain of 500TCcs and 525TCcs samples is always larger than that of samples 500cs and 525cs (figures 6.11b and 6.12b).

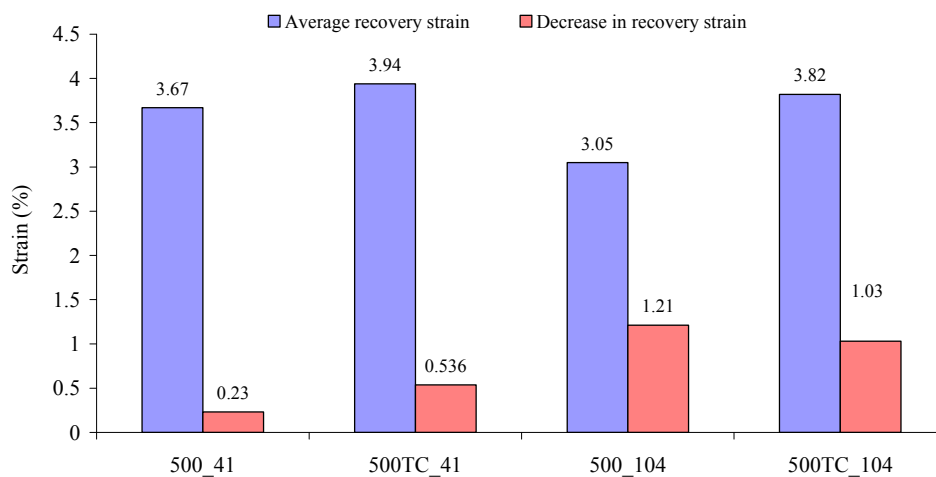
The decrease in residual strain is higher for samples thermally cycled prior to training (500TCcs and 525TCcs) than for samples 500cs and 525cs, excepting in sample 500TC₁₀₄. However, the highest difference between samples about the decrease in recovery strain is 0.3% for 500₄₁ and 500TC₄₁ samples and it is 0.28% for 525TC₄₁ and 525₄₁ samples (see figures 6.11b and 6.12b). The fact that samples thermally cycled 525TCcs and 500TCcs suffer higher decrease in recovery strain can be offset because of two facts (figure 6.13). Firstly, the irreversible strain accumulated during TWSME training by samples thermally cycled is lower than that accumulated by samples non-thermally cycled. Secondly, the recovery strain of samples thermally cycled is always higher than that of samples thermally cycled.

Comparison between the average work production of 500cs and 500TCcs samples



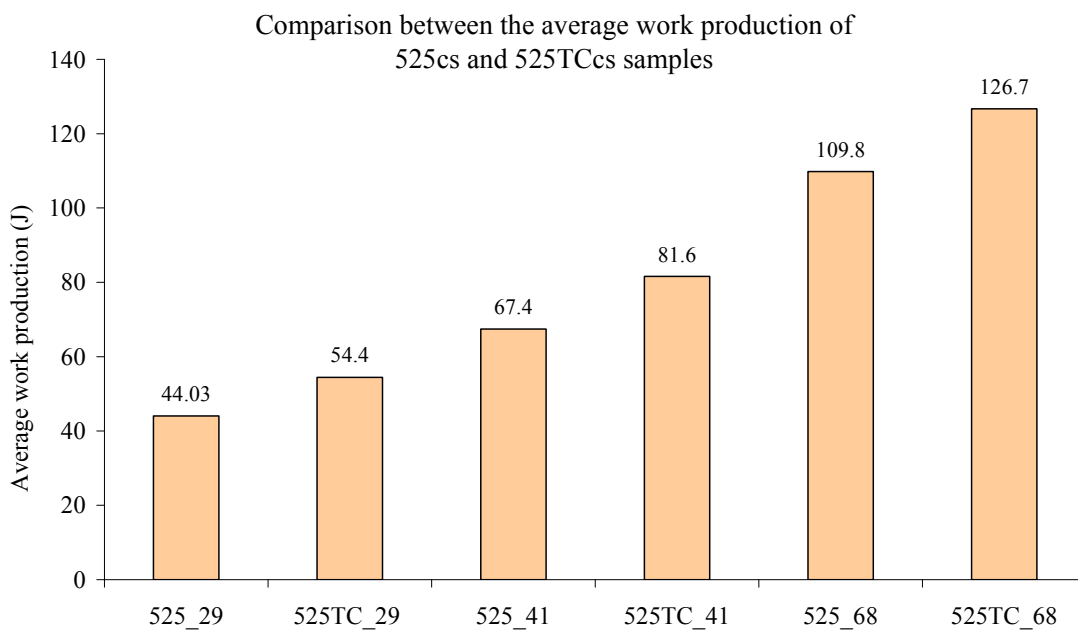
a)

Comparison between recovery strains of 500cs and 500TCcs samples

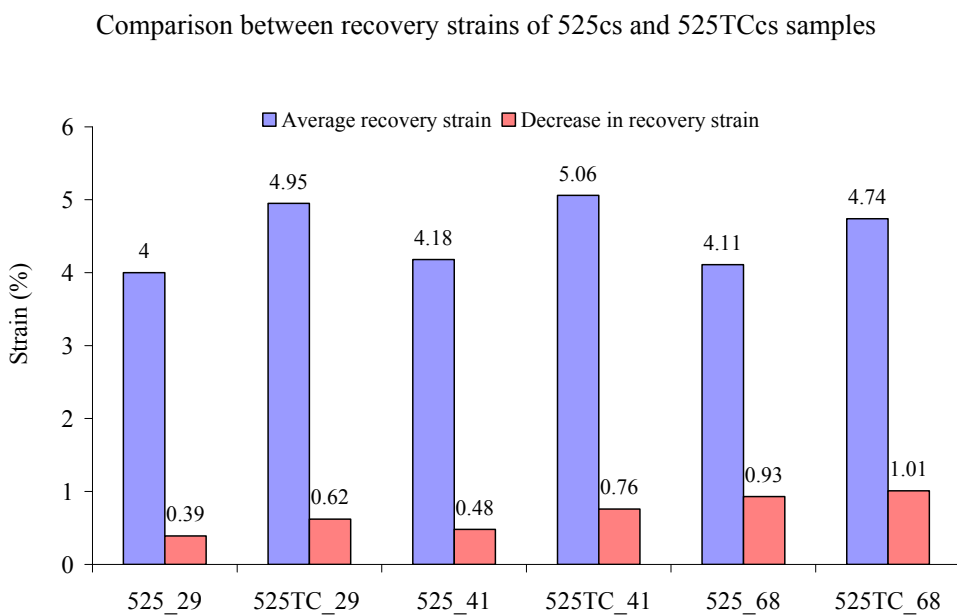


b)

Figures 6.11 Comparison between the thermomechanical behaviour of the non-improved samples (500cs) and the thermomechanical behaviour of the improved samples (500TCcs) for 50 working cycles: a) average work production and b) average recovery strain and net decrease in recovery strain.



a)



b)

Figures 6.12 Comparison between the thermomechanical behaviour of the non-improved samples (525cs) and the thermomechanical behaviour of the improved samples (525TCs) for 50 working cycles:
 a) average work production and b) average recovery strain and net decrease in recovery strain.

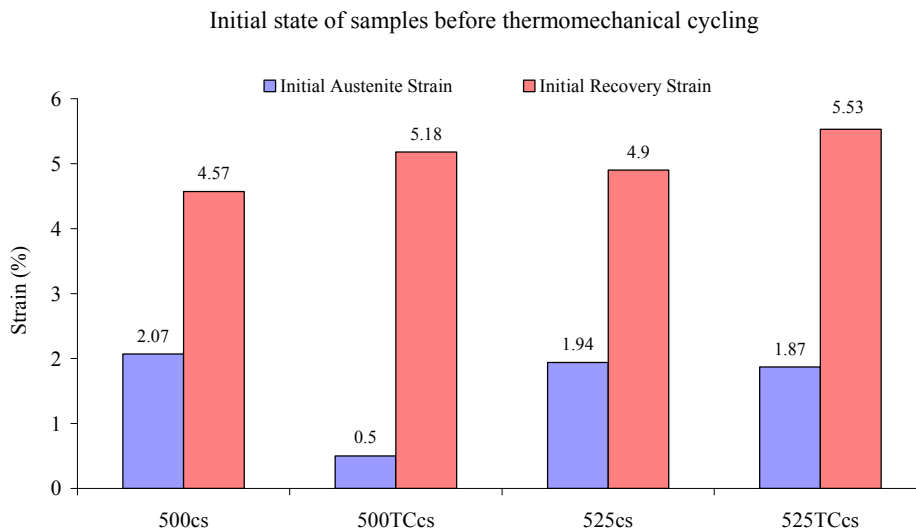


Figure 6.13 The recovery strain and the austenite strain developed by sample due to TWSME training.

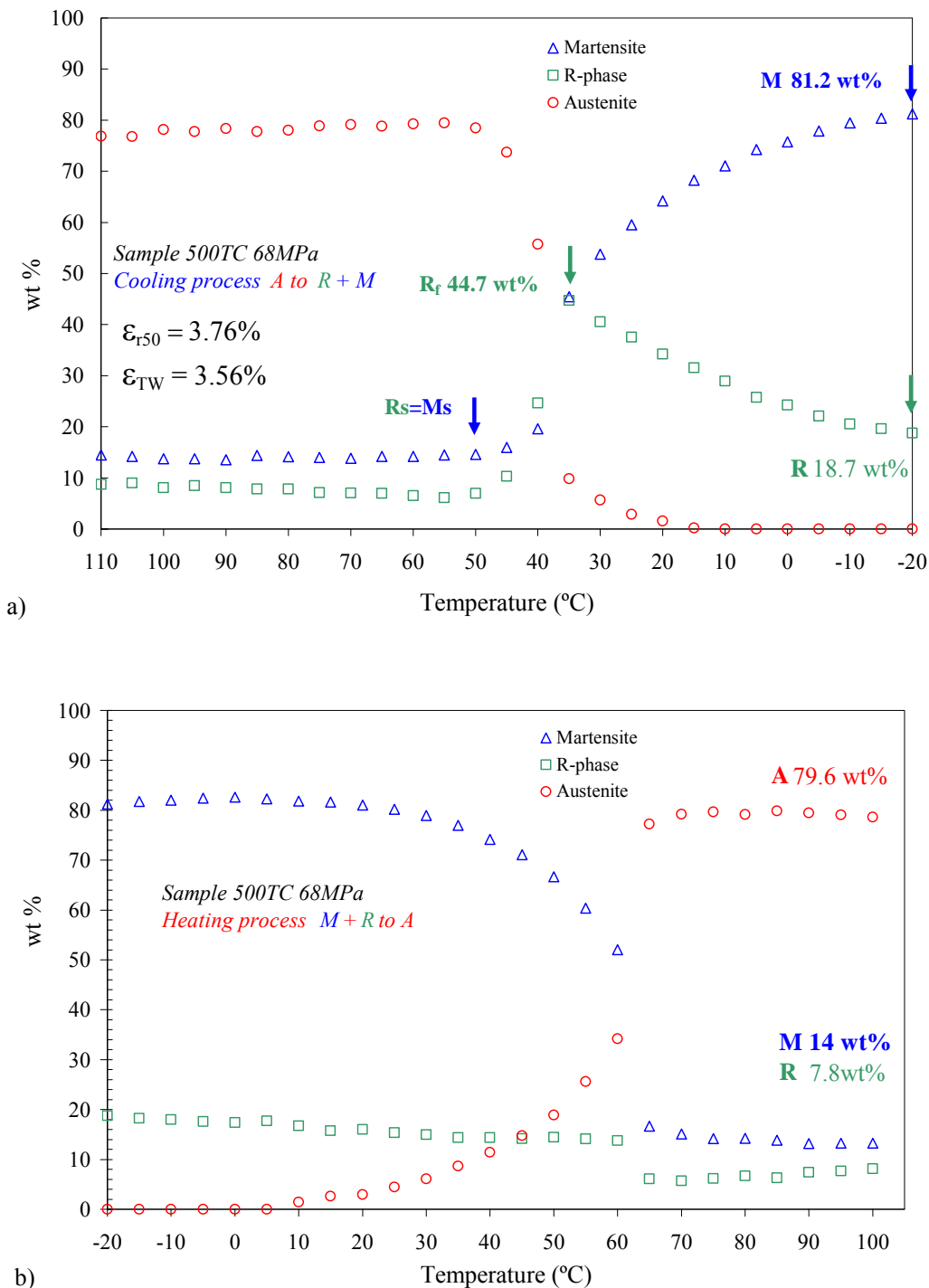
5 Quantification of the changes in phase transformation behaviour due to thermomechanical cycling

The changes in the phase transformation behaviour due to 50 thermomechanical cycles are shown in figures 6.14 and 6.15. The quantitative analysis are derived from XRD powder patterns using the Rietveld method and the software TOPAS. The results are given for each sample and each opposing stress as the % percent of the weight fraction (wt%) of each phase present in the sample as a function of temperature and through the completed temperature transformation range. The figures show the results for selected samples. They are 500TC₆₈, 500TC₁₂₈, 525TC₄₁, and 525TC₁₀₄. We show the results for values of working stress under and over the training stress. The value of the recovery strain at cycle 50 and the value of the two-way memory strain are included in the cooling part of the wt% diagram for each sample.

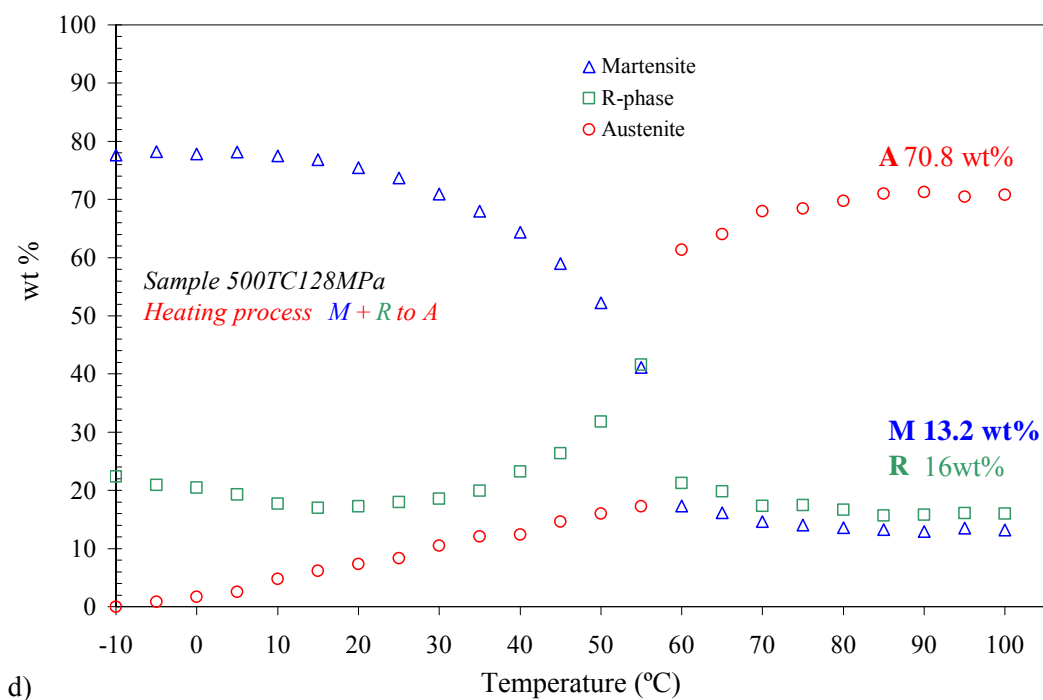
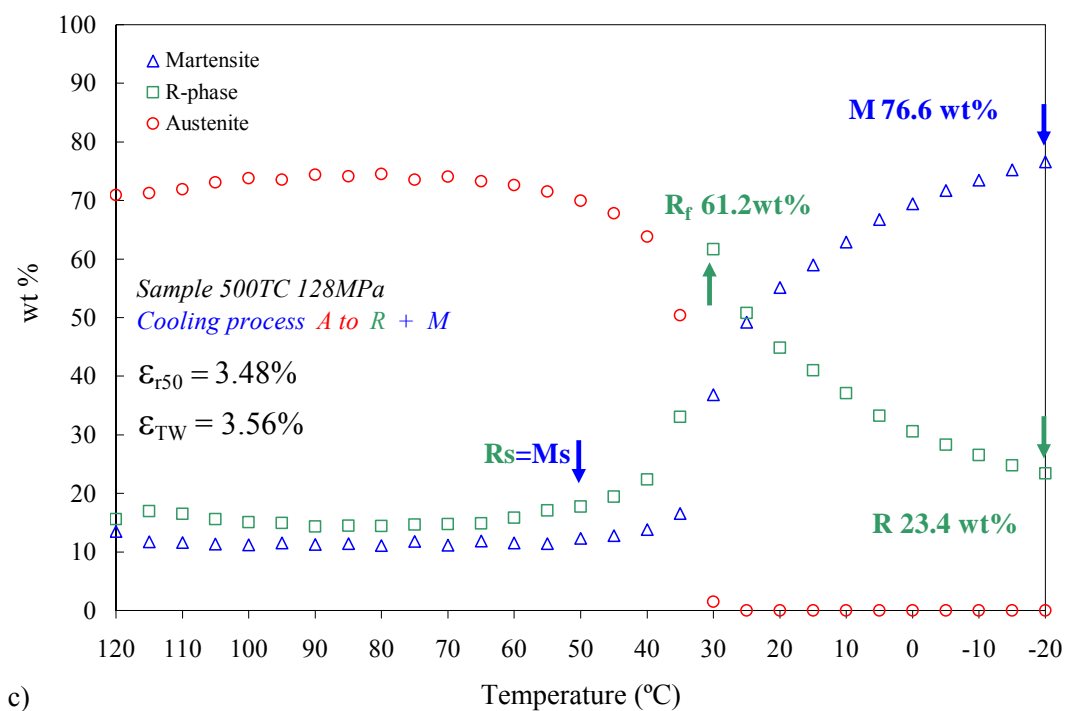
The effects of thermomechanical cycling on sample 500TC₆₈ are clearly shown in figures 6.14a and 6.14b. The transformation behaviour of 500TC₆₈ sample is scarcely modified respect to the TWSME sample 500TCcs (figures 5.9). During cooling, the martensite and the R-phase evolve together from austenite being the transformation simultaneous ($R_S=M_S=50^\circ\text{C}$), as occurs in TWSME sample 500TCcs. When the R-phase transformation ends the maximum level of R-phase is attained (44.7wt% at 35°C). Sample 500TC₆₈ develops similar quantity of R-phase under constant stress of 68MPa than sample 500TCcs under TWSME thermal cycling (0.4% more). From 35°C, the martensite is formed from austenite plus R-phase. At 20°C the austenite reaches the 0wt%. From this point, the martensite is formed only from contribution of the R-phase. At the end of the cooling process, there is lower martensite (81.2wt%) and higher R-phase (18.7wt%) in sample 500TC₆₈ than in sample TWSME 500TCcs (83wt% and 17wt% respectively, figure 5.9). The heating process for sample 500TC₆₈ is done with contribution of martensite and R-phase that transforms into austenite (figure 6.14b). During heating, the quantity of R-phase is increased up to 13.79wt% at 60 °C (12.65wt% for TWSME 500TCcs at similar temperature). At the end of transformation process, sample 500TC₆₈ has a minor quantity of austenite and a higher quantity of retained martensite (3.7% more) and R-phase (1.8% more) respect to 500TCcs TWSME sample.

The effects of constant stress training on sample 500TC₁₂₈ are exposed in figures 6.14c and 6.14d. The transformation behaviour of 500TC₁₂₈ sample is similar to that of sample 500TC₆₈. During cooling, the martensite and the R-phase evolve together from austenite being the transformation simultaneous ($R_S=M_S=50^\circ\text{C}$). When the R-phase transformation ends the maximum level of R-phase is attained (61.2wt% at 30°C), which is higher than that of sample 500TC₆₈ (and that of TWSME sample). Therefore, it seems that sample 500TC₁₂₈ develops larger quantity of R-phase under constant stress of 128MPa than sample 500TC₆₈. At the end of the cooling process there is less martensite (76.6%) and higher residual R-phase (23.4wt%) for sample 500TC₁₂₈ than for 500TC₆₈ and 500TCcs TWSME samples. The heating process is done with contribution of martensite and R-phase that transforms into austenite (figure 6.14d). During heating, the 500TC₁₂₈ R-phase is also increased up to 41wt% (60°C), which is considerably higher than that for 500TC₆₈ and TWSME samples. At the end of

transformation process, (90°C), sample 500TC₁₂₈ has an important decrease in austenite (11.8% less), an increase in retained martensite (3% more) and an important increase in R-phase (9% more) respect to the TWSME sample.

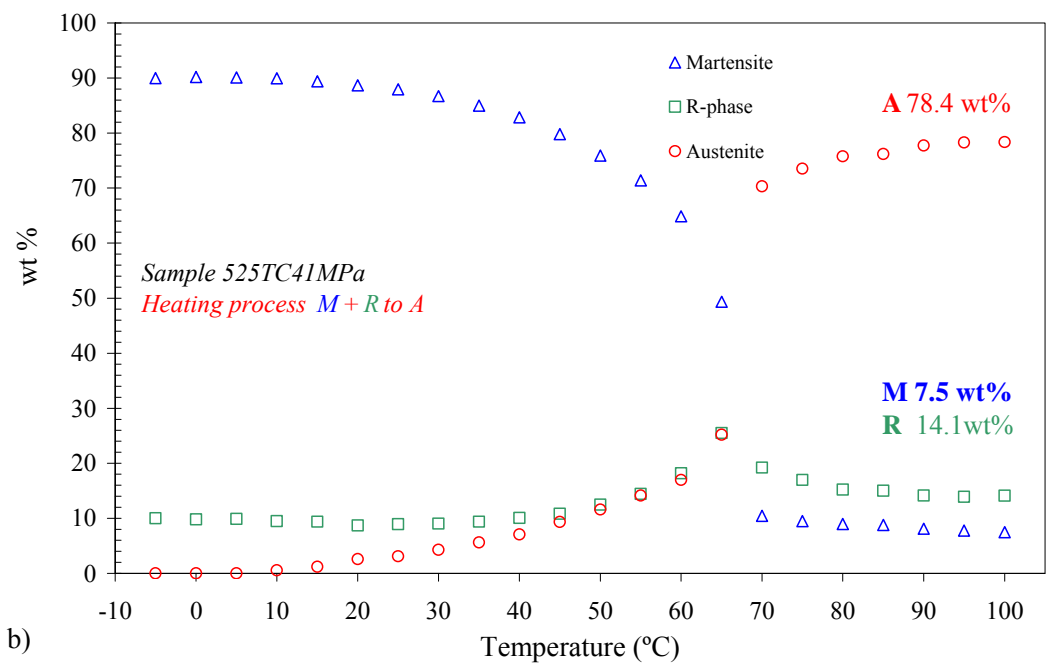
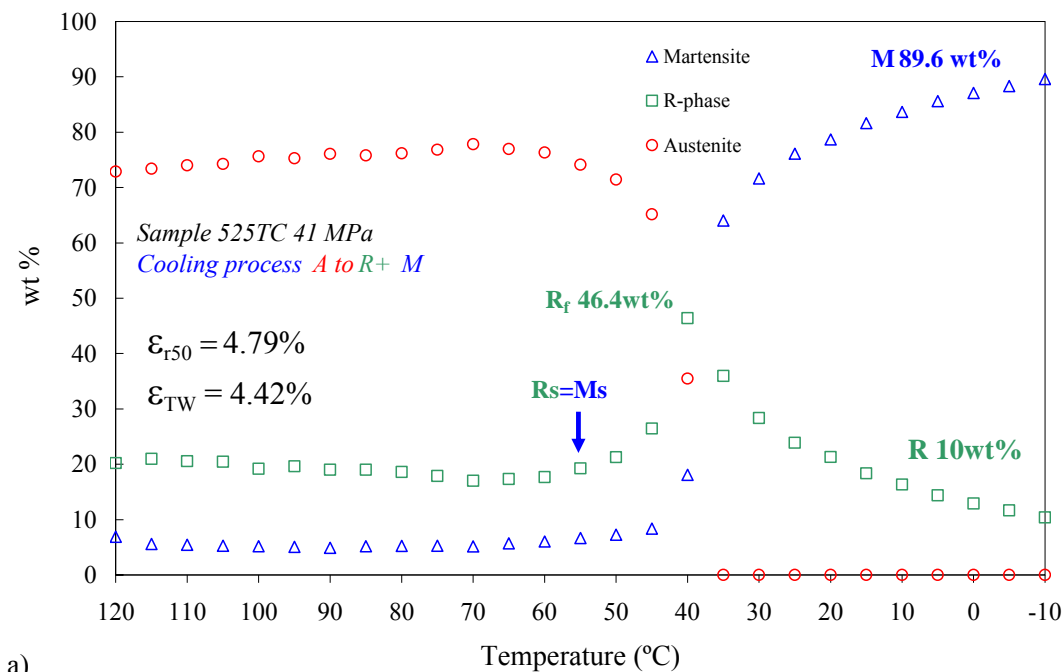


Figures 6.14a and b Evolution of the phase transformation behaviour due to 50 working cycles for samples 500TC₆₈; a) 500TC₆₈ cooling, b) 500TC₆₈ heating.

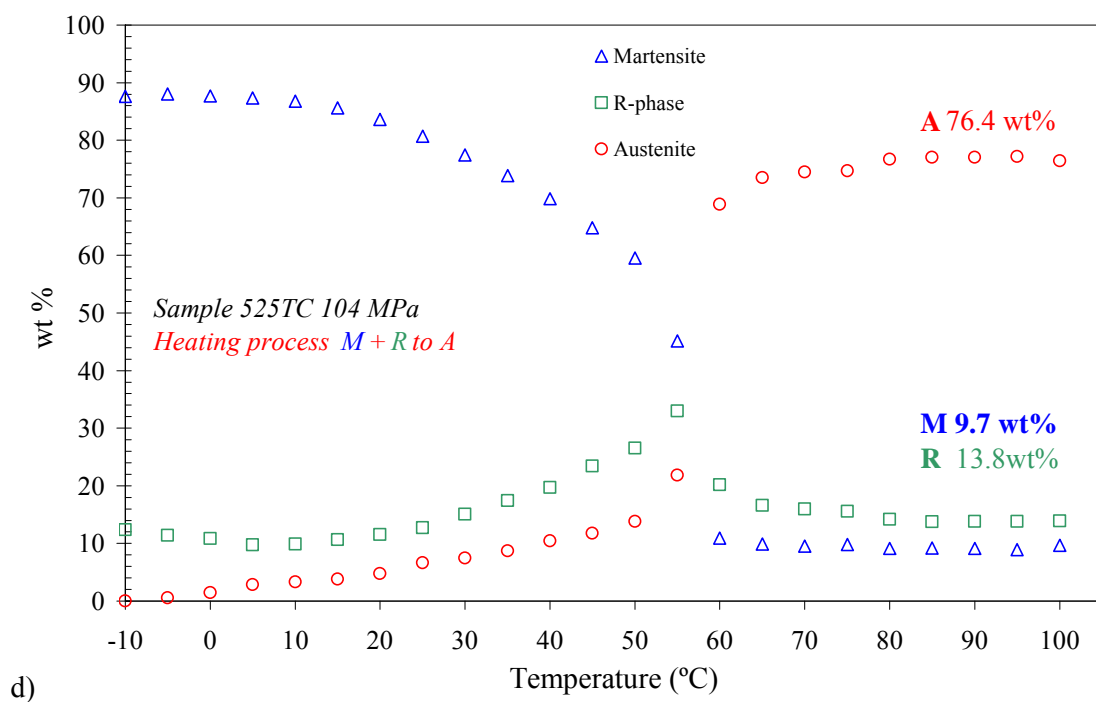
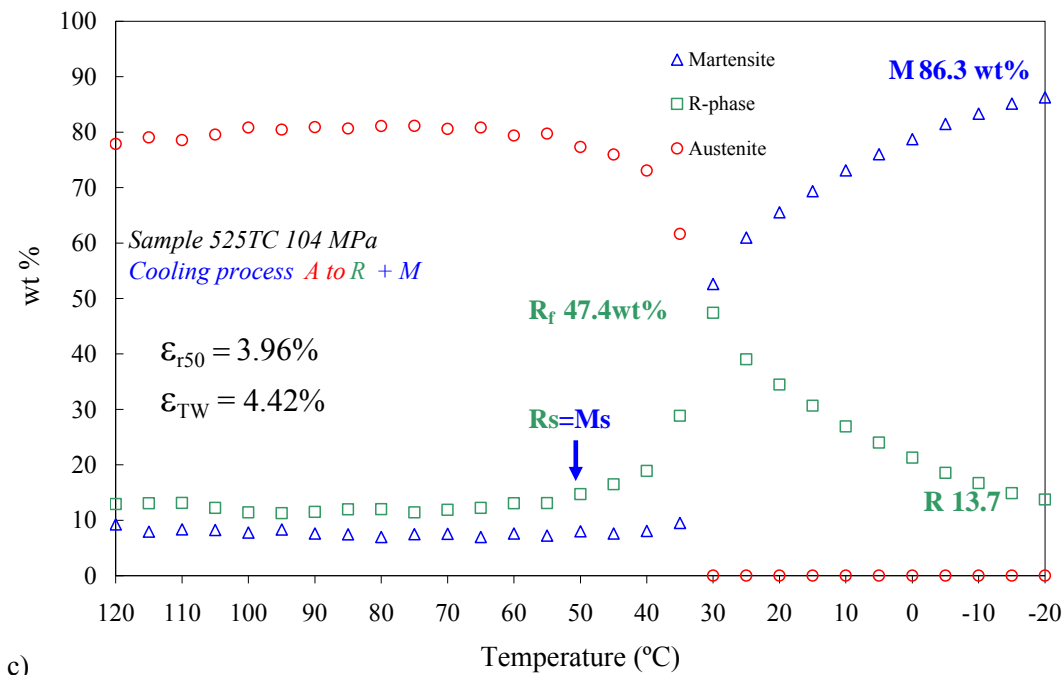


Figures 6.14c and d Evolution of the phase transformation behaviour due to 50 working cycles for samples 500TCs: c) 500TC₁₂₈ cooling and d) 500TC₁₂₈ heating.

The effects of the 50 working cycles on samples 525TC₄₁ and 525TC₁₀₄ are exposed in figures 6.15.



Figures 6.15a and b Evolution of the phase transformation behaviour due to 50 working cycles for samples 525TCs for a) 525TC₄₁ cooling, b) 525TC₄₁ heating.



Figures 6.15c and d Evolution of the phase transformation behaviour due to 50 working cycles for samples 525TCs for c) 525TC₁₀₄ cooling and d) 525TC₁₀₄ MPa heating.

The changes in the phase transformation behaviour of 525TC₄₁ and 525TC₁₀₄ samples due to thermomechanical working are similar to those commented for samples 500TC₆₈ and 500TC₁₂₈ respectively. During cooling, the martensite and the R-phase evolve together from austenite being the transformation simultaneous. When the R-phase transformation ends the maximum level of R-phase is attained, being slightly lower distribution of R-phase for sample 525TC₄₁ (46.4wt%) than for sample 525TC₁₀₄ (47.4wt%). At the end of the cooling process, there is less martensite (86.3%) and higher residual R-phase (13.7wt%) in sample 525TC₁₀₄ than in 525TC₄₁. The heating process for sample 525TC₄₁ and 525TC₁₀₄ is done with contribution of martensite and R-phase that transforms into austenite (figure 6.15 b and 6.15d). During heating, the quantity of R-phase is higher for sample 525TC₁₀₄ (33wt%) than for sample 525TC₄₁ (25.2wt%). At the end of heating process, sample 500TC₁₂₈ has little less austenite respect to 525TC₄₁.

To conclude, according to the values of the recovery strain displayed in figures 6.14 and 6.15, those working samples that develop the largest quantity of martensite and the lowest quantity of R-phase at the end of the cooling process are those that have the highest values of recovery strain (sample 500TC₆₈ and sample 525TC₄₁). In opposition, it seems that the sample that works at stress values higher than its training stress value (sample 500TC₁₂₈ and sample 525TC₁₀₄), an increment in the dislocation density of the sample occurs during working, that is, an increment in the quantity of R-phase is produced. This increment in the level of R-phase produces a decrement in the austenite-martensite transformation strain, and thus, a decrease in recovery strain respect to the TWSME sample is produced.

5. Summary and conclusions

The objective of this Chapter 6 was to measure the efficiency of the TWSME improvement by measuring the work production of the wires during 50 thermomechanical cycles under various levels of constant stress (from 29 to 128MPa). The wires used were those that had been heat treated at a temperature equal to or greater than 500°C, followed by repeated thermal cycling at zero stress and then trained by

constant stress training. These wires were called improved wires. All the improved wires were analyzed to determine the changes caused by this thermomechanical cycling in the work production, recovery strain, transformation temperatures and phase transformation behaviour. The process was repeated for the non-improved (non-thermally cycled) samples and then the results for both the non-improved and the improved samples were compared. Furthermore, we used XRD to quantify the phase transformation behaviour of the samples after the thermomechanical work production.

The main conclusions of this chapter six are:

(i) The results show that **samples that were thermally cycled prior to TWSME training produced higher work than samples that were non-thermally cycled prior to TWSME training** (15% higher). This fact is due to the recovery strains developed during thermomechanical work production, which were always larger for thermally cycled samples than for non-thermally cycled.

(ii) We analyzed the level and stability of the work production generated by the samples during 50 working cycles under different applied stresses. This analysis showed that the **500TCs and 525TCs samples developed their best mechanical performance under low levels of stress**. This range of working stress is between 29 to 70MPa for the 500TC samples and 29 to 50MPa for the 525TC samples.

(iii) The improved SMA wires develop higher recovery strains if they work under certain low values of constant stress than if they work under free stress conditions (TWSME thermal cycling). A saturation phenomenon occurs in the recovery strains depending on the heat treatment temperature and stress applied, with 29 to 70 MPa being the highest stress values for the recovery strain.

(iv) In addition, these 500TCs and 525TCs samples show recovery strain values that are higher than those obtained by other authors who tested non-trained samples under similar working conditions. Turenne et al. published a recovery strain value of 2.8% for a constant stress value of 55MPa after 50 cycles. This recovery strain was stable after 15 cycles [TUR, 2000]. Braisloski et al. obtained similar values to those of Turenne [BRA, 2001]. **The 500TCs samples showed a recovery strain of 3.7% for a constant stress value of 68 MPa after 50 cycles. For the 525TCs samples, the recovery strain was 4.4% for a constant stress of 68 MPa after 50 cycles.**

(v) These 500TCcs and 525TCcs samples show recovery strain values **working at high level of stress (525TC₁₀₄ and 500TC₁₀₄) that are also higher than the values of recovery strain obtained by other authors**. Uchil et al. published that samples thermally cycled under constant stress of 100MPa showed a recovery strain value of 3.1%, and those working under 200MPa showed a recovery strain value of 2.8% after 50 cycles [UCH, 2002]. **The samples 500TCcs showed a recovery strain of 3.61% for a constant stress value of 104 MPa and after 50 cycles.**

(vi) Finally, the phase transformation behaviour changes a little between working samples and TWSME samples, when these working samples were working under stress values that were lower than training stress values. This similitude in the phase transformation behaviour may indicate that at microscopic level, the same variants of martensite that were formed during training were formed in the same sequence during the working cycles. From this point of view, **the results presented in this chapter may confirm the reproducibility of the martensite transformation path formed during training under opposing constant stress working conditions.**

CHAPTER 7

CONCLUSIONS



CHAPTER SEVEN: CONCLUSIONS

1 Summary and Conclusions

307

1 Summary and Conclusions

The main objective of this thesis was to establish the relationships between the changes in Ti-Ni phase transformation behaviour caused by thermomechanical processes, and the functional properties of the Ti-Ni shape memory alloys. The aim was to determine which thermomechanical processes substantially improve the Ti-Ni one-way and two-way shape memory effects. The study has paid special attention to the development of the R-phase by these thermomechanical processes and to the influence of this R-phase on the functional properties of Ti-Ni alloys.

Several experimental techniques were used and included measuring variations of the electrical resistivity with temperature (ER), X-ray diffraction (XRD), isothermal tension test, thermal cycling under constant stress, and thermal cycling under zero stress. The quantitative characterizations of the SMA phases, which are derived from XRD profiles, were introduced to this thesis as a weight fraction (%wt) of the SMA phases as a function of temperature.

To achieve the main objective of this thesis, it was necessary to break it down into a series of smaller objectives. The first of these, which is described in Chapter 4, was to study experimentally how repeated thermal cycling at zero stress throughout the full transformation range affected the phase transformation behaviour and the R-phase depending on the temperature of the heat treatment previously applied. To achieve this objective, the study used different sets of Ti-Ni wires with a Ti-rich chemical composition (49.33at%Ni-50.67at%Ti). One set was heat treated at temperatures of 450, 475, 500, and 525°C. This was done for one hour before the set was quenched in water to obtain different levels of R-phase and different transformation paths. The other set had the same heat treatment followed by repeated thermal cycling at zero stress to

determine the changes in the wire's phase transformation behaviour. Fifty thermal cycles at zero stress were applied. The study then used electrical resistivity measurements and XRD weight fraction diagrams to analyze how heat treatment and thermal cycling affect the phase transformation behaviour of these samples. By comparing these two experimental techniques we were able to interpret the electrical resistivity measurements, regardless of whether there was an R-phase in the alloy or not, and we also obtained valuable information about the SMA's dynamic transformation behaviour between austenite, R-phase and martensite.

The second part of Chapter 4 describes the second objective of this thesis, which was to analyze and determine how the evolution of the phase transformation behaviour with heat treatment and subsequent thermal cycling at zero stress influenced the mechanical parameters of the SMA. We compared the mechanical parameters of samples that had been heat-treated and thermally cycled at zero stress and those of samples that had been heat treated and non-thermally cycled. The comparison paid special attention to the R-phase transformation zone and its parameters in order to detect a possible improvement in the SMA's functional properties as a result of applying a minimum number of thermal cycles at zero stress to the Ti-Ni wires. We used the tension test results to obtain and analyze the critical stress-temperature diagrams for non-thermally cycled samples and for thermally cycled samples. Table 4.7 summarizes the parameters obtained.

We have used different TWSME methods to train the wires that had been previously heat-treated or heat-treated and thermally cycled at zero stress **to investigate a possible improvement in the TWSME** (Chapter 5). Furthermore, we investigated **the changes caused by the training processes to the phase transformation behaviour** of the samples. These two important goals represent the third and four objectives of this thesis. To achieve these objectives we used a great variety of samples. We used two samples that did not show any improvement in their mechanical properties after thermal cycling at zero stress and that presented an initial full developed R-phase after heat treatment (450 and 475 samples); we also used samples that showed little or almost non-existent R-phase in their initial transformation path (500 and 525 samples), and finally, we used samples that had developed the R-phase after thermal cycling at zero stress and that showed an improvement in their mechanical properties after thermal cycling at zero

stress (500TC and 525TC samples). As can be seen, a wide variety of mechanical and phase transformation behaviours were used in the experimental study described in Chapter 5.

The first section of Chapter 5 discussed the results obtained for samples 475, 500, 525, 500TC and 525TC trained by thermal cycling under constant load. It also presented an in-depth analysis of the main parameters obtained during training (permanent strain, strain in the martensite state, and recovery strain). After this, the chapter presented the two-way memory strain that was obtained and its evolution with thermal cycling before finally analyzing and discussing the evolution of the TWSME activation temperatures after training. Following this, the resulting phase transformation behaviour was analyzed by ER and XRD for all the trained samples after constant stress training. The results of this analysis were correlated with the macroscopic TWSME behaviour (strain-temperature behaviour) of each sample. The second part of Chapter 5 presented the results obtained for the isothermal tensile deformation under M_f training in the same order as the results for the constant stress training.

Finally, the last objective of this thesis was to measure the efficiency of the TWSME improvement (Chapter 6) by measuring the work production of the wires during 50 thermomechanical cycles under various levels of constant stress (from 29 to 128MPa). The wires used were those that had been heat treated at a temperature equal to or greater than 500°C, followed by repeated thermal cycling at zero stress and then trained by constant stress training. These wires were called improved wires. All the improved wires were analyzed to determine the changes caused by this thermomechanical cycling in the work production, recovery strain, transformation temperatures and phase transformation behaviour. The process was repeated for the non-improved (non-thermally cycled) samples and then the results for both the non-improved and the improved samples were compared. Furthermore, we used XRD to quantify the phase transformation behaviour of the samples after the thermomechanical work production.

The following are the main conclusions of this thesis:

(i) **On the basis of the constitutive parameters and the critical stress-temperature diagrams** obtained, it is possible to establish that the most **effective way to use a near equiatomic Ti-rich Ni-Ti wire is to heat-treat the sample at**

temperatures equal to or greater than 500°C for one hour before quenching the sample in water. Then, the sample has to be thermally cycled at zero stress prior to use to achieve the best shape memory properties (12 cycles for 500 samples and 25 cycles for 525 samples).

(ii) Due to repeated thermal cycling at zero stress, 500TC and 525TC wires experience a hardening process that improves their mechanical and functional properties. The **apparent modulus** for martensite and R-phase for the load process E_M and E_R , the apparent modulus measured for oriented martensite E_S , and the **shape memory effect** are improved with respect to the corresponding values for non-thermally cycled SMA, 500 and 525 samples (Table 4.7).

(iii) The **improvement in TWSME** is found by **applying a heat treatment prior to training at a temperature equal to or greater than 500°C. This is followed by repeated thermal cycles at zero stress to develop the R-phase** (12 cycles for sample 500TCs and 25 cycles for sample 525TCs) **and training the sample by constant stress training**. After this complete sequence of processes, the TWSME is improved because the training efficiency and the two-way memory strain increase and the permanent strain decreases during training.

(iv) ER curves are very effective at detecting the R-phase in Ti-Ni SMAs. However, **to detect simultaneous transformations, the ER curves should be analyzed in detail together with the XRD results** because these transformations are not revealed in the ER curve alone. Moreover, none of the samples analyzed showed any significant jump in resistivity throughout the heating process, which suggests that the R-phase transformation is the most important cause of change in the ER curves' resistivity values. Therefore, the results have to be deduced using XRD. In any case, **a jump resistivity in the ER curve followed by a long plateau can be taken to mean that the SMA has a transformation path which is clearly separated into two stages and that, in this case, is $R_f=M_S$** . However, a jump resistivity without a plateau indicates that the austenite transforms simultaneously to R-phase and martensite.

(v) For samples with R-phase before thermal cycling (450 and 475) and for samples with R-phase after thermal cycling (450TC₅₀, 475TC₅₀, 500TC₅₀ and 525TC₅₀) **the end of the R-phase transformation (R_f) always corresponds to the end of the**

resistivity plateau that is formed after the sharp increase in the resistivity curve. Ling and Kaplow [LIN, 1980] considered this point to be M_S in the ER curve. Our results show that this point is, in fact, the end of the R-phase transformation (R_f) and that it only corresponds to M_S in some cases. Consequently, **we propose a new interpretation of the ER curves that takes into account the shape of the ER curve measured for the sample** (Figures 4.8).

(vi) It is found that the **R-phase increases after thermal cycling at zero stress** for the sample 500TC, which was heat treated at 500°C and thermally cycled. Moreover, for this sample 500TC, thermal cycling at zero stress **produced a well separated two stage transformation on cooling**; that is, the increase in the dislocation density due to thermal cycling increases the R-phase, thus retarding the martensite transformation and eliminating the simultaneous transformation that had the sample 500 non-thermally cycled. **However, the R-phase does not reach 100wt%**, in fact, it only reaches 65wt%. For sample 525, thermal cycling increases the R-phase to 36wt% after 50 thermal cycles, but does not increase it to 100wt% and does not separate the transformation process. Therefore, it can be said that for heat-treated samples that generate small quantity of R-phase, **thermal cycling at zero stress causes R-phase to develop beyond a certain number of thermal cycles at zero stress but only up to a certain saturation level, which depends on the initial level of the R-phase.** Moreover, if the initial R-phase is almost inexistent, as occurs with sample 525, repeated thermal cycling cannot fully modify the transformation behaviour (or separate the transformation process).

(vii) The **changes produced in the phase transformation behaviour by TWSME trainings** indicate that **to develop a substantial two-way memory strain, the training needs to promote a phase transformation path in the sample that is characterized by a simultaneous transformation of the austenite to the R-phase plus martensite.** To achieve this kind of transformation path, training has to increase the martensite transformation temperature and to make the R-phase and the martensite evolve together throughout the TWSME process. The best samples for obtaining this useful phase transformation behaviour (the simultaneous transformation from austenite to R-phase plus martensite) are those that are heat treated at temperatures equal to or greater than 500°C. These heat treatment temperatures ensure that samples are obtained

with a low dislocation density and similar phase transformation behaviour to those samples subjected to constant stress training or isothermal training. Consequently, the development of TWSME properties in these samples is fast and effective.

(viii) **The dislocations introduced by thermal cycling at zero stress seem to be rearranged by constant stress training.** Thus, in thermally cycled samples, not only is the process of reorienting the martensite easier than in non-thermally cycled samples, but also the increment of R-phase is little or non-existent, as has been experimentally demonstrated. Therefore, **samples that are thermally cycled prior to training generate higher two-way memory strain** than non-thermally cycled samples (0.6% higher).

(ix) **The two-way memory strain values attained for the 500TCcs and 525TCcs samples** are higher than the values published by other authors for similar materials, composition, and training. For example, Scherngell et al. [SCHE, 2002] obtained a two-way strain of around 2.8% and Prader et al. [PRA, 1997] obtained a two-way memory strain of 2.6%. We obtained a maximum value of the two-way memory strain of **4.8% for the 525TCcs samples and 3.8% for the 500TCcs samples.**

(x) **The analysis of effect of the aforementioned thermomechanical processes on the evolution of the phase transformation behaviour has led to the discovery of an important variety of behaviours** for this commercial SMA. These behaviours vary according to the heat treatment temperature, thermal cycling at zero stress, and the training method applied. **For TWSME applications**, the appropriate process is heat treatment at a temperature equal to or greater than 500°C, followed by repeated thermal cycling at zero stress and then constant stress training. **For one-way applications**, the appropriate heat treatment temperatures are 450 and 475°C. These samples are suitable for one-way memory effect applications because they are very stable during mechanical cycling at M_f . Sample 450 becomes stable after almost 36 isothermal cycles under M_f and sample 475 becomes stable after almost 26 isothermal cycles.

(xi) We should note that **the shape memory behaviour of the as-received (non-heat treated) material has been improved.** The number of isothermal cycles needed to obtain stable one-way shape memory behaviour is lower for the 450 and 475 samples

than for the as-received material. The as-received sample needs almost 50 isothermal cycles to reach stable behaviour [DFO, 2009]. Moreover, the values of the critical stress are always higher for the 450 and 475 samples than for the as-received material (almost 50MPa higher).

(xii) The results show that **samples that were thermally cycled prior to TWSME training produced higher work than samples that were non-thermally cycled prior to TWSME training** (15% higher). This fact is due to the recovery strains developed during thermomechanical work production, which were always larger for thermally cycled samples than for non-thermally cycled.

(xiii) We analyzed the level and stability of the work production generated by the samples during 50 working cycles under different applied stresses. This analysis showed that the **500TCs and 525TCs samples developed their best mechanical performance under low levels of stress**. This range of working stress is between 29 to 70MPa for the 500TC samples and 29 to 50MPa for the 525TC samples.

(xiv) In addition, these 500TCs and 525TCs samples show recovery strain values that are higher than those obtained by other authors who tested non-trained samples under similar working conditions. Turenne et al. published a recovery strain value of 2.8% for a constant stress value of 55MPa after 50 cycles. This recovery strain was stable after 15 cycles [TUR, 2000]. Braisloski et al. obtained similar values to those of Turenne [BRA, 2001]. **The 500TCs samples showed a recovery strain of 3.7% for a constant stress value of 68 MPa after 50 cycles. For the 525TCs samples, the recovery strain was 4.4% for a constant stress of 68 MPa after 50 cycles.**

The following interesting conclusions can be drawn from the analysis of how heat treatment and thermal cycling at zero stress influence the phase transformation behaviour:

a. The ER and XRD results show that the transformation behaviour for this 49.33Ni_{at}%-50.67Ti_{at}% SMA changes dramatically when the heat treatment temperature reaches 500°C, and again when the temperature is above 500°C. Samples annealed at $T < 500^{\circ}\text{C}$ retain a high density of dislocations, which leads to a well developed R-phase. Samples annealed at $T \geq 500^{\circ}\text{C}$ produce a little or almost no R-

phase because of the considerable decrease in defects and dislocations in the matrix caused by heat treatment.

b. The ER and XRD results show that the transformation path for samples heat-treated at $T < 500^{\circ}\text{C}$ leads to a well-separated two-stage transformation on cooling ($\text{B2} \rightarrow \text{R} \rightarrow \text{B19}'$) with a well-developed R-phase. It also shows that there is no temperature interval between the end of the R-phase transformation and the beginning of the martensite transformation; that is, $R_f = M_s$.

c. The XRD quantification shows that the transformation path for samples heat-treated at $T > 500^{\circ}\text{C}$ results in a simultaneous transformation on cooling ($\text{B2} \rightarrow \text{R} + \text{B19}'$) and a very poor quantity of R-phase. It also shows that there is no temperature interval between the beginning of the R-phase and the beginning of the martensite transformation; that is, $R_s = M_s$.

d. On heating, all samples presented a simultaneous transformation of the martensite and R-phase to austenite phase ($\text{B19}' + \text{R} \rightarrow \text{B2}$), which confirms that during heating the R-phase is not an intermediate phase. The fact that this simultaneous transformation is not detected by the ER measurements may be due to the poor quantity of R-phase that the alloy has to transform into austenite.

e. The XRD diagrams for all the samples show that the beginning of the transformation to martensite (M_s) corresponds to different points in the ER curves depending on the quantity of the R-phase that the alloy develops during the heat treatment or during thermal cycling at zero stress. Therefore, the ER curves should be combined with the XRD results to ascertain at which point the martensite transformation starts in the ER measurements.

f. The results published by [UCH, 2002] state that when the M_s attains fixed values, the R-phase is considered to have developed during repeated thermal cycling at zero stress. If we compare these results with those described in (ii) and e., we can deduce the following: the temperature that is taken from the ER curves and that indicates that the R-phase has developed is not the M_s temperature. Instead, this temperature seems to be the same temperature as the one at the end of the R-phase transformation (R_f), as all of the wt% diagrams suggest.

g. The ER curves of the samples heat-treated under 500°C show no effect on the transformation behaviour after thermal cycling at zero stress. The remaining high dislocation density resulting from the heat treatment, along with the increase in the internal stress field due to transformation, may act as an obstacle to the movements of the martensite interfaces and interfere with the transformation process, thus increasing the (non-transformed) martensite retained at the end of each thermal cycle. This may be responsible for the increase in retained martensite and the corresponding decrease in austenite and R-phase wt% found.

This thesis draws the following conclusions regarding the effects of TWSME training on Ti-Ni phase transformation behaviour and the role of the R-phase in the development of the TWSME:

a. For samples heat-treated at $T > 500^\circ\text{C}$, both trainings have the same effect on the phase transformation behaviour of these samples (i.e. an increase in martensite transformation temperatures). For samples heat-treated at $T < 500^\circ\text{C}$ both trainings have the same effect on the phase transformation behaviour of these samples (i.e. a decrease in the martensite transformation temperatures and an increase in the temperature interval of the R-phase). Therefore, it can be seen that these effects are only dependent on the heat treatment temperature applied to the Ti-Ni wire and are not dependent on the type of training applied.

b. In samples with an initial full-developed R-phase (the 450 and 475 samples), the trainings do not develop the TWSME. The initial high dislocation density, and thus, the high quantity of R-phase presented by these samples reduces the mobility of the martensite plates. Consequently, the necessary change in the phase transformation behaviour is not produced by training. In fact, training produces the opposite effect; that is, the martensite temperature decreases and the interval of the R-phase transformation increases, thus impeding the development of the TWSME in the 450 and 475 samples.

c. Samples non-thermally cycled prior to training 500cs and 525cs and samples thermally cycled prior to training 500TCs and 525TCs develop similar distributions of R-phase after training. This means that the net increase in R-phase is superior for those samples that are non-thermally cycled prior to training (500cs and 525cs). Thus,

training seems to rearrange the dislocations introduced by thermal cycling at zero stress, thus improving the mobility of martensite and limiting the increase in R-phase.

A comparison of the trainings gives the following conclusions:

- a. The results suggest that to obtain the best SMA performance, that is, to obtain a substantial two-way memory strain together with a minimum final irreversible strain and TWSME activation at room temperatures, the Ti-Ni wire should be trained by thermal cycling under constant stress.
- b. Isothermal training developed the largest two-way memory strain but the irreversible strain generated during this training is higher than that generated by constant stress training.

Chapter 6 provides the following additional conclusions:

- a. The improved SMA wires develop higher recovery strains if they work under certain low values of constant stress than if they work under free stress conditions (TWSME thermal cycling). A saturation phenomenon occurs in the recovery strains depending on the heat treatment temperature and stress applied, with 29 to 70 MPa being the highest stress values for the recovery strain.

The present exhaustive study of the phase transformation changes caused by the most commonly used thermomechanical processes in Ti-Ni SMAs, has led to a new way of interpreting resistivity curves in order to calculate the transformation temperatures. Moreover, we have determined how the R-phase influences the functional properties of SMAs and, finally, we have substantially improved the properties of the one-way and two-way shape memory effects by using thermal processes that prevent permanent deformation of the alloy.

REFERENCES



REFERENCES

A

- [ABE, 2004] Abel, E., Luo, H., Pridham, M., Slade, A., *Issues concerning the measurement of transformation temperatures of NiTi alloys*, Smart Materials and Structures, 13, pp.1110-1117.
- [ANT, 2007] Antonucci, A., Faiella, G., Giordano M., Mennella, F., Nicolais, L., *Electrical resistivity study and characterization during NiTi phase transformations*, Thermochemica Acta, 462, pp.64-69.
- [AIR, 1989] Airoidi, G., Riva, G., Rivolta, B., *A. Proc. MRS Int. Mtg. Adv. Mater.*, 9, pp.105.
- [AIR, 1994] Airoidi, G., Riva, G., Rivolta, B., Vanelli, M., *DSC calibration in the study of the shape memory alloys*, Journal of Thermal Analysis 42, pp.781-791.
- [AUR, 1997]a Auricchio, F., Lubliner, J., *A uniaxial model for superelastic Shape Memory Alloys*. International Journal of Solids and Structures 34(27), pp.3601-3618.
- [AUR, 1997]b Auricchio, F., Sacco, E., *A one dimensional model for superelastic Shape Memory Alloys with different elastic properties between austenite and martensite*. International Journal of non-linear mechanics, 32(6), pp.1101-1114.

B

- [BAT, 1998] Bataillard, L., Bidaux, J.E., Gotthardt, R., *Interaction between microstructure and multiple-step transformation in binary NiTi alloys using in-situ transmission electron microscopy observations*, Philosophical Magazine A 78(2), pp. 327-344.
- [BES, 1999] Besseghini, S., Villa, E., Tuissi, A., *NiTiHf shape memory alloy: effect of aging and thermal cycling*, Materials Science and Engineering A273-275, pp.390-394.
- [BIG, 1996] Bigeon, M.J., Morin, M., *Thermomechanical study of the stress assisted two way memory effect fatigue in TiNi and CuZnAl wires*. Scripta Materilia ,35(12), pp.1373-1378.
- [BRA, 2002] Brailovski, V., Terriault, P., Prokoshkin, P. S., *Influence of the post-deformation annealing heat treatment on the low-cycle fatigue of NiTi Shape Memory Alloys*, Journal of Material Eng. Perform., 11, pp.614-621.
- [BRI, 1993] Brinson, L.C., *One-dimensional constitutive behaviour of shape memory alloys: thermomechanical derivation with non-constant material functions and redefined*

martensite internal variable, Journal of intelligent material systems and structures 4, pp.229-242.

[BRU, 2003] **Bruker AXS GmbH**, TOPAS: General Profile, Structure Analysis Software for Powder Diffraction Data, Karlsruhe V3.1 Germany.

[BUE, 1968] **Buehler, W.J., Wang, F.E.**, *A summary of recent research on the Nitinol alloys and their potential application in ocean engineering*, Ocean Eng. 1, pp.105-120.

C

[CAT, 2005] www.hbm.com

[CAI, 2005] **Cai, W., Meng, L.C., Zhao, L.C.**, *Recent developments of TiNi based shape memory alloys*, Current Opinion in Solid State and Materials science 9, pp.296-302.

[CIN, 1999] **Cingolani, E., Ahlers, M.**, *On the origin of the two-way shape memory effect in Cu-Zn-Al single crystals*, Materials Science & Engineering A, 273-275, pp.595-599.

[CHA, 1951] **Chang, L.C., Read, T.A.**, *Plastic deformation and diffusionless phase changes in metals-the gold-cadmium beta phase*, Am. Inst. Min. Metall. Eng., J. Met. 191(1), pp.47-52.

[CHAN, 2001] **Chang, C., Vokoun, D.**, *Two-Way Shape Memory Effect of NiTi Alloy Induced by Constraint Aging Treatment at Room Temperature*, Metallurgical and Material Transaction A 32(7), pp.1629-1634.

[CHE, 1992] **Cheary, R.W., Coelho, A.A.**, *A fundamental parameters approach to X-ray line-profile fitting*, Journal of Applied. Cryst. 25, pp.109-121.

[CHK, 1976] **Chakravorty, S., Wayman, C.**, *Thermoelastic martensitic transformation in Ni-Al alloys: 1. Crystallography and morphology*, Metallurgical Transactions A 7A, pp.555-568.

[CHI, 1990] **Chi-Mei, M., Gang, L.**, *Contribution of the R transformation to the two-way memory effect in TiNi alloys*, Materials & Science and Engineering A127, pp.85-89.

[CHG, 2001] **Chang, C., Vokoun, D.**, *Two-way shape memory effect of NiTi alloy induced by constraint aging treatment at room temperature*, Metallurgica and Materials Transactions A 32, pp.1629-1634.

[CON, 1990] **Contardo, L., Guenin, G.**, *Training and two way memory effect in Cu-Zn-Al alloy*, Acta Metallurgica Materilia 38, pp.1267-1272.

D

- [DEL, 1991] **Delaey, L.**, *Difussionless transformations*. Materials Science and Technology 5: phase transformations in materials. Ed. P.Haasen. VCH. Verlagsgesellschaft. mbH. Weinheim. Germany. pp. 339-404.
- [DER, 1995] **Derek, H., Scott, R.**, *Effect of training conditions and extended thermal cycling on Nitinol two-way shape memory behaviour*, Smart materials Structures 4, pp.298-304.
- [DFO, 2005] **De la Flor, S.**, *Simulación numérica y correlación experimental de las propiedades mecánicas en las aleaciones con memoria de forma*, Chapter 3. Master Thesis. ETSEIB, UPC.
- [DFO, 2006] **De la Flor, S., Urbina, C., Ferrando, F.**, *Constitutive model of shape memory alloys: theoretical formulation and experimental validation*. Materials Science and Engineering A427, pp.112-122.
- [DFO, 2009] **De la Flor, S., Urbina, C., Ferrando, F.**, *Effect of mechanical cycling on stabilizing the transformation behaviour of NiTi shape memory alloys*, Journal of Alloys and Compounds 469 (1-2), pp.343-349.
- [DOL, 2001]_a **Dolce, M., Cardone, D.**, *Mechanical behaviour of shape memory alloys for seismic applications 1. Martensite and austenite NiTi bars subjected to torsion*. International Journal of Mechanical Sciences 43(11), pp.2631-2656.
- [DOL, 2001]_b **Dolce, M., Cardone, D.**, *Mechanical behaviour of shape memory alloys for seismic applications: 2. austenitic NiTi wires subjected to tension*. International Journal of Mechanical Sciences 43(11), pp.2657-2677.
- [DUE, 1990] **Duering, T.W., Zadno, G.R.**, *An engineering perspective of pseudoelasticity. Engineering aspects of shape memory alloys*, Ed. T.W. Duering, K.N. Melton, D. Stöckel, C.M. Wayman. Butterworth-Heinemann London.
- [DUE, 1996] **Duering, T.W., Pelton, A.R., Stockel, D.**, *The utility of superelasticity in medicine*, Biomedical. Materials and Engineering 6, pp.255-266.
- [DUE, 2006] **Duering, T.W.**, *Some unsolved aspects of Nitinol*, Biomedical. Materials Science and Engineering A 438-440, pp.69-74.
- [DUT, 2006] **Dutta, M., Fathi, H., Dabney, J.**, *Modeling and Control of a Shape Memory Alloy Actuator*, Proceedings of the 2005 IEEE, pp.27-29.
- [DWI, 1959] **Dwight, A.E.**, *CsCl-Type Equiatomic Phases in Binary Alloys of Transition Element*, Transactions of the Metallurgical Society of AIME, 215, pp.283-286.

E

- [ECK, 1976] **Eckelmeyer, K.**, *The effect of alloying on the shape memory phenomenon in nitinol*. Scripta Metallurgica 10 (8), pp.667-672.
- [EGG, 2004] **Eggeler, G., Hornbogen, E., yawny, A., Heckman, A., Wagner, M.**, *Structural and functional fatigue of Ni-Ti shape memory alloys*, Materials Science and Engineering A 378, pp.24-33.

F

- [FAL, 2007] **Falco, A., Furgiule, F., Maletta, C.**, *Two-way shape memory effect of a Ti rich NiTi alloy: experimental measurements and numerical simulations*, Smart Materials and Structures 16, pp.771-778.
- [FAL, 2008] **Falco, A., Furgiule, F., Maletta, C.**, *Functional behaviour of a NiTi/welded joint, Two/way shape memory effect*, Materials Science and Engineering A 481-482, pp.647-650.
- [FAV, 1993] **Favier, D., Liu, Y., McCormick, P.G.** *Three stage transformation behaviour in aged NiTi*, Scripta Metallurgica et Materialia, 28, pp.669-672.
- [FIL, 1994] **Filip, P., Mazanec, K.**, *Influence of cycling on the reversible martensitic transformation and shape memory phenomena in NiTi alloys*. Scripta Metallurgica et Materialia 34, pp.67-72.
- [FIL, 1995] **Filip, P., Mazanec, K.**, *Influence of work hardening and heat treatment on the substructure and deformation behaviour of NiTi shape memory alloys*. Metallurgica et Materialia 32(9), pp.1375-1380.
- [FIL, 1996] **Filip, P., Mazanec, K.**, *The two-way memory effect in TiNi alloys*, Scripta materialia 35(3), pp.349-354.
- [FIL, 2001] **Filip, P., Mazanec, K.**, *Investigation of physical metallurgy characteristics of the two-way shape memory effect in TiNi alloys*, Metallurgica et Materialia 39(1), pp.23-28.
- [FON, 2003] **Font, J., Cesari, E., Muntasell, J., Pons, J.**, *Thermomechanical cycling in Cu-Al-Ni based melt spun shape memory ribbons*, Materials Science and Engineering A 354, pp.207-211.
- [FOR, 1996] **Ford, D., White, S.**, *Thermomechanical behaviour of 55Ni45Ti nitinol* Acta Materialia 44(6), pp 2295-2307.
- [FU, 2004] **Fu, Y., Du H., Huang W., Zhang, S., Hu, M.**, *TiNi-based thin films in MEMS applications: a review*, Sensors and Actuators A 112, pp.395-408.
- [FUN, 1987] **Funakubo, H.**, *Shape memory alloys*, Gordon and Breach Science Publishers, New York.

- [FUK, 1997] **Fukuda, T., Deguchi, A., Kakeshita, T., Saburi, T.,** *Two-way shape memory properties of a Ni-rich Ti-Ni alloy aged under tensile stress.* Materials Transactions JIM, 38(6), pp.514-520.

G

- [GAD, 2002] **Gadaj, S.P., Nowacki, W.K., Pieczyska, E.A.,** *Temperature evolution in deformed shape memory alloy,* Infrared Physics & Technology 43, pp.151-155.
- [GAL, 1999] **Gall, K., Sehitoglu, H., Chumlakov, Y., Kireeva, I.,** *The Influence of Aging on Critical Transformation Stress Levels and Martensite Start Temperatures in NiTi: Part I—Aged Microstructure and Micro-Mechanical Modeling,* Eng. Material and Technology 121, pp.19.
- [GIL, 1998]_b **Gil, F.J., Planell, J.A.,** *Shape memory alloys for medical applications,* Proceedings of the institution of mechanical engineers, Part H-Journal of Engineering in medicine (112) NH6, pp.473-488.
- [GLE, 2000] **Glendenning, R.W., Hood, J.A.A., Enlow, R.L.,** *Orthodontic Applications of a Superelastic Shape-Memory Alloy model,* Proceedings of the International Symposium on Shape Memory Materials, Materials Science Forum 327-328, pp.71-74.
- [GOO, 1985] **Goo, E., Sinclair, R.,** *The B2 to R transformations in Ti50 Ni47Fe3 and Ti49.5 Ni50.5 alloys,* Acta Metallurgica 33 (9), pp.1717-1723.
- [GOR, 2006] **Gori, F., Carnevale, D., Altan, D., Nicosia, S., Pennestril, E.,** *A New Hysteretic Behavior in the Electrical Resistivity of Flexinol Shape Memory Alloys Versus Temperature,* International Journal of Thermophysics 27(3), pp.866-879.
- [GRE, 1938] **Greninger, A.B., Mooradian, V.G.,** *Strain transformation in metastable beta copper-zinc and beta copper-tin alloys,* Transactions AIME 128, pp.337-368.
- [GRY, 2004] **Goryczka, T., Morawiec, H.,** *Structure studies of the R-phase using X-ray diffraction methods,* Journal of Alloys and Compounds 367, pp.137-141.
- [GUI, 1987] **Guilemany, J.M., Gil, F.J., Miguel, J.R.,** *Ciencia y tecnología de materiales con memoria de forma: propiedades y aplicaciones,* Técnica Metalúrgica Barcelona, pp.25-37.
- [GYO, 1996] **Gyobu, A., Kawamura, Y., Horikawa, H., Saburi, T.** *Martensitic transformations in Sputter-Deposited Shape Memory Ti-Ni films,* Materials Transactions JIM 37(4), pp.697-702.

- [GYO, 2001] **Gyobu, A., Kawamura, Y., Horikawa, H., Saburi, T.,** *Two-way shape memory effect of sputter-deposited Ti-rich Ti-Ni alloy films*, Materials & Science and Engineering A312(1-2), pp.227-231.

H

- [HAR, 1990] **Harrison, J.H.,** *Measurable changes concomitant with the shape memory transformations*. In *Engineering aspects of shape memory alloys*. Ed. T.W. Duering., K.N. Melton., D.Stöckel, C. M. Wayman. Butterworth-Heinemann. London. pp.106-115.
- [HARA, 1997] **Hara, T., Ohba, T., Otsuka, K.,** *Phase transformation and crystal structures of Ti₂Ni₃ precipitates in Ti-Ni alloys*, Material Transactions JIM 38, pp.11.
- [HBM, 2010] <http://www.hbm.com/en>.
- [HE, 2006] **He, Z., Gall, K. R., Brinson, L. C.,** *Use of electrical resistance to redefine the transformation kinetics and phase diagram for shape memory alloys*, Materials Transactions 37A, pp.579-587.
- [HEB, 1995] **Hebda, D.A., White, S.R.,** *Effect of training conditions and extended thermal cycling on nitinol two-way shape memory behaviour*, Smart materials and structures 4, pp.298-304.
- [HEC, 2002] **Heckmann, A., Hornbogen, E.,** *Effects of Thermomechanical Pre-treatments on Pseudo-Elastic fatigue of a NiTi alloy*, Materials Science Forum 394-395, pp.325-328.
- [HOD, 1999] **Hodgson, D.E., Wu, M.H., Biermann, R.J.,** *Shape memory alloys*. Shape Memory Applications, Inc. www.sma-inc.com.
- [HON, 1980] **Honma, T., Matsumoto, M., Shugo, Y., Nishida, M., Yamazaki, I.,** *Effects of Thermal Cycles and Substitution Elements on the Phase Transformations of TiNi*, Proceedings of 4th Int. Conf. on Titanium, Kyoto. AIME., pp.1455-1460.
- [HOR, 2003] **Hornbogen, E., Heckmann, A.,** *Improved fatigue resistance of pseudo elastic NiTi alloys by thermo mechanical treatment*, Materialwissenschaft und Werkstofftechnik 34(5), pp.464-468.
- [HOR, 2004] **Hornbogen, E.,** *Review: Thermomechanical fatigue of shape memory alloys*, Journal of Materials science, 39, pp. 385-399.
- [HSI, 1998] **Hsieh, S.F., Wu, S.,** *Room temperature phases observed in Ti_{53-x}Ni₄₇-Zr_x high temperature shape memory alloys*, Journal of Alloys and Compounds 266, pp.276-282.
- [HUA, 2000] **Huang, W., Toh, W.,** *Training two-way shape memory alloy by reheat treatment*, Journal of Materials Science Letters 19, pp.1549-1550.

[HUA, 2001] **Huang, W., Goh, H.B.**, *On the long term stability of two-way shape memory alloy trained by reheat treatment*, Journal of Materials Science Letters 20, pp.1795-1797.

[HUAN, 2001] **Huang, X, Liu, Y.** *Effect of annealing on the transformation behaviour and superelasticity of NiTi shape memory alloy*, Scripta Materialia 45(2), pp.153-160.

I

[IIJ, 2004] **Iijima, M., Brantleyb, W. A., Kawashimac, I., Ohnoc, H., Guob, W., Yonekuraa, Y., Mizoguchia, I.**, *Micro-X-ray diffraction observation of nickel–titanium orthodontic wires in simulated oral environment*, Biomaterials 25(1), pp.171-176.

[IIJ, 2008] **Iijima, M., Brantleyb, W. A., Kawashimac, I., Ohnoc, H., Guob, W., Yonekuraa, Y., Mizoguchia, I.**, *X-ray diffraction study of low-temperature phase transformations in nickel–titanium orthodontic wires*, Dental Materials 24(11), pp.1454-1460.

[ISH, 2001] **Ishida, A., Sagawuchi, T., Sato, M.**, *Shape memory behaviour of Ti-rich Ti-Ni films formed by sputtering*, Journal of Physique IV 11, pp.409-414.

J

[JAN, 2005] **Janke, L.**, *Applications of shape memory alloys in civil engineering structures-overview, limits and new ideas*, Materials and Structures 38, pp.578-592.

[JIN, 1992] **Jinfang, G., Yuying, C.** *The influence of thermomechanical treatment on R-phase transition and shape memory effect*, Material Res. Society. Symposium Proceedings Vol. 246, pp.283-288.

K

[KAF, 1998] **Kafka, V., Vokoun, D.**, *Two-way shape memory: Its nature and modelling*, Acta Technica CSAV 43(4), pp.375-391.

[KAJ, 1986] **Kajiwara, S.**, *Roles of dislocations and grain boundaries in martensite nucleation*, Metallurgica and Materials Transactions A 17(10), pp.1693-1702.

[KAJ, 1996] **Kajiwara, S., Kikuchi, T., Ogawa, K., Matsunaga, T., Miyazaki, S.**, *Strengthening of Ti-Ni shape memory films by coherent subnanometric plate precipitates*, Philosophical Magazine A Letters 74(3), pp.697-702.

[KHA, 2002] **Khalil, K., Ren, X., Eggeler, G.**, *The mechanism of multistage martensitic transformations in aged Ni-rich NiTi shape memory alloys*, Acta Materilia 50, pp.793-803.

- [KHA, 2006] **Khalil-Allafi J., Schmahl W.W., Toebbens D.M.,** *Space group and crystal structure of the R-phase in binary NiTi shape memory alloys*, Acta Mater 54, pp.3171-3175.
- [KIM, 2005] **Kim, J.I., Miyazaki, S.,** *Comparison of Shape Memory Characteristics of a Ti-50.9 % Ni alloy aged at 473 and 673K*, Metallurgical and Materials transactions A 36, pp.3301-3310.
- [KIH, 2008] **Kim, H., Yoo, Y., Lee, J.,** *Development of a NiTi actuator using a two way shape memory effect induced by compressive loading cycles*, Sensors and Actuators A 148, pp.437-442.
- [KNE, 2008] **Kneissl A.C., Unterweger E., Bruncko M., Mehrabi K., Lojen G., Scherngell, H.,** *Microstructure and properties of NiTi and CuAlNi shape memory alloys*, Metallurgica14(2), pp.89-100.
- [KUD, 1985] **Kudoh, Y., Tokonami, M., Miyazaki, S., Otsuka, K.,** *Crystal structure of the martensite in Ti – 49.2 at. % Ni alloy analyzed by the single crystal X-ray diffraction method*, Acta Metallurgica 33, pp.2049-2056.
- [KUM, 2008] **Kumar, P.K., Lagoudas, D.C.,** *Introduction to Shape Memory alloys*, D.C. Lagoudas editorial, Springer Science Business Media, pp.29-42.

L

- [LAH, 2002] **Lahoz, R., Garcia-Villa L., Puertolas, J.A.,** *Training of the Two-Way Shape Memory Effect by Bending in NiTi Alloys*, Journal of Engineering. Material and Technology 124, pp.397-401.
- [LAH, 2004] **Lahoz, R., Garcia-Villa L., Puertolas, J.A.,** *Training and two-way shape memory in NiTi alloys: influence on thermal parameters* Journal of Alloys and Compounds 381, pp.130-136.
- [LAI, 2004] **Lai, BK., Kahn, K.J.,** *Quantitative phase transformation behaviour in TiNi shape memory alloy thin film,s* Material Res. 19(10), pp.2822-2840.
- [LAG, 1999] **Lagoudas, D., Bo, Z.,** *Thermomechanical modelling of polycrystalline shape memory alloy under cyclic loading. Part II: material characterization and experimental results for a stable transformation cycle*, International Journal of engineering science 37, pp.1141-1173.
- [LEX, 1996] **Lexcellent, C., Bourbon, G.,** *Thermodynamical model of cyclic behaviour of Ti-Ni and Cu-Zn-Al shape memory alloys under isothermal undulated tensile tests*, Mechanics of material 24(1), pp.59-73.

- [LI, 1991] **Li, D.Y., Wu, F., Ko, T.,** *The effect of stress on soft modes for the phase transformation in a Ti-Ni alloy II. Effects of ageing and thermal cycling on the phase transformation,* Philosophical magazine A 63(3), pp.603-616
- [LIA, 1990] **Liang, C., Rogers, CA.,** *One dimensional thermomechanical constitutive relations for shape memory materials,* Journal of Intelligent Materials Systems and Structures 1, pp.207-234.
- [LIA, 1992] **Liang, C., Rogers, CA.,** *Design of shape memory alloy actuators.,*Journal of Mechanical Design 114, pp.223-230.
- [LIM, 1994] **Lim, T.J., McDowell, D.L.,** *Degradation of a NiTi alloy during cyclic loading,* Proceedings of the Smart Structures and Materials, SPIE 2189, Orlando, FL, pp. 326–341.
- [LIN, 1980] **Ling, H.C., Kaplow, R.,** *Phase transitions and Shape Memory in NiTi,* Metallurgical Transactions A 11(77), pp.2101-2111.
- [LIN, 1981] **Ling, H.C., Kaplow, R.** *Stress induced shape changes and shape memory in the R and martensite transformations in equiatomic NiTi,* Metallurgical Transactions A 12, pp.2101-2111.
- [LIN, 1994] **Ling, H.C., Wu, S. K.,** *The tensile behaviour of a cold-rolled and reverse-transformed equiatomic TiNi Alloy,* Acta Metallurgica et Materialia 42, pp.1623-1630.
- [LINH, 2006] **Lin, H.C., Lin, K.M., Wang, T.P., Hsiao, Y.C.,** *Effects of thermomechanical training on a Fe59Mn30Si6Cr5 shape memory alloy,* Materials Science and Engineering A438-440, pp.791-795.
- [LIQ, 1990] **Lindquist, G., Wayman, C.,** *Shape memory and transformation behavior of martensitic Ti-Pd-Ni and Ti-Pt-Ni alloys,* In: Proceedings of the International Conference on Engineering Aspects of Shape Memory Alloys, pp.58–68.
- [LIU, 1988] **Liu, Y., McCormick, P.G.** *Transformation dependence of Two-way shape memory behaviour in NiTi,* Acta Metallurgica et Materialia 22, pp.1327-1330.
- [LIU, 1989] **Liu, Y., McCormick, P.G.** *Influence of heat treatment on the Mechanical behaviour of a NiTi Alloy,* ISIJ International 5, pp.417-422.
- [LIU, 1990] **Liu, Y., McCormick, P.G.** *Factors influencing the development of two-way shape memory in NiTi,* Acta Metallurgica et Materialia 38 (7), pp.1321-1326.
- [LIU, 1990]b **Liu, Y., McCormick, P.G.,** *Two way Shape memory effect in NiTi,* Material Science Forum 56, pp.585-590.

- [LIU, 1994] **Liu, Y., McCormick, P.G.**, *Thermodynamic analysis of the martensitic transformation in NiTi-II, Effect of transformation cycling*, Acta Metallurgica Materilia 42(7), pp.2407-2413.
- [LIU, 1994]b **Liu, Y, McCormick, P.G.**, *Thermodynamic analysis of the martensitic transformation in NiTi-I. Effect of heat treatment on transformation behavior*, Acta Metallurgica et Materilia 42 (7), pp.2401-2406.
- [LIU, 1997] **Liu, Y., Galvin, P.**, *Criteria for pseudoelasticity in near-equiatomic NiTi shape memory alloys*, Acta Materillia 45(11), pp.4431-4439.
- [LIU, 1998] **Liu, Y., Xiang, H.**, *Apparent modulus of elasticity of near equiatomic Ni-Ti*, Journal of Alloys and Compounds 270, pp.154-159.
- [LIU, 1999] **Liu, Y., Van Humbeeck, J.**, *Two-way shape memory effect developed by martensite deformation in Ni-Ti*, Acta Metallurgica et Materilia 47(1), pp.199-209.
- [LIU, 1999]b **Liu, Y., Xie, Z., Van Humbeeck, J.**, *Cyclic deformation of NiTi SMA*, Materials Science and Engineering A273-275, pp.134-138.
- [LIU, 1999]c **Liu, Y., Yang, H.**, *The concern of elasticity in stress-induced martensite transformation in Ni-Ti*, Materials Science and Engineering A260, pp.240-245.
- [LIU, 2000] **Liu, Y., Xie, Z., Van Humbeeck, J., Delaey, L., Liu, Y.**, *On the deformation of the twinned domain in NiTi shape memory alloy*, Philosophical magazine A 80(8), pp.1935-1953.
- [LIU, 2000]b **Liu, Y., Favier, D.**, *Stabilisation of martensite due to shear deformation via variant reorientation in polycrystalline*, Acta Materilia 48, pp.3489-3499.
- [LIU, 2002] **Liu, Y., Favier, D., Yang, H.**, *Effect of Ferroelastic Cycling via Martensite Reorientation on the Transformation Behaviour of Nickel-Titanium*, Materials Transaction JIM 43(5), pp.792-797.
- [LIU, 2006] **Liu, Y., Laeng, J., Chin, T.V., Nam, T.H.**, *Effect of incomplete thermal cycling on the transformation behaviour of Ni-Ti*, Materials Science and Engineering A 435-436, pp.251-257.
- [LIU, 2006]b **Liu, Y., Blanc, M., Tan, G., Kim, J.I., Miyazaki, S.**, *Effect of ageing on the transformation behaviour of Ti-49.5at%Ni*, Materials Science and Engineering A 438-440, pp.617-621.
- [LIUY, 2004] **Liu, Y.**, *The work production of shape memory alloy*, Smart Materials and Structures 13, pp.552-561.

- [LOP, 2003] **Lopez Cuellar, E., Guenin, G., Morin, M.,** *Study of the stress-assisted two-way memory effect of a TiNiCu alloy using resistivity and thermoelectric power techniques*, Materials Science and Engineering A 358, pp.350-353.
- [LUO, 007] **Luo H.Y., Abel E.W.,** *A comparison of methods for the training of Ni-Ti two-way shape memory alloy*, Smart Materials and Structures 16, pp.2543-2549.
- [LUK, 2002] **Lukas, P., Sittner, P., Lugovoy, D., Neov, A., Ceretti, M.** *In situ neutron diffraction studies of the R-phase transformation in the NiTi shape memory alloys*, Applied Physics 74 (1), pp.1121-s1123.

M

- [McN, 2003] **McNaney, J.M., Imbeni, V., Jung,Y., Papadopoulos, P., Ritchie,R.O.,** *An experimental study of the superelastic effect in a shape-memory Nitinol alloy under biaxial loading*, Mechanics of Materials 35, pp.969-986.
- [MAC, 2003] **Machado, L.G., Savi, M.A.,** *Medical applications of shape memory alloys*, Brazial Journal of Medical and Biological Research 36(6), pp.683-691.
- [MAN, 1993] **Manach, P. Y., Favier, D.,** *Origin of the Two-way memory effect in NiTi shape memory alloys*, Scripta Metallurgica et Materilia 28, pp.1417-1421.
- [MAR, 1932] **March, A., Krist, Z.,** *Mathematische Theorie der Regelung nach der Korngestalt bei affiner Deformation*, pp.285-297.
- [MAT, 1992] **Matsumoto, H.,** *Electrical resistivity of NiTi with a high transformation temperature*, Journal of Material Science Letters 11, pp.367-368.
- [MAT, 1993] **Matsumoto, H.,** *Transformation behaviour of Ni-Ti in relation to thermal cycling and deformation*, Physica B: Condensed Material 190(2-3), pp.115-120
- [MAT, 2003] **Matsumoto, H.,** *Transformation behaviour with thermal cycling in NiTi alloys*, Journal of Alloys and Compounds 350, pp.213-217.
- [MAT, 2004] **Matsumoto, H.,** *Irreversibility in transformation behavior of equiatomic nickel-titanium alloy by electrical resistivity measurement*, Journal of Alloys and Compounds 368, pp.182-186.
- [MATS, 1987] **Matsumoto, O., Miyazaki, S., Otsuka, K., Tamura, H.,** *Crystallography of martensitic transformation in Ti-Ni single crystals*, Acta Metallurgica 35(8), pp.2138-2144.
- [MATO, 2010] **Matovic, J., Reichenberger, K.,** *Two-way SMA actuators for space application, performances and reliability*, Procedia Engineering 5, pp.1372-1375.

- [MEL, 1990] **Melton, K.R.** *NiTi based Shape Memory Alloys*. En *Engineering aspects of shape memory alloys*. Ed. T.W. Duering., K.N. Melton., D.Stöckel, C. M. Wayman. Butterworth-Heinemann. London. pp.21-36.
- [MEL, 1999] **Melton, K.R.** *general applications of shape memory alloys and smart materials*, Ed. C. M. Wayman, Shape Memory Materials, Cambridge University Press, Cambridge pp.220-239.
- [MEN, 2002] **Meng, X.L., Tong, Y.X., Lau, K.T., Cai, W., Zhou, L.M., Zhao, L.C.**, *Effect of Cu addition on phase transformation of Ti-Ni-Hf high-temperature shape memory alloys*, Material Letters 57, pp.452-456.
- [MIL, 2000] **Miller, D.A., Lagoudas, D.C.**, *Thermo-mechanical characterization of NiTiCu y NiTi actuators: influence of plastic strains*, Smart Materials & Structures 9(5), pp.640-652.
- [MIL, 2001] **Miller, D.A., Lagoudas, D.C.**, *Influence of cold work and heat treatment on the shape memory effect and plastic strain development of NiTi*, Materials Science and Engineering A 308, pp.161-175.
- [MIY, 1981] **Miyazaki, S., Otsuka, K., Suzuki, Y.** *Transformation pseudoelasticity and deformation behaviour in a Ti-50.6%Ni alloy*. Scripta Metallurgica 15, pp.287-292.
- [MIY, 1984] **Miyazaki, S., Otsuka, K.**, *Mechanical behaviour associated with the premartensitic rhombohedral-phase transition in a Ti50-Ni47-Fe3 alloy*. Philosophical magazine A50, pp.393-408.
- [MIY, 1986] **Miyazaki, S., Imai, T., Igo, Y., Otsuka, K.**, *Effect of cyclic deformation on the pseudoelasticity characteristics of Ti-Ni alloys*, Metallurgical Transactions A 17A, pp.115-120.
- [MIY, 1986]b **Miyazaki, S., Igo, Y., Otsuka, K.**, *Effect of thermal cycling on the transformation temperatures of TiNi alloy*, Acta metallurgica 34, pp.2045-2051.
- [MIY, 1986]c **Miyazaki, S., Otsuka, K.**, *Deformation and transition behavior associated with the R-phase in titanium-nickel alloys*, Metallurgical Transactions 17A, pp.53-63.
- [MIY, 1988] **Miyazaki, S., Kimura, S., Otsuka, K.**, *Shape memory effect and pseudoelasticity associated with R-phase transition in Ti50.5at%Ni single crystals*, Philosophical magazine A 57, pp.467-478.
- [MIY, 1989] **Miyazaki, S., Otsuka, K.** Proceedings of the MRS international symposium on Advanced Materials 9, pp.93-101.
- [MOB, 1990] **Moberly, W., Melton, K.N.**, *NiTiCu Shape Memory Alloys*. In *Engineering aspects of shape memory alloys*. Ed. T.W. Duering., K.N. Melton., D.Stöckel, C. M. Wayman. Butterworth-Heinemann. London. pp. 46-57.

- [MOR, 2001] **Morgan, N.B., Friend, C.M.**, *A review of shape memory stability in NiTi alloys*, Journal de Physique IV.11, pp.325-332.
- [MOR, 2003] **Morgan, N.B., Friend, C.M.**, *The effect of thermal cycling and applied stress level on post cycling-Stress free transformation behaviour in NiTi alloys*, Journal de Physique IV 112, pp.815-818.
- [MOR, 2004] **Morgan, N.B.**, *Medical shape memory applications-the market and its products*, Materials Science and Engineering A 378, pp.16-23.

N

- [NAG, 1974] **Nagasawa A, Enami K, Ishino Y, Abe Y, Nenno S.**, *Reversible shape memory effect*, Scripta Metallurgica 8, pp.1055-1060.
- [NAM, 2002] **Nam, T.H., Kim, J.H., Choi, M.S., Lee, H.W.**, *Effect of alloy compositions on the R phase transformation in Ti-Ni alloy ribbons fabricated by rapid solidification*, Journal of Material Science Letters 21, pp.799-801.
- [NAM, 2007] **Nam, T.H, Lee, H.W., Jung, D., Yu, C., Liu, Y.**, *Transformation behavior of Ti-Ni and Ti-Ni-Cu alloy ribbons with nano Ti₂Ni particles*, Materials Science and Engineering A 449-451, pp.1041-1044.
- [NIS, 1984] **Nishida, M., Honma, T.**, *All-round shape memory effect in Ni-rich TiNi alloys generated by constrained aging*, Scripta Metallurgica 18, pp.1293-1298.
- [NIS, 1984]b **Nishida, M., Wayman C.M.**, *Electron microscopy studies of the all-round shape memory effect in a Ti-51 at%Ni alloy*, Scripta Metallurgica 18, pp.1389-1394.
- [NG, 2006] **Ng, K.L., Sun, Q.P.**, *Stress induced phase transformation and detwinning in NiTi polycrystalline shape memory alloy tubes*, Mechanics of Materials 38, pp.41-56.
- [NOV, 2008] **Novak, V.**, *Electric resistance variation of NiTi shape memory alloy wires in thermomechanical tests: Experiments and simulation*, Materials Science and Engineering A 481-482, pp.127-133.
- [NUR, 2008] **Nurveren, K., Akdogan, A., Huang, W.M.**, *Evolution of transformation characteristics with heating/cooling rate in NiTi shape memory alloys*, Journal of Material Processing Technology 196, pp.129-134.

O

- [OLA, 1932] **Ölander, A. Z.** Kristallograf 83(A), p.145.

- [OLS, 1982] **Olson G.B., Cohen, M.**, *Stress assisted isothermal martensitic transformation: application to TRIP steels*, Metallurgical Transactions A 13, pp.1907-1914.
- [OTS, 1970] **Otsuka, K., Shimizu, K.**, *Memory effect and thermoelastic martensite transformation in Cu-Al-Ni alloy*, Scripta Metallurgica 4 (6), pp.469-472.
- [OTS, 1979] **Otsuka, K., Sakamoto, H., Shimizu, K.**, *Successive stress-induced martensitic transformations and associated transformation pseudoelasticity in Cu-Al-Ni alloys*, Acta Metallurgica 27, pp.585-601.
- [OTS, 1990] **Otsuka, K.**, *An introduction to the R phase transition*. En *Engineering aspects of shape memory alloys*. Ed. T.W. Duering., K.N. Melton., D.Stöckel, C. M. Wayman. Butterworth-Heinemann. London. pp.36-46.
- [OTS, 1999] **Otsuka, K., Wayman, C.M.**, *Mechanism of shape memory effect and superelasticity*, In *Shape memory Materials* Ed. Otsuka, K., Wayman, C.M. Cambridge University Press. Cambridge. pp.27-48.
- [OTS, 2002] **Otsuka, K., Ren, X.**, *Factors affecting the M_s temperature and its control in Shape Memory alloys*, Materials Science Forum 394-395, pp.177-184.
- [OTS, 2002]b **Otsuka, K., Kakeshita, T.**, *Science and technology of Shape Memory Alloys: new developments*, MRS Bulletin. Materials Research Society 27(2). pp.91-100.
- [OTS, 2005]c **Otsuka, K., Ren, X.** *Physical metallurgy of Ti-Ni based shape memory alloys*. Progress in Materials Science 50, pp.511-678.

P

- [PAU, 2004] **Paula, A.S., Canejo, J.P.H.G., Martins, R.M.S., Fernandes, F.M.B.**, *Effect of thermal cycling on the transformation temperatures ranges of a Ni-Ti shape memory alloy*, Materials Science and Engineering A 378, pp.92-96.
- [PAU, 2006] **Paula, A.S., Canejo, J.H.P.G., Manesh, Da Silva, R.J.C.**, *Study of the textural evolution in Ti-rich NiTi using synchrotron radiation*, Nuclear instruments and Methods in Physics research B 246, pp.206-210.
- [PAU, 2008] **Paula, A.S., Manesh, K.K., dos Santos, C.M.L., Fernandes, F.M.B., Viana, C.S.**, *Thermomechanical behaviour of Ti-rich NiTi shape memory alloys*, Materials Science and Engineering A 481-482, pp.146-150.
- [PAT, 2006] **Patoor, E., Lagoudas, C.D., Entchev, P.B., Brinson, L.C., Gao, X.**, *Shape memory alloys, Part I: General properties and modelling of single crystals*, Mechanics of Materials 38, pp.391-429.

- [PATT, 2007] **M. Pattabi, K. Ramakrishna, K. Mahesh**, *Effect of thermal cycling on the shape memory transformation behaviour of NiTi alloy: Powder X-ray diffraction study*, *Materials Science and Engineering A* 448(1-2), pp.33-38.
- [PEL, 1998] **Pelosin, V., Riviere, A.**, *Effect of thermal cycling on the R-phase and martensitic transformations in a Ti-rich NiTi alloy*, *Metallurgical and Materials Transactions A: Physical Metallurgy and Materials Science* 29 (4), pp.1175-1180.
- [PELT, 2003] **Pelton, A.R., Scott, M., DiCello, J.**, *The Physical Metallurgy of Nitinol for Medical Applications*, *JOM*, pp.33-37.
- [PELT, 2008] **Pelton, A.R., Schroeder, V., Mitchell, M.R., Gong, X., Barney, M.**, *Fatigue and durability of Nitinol stents*, *Journal of the mechanical behaviour of biomedical materials* I, pp.153-164.
- [PER, 1974] **Perkins, J.**, *Residual stresses and the origin of reversible two-way shape memory effect*, *Scripta Metallurgica* 8, pp.1469-1476.
- [PER, 1983] **Perkins, J., Muesing, W.E.**, *Martensitic transformation cycling effects in Cu-Zn-Al shape memory alloys*, *Metallurgical Transactions* 14A, pp.33-39.
- [PER, 1984] **Perkins, J., Spoholz, R.O.**, *Stress-Induced Martensitic transformation cycling and Two way shape memory training in Cu-Zn-Al Alloys*, *Metallurgical Transactions A* 3(15A), pp.313-321.
- [PIEC, 2006] **Pieczyska, E.A., Gadaj, S.P., Nowacki, W.K., Tobushi, H.**, *Phase transformation Fronts Evolution for stress and strain controlled tension tests in TiNi Shape Memory alloy*, *Experimental Mechanics* 46, pp.531-542.
- [PIE, 2003] **Pietikäinen, J., Söderberg, O.**, *Editores de: Proceedings of the International Conference on Martensitic Transformations. ICOMAT 2002. Espoo. Finland.*
- [POZ, 1999] **Pozzi, M., Airoidi, G.**, *The electrical transport properties of shape memory alloys*, *Materials Science and Engineering A* 273-275, pp.300-304.
- [PRA, 1997] **Prader, P., Kneissl, A.**, *Deformation behaviour and two way shape memory effect of NiTi alloys*, *Zeitschrift für metallkunde* 88(5), pp.410-415.
- [PRE, 2008] **Predki W., Knopik A., Bauer B.**, *Engineering applications of NiTi shape memory alloys*, *Materials Science and Engineering A* 481-482, pp.598-601

R

- [REN, 2001] **Ren, X., Miura, N., Zhang, , Otsuka, K., Koiwa, M., Suzuki T.**, *A Comparative study of elastic constants of Ti-Ni-based alloys prior to martensitic transformation*, *Materials Science and Engineering A* 312, pp.196-206.

- [REY, 1986] **Reyhani, M.M., Mckormik, P.G.,** *Two-Way Shape Memory in a CuZnAl Alloy*, Proceedings of the International Conference on Martensitic Transformations, ICOMAT-86; Nara, Japan, pp.896-901.
- [RIE, 1969] **Rietveld, H.M.,** *A Profile Refinement Method for Nuclear and Magnetic Structures*, Applied Crystallography 2, pp.65-71.
- [RIO, 1987] **Rios-Jara, D., Guenin, G.,** *On the characterization and origin of the Dislocations Associated with the two-way shape memory effect in Cu-Zn-Al thermoelastic alloys*, Acta Metallurgica 35, pp.109-119 and pp.121-129.
- [RYA, 1999] **Ryhänen, J.,** *Biocompatibility evaluation of nickel-titanium shape memory alloy*. Master Thesis. Faculty of Medicine. University of Oulu. Sweden.
- [RYK, 2006] **Ryklina, E.P., Khmelevskaya, I., Prokoshkin, S.D., Inaekyan, K.E., Ipatkin, R.V.,** *Effects of strain aging on two-way shape memory effect in a nickel-titanium alloy for medical application*, Materials Science and Engineering A 438-440, pp.1093-1096.
- [RYK, 2008] **Ryklina, E.P., Prokoshkin, S.D., Khmelevskaya, I.,** *One way and two-way shape memory effect in thermomechanically treated TiNi-based alloys*, Materials Science and Engineering A 481-482, pp.134-137.

S

- [SAA, 2002] **Saadat, S.** *An overview of vibration and seismic applications of NiTi shape memory alloy*. Smart materials and structures 11, pp.218-229.
- [SAB, 1974] **Saburi, T., Nenno, S.,** *Reversible Shape Memory in Cu-Zn-Ga*, Scripta Metallurgica 8, pp.1363-1368.
- [SAB, 2000] **Saburi, T.,** Editor de *Shape Memory Materials*. Proceedings of the Internacional symposium and Exhibition on Shape Memory Materials. SMM'99. Materials Science Forum. pp.327-328.
- [SAI, 2006] **Saikrishna, C. N., Ramaiah, K. V., Bhaumik, S. K.,** *Effects of thermo-mechanical cycling on the strain response of Ni-Ti-Cu shape memory alloy wire actuator*, Materials & Science and Engineering A428, pp.217-224.
- [SAL, 1985] **Salomon, M.B., Meichle, M.E., Wayman, C.M.,** *Premartensitic phases in Ti₅₀Ni₄₇Fe₃*, Physical Rev. B (11), pp.7306-7311.
- [SAT, 1998] **Sato, M.,** *Two-way shape memory effect of sputter-deposited thin films of Ti 51.3 at% Ni*, Thin Solid Films 315(1-2), pp.305-309.

- [SHA, 2009] **Shakeri, M.S., Khalil-Allafi, J., Abbasi-Chianeh, V., Ghabchi, A.,** *The influence of Ni₄Ti₃ precipitates orientation on two-way shape memory effect in a Ti-rich niTi alloy*, Journal of alloys and Compounds 485, pp.320-323.
- [SCH, 2000] **Schetky, L.McD.,** *The industrial applications of Shape memory alloys in North America*, Materials Science Forum 327-328, pp.9-16.
- [SCHE, 1998] **Scherngell, H., Kneissl, A.C.,** *Training and stability of the intrinsic two-way shape memory effect in NiTi alloys*, Scripta Materilia 39(2), pp.205-212.
- [SCHE, 1999] **Scherngell, H., Kneissl, A.C.,** *Influence of the microstructure on the stability of the intrinsic two-way shape memory effect*, Materials Science and Engineering A273-275, pp.400-403.
- [SCHE, 2002] **Scherngell, H., Kneissl, A.C.,** *Generation, development, and degradation of the intrinsic two-way shape memory effect in different alloy systems*, Acta Materilia 50, pp.327-341.
- [SCHR, 1977] **Schroeder, T.R., Wayman, C.M.,** *The two way shape memory effect and other training phenomena in Cu-Zn single crystals*, Scripta Metallurgica 11, pp. 225-230.
- [SCHY, 2002] **Schryver, D., Potapov, P.,** *R-phase structure refinement using electron diffraction data*, Special issue on smart materials-fundamentals and applications, Materials Transactions 43(5), pp.774-779.
- [SHAW,1995] **Shaw, J.A., Kyriakides, S.,** *Thermomechanical aspects of NiTi*, Mechanics and Physics of Solids 43(8), pp.1243-1281.
- [SIT, 2006] **Sittner, P., Landa, M., Lukas, P., Novak, V.,** *R-phase transformation phenomena in thermomechanically loaded NiTi polycrystals*, Mechanics of Materials 38, pp.475-492.
- [SIT, 2006]b **Sittner, P., Sedlak, P., Landa, M., Novak, V., Lukas, P.,** *In situ experimental evidence on R-phase related deformation processes in activated NiTi wires*, Materials Science and Engineering A 438-440, pp.579-584.
- [SITE, 2002] **Sitepu, H., Shamal, W.W., Allaf, J.K., Eggeler, G., Dlouhy, A., Toebbeus, D.M., Tovar, M.,** *Neutron diffraction phase analysis during thermal cycling of a Ni-rich NiTi shape memory alloy using the Rietveld method*, Scripta Materilia 46, pp.543-548.
- [SOM, 1999] **Somsen, H., Záhres, E., Wasserma, F., Kakeshita, T. Saburi, T.,** *Influence of thermal annealing on the martensitic transitions in Ni-Ti shape memory alloys*, Materials Science and Engineering A273-275, pp.310-314.
- [STA, 1991] **Stalmans, R., Van Humbeeck, J., Delaey, L.,** *Training and the two way memory effect in copper based Shape Memory Alloys*. Journal de Physique IV C4(1), pp.45-62.

- [STA, 1992] **Stalmans, R., Van Humbeeck, J., Delaey, L.,** *Thermomechanical cycling, two way memory and concomitant effects in Cu-Zn-Al alloys*, Acta Metallurgica Materilia 40(3), pp.501-511.
- [STA, 1992]b **Stalmans, R., Van Humbeeck, J., Delaey, L.,** *The Two way memory effect in cooper-based shape memory alloys- thermodynamics and mechanisms*, Acta Metallurgica Materilia 40(11), pp.2921-2931.
- [STA, 1992]c **Stalmans, R., Van Humbeeck, J., Delaey, L.,** *Effects of training on the Shape Memory behaviour of Cu-Zn-Al*, Materials Transactions 33, pp.289-293.
- [STAC, 1988] **Stachowiak, G.B., McCormick, P.G.,** *Shape memory behaviour associated with the R and martensitic transformations in a NiTi alloy*, Acta Metallurgica 36(2), pp.291-297.
- [STI, 2007] **Stinton, G., Evans, J.,** *Parametric Rietveld refinement*, Journal of Applied Crystallography 40, pp.87-95.
- [STO, 1942] **Stokes, A.R., Wilson, A.J.C.,** *A method of calculating the integral breadths of Debye-Scherrer lines*, Proc. Camb. Philosophical Society 38, pp.313-322.
- [STÖ, 2001] **Stöckel, D.,** *The Shape Memory Effect: Phenomenon, Alloys and applications*, NCD Nitinol Devices and components. Inc. Fremont. CA.
- [STR, 1995] **Strnadel, B., Ohashi, S., Otsuka, H., Ishihara, T., Miyazaki, S.,** *Cyclic stress-strain characteristics of NiTi and TiNiCu shape memory alloys*. Materials Science and Engineering A202, pp.148-156.

T

- [TAD, 1999] **Tadaki, T.,** *Cu based shape memory alloys*, Shape Memory Materials, Cambridge University Press, pp.97-116.
- [TAM, 1984] **Tamura, H., Suzuki, Y., Todoroki, T.,** Proceedings of International Conference on Martensitic Transformations, Nara, Japan, pp.736.
- [TAS, 1972] **Tas, H., Delay, L., Deruyttere, A.,** *Stress-induced transformations and the shape-memory effect*, Journal of Less-common Materials 28, pp.141-151
- [TAN, 1986] **Tanaka, K.,** *A thermomechanical sketch of shape memory effect: one dimensional tensile behaviour*, Res. Mechanica 18, pp.251-263.
- [TAN, 1992] **Tanaka, K., Hayashi, T., Itoh, Y., Tobushi, H.,** *Analysis of thermomechanical behaviour of shape memory alloys*, Mechanics of Materials 13, pp.207-215.
- [TIA, 2002] **Tian, Q., Wu, J.,** *Tensile behavior of Ti50.6Pd30Ni19.4 alloy under different tensile conditions*, Materials & Science and Engineering A325, pp.249-254.

- [TIR, 2005] Tirry, W., Schryvers, D., *Quantitative determination of the strain fields around Ni₄Ti₂ precipitates*, Acta Materilia 53, pp.1041-1049.
- [TOB, 1990] Tobushi, H., Iwanaga, H., *Cyclic characteristics of the shape memory effect in TiNi alloy wires and helical springs*, JSME International Journal, series I, 33, 2, pp.256-262.
- [TOB, 1991] Tobushi, H., Iwanaga, H., Tanaka, K., Hori, T., Sawada, T., *Deformation behaviour of NiTi SMA subjected to variable stress and temperature*, Continuum mechanics and thermodynamics (3), pp 79-93.
- [TOB, 1992] Tobushi, H., Ohashi, Y., Saida, H., Hori, T., Shirai, S., *Recovery stress and recovery strain of NiTi SMA. Cyclic properties under constant residual strain and constant residual stress*, JSME International Journal I (35), pp. 84-90.
- [TOB, 1992]b Tobushi, H., Iwanaga, H., Tanaka, K., Hori, T., Sawada, T., *Stress-strain-temperature relationships of TiNi shape memory alloy suitable for thermomechanical cycling*, Mechanics JSME International Journal 1 (35-3), pp.271-277.
- [TOB, 1994] Tobushi, H., Kiwura, K., Sawada, T., Hattori, Lin, P.H., *Recovery stress associated with the R-phase transformation in TiNi shape memory alloys*, JSME International Journal I 37, pp.138-142.
- [TOB, 1996] Tobushi, H., Yamada, S., Hachisuka, T., Ikai, A., Tanaka, K., *Thermomechanical properties due to martensitic and R-phase transformations of TiNi shape memory alloy subjected to cyclic loadings*, Smart Material and Structures 5, pp.788-795.
- [TOB, 1998] Tobushi, H., Shimeno, Y., Hachisuka, T., Tanaka, K., *Influence of strain rate in superelastic properties of NiTi shape memory alloy*, Mechanics of Materials 30, pp.141-150.
- [TOD, 1986] Todoroki, T., Tamura, H., Suzuki, Y., *Variable temperature stress-induced martensitic transformation training of Ti-Ni alloy*, Proceedings of the international Conference on Martensitic Transformations, pp.748-753.
- [TOH, 1999] Thoma, P.E., Boehm, J.J., *Effect of composition on the amount of second phase and transformation temperatures of NixTi90-xHf10 shape memory alloys*, Materials Science and Engineering A 273-275, pp.385-389.
- [TOM, 2006] Tomozawa, M., Kim, H.Y., Miyazaki, S., *Micro actuators Using R-phase Transformation of Sputter-deposited Ti-47.3Ni Shape Memory Alloy Thin Film*, Journal of Intelligent Materials System and Structures 17, pp.1049-1058.
- [TUR, 2000] Turenne, S., Prokoshkin, S., Braislovski, V., Sacépé N., *Mechanical and X-Ray Characterization of the Assisted Two-Way Shape Memory Effect in NiTi*, Canadian Metallurgical Quart 39, pp.217-224.

U

- [UCH, 1998] Uchil, J., Mohanchandra, K.P., Kumara, K., Mahesh, K.K., *Study of critical dependence of stable phases in Nitinol on heat treatment using electrical resistivity probe*, Materials Science and Engineering A251(1-2), pp.58-63.
- [UCH, 1999] Uchil, J., Mohanchandra, K.P., Kumara K., Mahesh, K.K., Murali, T.P., *Thermal expansion in various phases of Nitinol using TMA*, Physica B 270, pp.289-297.
- [UCH, 2002] Uchil, J., Kumara K., Mahesh, K.K., *Effect of thermal cycling on R-phase stability in a NiTi shape memory alloy*, Materials Science and Engineering A332, pp.25-28.
- [UCH, 2002]b Uchil, J., Mahesh, K.K., Kumara K., *Electrical resistivity and strain recovery studies on the effect of thermal cycling under constant stress on R-phase in a NiTi shape memory alloy*, Physica B, 324, pp.419-428.
- [UCH, 2002]c Uchil, J., Ganesh,, K., Mahesh, K.K., Kumara K., *Characterization techniques*, Smart Structures and Materials 470(1), pp.435-442.
- [UCH, 2007] Uchil, J., Fernandes, F.M., Mahesh, K.K., *X-ray diffraction study of the phase transformations in NiTi shape memory alloy*, Material Characterizations 58, pp.243-248.
- [URB, 2002] Urbina, C., *Proyecto de adaptación de una máquina Zwick 1445 para la realización de ensayos mecánicos de aleaciones con memoria de forma*, Master Degree in Industrial Engineering, Escola Tècnica Superior d'Enginyeria Industrial de Barcelona (ETSEIB), Universitat Politècnica de Catalunya (UPC).
- [URB, 2002]b Urbina, C., De la Flor, S., Ferrando, F., *Operativa de ensayo para la determinación de las características mecánicas de Alambres con Memoria de forma*, XV Congreso Nacional de Ingeniería Mecánica, Cadiz, (España).
- [URB, 2002]c Urbina, C., De la Flor, S., Ferrando, F., *Adaptación de una máquina de ensayos Zwick 1445 para la realización de ensayos de alambres de aleaciones con memoria de forma níquel titanio*, VIII Congreso nacional de propiedades mecánicas de sólidos, Gandia (España).
- [URB, 2009] Urbina, C., De la Flor, S., Ferrando, F., *Effect of thermal cycling on the thermomechanical behaviour of NiTi Shape Memory Alloys*, Materials Science and Engineering A501 (1-2), pp.197-206.
- [URB, 2009]b Urbina, C., De la Flor, S., Ferrando, F., *TWSME improvement by thermal cycling at zero stress in NiTi shape memory alloys*, Proceedings of SPIE, 7493-74930L.
- [URB, 2010] Urbina, C., De la Flor S., Gispert-Guirado, F., Ferrando, F., *Quantitative XRD analysis of the evolution of the TiNi phase transformation behavior in relation to thermal treatments*, Intermetallics 18 (8), pp.1632-1641.

- [URB, 2010]b **Urbina, C., De la Flor, S., Ferrando, F.,** *R-phase influence on different two-way shape memory training methods in NiTi shape memory alloys*, Journal of Alloys and Compounds 490, pp.499-507.
- [URB, 2010]c **Urbina, C., De la Flor, S., Gispert-Guirado, F., Fabregat, A., Ferrando, F.,** *Characterization of phase transformation and shape memory behaviour of Ti-Ni 54.4 wt% by heat and thermal treatments*, Proceedings of the ESDA 2010-25071.

V

- [VEL, 2005] **Velazquez, R., Pissaloux, E., Szewcyk, J.,** *Miniature Shape Memory alloy Actuator for tactile Binary information display*, Proceedings of the 2005 IEEE, pp.1344-1349.
- [VHU, 1991] **Van Humbeeck, J.,** *Cycling effects, fatigue and degradation of shape memory alloys*, Journal of Physique IV C4 1, pp.189-197.
- [VHU, 1999] **Van Humbeeck, J.,** *Non medical applications of Shape Memory Alloys*, Materials Science and Engineering A273-275, pp.134-148.
- [VHU, 2001] **Van Humbeeck, J.,** *Shape Memory Alloys: a material and a technology*, Advanced Engineering materials 3(11), pp.837-850.
- [VIT, 2005] **Vitello, A., Giorleo, G. Morace, E.,** *Analysis of thermomechanical behaviour of Nitinol wires with high strain rates*, Smart Materials and Structures 14, pp.215-221.

W

- [WAD, 2005] **Wada, K., Liu, Y.,** *Shape recovery of NiTi shape memory alloy under various pre-strain and constraint conditions*, Smart Materials and Structures 14, pp.S273-S286.
- [WAD, 2005]b **Wada, K., Liu, Y.,** *Factors affecting the generation of stress-assisted two-way memory effect in NiTi shape memory alloy*, Journal of Alloys and Compounds 400, pp.163-170.
- [WAD, 2008] **Wada, K., Liu, Y.,** *On the two-way shape memory behaviour in NiTi alloy-An experimental analysis*, Acta Materilia 56(3), pp.3266-3277.
- [WAD, 2008]b **Wada, K., Liu, Y.,** *On the mechanisms of two-way memory effect and stress-assisted two-way memory effect in NiTi shape memory alloys*, Journal of Alloys and Compounds 409, pp.125-128.
- [WAN, 1999] **Wang, Y., Zheng, Y.F, Cai, W., Meng, X., Zhao, L.,** *The tensile behavior of Ti36Ni49Hf15 high temperature shape memory alloy*, Scripta Materilia 40, pp.1327-1331.

- [WANF, 1972] **Wang, F., Buehler, W.,** *Additional unique properties changes observed during TiNi transition*, Applied Physics Letters 21(3), pp.105-106.
- [WANZ, 2002] **Wang, Z.G., Zu, X., Feng, X.,** *Effect of thermomechanical treatment on the two-way shape memory effect of NiTi alloy spring*, Materials Letters, Journal of Materials Letters 54, pp.55-61.
- [WANZ, 2003] **Wang, Z.G., Zu, X., Fu, T.P., Dai, Y., Zhu S, Whang, L.M.,** *Two-way shape memory effect of TiNi alloy coil extension springs*, Materials & Science and Engineering A360, pp.126-131.
- [WANZ, 2003]b **Wang, Z. G., Zu, X., Feng, X., Lin, L.B.,Zhu, S., You, L.P., Wang, L.M.,** *Design of TiNi alloy two-way shape memory coil extension spring*, Materials & Science and Engineering A345, pp.249-254.
- [WANZ, 2004] **Wang, Z., Zu, X.,** *Two-way shape memory effect and alternating current driving characteristics of a TiNi alloy spring*, Rare Metals 23(3), pp.250-254.
- [WAY, 1990] **Wayman, C.M., Duering, T.W.,** *An introduction to martensite and shape memory*, In *Engineering aspects of shape memory alloys.*, Ed. T.W. Duering., K.N. Melton., D. Stöckel, C. M. Wayman. Butterworth-Heinemann. London. pp.3-20.
- [WAY, 1992] **Wayman,C.M.** *Shape memory alloys and related phenomena*, Progress in Materials Science 36, pp.203-224.
- [WU, 1989] **Wu, M.H., Wayman, C.M.,** *On the reciprocal lattice of the premartensitic R-phase in TiNi shape memory alloys*, Acta Metallurgia 37, pp.11-17.
- [WU, 1990] **Wu, M.H.** *Cu based Shape Memory Alloys.* In *Engineering aspects of shape memory alloys*, Ed. T.W. Duering., K.N. Melton., D.Stöckel, C. M. Wayman. Butterworth-Heinemann. London. pp.69-89.
- [WUJ, 2003] **Wu, J., Tian, Q.,** *The superelasticity of TiPdNi high temperature shape memory alloy*, Intermetallics 11, pp.773–778.
- [WUK, 1999] **Wu, S.K., Lin, H.C., Cheng P.C.,** *Multi-strengthening effects on the martensitic transformation temperatures of TiNi shape memory alloys*, Journal of Materials Science 34, pp.5669-5675.
- [WUK, 2006] **Wu, S.K., Lin, H.C., Lin., T.C.,** *Electrical resistivity of Ti–Ni binary and Ti–Ni–X (X = Fe, Cu) ternary shape memory alloys*, Materials Science and Engineering A 438–440, pp.536–539.
- [WUX, 2000] **Wu, X.D., Fan, Y.Z., Wu, J.S.,** *A study on the variations of the electrical resistance for Ni-Ti shape memory alloy wires during the thermo-mechanical loading*, Materials letters 57, pp.1334-1338.

- [WUX, 2003] **Wu, X.D., Fan, Y.Z.,** Wu, J.S., *The nonlinear relationship between transformation strain and applied stress for Nitinol*, Materials & Design 54, pp.114-119.

Y

- [YOO, 2008] **Yoo, S., Yeo, J., Kim, Y.H., Hur, S.G., Kim, E.,** *Application of a NiTi alloy two-way shape memory helical coil for a versatile insulating jacket*, Materials Science and Engineering A 481-482, pp.662-667.
- [YUR, 1959] **Yurko, G. A., Burton, J.W., Pau, J.G.,** *The Crystal Structure of Ti₂Ni*, Acta Crystallina 12, pp.909-911.

Z

- [ZEL, 2003] **Zel'dovich, V.I., Frolova, N.Y., Khomsakaya, I.V., Epanechnikov, E.A.,** *Dilatometric study of SME and TWSME in Ti-Ni alloy*, Journal de Physique IV 113, pp.773-776.
- [ZHA, 1997] **Zhang, X., Rogers, C.A., Liang, C.,** *Modelling of the Two-way shape memory effect*. Journal of intelligent material systems and structures 8. pp.353-362.
- [ZHA, 2006] **Zhang, X., Fernandez, J., Guilemany, J.M.,** *Role of external applied stress on the two-way shape memory effect*. Materials Science and Engineering A 438-440, pp.431-435.
- [ZHO, 2006] **Zhong, Z.W., Yeong, C.K.,** *Development of a gripper using SMA wire*, Sensors and Actuators A 129, pp.375-381.
- [ZHU, 1988] **Zhu, J.S., Gotthardt, R.,** *New phase transition peak in NiTi*, Physical Letters A 132, pp.279-282.
- [ZHUI, 2008] **Zhuiyok, S.,** *Novel sensor-actuator device for early detection of fire*, Sensors and Actuators A 141, pp.89-96.

ANNEX 1

SM495 QUALITY CERTIFICATE





47533 Westinghouse Drive
 Fremont, CA 94539
 Phone: 510-623-6996
 FAX: 510-623-6995

Certificate of Conformance

It is hereby certified that the material or product described meets the requirements of the cited Purchase Order, including referenced specifications or other documents and mutually agreed exceptions, if any.

Euroflex G. Rau GmbH
 Dennigstrasse 7
 D-75179 Pforzheim


Date 20 Dec, 99
 Cust PO 500137
 Work Order WO99-4812
 Lot # 10474
 Certification # 5778

Description SM-495 Wire 1.00±0.01 mm straight, oxide, Af=60-80°C.

Quantity

Material		Parameters	Requirements	Properties
Alloy Type	SM-495	OD (mm)	1.00 + 0.01	0.993 / 0.101
Material Lot #	10474	Length (m)	n/a	n/a / n/a
Ingot Lot #	833080	Load Plateau (ksi)	n/a	n/a / n/a
Ni wt%	54.4	UTS (ksi)		171.5 / 171.5
Ti wt%	Balance	Perm Set %	n/a	n/a / n/a
O wt%	0.033	Elongation %		9.7 / 11.6
H wt%	0.001	Surface Finish	Black Oxide	Black Oxide
C wt%	0.0046	Straightness	Straight	Straight
		Af (°C)	60 -80	66.3 / 74

20 Dec 99 14:23
 30.67%


 Jeff Langan, QA Manager

Wire:SL

ANNEX 2
XRD ANALYSIS



Quantification of the XRD profiles

In recent years, XRD profiles have provided a quantitative understanding that clarifies and relates the phase transformation behaviour to the macroscopic properties and the microstructure of the SMAs. However, the literature contains no quantitative studies of the Ni-Ti phase fraction evolution after heat treatment or after repeated thermomechanical cycling through the complete temperature transformation range.

XRD measurements were made using a Siemens D5000 diffractometer equipped with an Anton-Paar TTK low temperature chamber. The angular 2θ diffraction range was between 37° and 48° , step size 0.016° and 0.4s of step time. Ni-filtered $\text{Cu}_{k\alpha}$ radiation (30 mA, 40 kV) and a Braun position sensitive detector (PSD) were used. The profiles were collected at $\Delta T=1^\circ\text{C}$ after 30s of delay time and at a heating/cooling rate of 0.1°C/s . A static air-atmosphere was used throughout the measurement. All samples were heated at 130°C , cooled at 0.1°C/s down to -20°C , and heated again up to 100°C , and one diffractogram was taken every 1°C during both the cooling and heating processes.

Quantitative phase analysis was carried out on the XRD powder profiles using the Rietveld [RIE, 1969] method and TOPAS 4.2 [BRU, 2003] software. This software was operated under the so called “launch mode” that permits a large number of diffractograms to be fitted in a sequential way. In the present study, up to 137 diffractogram were taken for each sample.

TOPAS had to be configured beforehand so that it could accept the diffractogram obtained with this detector. For this purpose, a sample of LaB_6 from the NIST (SRM 676b) was analyzed in order to obtain the Instrumental Resolution Function of the diffractometer. This function was therefore used for Ni-Ti profiles. The background for each Ni-Ti diffraction profile was fitted as straight line with an adjustable slope. The zero shift, the overall scale factor, the cell parameters and the Lorentzian contribution to the peak width produced by the crystallite size were refined for each phase in all the profiles. The preferred orientation of the martensite and R-phase needed to be corrected [MAR, 1931] because of the samples' wire shape. Martensite needed two hkl directions to correct the preferred orientation. The crystal structures and lattice parameters used for

austenite, martensite and R-phase are reported by [DWI, 1959], [KUD, 1985], [GRY, 2004]. These are summarized on table A2.1.

Following the Rietveld method, the quantitative phase analysis consisted of fitting a calculated X-ray diffractogram to the experimental diffractogram and minimizing, by least squares, the difference between them. All algorithms that are used in the Rietveld method try to minimize the difference between the intensity in each point of the observed profile (I_i) and the calculated intensity in the same point (I_{ci}) of the diffractogram. The quantity to be minimized during the refinement is:

$$R_y = \sum_i \omega_i (I_i - I_{ci})^2 \quad (\text{eq.A2.1})$$

Where $\omega_i = 1/I_i$.

The summation is performed for all points in the diffractogram. The calculated X-ray diffractogram is obtained from the crystal structure of each phase and from geometrical considerations of the diffractometer. The weight fraction, w_i , of a phase in a system of n crystalline phases is given by the expression:

$$W_i = \frac{S_i \rho_i V_i^2}{\sum_{j=1}^n S_j \rho_j V_j^2} \quad (\text{eq.A2.2})$$

Where ρ_i is the crystal density, V_i is the unit cell volume and S_i is the refinable scale factor for phase i . The expression (3.2) is applicable when all phases considered in the sample are crystalline so that:

$$\sum_i W_i = 1 \quad (\text{eq.A2.3})$$

Composition Phase name	System, space group	Crystal Cell parameters	Atomic positions (x, y, z)	Preferred orientation vector	Reference
Ni-Ti Austenite	Cubic $Pm\bar{3}m$	a: 3.015 Å	Ni (0, 0, 0) Ti ($\frac{1}{2}$, $\frac{1}{2}$, $\frac{1}{2}$)		[DWI, 1959]
Ni-Ti Martensite	Monoclinic $P2_1/m$	a: 2.898 Å b: 4.108 Å c: 4.646 Å β : 97.78°	Ti (0.2164, $\frac{1}{4}$, 0.4176) Ni (0.6752, $\frac{1}{4}$, 0.0372)	010 101	[KUD, 1985]
Ni-Ti R-phase	Hexagonal $P\bar{3}$	a: 7.3451 Å c : 5.2718 Å	Ti (0, 0, 0) Ti ($\frac{1}{3}$, $\frac{2}{3}$, 0.045) Ti (0.663, 0.658, 0.651) Ni (0, 0, $\frac{1}{2}$) Ni ($\frac{1}{3}$, $\frac{2}{3}$, 0.544) Ni (0.684, 0.670, 0.152)	(010)	[GRY, 2004]

Table A2.1 Crystal Structures and Lattice Parameters used for austenite, martensite and R-phase.

In order to illustrate this process, figure A2.1 shows the observed (black), calculated (red) and difference (grey) profile for sample 475 during the cooling process. The conventional Rietveld agreement factor, R_{wp} , for this profile is 4.99.

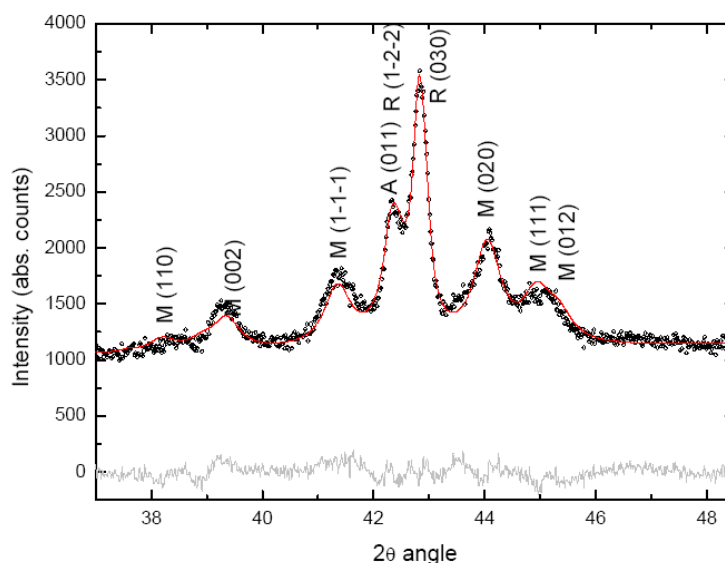


Figure A2.1 Observed (black), calculated (red) and difference (grey) profile for sample 475 during the cooling process at 75°C. Labels indicate the hkl indexes of the Bragg reflections for M (Martensite), A (Austenite) and R (R-phase) phases. The calculated weight % for each phase in this profile is: M: 65.21%, A: 12.58% and R: 22.21%.

To make an accurate analysis of the Ti-Ni phase transformation behaviour by XRD, two different analysis of the XRD profiles using the Rietveld method are made, that is, **Conventional Rietveld analysis and Parametric Rietveld analysis**. In the Conventional Rietveld analysis of the XRD temperature diffractogram, the changes are considered in a sequential way. It means that firstly is analyzed the diffractogram corresponding to temperature T_1 , later on, the diffractogram that corresponds to T_2 and successively until the last temperature, T_n . The parameters fitted for T_i (cell parameters, wt%, crystallite size, etc...) are completely independent from the parameters fitted for T_{1-i} . This way of using the Rietveld method is correct for many cases [URB, 2010], as analysis of the phase transformation behaviour after heat treatments or after thermal cycling at zero stress.

However, a new approach was made in order to improve the XRD results. The reason is the strong correlation between the wt% of austenite and R-phase that was observed in the XRD patterns. The weight fraction diagram of 500 sample, which has

been trained under constant load, is shown in figure A2.2. As seen, the resulting austenite and R-phase wt% variation appears as a cloud of points that makes difficult any interpretation of the results.

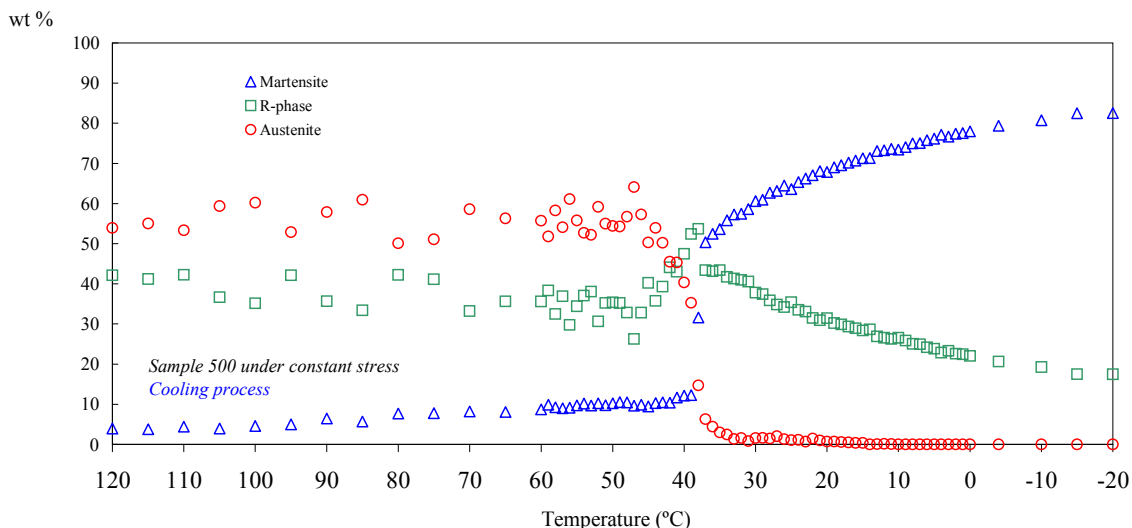


Figure A2.2 From 120 °C to 40 °C is observed a cloud of points composed by austenite and R-phase wt% variations.

Therefore, a second approach to the wt% of phases as a function of temperature by using the Rietveld method was performed. This second approach was made with the so-called **Parametric Rietveld** [STI, 2007]. Stinton and Evans called this approach as “Parametric Rietveld refinement” to emphasize that the calculus to refine fits parametrically in a three-dimensional surface composed by 2θ , intensity and temperature (or time, pressure, etc) space.

In Conventional Rietveld refinement, the parameters refined at T_i are considered independent from those parameters at T_j , T_k or any other temperature. This is a hard assumption because not all the parameters involved in a refinement are completely independent from one temperature to the next. On the other hand, Parametric Rietveld consists on refining several consecutive diffractogram in a simultaneous way, taking into account that the change of some parameters depend on the temperature changes. In the case of the cell parameters, the function that controls such change is the thermal expansion coefficient. During the Ni-Ti phase transformation, there is a change in the size of the sample and hence changes in the coefficient of thermal expansion. The

change in the coefficient of thermal expansion for the characterization of different phases in Nitinol is used [UCH, 1999]. Therefore, the thermal expansion coefficient of the cell parameters is considered that changes in a linear way during all the Parametric Rietveld analysis, especially in the short temperature range studied.

Therefore, in our case, the refinement of the linear expansion coefficient was used to control that the change of the cell parameters varying in a lineal way. The high-temperature phase of Nitinol has the BCC structure; therefore the linear expansion coefficient given for Austenite in literature was used for the refinement ($11 \cdot 10^{-6} \text{C}^{-1}$, [UCH, 1999]). The low-temperature phase has a monoclinic unit cell, so is considered that the thermal expansion is lineal in each of the 3 directions, taking three coefficients to refine: a, b, and c axis. For the intermediate R-phase is considered two coefficients to refine, a-b and c axis, considering the thermal expansion lineal in these two directions.

With this refinement of the cell parameters, the peak position with temperature is limited:

$$a_i = a_R (1 + \alpha_a (T_i - T_R)) \quad (\text{eq. A2.4})$$

Where a_i is the cell parameter at temperature T_i , a_R is the cell parameter at room temperature T_R and α_a is the linear expansion coefficient. Both a_R and α_a are refined and constrained parameters.

Moreover, the width of the diffraction peak that is an independent parameter for each phase is also used to perform the refinement. The crystallite size of Austenite, R-phase and Martensite phase is different, as it would be expected. Austenite phase presents the highest crystallite size up to 300 nm at the highest temperatures whereas Martensite presents the lowest crystallite size around 15 nm at all temperatures where this phase is present. R-phase presents a crystallite size ranging from 50 up to 150 nm. Therefore, the width of the diffraction peak (integral breadth, β_i) is another independent parameter to refine used in the Parametric Rietveld. The crystallite size was calculated from the integral breadth of the diffraction peak [STO, 1942] according to the following formula that comes from the Scherrer expression:

$$\beta_i = \lambda / \varepsilon \cos \theta \quad (\text{eq. A2.5})$$

Where λ is the wavelength, ε is the crystallite size and θ is the Bragg angle.

Because of the Parametric Rietveld analysis, the position of austenite and R-phase peaks are predicted at each temperature minimizing the peak overlapping of these two phases. Therefore, the hard correlation between wt% variation of austenite and R-phase is minimized. As shown in figure A2.3, the cloud of points that exists in the figure A2.2 disappears for the same sample 500, using the Parametric Rietveld method.

The resulting wt% variation as a function of temperature obtained with the Parametric Rietveld refinement is more clear than the obtained with the conventional Rietveld refinement (figures 3.18 and 3.19). Moreover, the number of diffractograms refined by this last mode is reduced up to 59 ($\Delta T=5^{\circ}\text{C}$), while with the conventional Rietveld the number of diffractogram was 187 ($\Delta T=1^{\circ}\text{C}$), resulting the refinement process more easy to perform and the results obtained easier to interpret.

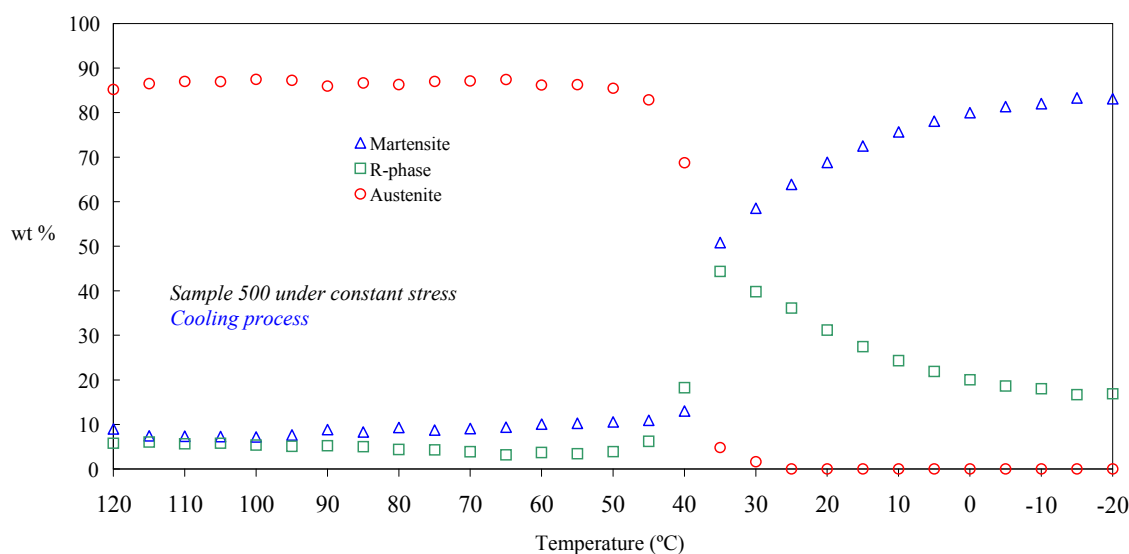


Figure A2.3 Using the Parametric Rietveld method the overlapping between austenite and R-phase disappears and is possible to interpret the phase transformation behaviour of this sample.

On the other hand, Ti_2Ni precipitates may form by annealing Ti-rich Ti-Ni thin films [GYO, 1996], [KAJ, 1996]. However, the X-ray data obtained showed no clear

evidence of the presence of Ti_2Ni precipitates in the wires analyzed [PEL, 1998]. Given the Ni content of the wires analyzed, the maximum expected amount of intermetallic Ti_2Ni is about 2.02 wt %, considering that austenite, martensite and R-phase are stoichiometric Ni-Ti phases and that no other precipitates occurs. Ti_2Ni has a cubic structure [YUR, 1959]. Its strongest peak (511) is located at 41.41° 2θ degrees (ICDD card 72-442). This peak is partially overlapped by (111) martensite reflection. This overlapping, together with the low expected weight and crystallite size of Ti_2Ni [NAM, 2002], produces broad diffraction peaks that make it impossible to identify the Ti_2Ni phase with the present XRD diffractogram. Consequently, the presence of precipitates in the quantitative phase is not indicated in the X-ray data.

